Gene therapy for a novel mouse model of Canavan disease

Dissertation
zur Erlangung des Grades
„Doktor der Naturwissenschaften“
am Fachbereich Biologie
der Johannes Gutenberg-Universität
in Mainz

Nadine Mersmann

Mainz, 2011

Dekan:

1. Berichterstatter:
2. Berichterstatter:

Tag der mündlichen Prüfung: 02.12.2011

TABLE OF CONTENTS

Chapter 1

Summary & Zusammenfassung

1.1. Summary

Canavan disease (CD) is a rare leukodystrophy caused by loss-of-function mutations in the gene encoding aspartoacylase (ASPA), an oligodendrocyte-enriched enzyme. It is characterised by the accumulation of the ASPA substrate N-acetylaspartate (NAA) in brain, blood and urine, leading to a spongiform vacuolisation of the brain, severe motoric and cognitive impairments and premature death. To date, no therapy is available due to the lack of a gene-transfer system allowing transgene expression in oligodendrocytes (OLs) and the restoration of the missing enzyme. Hence, the aim of this study was to establish a novel gene-transfer system and its preclinical evaluation in a CD animal model.

In the first part of this thesis, a novel ASPA mouse mutant was generated. A βgeo cassette (including the genes encoding β-galactosidase and neomycin) flanked by frt sites was inserted into intron 1 of the intact *aspa* gene. Additionally, exon 2 was flanked by loxP sites for optional conditional deletion of the targeted locus. The resulting ASPA-deficient *aspa*$^{lacZ/lacZ}$-mouse was found to be an accurate model of CD and an important tool to identify novel aspects of its complex pathology. Homozygous mutants showed a CD-like histopathology, neurological impairment, behavioural deficits as well as a reduced body weight. Additionally, MRI data revealed changes in brain metabolite composition.

Recombinant adeno-associated viral (rAAV) vectors have become a versatile tool for gene transfer to the central nervous system because they are efficient, non-toxic and replication-deficient. Based on the natural neurotropism of AAV vectors, AAV-based gene delivery has entered the clinics for the treatment of neurodegenerative diseases. However, the lack of AAV vectors with oligodendroglial tropism has precluded gene therapy for leukodystrophies. In the second part of this work, it was shown that the transduction profile of established AAV serotypes can be targeted towards OLs in a transcriptional approach, using the oligodendrocyte-specific myelin basic protein (MBP) promoter to drive transgene expression in OLs.

In the last part of this work, the therapeutic efficacy of AAV-mediated *aspa* gene transfer to OLs of juvenile *aspa*$^{lacZ/lacZ}$ mice was evaluated. AAV-aspa injections into multiple sites of the brain parenchyma resulted in transduction of OLs in the grey and white matter throughout the brain. Histological abnormalities in the brain of ASPA-deficient mice were ameliorated and accompanied by a reduction of NAA levels. Furthermore, the treatment resulted in normalisation of body weight, motor function and nest-building behaviour. These data provide a proof-of-concept for a successful gene therapy of Canavan disease. This might pave the way towards translation into clinical application and serve as the basis for the genetic treatment of other leukodystrophies.

1.2. Zusammenfassung

Morbus Canavan (CD) ist eine seltene Leukodystrophie, die durch eine „loss-of-function"-Mutation im *aspa*-Gen entsteht. Dieses Gen kodiert für das ASPA-Protein, das in Oligodendrozyten angereichert ist. Kennzeichnend für CD ist die Akkumulation des ASPA-Substrats N-Acetylaspartat (NAA) im Gehirn, Blut und Urin. Dies führt bei CD-Patienten zu einer spongiformen Vakuolisierung des Gehirns, zu schweren motorischen und kognitiven Defiziten sowie zum Tode vor Erreichen des Erwachsenenalters. Bisher gibt es keine kurative Therapiemöglichkeit, da ein virales Gentransfersystems fehlt, welches es ermöglicht, Transgene in Oligodendrozyten zu exprimieren und dadurch das fehlende Enzym zu ersetzen. Das Ziel dieser Arbeit war die Etablierung eines solchen Gentransfersystems und dessen präklinische Evaluierung in einem CD-Mausmodell.

Im ersten Teil dieser Arbeit wurde zunächst ein neues ASPA-defizientes Mausmodell hergestellt. Dazu wurde eine von frt-Sequenzen flankierte βgeo-Kassette, die für β-Galaktosidase und Neomycin kodiert, in das Intron 1 des *aspa*-Gens eingefügt. Außerdem wurde zur optionalen konditionalen Deletion das Exon 2 des *aspa*-Gens mit loxP-Stellen flankiert. Es konnte gezeigt werden, dass dieses Mausmodell das klinische Bild der Krankheit widerspiegelt und als wichtiges Instrument zur Aufklärung der komplexen Pathologie dienen kann. Homozygote *aspa*$^{lacZ/lacZ}$-Mäuse zeigen eine CD-typische Histopathologie, neurologische Störungen, motorische Defizite sowie ein verringertes Körpergewicht. Außerdem zeigen MRT-Daten Veränderungen in der Metabolitzusammensetzung des Gehirns.

Rekombinante adeno-assoziierte virale (rAAV)-Vektoren haben sich zu einem vielseitigen Werkzeug für den Gentransfer in das zentrale Nervensystem entwickelt, da sie effizient, nicht-toxisch und replikationsdefizient sind. Aufgrund ihres inherenten Neurotropismus werden sie bereits klinisch in der Behandlung neurodegenerativer Erkrankungen eingesetzt. Allerdings ist die Verwendung der Vektoren zur Therapie von Leukodystrophien bisher nicht möglich, da Vektoren mit oligodendroglialem Tropismus fehlen. Im zweiten Teil dieser Arbeit konnte gezeigt werden, dass das Transduktionsprofil schon etablierter AAV-Vektoren zugunsten von Oligodendrozyten verschoben werden kann. Dies wurde durch die Verwendung des Myelin-basisches-Protein-Promotors (MBP-Promotors) erreicht, der auf transkriptioneller Ebene die Expression von Transgenen in Oligodendrozyten ermöglicht.

Im letzten Teil der Arbeit wurde die therapeutische Effizienz des AAV-vermittelten *aspa*-Gentransfers in Oligodendrozyten junger, ASPA-defizienter Mäuse untersucht. Multiple, parenchymale AAV-*aspa* Injektionen resultierten in einer Transduktion von Oligodendrozyten, sowohl in der weißen, als auch in der grauen Substanz im gesamten Gehirn. Dies führte zu einer

Verringerung der NAA-Konzentration im Gehirn der behandelten Tiere und zu einer deutlichen Abnahme der histologischen Schäden des Gehirns. Außerdem führte die Behandlung zur Normalisierung des Köpergewichts und zur Verbesserung motorischer Fähigkeiten.

Diese Arbeit stellt damit eine „proof-of-concept“-Studie für die erfolgreiche gentherapeutische Behandlung von Morbus Canavan dar. Außerdem können diese Ergebnisse den Weg in die klinische Anwendung ebnen und als Ausgangspunkt für die Entwicklung neuer Therapiestrategien für weitere Leukodystrophien dienen.

Chapter 2:

Introduction on leukodystrophies and gene therapy in the CNS

2. Introduction on leukodystrophies and gene therapy in the CNS

2.1. Cell types of the central nervous system

In the course of evolution, higher eukaryotes were forced to adapt to ever growing challenges resulting in an increase of size and complexity of the nervous system. The vertebrate nervous system is organised in the central nervous system (CNS) comprising the brain and the spinal cord, and the remaining part of the nervous system, the peripheral nervous system (PNS), which is subdivided into somatic and autonomic PNS.

Our brain constitutes only ~2% of the body weight, but consumes ~20% of total body oxygen and ~25% of glucose (SHERWOOD *et al.* 2006), showing the vast activity and fundamental importance of this organ. Beyond that, the human brain contains billions of cells, each with distinct roles, and forms more than 100 trillion (10^{14}) synapses, demonstrating the complexity of this organ. Cell types are classified into neurons and glial cells and the latter are further subdivided into macroglia (astrocytes and oligodendrocytes) and microglia.

Glial cells were discovered in the 19th century by Rudolph Virchow (VIRCHOW 1846), who erroneously considered them to be `brain glue´ (Greek `g*lia´*= glue), providing a scaffold to support neuronal function. However, the work of the last twenty years indicate a more versatile role for these cells and their dysfunction in disease highlights the fundamental importance of glial cells in the maintenance of the brain cell network.

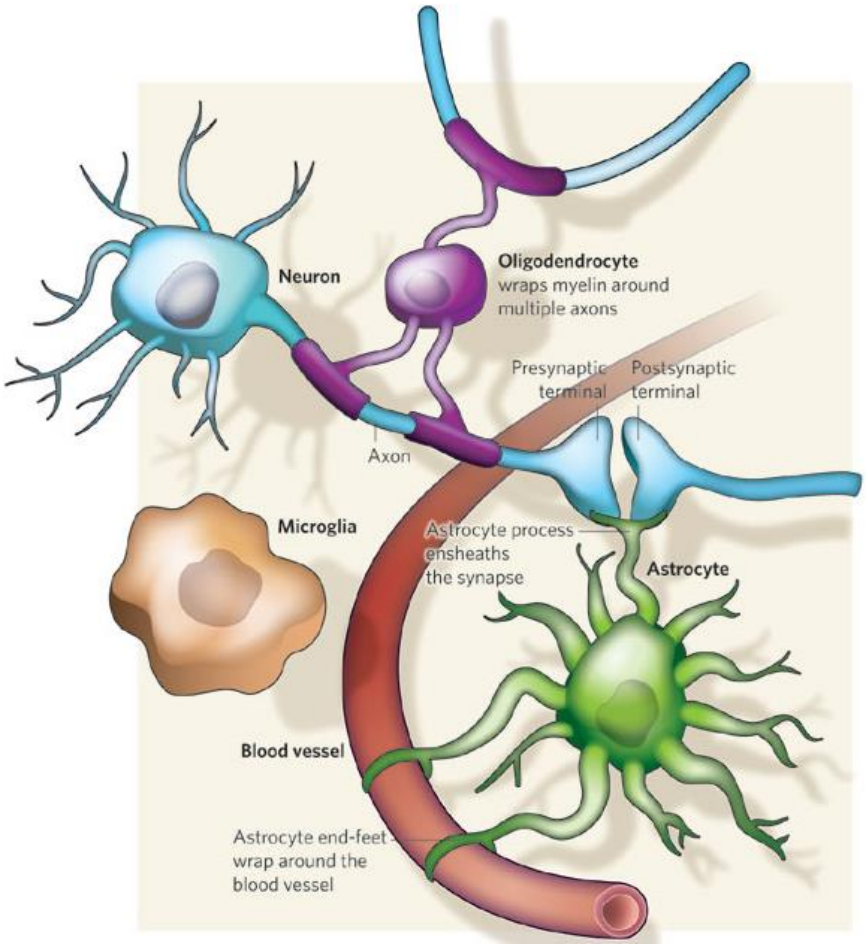

Figure 2.1: The brain cell network.
Aside from neurons, the brain contains different types of glial cells. Oligodendrocytes wrap up axons with myelin to fasten signal propagation. Astrocytes ensheath synapses and assist in signal transmission as well as in the exchange of factors with the blood system and microglia are the resident immune cells of the brain (adapted from (ALLEN and BARRES 2009)).

2.1.1. Neurons

The human brain contains about 100 billion (10^{11}) neurons, or nerve cells, processing and forwarding information via electric or chemical signaling. Neurons are classified either by their connections and inputs, by the neurotransmitters they use or by their electrophysiological properties. The functional classification subdivides neurons into efferent neurons, also called sensory neurons, conveying stimuli such as light, touch and sound from the organs to the CNS, and afferent neurons, also referred to as motor neurons, transferring information from the CNS to the effector cell such as muscle, gland and organ cells.

Although neurons show a broad variety in shape, the cells can be divided into three parts: The perikaryon, or soma, and the axon and dendrites extending from the soma. Dendrites are multiple fine filaments, forming the dendritic arbor, receive most of the synaptic input and can be

modulated in number and structure in response to neuronal activity. The cell body is the compact part of the nerve cell and contains the nucleus as well as major cytoplasmatic organelles. Aggregations of cell bodies form the grey matter of the brain, as they appear grey on freshly cut brain sections. In contrast, myelin-rich regions appear white due to the high amount of lipids in myelin and form the white matter. When incoming signals are received by the neuron, they are processed, integrated and transferred to the axon, where action potentials are formed and the electrical signal is transmitted to the axon terminals and via synapses to other cells. Axon length can vary from less than a millimetre to more than a metre for motor neurons projecting into the extremities.

Neuronal communication depends on both electrical and chemical signaling. With exception of electrical synapses, neurons use different kinds of neurotransmitters binding to chemical receptors to transmit information. Based on the nature of the neurotransmitter these interactions can either be inhibitory, excitatory or modulating.

2.1.2. Microglia

Micoglial cells have a variety of functions in CNS, mainly associated with tissue homeostastis and immune response, as they are the resident macrophages in the brain. They secrete cytokines and growth factors and are involved in CNS development, gliogenesis and angiogenesis. Inflammatory processes, viral infections and neurodegeneration are capable of inducing `reactive´ microglia. One of the main characteristics of activated microglia is the change in morphology upon activation from a bushy appearance in the healthy adult CNS towards an amoeboid morphology in the disease state. During phagocytosis they engulf cellular debris and apoptotic cells and also viruses and bacteria after infection. Furthermore, microglia activation results in an upregulation of the secretion of cytotoxic and/or inflammatory mediators and in antigen presentation, as for example in MS, microglia activation induces T-cell response (OLSON *et al.* 2001).

2.1.3. Astrocytes

Although astrocytes have been named after their star shaped morphology, their form varies widely. Histologically they are identified by staining the intermediate filaments composed of glial fibrillary acidic protein (GFAP) and classified into protoplasmatic astrocytes, which are predominantly found in the grey matter, and fibrous astrocytes in the white matter.

Embryonically, astrocytes derive from radial glial cells, which provide structural support in patterning and neuronal migration. Therefore, radial glia play a crucial role in development and serve as precursors during neurogenesis in adulthood (NOCTOR *et al.* 2001). Astrocytes express adhesion molecules and extracellular matrix proteins such as cell adhesion molecules (CAMs), fibronectin, laminin and growth factors and collaborate in forming the neural network. As they are involved in the regulation of ion concentration, they express potassium channels, which are needed to balance the extracellular milieu for synaptic transmission. Further functions include the building and maintenance of the blood-brain-barrier and the promotion of myelination by the secretion of leukemia inhibitory factor (LIF) in response to ATP released by firing neurons (ISHIBASHI *et al.* 2006). Astrocytes modulate and control synaptic transmission by the uptake of neurotransmitters, the release of so called `gliotransmitters´ upon activation of G-protein coupled receptors (GPCRs) and the elevation of Ca^{2+}-concentration by releasing Ca^{2+} from stores in the endoplasmatic reticulum (SANTELLO and VOLTERRA 2009). Furthermore, astrocytes play a crucial role in detoxification of the CNS. They are thought to be involved in the clearing of amyloid-β (Aβ), the protein that accumulates in the plaques in Alzheimer´s disease (WYSS-CORAY *et al.* 2003). After brain injury, viral infections, or in response to neuronal degeneration and inflammatory demyelinating diseases, astrocytes can become hypertrophic and may proliferate, leading to a so called `reactive gliosis´ (ENG and GHIRNIKAR 1994). This is accompanied by structural changes such as the upregulation of intermediate filament proteins GFAP, vimentin and the re-expression of nestin (PEKNY and NILSSON 2005). In addition, there are functional changes leading to the upregulation of proteolytic enzymes such as cathepsines and calpain to degrade myelin proteins in demyelinating diseases (EDDLESTON and MUCKE 1993; SHIELDS *et al.* 1999).

2.1.4. Oligodendrocytes

As communication from and to the extremities and within the brain depends on rapid signal propagation, the conduction velocity in axons is a crucial factor. The increase of conduction velocity is either achieved by the enlargement of the axon diameter, as for example in the case of the squid giant axon, or by the insulation of the axon with large sheets of membranes – the myelin sheath. Both mechanisms lead to an increase in conduction velocity making it possible to transfer information over long distances and are employed in the nervous system of many taxa, both vertebrate and invertebrate (HARTLINE and COLMAN 2007).

In the mammalian CNS oligodendrocytes are the myelinating cells and, in contrast to PNS, where Schwann cells are the myelinating cells, oligodendrocytes can wrap up multiple axons. They

derive from oligodendrocyte precursors (OPCs) from the neuroepithelial cells of the ventricular and subventricular zone (DOETSCH *et al.* 1997). Their number increases for six postnatal weeks in rodents (BARRES and RAFF 1994) and is regulated by apoptosis in the maturating brain. OPCs migrate extensively throughout the brain (SMALL *et al.* 1987), settle in the future white matter tracts, become post-mitotic and differentiate driven by factors from neurons as well as astrocytes. Each stage of oligodendrocyte maturation is characterised by the expression of different transcription factors, proteins and lipids. During myelination oligodendrocytes build a large sheet of plasma membrane, which gets spirally wrapped around the axon. Long myelin segments are interspersed with by the so called `nodes of Ranvier´, where sodium channels are clustered to facilitate the saltatory impulse propagation of action potentials. Furthermore, oligodendrocytes are involved in the development and the regulation of the axonal caliber and the inhibition and regeneration of axonal growth (BAUMANN and PHAM-DINH 2001). Independent of myelin formation, oligodendrocytes contribute to axonal integrity by trophic support (NAVE 2010). Additionally, the abnormal expression of myelin- and oligodendrocyte-related genes in schizophrenia and bipolar disorder suggests oligodendrocyte dysfunction in these diseases (DAVIS and HAROUTUNIAN 2003; TKACHEV *et al.* 2003). Most importantly, oligodendrocyte dysfunction leads to severe de- and dysmyelininating diseases such as multiple sclerosis or leukodystrophies, highlighting the pivotal role of oligodendrocytes in the maintenance of CNS homeostasis.

2.2. Leukodystrophies

The word `leukodystrophy´ is of Greek origin (leukos – white, dys – impaired, trophe – nutrition) and terms a group of mostly hereditary neurodegenerative disorders characterised by defects in myelin sheath formation or maintenance (de-/dysmyelination) in the CNS and often also in peripheral nerves. The molecular basis of these diseases are genetic mutations in the myelin-forming cells, the oligodendrocytes, or failure in myelination secondary to neuronal or astroglial dysfunctions. This leads to a breakdown of the oligodendrocyte-neuron interaction and subsequently to a disruption of information processing (KUMAR *et al.* 2006). By now, more than 20 diseases have been identified as leukodystrophies and are classified by their affected cell organelle or histological characteristics. Table 1 summarises different types of leukodystrophies and their causes and effects.

Table 2.1: Overview on leukodystrophies.

Disease	Gene affected	Cellular defect
X-linked Adrenoleukodystrophy (X-ALD)	ABCD1	Peroxisomal disease, reduced β-oxidation of VLCFA, VLCFA accumulation
Metachromatic leukodystrophy (MLD)	Aryl sulfatase A (ARSA)	Lysosomal disease, Accumulation of sulfatides in brain and kidney
Globoid cell leukodystrophy (Krabbe disease)	Galactocerebrosidase (GALC)	Lysosomal disease, Accumulation of galactocerebrosid
Canavan disease (CD)	Aspartoacylase (ASPA)	N-acetylaspartate (NAA) accumulation; impaired lipid synthesis
Pelizaeus-Merzbacher Disease (PMD)	Proteolipid protein (PLP)	Unfolded protein response
Spastic Paraplegia Type 2	Proteolipid protein (PLP)	Protein turnover, protein mistrafficking

2.2.1. Canavan disease (CD)

Canavan disease is an autosomal recessive disorder caused by loss-of-function mutations in the gene encoding aspartoacylase (ASPA). It was described based on histological findings by Myrtelle M. Canavan in 1931 (CANAVAN 1931) and further characterised by van Bogaert and Bertrand (VAN BOGAERT and BERTRAND 1949), but it took nearly 60 years to find the molecular cause for CD (HAGENFELDT *et al.* 1987; MATALON *et al.* 1988).

The single gene mutation has pleiotropic effects. Histopathological findings are a spongiform vacuolisation of the brain, dilated ventricles and dysmyelination. The number of protoplasmatic astrocytes increases and also their mitochondria were observed to be abnormally elongated with distorted cristae, suggesting an impaired energy metabolism (ADACHI *et al.* 1973; ADACHI *et al.* 1972; KUMAR *et al.* 2006). Due to the lack of aspartoacylase its substrate N-acetyl-L-aspartate (NAA), a major osmolyte of the brain, accumulates and leads to water accumulation (BASLOW 1999b). These findings on cellular level lead to developmental delay, mental retardation, macrocephaly, hypotonia and later spasticity, optic atrophy and seizures in CD patients (MATALON and MICHALS-MATALON 2000; SURENDRAN *et al.* 2003b).

Besides genetic testing the clinical diagnosis includes measuring NAA levels in blood and urine. NAA levels in blood and cerebrospinal fluid are elevated about 3-fold and urinary levels are increased up to 50 times compared to normal levels (SURENDRAN *et al.* 2003b). NAA levels are also increased in the amniotic fluid and allow prenatal testing. Computed tomography as well as magnetic resonance imaging (MRI) of the brain of CD patients reveal diffuse white matter degeneration

(BRISMAR *et al.* 1990) and an elevated NAA peak is found in nuclear magnetic resonance spectroscopy (WITTSACK *et al.* 1996).

There is a broad variation in the clinical course of CD and the different forms are classified depending on the onset of the disease into a congenital, infantile and juvenile form. Although CD patients have a drastically reduced lifespan and usually die before the age of ten, some patients, however, reach the second and some even the third decade of life (MATALON and MICHALS-MATALON 1999).

2.2.2. The enzyme: Aspartoacylase (ASPA)

The human aspartoacylase gene was cloned in 1993 and is localised on the short arm of chromosome 17 (17p13-ter) (KAUL *et al.* 1994; KAUL *et al.* 1993). The gene spans 30 kb and consists of five introns and six exons. The cDNA comprises 1,435 bp with 158 bp 5´ and 316 bp 3´ untranslated regions and codes for a protein (EC3.5.1.15) with 313 aminoacids (312 aminoacids in rat and mouse) with a predicted molecular weight of 36 kDa (KAUL *et al.* 1994). The human *aspa* coding sequence cross-hybridises with genomic DNA from yeast, chicken, rabbit, cow, dog, mouse, rat, and monkey suggesting that ASPA is highly conserved during evolution (KAUL *et al.* 1994; KAUL *et al.* 1991). Studies on the structure of ASPA revealed that recombinant ASPA forms dimers *in vitro* (BITTO *et al.* 2007; LE COQ *et al.* 2006), however, the active form of the native protein is a monomer (HERSHFIELD *et al.* 2006). ASPA belongs to the zinc-carboxypeptidase family (BITTO *et al.* 2007; HERGA *et al.* 2006; LE COQ *et al.* 2006; MAKAROVA and GRISHIN 1999).

Although CD is pan-ethnic, it is more prevalent among Ashkenazi Jews of Eastern European origin and in this group two predominant gene mutations have been identified, which account for 96% of the mutation in this population (KRONN *et al.* 1995). The missense mutation E285A leads to a loss of the hydrogen bonding network at the active site and the nonsense mutation Y231X leads to a truncated protein, which is likely to be degraded *in vivo* (BITTO *et al.* 2007).

Histologically, the most abundant expression is observed in white matter tracts and the thalamus. On cellular level ASPA expression is restricted to oligodendrocytes (BHAKOO *et al.* 2001; KIRMANI *et al.* 2003; KLUGMANN *et al.* 2003). However, there is one study reporting the immunostaining of a small number of large reticular and motor neurons in the brain stem and spinal cord of rats, and of microglia, which were faintly to moderately stained (MADHAVARAO *et al.* 2004). The subcellular localisation, however, is still a matter of debate. Early studies suggested that ASPA is an integral component of the myelin sheath where it is ideally located to produce acetyl groups from NAA for the synthesis of myelin lipids (CHAKRABORTY *et al.* 2001). Later studies revealed ASPA

immunoreactivity in both cytoplasm and nucleus of oligodendrocytes (HERSHFIELD *et al.* 2006; KLUGMANN *et al.* 2003), but all studies lack consistency in the techniques used, pre-treatment of the samples and antibodies used for the determination of ASPA expression. Another study combining immunoblot, proteomic and biochemical approaches demonstrated the bimodal occurrence of ASPA in the cytosol as well as in the myelin of the brain (WANG *et al.* 2007).

In wildtype mice, ASPA expression coincides with oligodendrocyte maturation and myelinogenesis (BHAKOO *et al.* 2001; KLUGMANN *et al.* 2003), but recent studies showing that ASPA is already expressed as early as E12.5 raised the question of the developmental effects of this protein in the brain (KUMAR *et al.* 2009). In the absence of ASPA immature oligodendrocytes die particularly in the white matter and, simultaneously, a massive increase in the number of undifferentiated neural stem/progenitor cells is observed suggesting an attempt to repair the damage. A study by Kumar and co-workers revealed that neural progenitors have an increased proliferation rate due to a loss of cell cycle arrest (KUMAR *et al.* 2009). Hence, there is a concurrent genesis of oligodendrocyte progenitors and apoptosis of immature oligodendrocytes. Furthermore, it was speculated that ASPA is involved in chromatin remodeling due to its function as a deacetylase. Indeed, a second study by Mattan and colleagues (MATTAN *et al.* 2010) showed an increased level of acetylated histone H3 in oligodendrocytes of ASPA-deficient mice subsequently leading to a more dispersed chromatin, which is an indication of progenitor-like cells. These findings suggest the involvement of ASPA in early postnatal development affecting oligodendrocyte maturation and myelination and are further supported by study reporting increased postnatal mortality of ASPA-knockout mice (SURENDRAN *et al.* 2005b).

2.2.3. The substrate: N-acetyl-L-aspartate (NAA)

NAA is among the most abundant free amino acids in the brain and was first isolated from cat and rat brain (TALLAN 1957; TALLAN *et al.* 1956). It is an amino acid derivate with an acetylated amino group, carrying two negative charges at physiological pH.

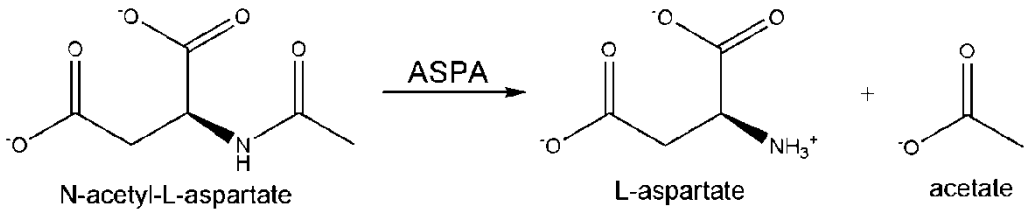

Figure 2.2: The chemical structure of NAA.
The cleavage into aspartate and acetate is catalysed by ASPA.

NAA localisation and distribution

Although the highest amounts of NAA were found in the brains of mammals and birds, amphibians and fish contain NAA as well. Furthermore, it is not restricted to the CNS, but was observed in the PNS and the vertebrate eye, yet in very low amounts (BASLOW and YAMADA 1997; MIYAKE *et al.* 1981; NADLER and COOPER 1972). Early studies showed, that in the CNS NAA is predominantly found in neurons (NADLER and COOPER 1972). However, more recent studies revealed that oligodendrocyte progenitors, and probably mature oligodendrocytes, contain NAA as well (BHAKOO and PEARCE 2000; URENJAK *et al.* 1992). The establishment of specific antibodies against NAA enabled the determination of cellular localisation (MOFFETT *et al.* 1991; SIMMONS *et al.* 1991). Thus, NAA was present in most neuronal cell populations, yet in varying concentrations (MOFFETT and NAMBOODIRI 1995; URENJAK *et al.* 1992). Due to its high concentrations in the brain and its well characterised MRI profile (MICHAELIS *et al.* 1993), it is used as a surrogate marker for the non-invasive determination of neuronal density and integrity.

NAA metabolism

The NAA metabolic cycle is remarkably compartmentalised and involves neurons, astrocytes and oligodendrocytes. NAA is synthesised from acetyl-coenzyme A (AcCoA) and aspartate in the mitochondria of neurons by acetyl CoA/aspartate N-acetyltransferase 8L (ANAT, Nat8L, EC2.3.1.17) (WIAME *et al.* 2010) in an oxygen and ADP-dependent manner (PATEL and CLARK 1979). Probably, NAA is produced in microsomes as well (LU *et al.* 2004). Intracellular NAA levels maintain at a concentration of 20 mM with an intracellular/extracellular gradient of >200 (BASLOW 2010). Upon stimulation, NAA is released to the extracellular fluid (ECF), taken up by oligodendrocytes, where NAA is cleaved into aspartate and acetate. The latter may serve as acetate source for myelin lipid synthesis, while aspartate is recycled in neurons.

Another source for NAA is the dipeptide N-acetyl-aspartylglutamate (NAAG). Like NAA, NAAG is synthesised in neurons from NAA and glutamate catalysed by NAAG synthase (NAAGS, EC.2.3.1.1) (BECKER *et al.* 2010) and the cellular concentration is maintained at 1 mM (BASLOW 2010). After release into the ECF, NAAG can be cleaved by NAAG peptidase (glutamate carboxypeptidase II; folh1; EC 3.4.17.21), which is located on the surface of astrocytes. Whereas NAA is further metabolised in oligodendrocytes, glutamate is taken up by astrocytes and converted into glutamine prior to the transport back to neurons (BASLOW 2010). Taken together, the NAA system ties up the intercellular communication between neurons, astrocytes and oligodendrocytes and is therefore termed `the operating system´ of the brain (BASLOW 2010).

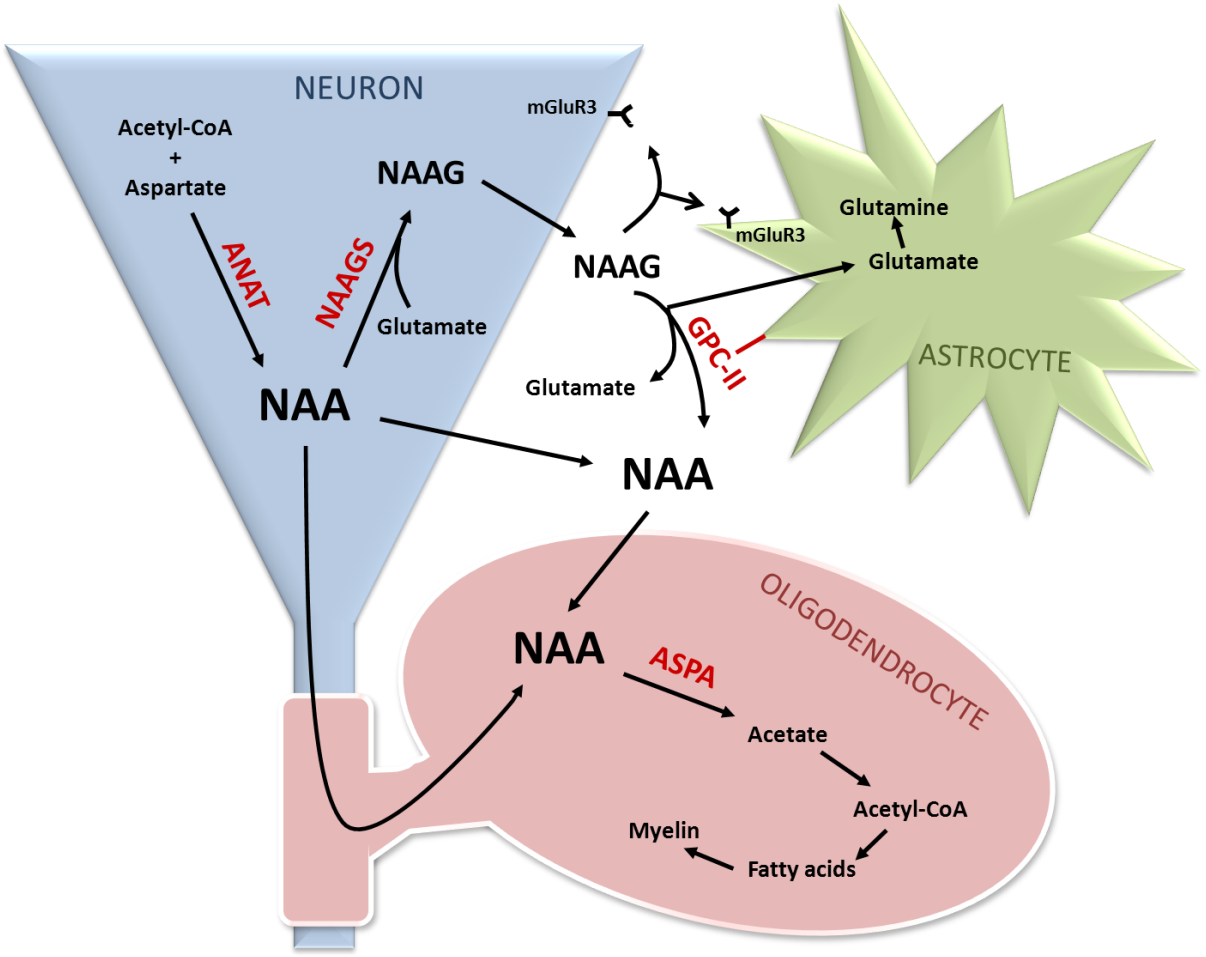

Figure 2.3: Schematic representation of NAA metabolism.
See text for details. NAA, N-acetyl-L-aspartate; NAAG, N-acetyl-aspartylglutamate; ANAT, acetyl CoA/aspartate N-acetyltransferase; NAAGS, N-acetyl-aspartylglutamate synthase; GPC-II, glutamate carboxypeptidase II; ASPA, aspartoacylase.

NAA functions

***Osmoregulation*:**

Unlike glial cells, neurons do not express aquaporins and their membrane seems to be largely water impermeable due to the fact that large part of their axons are insulated by myelin (ANDREW *et al.* 2007; BUFFOLI 2010). Therefore, neurons have established other mechanisms to regulate their osmolarity by co-transporting water against the gradient and the co-transporters have subsequently been named `molecular-water-pump´ (BASLOW 1999a; BASLOW 2002). The export of water is coupled to the release of NAA leading to the co-transport of at least 32 molecules of water per molecule NAA (BASLOW 2010). It was proposed for CD that excessive NAA levels lead to an increase in osmotic-hydrostatic pressure and initiation of the demyelination process (BASLOW and GUILFOYLE 2009).

Acetate source for myelin lipids:

The incorporation of the acetate moiety of NAA in brain lipids was already suggested in the 1960s (D'ADAMO *et al.* 1968; D'ADAMO and YATSU 1966) but confirmed first in 1991 by Burri and co-workers. They could show that acetate from NAA was incorporated in brain lipids particularly during early postnatal stages concurrent with myelination (BURRI *et al.* 1991). Acetyl groups from NAA can be traced to myelin lipids as demonstrated by Chakraborty in the optic system of the rat (CHAKRABORTY *et al.* 2001). Furthermore, studies on an ASPA-ko mouse revealed dramatically lowered free-acetate levels and myelin lipid synthesis supporting the hypothesis of NAA being an important source of brain acetate (MADHAVARAO *et al.* 2005; NAMBOODIRI *et al.* 2006). According to these findings hypomyelination in CD is not surprising, but as acetate can also be transported from other organs into the brain (BALLARD 1972; DEELCHAND *et al.* 2009) it may not be the sole cause of CD.

Neurotransmitter/ neuromodulator:

NAA is known to induce seizures after intracerebroventricular administration into rats, probably due to the overexcitation of glutamate receptors (AKIMITSU *et al.* 2000; KITADA *et al.* 2000; YAN *et al.* 2003). Furthermore, excess levels of NAA can promote oxidative stress by stimulating lipid peroxidation, protein oxidation and by decreasing non-enzymatic antioxidant defenses in rat brain (PEDERZOLLI *et al.* 2007; PEDERZOLLI *et al.* 2009). Additionally, excess levels of NAA can elevate hydrogen peroxide levels (PEDERZOLLI *et al.* 2010a) and induce the inducible nitric oxide synthase (iNOS) to produce nitric oxide (SURENDRAN 2010). In contrast, NAAG acts as a neurotransmitter on N-methyl-D-aspartate (NMDA) receptors and the metabotropic glutamate receptor $mGluR_3$. The activation of $mGluR_3$ at the presynapse inhibits the release of excitatory neurotransmitters such as glutamate, and the activation on glial cells stimulates the release of neuroprotective growth factors from these cells (NEALE *et al.* 2000; NEALE *et al.* 2005). Taken together, these data suggest a neuroprotective role for NAAG. In CD, NAA as well as NAAG levels are increased (KRAWCZYK and GRADOWSKA 2003), indicating an attempt to balance the neurotoxic effects of NAA.

In addition, the expression of the NAA synthesising enzyme nat8L can be induced by methamphetamine treatment (ARIYANNUR *et al.* 2010; NIWA *et al.* 2007) and the upregulation of this enzyme in the nucleus accumbens in mice suggests the involvement of NAA in reward circuits and the reinforcement of addictive drugs.

2.2.4. Animal models of CD

Different mouse and rat models are available to study CD, which exhibit most characteristics of the human disease regarding biochemical and histological abnormalities.

Tremor Rat *(tm/tm):*

A natural occurring ASPA null mutant, termed tremor *(tm)* rat, was identified to carry a genomic deletion spanning the entire *aspa* gene locus. This mutant shows the histological abnormalities and biochemical characteristics of CD. (KITADA *et al.* 2000; WANG *et al.* 2009). Furthermore, these rats suffer from epileptic seizures beginning at 7-8 weeks of age (SERIKAWA and YAMADA 1986), and the heterozygous *tm/+* mutants show the same type of epilepsy, but with a later onset (HIGASHIGUCHI *et al.* 1991). Although tremor rats have been used to study CD and develop therapeutic interventions, deductions from this mutant are hampered by the fact that the tremor mutation encompasses a chromosomal aberration of *aspa* and at least two more gene loci.

ASPA-knockout (ko) mouse:

The murine *aspa* gene has been targeted to generate a 10 bp deletion in exon 4 in SV129 ES cells leading to a truncated ASPA protein (MATALON *et al.* 2000). Although this mouse showed 3.4% residual enzyme activity in the brain, it is most severely affected, with an early onset phenotype and premature death at 2-6 months. Expectedly, these mice exhibit neurological abnormalities, motor deficits, metabolic changes including reduction of acetate, glutamate and GABA levels and a strong vacuolisation in the WM and some GM areas of the brain and throughout the spinal cord (MADHAVARAO *et al.* 2005; MATALON *et al.* 2000; SURENDRAN *et al.* 2005a; SURENDRAN *et al.* 2004b; SURENDRAN *et al.* 2003a). Interestingly, in this mouse neither NAAG nor glutamate carboxypeptidase II levels are altered (SURENDRAN *et al.* 2004a). To generate the ASPA-ko mouse the allele was targeted with the *neo* gene as a selection marker driven by the strong *pgk* promoter that has been suggested to interfere with the activity of genes adjacent to *aspa* (OLSON et al. 1996). Hence, the severe phenotype of the ASPA-ko mouse was suggested to be caused by multiple gene effects (TRAKA *et al.* 2008).

aspa^{Nur7}:

Recently, another mouse model generated in an *N*-ethyl-*N*-nitrosourea (ENU)-based mutagenesis approach was identified as a functional ASPA null mutant (TRAKA *et al.* 2008). This mouse is on the C57BL/6J background and carries a nonsense-mutation (Q193X) leading to the truncation of ASPA at D192. While mRNA levels were reduced to 60%, no ASPA protein, including the

truncated version, was detectable. These mice are less severely affected and survive >1 year (M. Traka, pers. communication) but show the pathological signs of CD including vacuolisation and increased NAA levels. However, they show less vacuolisation in WM tracts of brain and spinal cord, but increased levels in GM areas compared to the ASPA-ko mouse. Despite the fact that at postnatal day (P) P70 many axons show a reduced myelin sheath thickness, 6-month-old animals still exhibited axons with a normal myelin sheath suggesting remyelination efforts and contradicting the hypothesis that ASPA´s biosynthetic role in supplying acetate through NAA hydrolysis is critical for myelin maintenance (TRAKA *et al.* 2008)

Taken together, there is a broad variation in the severity of the phenotype among these animals, which could reflect the course of the human disease, but are difficult to reconcile. Furthermore, a genetic dissection of the role of ASPA in different cell types and tissues is precluded as conditional mutagenesis is required to address this aspect.

2.3. Gene therapy in the central nervous system

Gene therapy was originally defined as treatment to correct genetically linked disorders by swapping a non-functional gene for a functional copy (FRIEDMANN and ROBLIN 1972). Today, gene-based therapeutics are broadly defined as the introduction of nucleic acids into cells using a vector with the intention of altering gene expression to prevent, halt or reverse a pathological process (KAY 2011). This includes gene addition, gene correction/alteration and gene knockdown or a combination of these. While conventional pharmaceutical interventions are based on the repeated application of a drug, gene therapy aims to ultimately correct dysfunctions.

The modification of the target cell can either be achieved *in vivo*, where the vector is administered directly to the host or *ex vivo* using autologous cells derived from a patient. These cells are manipulated *ex vivo* and then transplanted back into the patient. Delivery of DNA can be achieved by either non-viral or viral gene transfer methods. The non-viral strategy includes liposomal or nanoparticle-based DNA delivery as well as *in vivo* electroporation, and offers several potential advantages: These vectors are easy to produce, they do not contain viral contaminants nor do they stimulate any pre-existing antigen-dependent immunity, and there is no size limit on the amount of DNA that they can deliver (KAY 2011). However, the use of non-viral vectors for *in vivo* gene transfer remains relatively sparse especially in the CNS due to low transfection efficiency (LEONE *et al.* 2000). Most viral vectors are derived from common human viral pathogens and are naturally able to

transduce mammalian cells. The usage of these vectors lead to sustained and high-level gene expression and therefore shows great promise in both basic research as well as therapeutic applications.

Currently, more than ten vector types are in use (DAVIDSON and BREAKEFIELD 2003). This includes simple capsid virions such as adenovirus and adeno-associated virus, and enveloped virions like retrovirus, lentivirus or herpes-simplex virus, which all differ by their genetic material encased (DNA/RNA), size, maximum packaging capacity, target cell specificity (tropism) and their affinity to integrate into the host cell genome.

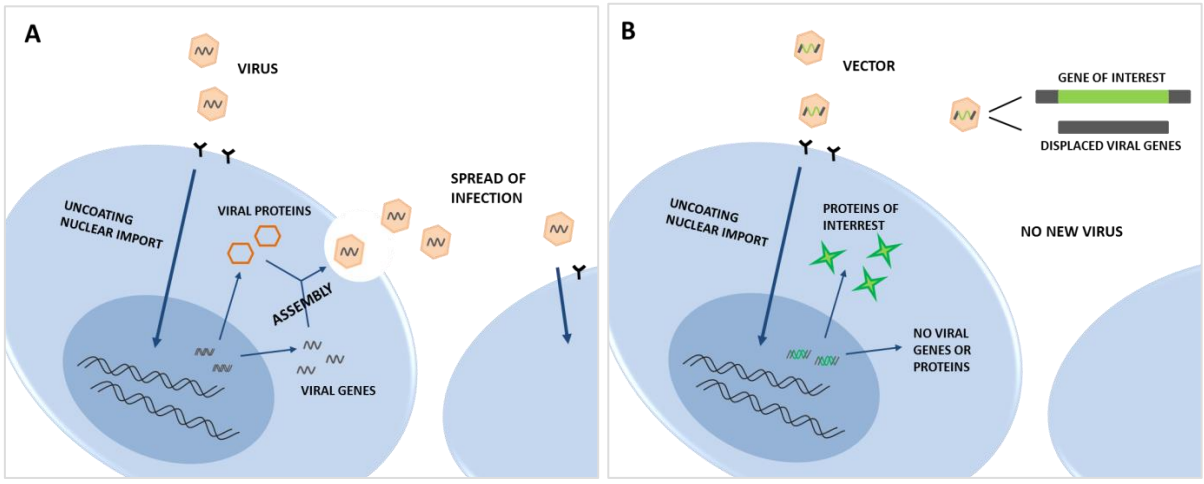

Figure 2.4: Gene therapy using viral vectors.
(A) A normal life cycle of a virus starts with receptor binding and internalisation of the virus, viral uncoating and the transport of viral DNA into the nucleus. The expression of viral genes leads to the production of capsid proteins and enzymes for the replication of viral genomes. After the assembly, new virions are released and start a new infectious cycle. **(B)** In recombinant vectors, viral genes are replaced by a gene of interest (green), and the proteins of interest, but no viral proteins are produced. The figure was redesigned based on (KLUGMANN 2007).

An ideal gene therapy vector for the CNS should match the following characteristics (KLUGMANN 2007; SOMIA and VERMA 2000):

- Infection of non-dividing cells as most brain cells are post-mitotic;
- Allowing for site-specific integration or episomal persistence, to avoid mutations in the host cell genome or position effects;
- Large packaging size capacity to enable the transfer of large genetic material;
- Tissue or cell-type specificity to minimise side effects due to off target transduction;
- Non-immunogenicity to avoid a neutralising response after repeated application and inflammatory reactions

- Sustained and regulated transgene expression for potential life-long gene expression;
- Simple and cost-effective production of high-titer vector stocks.

There is no vector available meeting all criteria, but adeno-associated viral vectors are the most promising so far.

2.3.1. Wildtype adeno-associated virus (wtAAV)

Adeno-associated viruses (AAV) were first found as a contamination in an adenovirus preparation and named accordingly (ATCHISON *et al.* 1965). They are classified into the family of *Parvoviridae* and the genus Dependovirus. As the name indicates, the lytic cycle of this virus requires the coinfection with a helper-virus, such as adenovirus or herpes-simplex virus. All AAV serotypes contain a single-stranded DNA genome of 4.7 kb, which is packed into an icosahedral non-enveloped capsid of approximately 25 nm in diameter. The wtAAV genome consists of two open-reading frames (ORF) flanked by palindromic hairpin structures, the inverted terminal repeats (ITR). The 3´ORF *rep* encodes for four proteins (Rep78, Rep 68, Rep52, Rep40), that are involved in replication, transcriptional control and site-specific integration. The 5´-ORF *cap* encodes the viral structural proteins VP1, VP2 and VP3, which build up the capsid containing 60 copies of these proteins in a ratio ranging from 1:1:10 (ZOLOTUKHIN *et al.* 2002) to 1:1:18 (WU *et al.* 2006) and with a molecular mass of 87 kDa, 72 kDa and 62 kDa, respectively.

AAV biology is best studied on AAV serotype 2 (AAV2) as this was the first AAV genome cloned into a bacterial plasmid (SAMULSKI *et al.* 1982). Viral entry is mediated by cell surface glycosaminoglycan or sialic acid receptors and subsequent interactions with co-receptors. AAV2 virus internalisation depends on the binding to heparan sulfate proteoglycan (HSPG) (SUMMERFORD and SAMULSKI 1998) and until now, five co-receptors have been identified. Fibroblast growth factor receptor 1 (FGFR-1) (QING *et al.* 1999), hepatocyte growth factor receptor (HGFR) (KASHIWAKURA *et al.* 2005) and laminin receptors, e.g. $\alpha_v\beta_5/\alpha_5\beta_1$ integrins, are thought to enhance virus-cell contact and are likely to facilitate cell entry (AKACHE *et al.* 2006; SUMMERFORD *et al.* 1999). Upon receptor binding, virions are internalised by receptor-mediated endocytosis (BARTLETT *et al.* 2000). Mechanisms of endosomal release and viral uncoating are still a matter debate and may be cell type specific, and studies of the nuclear import of viral DNA are contradictory as well. Sonntag *et al.* (SONNTAG *et al.* 2006) could completely block AAV2 infection by injecting capsid-specific antibodies into the nucleus, suggesting that viral uncoating takes place in the nucleus. However, Lux and colleagues could show, that the nuclear entry of viral capsids is a rare event, only achieved with high-titer virus and further

enhanced by adenovirus co-infection (BUNING *et al.* 2008; LUX *et al.* 2005). Inside the nucleus the next steps depend on the existence of helper viruses. In the presence of such, AAV enters the lytic cycle, instantly starting gene expression, replication and packaging. In the absence of helper viruses AAV enters a latent cycle where it persists mostly episomal in circular intermediates or concatamerisation through intermolecular recombination (DUAN *et al.* 1998; YANG *et al.* 1999). Less frequently AAV integrates site-specifically into a locus on chromosome 19 (19q13.3-qter; AASV1) (KOTIN *et al.* 1992).

2.3.2. AAV Serotypes

Within the *Dependoviridae* AAVs are formally grouped into serotypes. A serotype is a newly isolated virus, which does not efficiently cross-react with neutralising sera specific for all other existing and characterised serotypes (WU *et al.* 2006). By this definition only AAV1-4 and AAV7-9 can be classified as individual serotypes. Furthermore, AAV cap sequences were analysed for phylogenetic relationships by using a variety of computational approaches and then grouped into clades (GAO *et al.* 2004).

AAV1-4 and AAV6 were isolated as contaminants from adenoviral stocks and AAV5 from a human condylomatous wart and in the last decade over 100 new AAV variants have been found in human and non-human primate tissues via PCR-based DNA isolation (GAO *et al.* 2002; MORI *et al.* 2004; SCHMIDT *et al.* 2006). In addition, AAV genomes have also been isolated from other species such as horse, cow, chicken, snake, lizard and goat. Bovine, avian and caprine AAVs have already been used in gene transfer studies (reviewed in(WU *et al.* 2006)).

With regard to the application of AAVs as a gene transfer shuttle in humans, the advantage of these novel vectors is the lack of neutralising antibodies against them, which could reduce or impair AAV-mediated gene transfer. It has been estimated that, depending on age and ethnic group, between 50% and 95% of the human population is seropositive for AAV2 (BUNING *et al.* 2008), which is a consequence of respiratory infection during childhood (WARRINGTON and HERZOG 2006). Moreover, readministration of AAVs in a patient lacking neutralising antibodies can elicit an antibody response, which can hamper further applications (HALBERT *et al.* 2000). However, for CNS application pre-existing immunity may not cause major problems, since the brain is generally regarded as an immune-privileged organ.

2.3.3. Recombinant AAV

In recombinant AAV (rAAV) *rep* and *cap* open reading frames (ORFs) have been replaced with an expression cassette containing a transgene of interest (GOI). However, the only remaining *cis*

elements of the wtAAV are the ITRs, which are crucial for genome replication and packaging into capsids, while *rep* and *cap* genes can be provided in *trans*.

rAAV production and purification

For helper-virus free AAV production the standard technique is the transient co-transfection of human embryonic kidney cells 293 (HEK293) with the rAAV vector plasmid encoding the GOI, the AAV helper plasmid containing *rep* and *cap* genes, but no ITRs, and one plasmid providing adenoviral helper functions (E2A, E4, VA, with E1 encoded in the HEK293 cell genome). Commonly used is a cross-packaging strategy, also called vector pseudotyping, were *cap* genes from different serotypes and AAV2 *rep* genes are cloned into one plasmid. This strategy makes it possible to compare the role of serotype-specific virion shells on vector transduction without the influence of the ITRs on transgene expression (RABINOWITZ *et al.* 2002). Vector purification depends on the AAV serotype. Taking advantage of the fact that AAV2 binds to HSPG on the extracellular surface, this serotype can be purified via heparin-affinity chromatography. As yet, other serotypes are commonly purified by ultracentrifugation of caesium chloride density or iodixanol gradients followed by ion-exchange chromatography (ZOLOTUKHIN *et al.* 2002).

In the last years progress has been made regarding the up-scaling of the production process to generate highly potent, clinical-grade purity vector stocks. For this purpose, suspension-grown baby hamster kidney cells (sBHK) are co-infected with two recombinant herpes-simplex viruses (rHSV), one encoding the transgene flanked by AAV2 ITRs and one harbouring the AAV *rep2* and *capX* genes (where X is any rAAV serotype) (THOMAS *et al.* 2009). Another strategy, compatible with current good manufacturing practice, includes the co-infection of insect cells (Sf9) with baculoviruses containing *rep*, *cap* and the transgene vector and subsequent purification from up to 200 litre bioreactors (CECCHINI *et al.* 2011).

Progress has also been made to overcome the major drawback of AAVs: the small packaging capacity. Wu and co-workers could show that packaged AAV vector genomes never exceeded 5.2 kb in length irrespective of the size of the plasmid-encoded vector. Packaged vector genomes derived from plasmid-encoded vectors exceeding 5 kb were heterogeneous in length and truncated on the 5' end (WU *et al.* 2010). In a so called `trans-splicing´-approach gene expression can be reconstituted from two independent rAAV vectors, each encoding unique, non-overlapping halves of a transgene. This process requires intermolecular concatamerisation and subsequent splicing between independent vectors (DUAN *et al.* 2001; DUAN *et al.* 2000). However, the major drawbacks of this method are the poor efficiency and reliability.

2.3.4. Engineering AAV vectors

Despite the discovery of many new AAV serotypes and the study of their tropism, some organs or cell types are still more prone to AAV infection than others. To overcome this limitation, there is a need for engineering custom-designed AAV capsids and hybrid vectors to expand the range of AAV applications to cell-types refractory to the infection with known serotypes, such as glial cells.

The following section describes strategies to design rAAV vectors with novel properties.

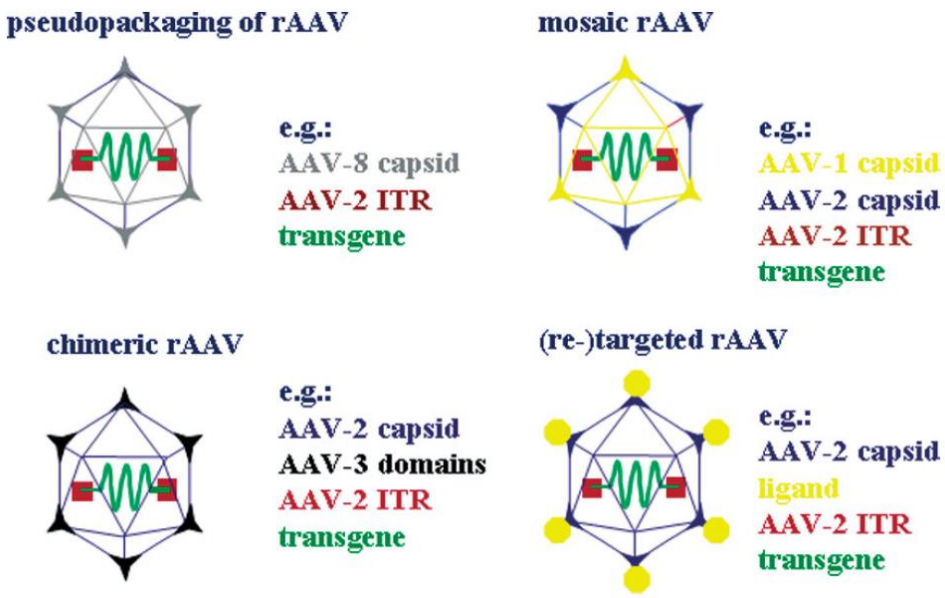

Figure 2.5: Overview on engineered AAV vectors.
In pseudopacked vectors, transgenes are flanked by identical ITRs (e.g. by AAV2-ITRs) and packaged into different serotypes in order to facilitate the comparison vector transduction without the influence of the ITRs on transgene expression. The capsid of mosaic vectors is composed of a mixture of different AAV serotypes capsids combining the properties of the parental serotypes. In chimeric vectors, capsid domains or short stretches of amino acids are exchanged. The capsids of targeting vectors have been modified by insertion of a peptide ligand to the capsid surface (from (BUNING *et al.* 2008)).

Mosaic vectors

A mosaic virion can be defined as the capsid structure composed of a mixture of capsid subunits from different serotypes (WU *et al.* 2006). These vectors can be generated by co-transfecting a mixture of helper constructs encoding capsid genes from different serotypes either wildtype or already mutated. Theoretically, the generated virions should be composed in a ratio that reflects the input amount of the helper plasmids used, but in practice such viral preparations consist of virions with a non-uniform capsid composition (BUNING *et al.* 2008). Furthermore, each batch can

contain a non-identical ratio of helper plasmids, making this approach difficult to standardise. However, the main advantage of this technique is the ability to synergistically combine qualities of the respective parental serotypes. Hence, most mosaic AAV2/X vectors (where X is any AAV serotype) inherit the heparin-binding capability of AAV2, which can be used for purification. Moreover, these viruses can gain new features distinct from their parental virus depending on the input ratio of the corresponding helper plasmids (RABINOWITZ *et al.* 2004). A study by Richichi and colleagues demonstrated that mosaic AAV1/2 show a more widespread transgene expression in the hippocampus compared to AAV2 alone (RICHICHI *et al.* 2004).

Chimeric AAV vectors

Chimeric vectors usually contain capsid proteins that have been modified by domain or amino acid swapping between different serotypes (WU *et al.* 2006). Domain swapping involves the transfer of specific capsid domains such as surface loops or specific residues from one serotype to another. In a marker rescue experiment Bowles and colleagues co-transfected AAV2 genomes with a non-functional *cap* mutation and AAV3 *cap* sequences. Chimeric Vectors generated via homologous recombination of the virus genomes could rescue the non-infecting and non-heparin binding phenotype of this vector. The resulting mixed population of viral genomes can be amplified via polymerase chain reaction (PCR), subcloned and individual clones can then be assessed for biological properties (BOWLES *et al.* 2003). Hence, this approach can contribute to gain further insights in structure-function relationships and help with the determination of regions responsible for tissue tropism.

Receptor targeting via chemical and genetic engineering

To target AAVs towards cell type specific receptors two strategies have been developed: a non-genetic (indirect) and a genetic (direct) targeting approach (BUNING *et al.* 2008). The non-genetic strategy includes the linkage of AAV capsid structures on the one hand and cell type specific receptors on the other with bispecific antibodies. This can be complemented with a genetic approach. Therefore, a peptide ligand for a cell type specific receptor is commonly fused to the N-terminus of either VP1 or VP2 and, additionally, domains determining the natural receptor binding can be mutated to ensure selective targeting.

Recent work includes combinatorial engineered capsids. Via error-prone PCR or DNA shuffling, where capsid genomes from different serotypes are randomly fragmented and rearranged, capsid libraries are generated. Advances in high-throughput screening and selection make it possible to characterise the resulting clones for their biological properties and screen for AAVs infecting yet

non-permissive cell-types. A study by Koerber and co-workers implemented a direct evolution approach to engineer a novel AAV vector capable of efficiently delivering genes to astrocytes and potentially other glial cells (KOERBER *et al.* 2009). They identified new vectors with an enhanced infection rate of astrocytes upon injection into the rat striatum (levels up to 16% of the total transduced cell population) and Müller glia within the rat retina. In a similar study Jang and colleagues created an AAV vector with enhanced delivery efficiency for rat, mouse and human neural stems cells (NSCs) including adult NSCs (JANG *et al.* 2011).

Promoter targeting

The natural tropism of AAVs in the CNS leads to a predominant infection of neural and epithelial cells and is opposing the urgent need for AAVs targeting glial cells. This can be achieved by replacing the commonly used strong, small and ubiquitous promoters like cytomegalovirus (CMV) promoter, chicken beta-actin (CBA) promoter or variants of both, with cell type specific promoters. As gene transfer with newly identified serotypes like AAV8 in combination with the strong hybrid cytomegalovirus/chicken β-actin (CAG) promoter can lead to neurotoxic overexpression of transgenes (GAO *et al.* 2002; KLEIN *et al.* 2006), the choice of a cell type specific promoter can also prevent transgene overdose.

First attempts to target astrocytes by using a 2.2 kb rat GFAP promoter in an AAV2 vector resulted in a limited (only up to 5% of glia showed transgene expression) and non-exclusive (also neurons showed transgene expression) transduction profile (XU *et al.* 2001). Further studies, combining serotypes known for a more widespread transduction pattern such as AAV8 and rh43 and the human 2.2 kb GFAP promoter could improve the transduction pattern, but still exhibited residual transgene expression in other cell types (LAWLOR *et al.* 2009).

With regard to gene therapy for demyelinating disorders such as Canavan disease or multiple sclerosis, there is a need for AAV vectors that target oligodendrocytes. First studies with a 1.9 kb fragment of the murine myelin basic protein (MBP) promoter (GOW *et al.* 1992) could show the possibility of transgene expression in oligodendrocytes *in vitro* and *in vivo*, but this approach failed to a generate long-lasting and widespread transduction (CHEN *et al.* 1998; CHEN *et al.* 1999). Another attempt with a 1.35 kb fragment of the murine MBP promoter packed into AAV8 and rh43 resulted in a more robust transgene expression, yet not oligodendroglia exclusive (LAWLOR *et al.* 2009).

Eukaryotic promoters consist of large *cis* acting elements to regulate cell-type specific gene expression and one of the main drawbacks of the AAV vector system is the rather small packaging capacity. Hence, compromises have to be made to generate a specific transduction pattern on the

one hand and not exceed the packaging limit on the other hand. It therefore might not be possible to generate cell type specific transduction by using only parts of promoter/enhancer regions.

2.3.5. AAV cell tropism

Tropism is the specificity of a virus for a distinct host tissue. This is achieved by the interaction of the viral surface with cell surface structures and receptors. Variances in the amino acid composition of the capsid lead to differences in the affinity towards distinct cell surface receptors. Hence, it was hypothesised that different serotypes would target different cell types in the CNS (BURGER *et al.* 2005). Until now, different receptors and co-receptors have been proposed for each serotype (reviewed (BUNING *et al.* 2008)). For AAV2 and also AAV3 heparan sulfate proteoglycan (HSPG) is the primary receptor (BLACKBURN *et al.* 2006; SUMMERFORD and SAMULSKI 1998), AAV4 uses α-2,3-O-linked sialic acid, while AAV5 requires α-2,3-N-linked sialic acid (KALUDOV *et al.* 2001). Although the cross-packaging strategy has been applied to study the transduction efficiencies of rAAVs, studies are often difficult to interpret due to their variations in vector titers and doses, promoters, transgenes or purification methods (WU *et al.* 2006). In a number of studies the delivery of AAV1, 5, 7, 8 and 9 resulted in a more widespread transduction than achieved with AAV2 (CEARLEY *et al.* 2008; CEARLEY and WOLFE 2006; KLEIN *et al.* 2006; TAYMANS *et al.* 2007) and that was even surpassed by newly identified AAV variants such as cy5, rh20 and rh39 (LAWLOR *et al.* 2009). A study by Klein and colleages (KLEIN *et al.* 2008b) investigated the effect of the purification method on the tropism of AAVs by injecting AAV8 expressing GFP either purified by CsCl- or iodixanol-gradient ultracentrifugation into adult rats. An astroglial transduction pattern was observed after the injection of the CsCl-purified vector, while the iodixanol-purified vector led to the transduction of neurons. In the same study they compared the cytomegalovirus promoter with the hybrid cytomegalovirus/chicken β-actin promoter and found the latter to yield a stronger transgene expression. The age of the animals treated and the application route can also influence the tropism. Gene delivery can either target widespread transgene expression (global), for example in Alzheimer´s disease, where the whole brain is affected, or the transduction of specific brain areas (focal), such as the dopaminergic neurons in the substantia nigra in Parkinson´s disease. Furthermore, viral vectors can be delivered into the brain tissue (intraparenchymal, i.p.), resulting in a more focal gene delivery, or into the ventricles of neonatal animals (intracerebroventricular, i.c.v.), yielding a transgene expression throughout the brain (BROEKMAN *et al.* 2007; PILPEL *et al.* 2009). The difference in transduction profile after intravenous injection of AAV9, which bypasses the blood-brain barrier and

efficiently targets CNS cells in neonatal and adult mice, was investigated by Foust and co-workers (FOUST *et al.* 2009). Neonatal injections led to a widespread transduction of dorsal root ganglia, motor neurons and neurons throughout the brain, while injections into adult mice resulted in a robust transduction of astrocytes and only limited neuronal transduction. Finally, the tertiary structure of the harboured DNA can alter the AAV capsid structure, thus leading to tropism influenced by the vector genome (MASTAKOV *et al.* 2002).

This section shows that the change of parameters can result in dramatic changes of transduction efficiency and transduction profiles. Hence, determination of the best conditions for a specific therapeutic intervention regarding efficiency as well as specificity is a pivotal task.

2.3.6. rAAV as a tool for gene transfer into the CNS

Since it has been shown that safe and efficient gene transfer to the CNS can be achieved using AAVs (KAPLITT *et al.* 1994), the usage of rAAVs in clinical as well as preclinical studies emerged rapidly. Transgene expression can persist up to 19 months in the rat brain (PEEL and KLEIN 2000) and for more than 3 years in the primate brain (DAADI *et al.* 2006). This and the inherent safety profiles makes AAV a logical choice for sustained gene therapy in the CNS. To date, AAVs have been used in clinical studies for CD (JANSON *et al.* 2002a; MCPHEE *et al.* 2006) Parkinson´s disease (CHRISTINE *et al.* 2009; KAPLITT *et al.* 2007; LEWITT *et al.* 2011) and Alzheimer´s disease (TUSZYNSKI 2007). Preclinical studies involve amyotrophic lateral sclerosis (ALS), Huntington´s disease, epilepsy and leukodystrophies (reviewed in (BIFFI *et al.* 2011a; MANDEL *et al.* 2006)).

2.3.7. CD therapy

CD is a rare disease, but the loss-of-function mutation and its pathology restricted to the CNS makes it a prototype for a gene replacement strategy, aiming to be a curative treatment, in contrast to other symptomatic and palliative therapies. The pioneering studies by During, Leone and colleagues were the first gene therapy attempt worldwide for a non-malignant CNS disease (DURING 1996; LEONE *et al.* 2000; LEONE *et al.* 1999). A recombinant *aspa* plasmid in a non-viral liposome delivery system was administered intracerebroventricular first to two CD patients and in follow-up studies with improved vectors and delivery protocols to more patients. The delivery system was tested to be safe, but clinical changes were transient and not pronounced due to inadequacies of the delivery system (JANSON *et al.* 2002a). The lack of efficient gene transfer using liposomes led to the implementation of AAV2 as a vector and this trial represented the first clinical use of AAV in the

human brain and the first application of viral gene transfer for a neurodegenerative disease (JANSON *et al.* 2002a). The rationale for the usage of a neurotropic vector, although ASPA is an oligodendrocyte-enriched enzyme, is based on the hypothesis that excess NAA has neurotoxic effects and the degradation at the origin of its synthesis can ameliorate CD symptoms. Vector administration was well tolerated (MCPHEE *et al.* 2006) but no results presenting the clinical outcome have been published yet.

Several years after clinical trials started, mice and rat models of CD became available for preclinical studies. Seki and co-workers could ameliorate absence-like seizures and tonic convulsions in the tremor rat using an adenoviral vector (SEKI *et al.* 2002; SEKI *et al.* 2004). Matalon and colleagues injected a hASPA-GFP fusion construct packaged into AAV2 into the striatum and thalamus of 3-month-old ASPA-ko mice. They demonstrated a reduction of vacuolisation at the sites of injection but did not provide information on the efficiency of transgene expression, neurological findings and the effect on motor functions (MATALON *et al.* 2003). A preclinical study with the AAV2 vector used in the 2002 clinical study (JANSON *et al.* 2002a) was performed on aged (30-week-old) tremor rats which resulted in elevated aspartoacylase bioactivity compared to untreated mutant animals and elicited a decrease in whole-brain NAA levels (MCPHEE *et al.* 2005a). Further studies were performed with a more efficient AAV1/2 vector system in juvenile *tm/tm* (KLUGMANN et al. 2005). ASPA protein and enzyme activity were restored, NAA levels reduced and the seizure phenotype rescued. However, histology and motor functions remained unchanged suggesting that NAA-mediated neuronal hyperexcitation but not oligodendrocyte dysfunction can be compensated by neuronal ASPA expression and that the time point of the treatment is crucial.

Taken together, ectopic neuronal overexpression of ASPA does not reverse CD pathology. Most importantly, none of the studies so far has shown any significant improvements of the motor deficits indicating the urgent need for a vector restoring ASPA expression at its site of action.

In addition to gene therapy, there are different palliative, symptomatic or curative CD treatment strategies, but to date none of them ameliorated all clinical signs. Hence, a curative treatment is still missing and this section is intended to give an overview on current clinical and pre-clinical approaches to treat CD.

Acetate substitution:

Based on the hypothesis that NAA-derived acetate plays a pivotal role in myelination, the supplementation of acetate should ameliorate clinical signs of CD. In a pilot study, glyceryltriacetate (GTA) was administered as food additive to C57BL/6 mice (MATHEW *et al.* 2005). As a result brain

acetate levels increased, suggesting further preclinical studies. Indeed, the administration of GTA to tremor rats starting at P7 led to an improved motor phenotype, increased myelin galactocerebrosid content and reduced brain vacuolisation (ARUN *et al.* 2010). However, two clinical trials, one with low and one with high doses of GTA, demonstrated that this treatment is well tolerated, but without any effects on the CD phenotype (MADHAVARAO *et al.* 2009; SEGEL *et al.* 2011).

Reduction of NAA:

As increased levels of NAA may contribute to the induction of seizures, osmotic imbalances and cause oxidative stress, the reduction of NAA is a pivotal aim in CD treatment. Baslow and colleagues demonstrated in the tremor rat that repeated i.p. injections of LiCl resulted in a reduction of about 13% of NAA brain levels (BASLOW 2002). In a first clinical trial and a follow-up study with a larger cohort lithium citrate was administered to CD patients and shown to be safe (ASSADI *et al.* 2010; JANSON *et al.* 2005). They demonstrated a drop in NAA levels, although a statistically significant reduction was only achieved in the basal ganglia, and probably mild improvements in the myelination in the frontal white matter. However, motor functions remained unchanged.

Elevated NAA can also cause oxidative stress, which can possibly be prevented by the administration of antioxidants (PEDERZOLLI *et al.* 2010a; PEDERZOLLI *et al.* 2007; PEDERZOLLI *et al.* 2009; SURENDRAN 2010). A study by Pederzolli and co-workes demonstrated that the brain of rats showed less signs of oxidative stress after NAA treatment when the animals were pre-treated with lipoic acid (PEDERZOLLI *et al.* 2010b). Hence, the administration of antioxidants may have beneficial effects on CD patients.

Enzyme replacement:

Enzyme replacement strategies have been applied to many metabolic disorders and recently a pilot study paved the way for this treatment in CD (ZANO *et al.* 2011). Purified ASPA protein was PEGylated (polyethylenglycol, PEG) to decrease immunogenicity and administered to ASPA-ko mice. It was demonstrated that the modified ASPA protein was able to traverse the blood-brain-barrier and caused a significant increase in enzyme activity in the brain as well as a decrease of NAA levels. Now, further studies have to reveal the efficiency of this treatment.

Transplantation of neural progenitor cells:

CD is accompanied with oligodendrocyte loss (KUMAR *et al.* 2009) and an increase in the number of undifferentiated neural stem/progenitor cells (NPCs) - an indication of repair mechanisms. Hence, the implantation of NPCs may enhance these attempts. Surendran and co-workers implanted

neural progenitor cells (NPCs) in both juvenile and adult ASPA-ko mice and demonstrated that these cells survive, migrate and differentiate into oligodendrocytes and fibrous astrocytes (SURENDRAN *et al.* 2004c). Thus, they provide a first step towards a cell therapy for CD.

2.4. Aim and outline of this thesis

To date, none of the current CD treatments has ameliorated all pathological signs of CD, including histology and biochemical abnormalities as well as locomoter deficits pointing out the urgent need for new treatment strategies. Hence, the aim of this study was to establish a novel gene-transfer system and its preclinical evaluation in a CD animal model.

Animal models of human diseases are an important prerequisite to develop effective therapies. Hence, an engineered mouse model of ASPA-deficiency expressing the bacterial *lacZ* gene under the control of the *aspa* promoter had to be established and validated as a new CD model in the first experimental part of this thesis (**Chapter 3**). Furthermore, this mouse-line was used to gain new insights at CD pathophysiology and ASPA expression and served as a tool for preclinical *aspa* gene transfer. The goal of the second part (**Chapter 4**) was to identify novel AAV-based vectors that are capable of transducing oligodendrocytes to allow gene transfer into these cells. Therefore two strategies were applied: Firstly, in a transcriptional approach a reporter gene (EGFP) was cloned under the control of different (ubiquitous and cell-type specific) promoters to address the question whether promoter targeting is sufficient to re-target the natural AAV neurotropism. Secondly, in a transductional approach these expression cassettes were packaged as different serotypes. The tropisms and efficacies of these vectors were evaluated *in vitro* and *in vivo* in order to identify the most efficient combination of promoter and serotype. In the last part (**Chapter 5**), the reporter gene was then replaced by human *aspa* cDNA and injected into the brain of the newly established CD mouse model to restore ASPA function in oligodendrocytes. Therapeutic efficiency was evaluated by biochemical, histological and behavioural analysis.

Chapter 3:

Aspartoacylase-lacZ knockin mice: An engineered model of Canavan disease

3. Aspartoacylase-lacZ knockin mice: An engineered model of Canavan disease

Canavan disease (CD) is a recessive leukodystrophy caused by loss-of-function mutations in the gene encoding aspartoacylase (ASPA), an oligodendrocyte-enriched enzyme that catalyses hydrolysis of N-acetylaspartate (NAA) to acetate and aspartate. The neurological phenotypes of different rodent models of CD vary considerably. This study reports on a novel targeted ASPA mouse mutant expressing the bacterial *β-galactosidase* (*lacZ*) gene under the control of the *aspa* regulatory elements. X-Gal staining in known ASPA expression domains confirms the integrity of the modified locus in heterozygous aspa lacZ-knockin ($aspa^{lacZ/+}$) mice. In addition, abundant ASPA expression was detected in Schwann cells. Homozygous ($aspa^{lacZ/lacZ}$) mutants are ASPA-deficient, show CD-like histopathology and moderate neurological impairment with behavioural deficits that are more pronounced in $aspa^{lacZ/lacZ}$ males than females. Non-invasive ultrahigh-field proton magnetic resonance spectroscopy revealed increased levels of NAA, myo-inositol and taurine in the $aspa^{lacZ/lacZ}$ brain. Spongy degeneration was prominent in hippocampus, thalamus, brain stem, and cerebellum, whereas white matter of optic nerve and corpus callosum was spared. Intracellular vacuolisation in astrocytes coincides with axonal swellings in cerebellum and brain stem of $aspa^{lacZ/lacZ}$ mutants indicating that astroglia may act as an osmolyte buffer in the ASPA-deficient CNS. In summary, the $aspa^{lacZ}$ mouse is an accurate model of CD and an important tool to identify novel aspects of its complex pathology.

3.1. Introduction

Aspartoacylase (ASPA) deacetylates N-acetyl-aspartate (NAA) to produce acetate and L-aspartate. This enzyme is a marker of mature oligodendrocytes (DUGAS *et al.* 2006; KLUGMANN *et al.* 2003; MADHAVARAO *et al.* 2004) and mutations of the *aspa* gene cause the fatal recessive leukodystrophy Canavan disease (CD) (CANAVAN 1931; KAUL *et al.* 1993). Patients suffer from mental retardation, hypotonia, seizures and death usually before the age of ten. Pathological changes include strongly elevated NAA levels in blood and urine, oligodendrocyte death and a progressive CNS vacuolisation (MATALON *et al.* 1995). The underlying mechanisms of these multifaceted abnormalities are not understood and it is not clear to what extent the deficiency of ASPA in cell types other than oligodendroglia contributes to the development of clinical signs observed in CD. The monogenic nature of CD, and the lack of an effective treatment have provided the rationale for *in vivo* gene transfer into the CNS of patients and ASPA-deficient animals (KLUGMANN and LEICHTLEIN

2006). While these animal models generally reprise the pathological hallmarks observed in CD, they show substantial differences in disease severity and longevity (KITADA *et al.* 2000; MATALON *et al.* 2000; TRAKA *et al.* 2008). The vast majority of clinical cases can be assigned to the relatively moderate infantile form of CD suggesting that an accurate animal model is expected to display a mild disease severity. Moreover, the identification of all ASPA expression domains is essential to gain a comprehensive picture of the complex CD pathology and design effective therapies.

The present study describes an engineered mouse line expressing the bacterial *lacZ* gene under the control of the *aspa* promoter. Homozygous lacZ-knockin ($aspa^{lacZ/lacZ}$) mutants are ASPA-deficient and show distinct abnormalities reminiscent of CD.

3.2. Materials and Methods

3.2.1. Generation of $aspa^{lacZ}$ mutant mice

Using homologous recombination in C57BL/6 embryonic stem (ES) cells, the βgeo cassette (including the genes encoding β-galactosidase and neomycin) flanked by frt sites was introduced into intron 1 of the *aspa* gene by the European Mouse Mutagenesis Consortium (EUCOMM). In addition, the critical exon 2 was flanked by loxP sites. An automated high-throughput approach and genotyping by long-range PCR (for technical see http://www.eucomm.org/) led to the identification of two independent aspa-lacZ C57BL/6 ES cell clones (Aspa clone EPD0038_4_C09 and EPD0038_4_H09) showing homologous targeting. Both clones were injected into BALB/c blastocysts and chimeric males were bred to C57BL/6J females to produce germ line transmission. The C09-derived line was used for further experiments. Heterozygous ($aspa^{lacZ/+}$) offspring intercrossed to obtain homozygous mutant mice ($aspa^{lacZ/lacZ}$) on the C57BL/6J backround. $aspa^{f/f}$ mice were generated via Flp-mediated recombination and deletion of the ßgeo cassette after crossing $aspa^{lacZ/+}$ animals with Flp-deleter mice (RODRIGUEZ *et al.* 2000).

3.2.2. Culture of embryonic stem cells

Tissue culture dishes were purchased from NUNC (Langenselbold, Germany)**.** Sterile plastic tubes (50 ml and 15 ml) were purchased from Greiner (Solingen, Germany). All cell culture reagents

were purchased from LIFE Technologies GIBCO (Darmstadt, Germany), if not stated otherwise. Fetal calf serum (FCS) was purchased from PAA (Cölbe, Germany), DMSO from Carl Roth (Karlsruhe, Germany) and mitomycin C and β-mercaptoethanol from Sigma Aldrich (Munich, Germany).

3.2.2.1. Preparation of embryonic mouse fibroblast (MEF) feeder cells

In order to maintain their undifferentiated and totipotent status, embryonic stem cells (ESCs) need the presence of factors that inhibit differentiation. Early experiments showed that primary embryonic mouse fibroblasts constitute a very good source of these factors (BRADLEY *et al.* 1984). Primary embryonic fibroblast cells were obtained from mice embryos at embryonic day 14-16. The pregnant mouse was sacrificed and embryos were isolated from the uterus. Embryos without any extraembryonal tissue were transferred to a petri dish containing sterile PBS (Ca^{2+} and Mg^{2+} free) and heads, inner organs and limbs were removed. Carcasses were washed three times in 35 ml of sterile PBS. After the PBS washes, 5-7 carcasses were pooled and quickly minced on ice with a sterile scalpel, 5 ml PBS was added and homogenised by passing through a syringe equipped with a 20-23 G needle). 25 ml 0.5% trypsin/1 mM EDTA (LIFE Technologies GIBCO, Darmstadt, Germany) supplemented with 200 µg/ml of DNase I (Roche Applied Science, Mannheim, Germany) was added and incubated at 37°C for 10 minutes. A teflon mesh was sterilised for 30 minutes in boiling Ampuwa water (Fresenius Medical Care, Bad Homburg, Germany). After cooling to room temperature and sequential washing in PBS and trypsin/EDTA solution, the mesh was placed into a 250 ml Erlenmeyer flask. After trypsin incubation, the minced embryos were pressed with a sterile 5 ml syringe plunger through the mesh, which was afterwards washed with trypsin/EDTA. The reaction was stopped by adding complete MEF feeder medium (MEF feeder medium: Dulbecco´s Modified Eagles Medium (DMEM, with glutamax, high glucose, GIBCO, Germany), supplemented with 10% FCS, 0.1 mM non-essential amino-acids (10 mM stock), 1 mM sodium pyruvate (100 mM stock), 100 U/ml penicillin and 100 U/ml streptomycin (10000 U/ml penicillin/streptomycin stock solution)). Cell-clumps were allowed to sediment for 1 min and the supernatant was centrifuged at 180 rcf for 10 min. The cell pellet was resuspended in 10 ml of complete medium. Cells were plated at the density of 5 x 10^6 cells/dish (~one embryo/dish) onto 15 cm cell culture dishes containing 20 ml of complete MEF feeder medium. After overnight culture at 37°C, 5% CO_2 (cell culture incubator: Haereus, Germany), the medium was replaced with fresh medium. After 2-3 days, when the cells formed a confluent monolayer, they were washed twice in PBS and trypsinised in 0.5% trypsin/1 mM EDTA for 5 min at 37°C. Cells were then centrifuged at 180 rcf and replated at a dilution of 1:5 and further incubated. After another 2-3 days, the cells were confluent. The cells were trypsinised as described above and resuspended at a concentration of 10-20 x 10^6 cells/ml. Cell suspensions were pipetted in 0.5 ml aliquots into 2 ml-freezing vials (Nalgene, Germany). The content of each vial was mixed with 0.5 ml

of ice-chilled 2x concentrated freezing medium (2x freezing medium: 6 ml of complete MEF feeder medium supplemented with 2 ml of FCS and 2 ml of DMSO). Cells were frozen at -80°C and then stored in liquid nitrogen.

MEF feeder cells were a produced by the group of Ari Waisman, 1. Medical Clinic, University Medical Centre, Mainz, Germany.

3.2.2.2. MEF cell culture

One aliquot of MEF passage 0 (EF0) was thawed in a 37°C water bath, transferred to a tube containing 10 ml of pre-warmed MEF feeder medium and pelleted by centrifugation at 180 rcf in a bench-top centrifuge for 4 min. Cells are resuspended in a final volume of 80 ml, split onto 4 plates (15 cm diameter) and cultured at 37°C with 10% CO_2 in a humidified incubator (Sanyo, Wood Dale IL, USA). The cell culture medium is changed on the next day. After 3-5 days, when the cells were confluent, they were washed twice with PBS and trypsinised for 4 min with 1x Trypsin supplemented with 1% chicken serum. After stopping the reaction with 5 ml MEF medium per plate the cell suspension was pelleted, resuspended in MEF medium and plated in a 1:4 dilution. These steps were repeated once to obtain 64 plates out of one vial EF0.

To freeze MEF the cells were resuspend in 0.5 ml MEF feeder medium per 15 cm culture dish, then put on ice and 0.5 ml ice cold 2x freezing medium (4 ml MEF feeder medium + 4 ml FCS + 2 ml DMSO) was added drop-wise whilst shaking the tube. 1 ml of cell suspension was transferred to each vial and the cells were frozen in a pre-cooled isopropanol cryobox to -80°C. After 24 h the cells are transferred to liquid nitrogen for longer storage.

3.2.2.3. Mitotically inactivation of MEF with Mitomycin

In order to block cell proliferation, MEFs were mitotically inactivated with mitomycin c. Therefore, the medium on confluent MEF cells was replaced with 10 ml inactivation medium (MEF feeder medium + 10 µg/ml mitomycin c dissolved in DMSO) and incubated for 2-4 h at 37°C. Cells were then washed twice in PBS, trypsinised as above, counted and plated at a concentration of 3.5 x 10^6 cells/10 cm culture dish or frozen at a concentration of 4 x 10^6 cells/vial in freezing medium. To prepare feeder plates, either one vial of frozen mitomycin-treated primary mouse embryonic fibroblasts per 10 cm culture dish was thawed one day prior to ESC plating, or freshly mitomycin-treated cells were used.

3.2.2.4. Embryonic stem cell culture

One aliquot of embryonic stem cells obtained from EUCOMM was quickly thawed in a 37°C water bath and then transferred to a 15 ml tube containing 7 ml of pre-warmed ESC medium (Complete ESC medium: Dulbecco´s Modified Eagles Medium (DMEM, without glutamax, high

glucose), supplemented with 10% FCS, 2 mM L-glutamine (200 mM stock), 0.1 mM non-essential amino-acids (10 mM stock), 1 mM sodium pyruvate (100 mM stock), 100 U/ml penicillin and 100 U/ml streptomycin (10000 U/ml penicillin/streptomycin stock), 0.1 mM β-mercaptoethanol (100 mM stock) and leukemia inhibitory factor (LIF, medium supernatant from HEK-cells transfected with LIF-plasmid, kind gift of Prof Ari Waisman, University Medical Center, Mainz, Germany)). The cells were centrifuged for 4 min at 180 rcf and the pellet was resuspended in 2 ml ESC medium. Then, the cell suspension was plated onto one well of a 6 well plate (clone C09) and one well of a 24 well plate (clone H09), respectively, on a feeder plate. For the resuspension of ESCs fire-polished Pasteur pipettes were used, the medium was changed daily and cells were grown in a humidified cell culture incubator (Sanyo, Wood Dale IL, USA) at 37°C with 10% CO_2. For the expansion of ESCs cells were split progressively onto larger feeder plates (24 well-plates, 6 well-plates, 6 cm-plates, 10 cm-plates). When sufficient numbers of cells were obtained aliquots of cells were frozen. Medium was changed 2 h prior to splitting. The cells were washed twice with PBS, trypsinised for 4 min at 37°C and homogenised in trypsin in order to obtain a single cell suspension. After transferring the cell suspension to a tube with pre-warmed ESC medium and centrifugation, cells were resuspended in ESC medium and plated at a concentration of 1.5 x 10^6 cells/ 10 cm feeder plate.

To freeze ESCs, follow the splitting procedure and resuspend the cells in half the final volume ECS medium. Then, put the cells on ice and drop-wise add ice cold 2x freezing medium (4 ml ESC medium + 4 ml FCS + 2 ml DMSO) whilst shaking the tube. Transfer 1 ml to each cryo-vial and freeze the cells in a pre-cooled isopropanol cryobox. After 24 h the cells are transferred to liquid nitrogen for longer storage. Cells were frozen at a concentration of 1 x 10^6 cells/ vial.

3.2.2.5. Preparation of ESC for blastocyst injection

To prepare the cells for injection into blastocysts follow the splitting procedure and re-plate all cells on a 10 cm culture dish and incubate at 37°C for 20 min. As feeder cells sediment faster than ECS, they will start to get adherent, while ESCs are still in the medium. Transfer the cell-suspension to a new 10 cm plate, gently wash the old plate with 2 ml fresh medium and also transfer the medium. After 15 min incubation transfer the medium to a 15 ml tube, count the cells while centrifuging for 3 min at 180 rcf. Resuspend the cells in cold MEF feeder medium at a concentration of 3 x 10^6 cells/ 1 ml. After 5 min incubation on ice, when residual cell clumps have sedimented, carefully transfer the cell suspension without any clumps to a new tube, spin down in a pre-cooled centrifuge for 3 min at 1000 rpm and resuspend the cells in cold HEPES buffered MEF feeder medium (20 µl HEPES/ 1 ml MEF feeder medium).

Blastocyst injections were performed by staff of the ZVTE (Zentrale Versuchstiereinrichtung), University Medical Center, Mainz, Germany.

3.2.3. Isolation of genomic DNA

3.2.3.1. DNA preparation from mouse tails

A mouse tail tip (approximately 1-2mm) was cut and incubated overnight on a thermo mixer at 56°C in 500 µl TENS- buffer (1 M Tris-HCl pH 8.0, 0.5 M EDTA, 5 M NaCl, 10% SDS). Proteinase K (25 µl of 10 mg/ml stock) was freshly added. After centrifugation at room temperature for 10 min at 18000 rpm, 500 µl of the supernatant was transferred to a fresh reaction tube containing 500 µl isopropanol. After mixing by inversion and centrifugation as above the supernatant was removed, precipitated DNA washed once with 70% ethanol, air-dried, dissolved in 200 µl $T^{1/10}E$ buffer (1 ml of 1 M Tris-HCl pH 8.0, 20 µl 0.5 M Na_2EDTA add 100 ml H_20, sterilised by autoclaving) and stored at 4°C until further use.

3.2.3.2. DNA preparation from embryonic stem cells

Embryonic stem cell clones were grown on a 10 cm cell-culture dish on feeder cells until they reached confluence. Then, cells were rinsed with twice with PBS (139.9 mM NaCl, 2.7 mM KCl, 10.1 mM Na_2HPO_4-H_2O, 1.8 mM KH_2PO_4, pH 7.4), trypsinised and centrifuged for 4 min at 180 rcf. The supernatant was discarded and the cell pellet was resuspended in TEN-buffer (1 M Tris-HCl pH 8.0, 0.5 M EDTA, 5 M NaCl). Afterwards, 10% SDS to a final concentration of 0.2% and 100 µl Proteinase K (10 mg/ml stock) was added and the reaction mixture was incubated overnight at 56°C on a thermomixer. Then, it was continued according to the “DNA preparation from mouse tail”-protocol.

3.2.4. Southern Blotting

Correct targeting of the locus was confirmed by Southern blot analysis.

3.2.4.1. DNA digest

Enzymes and buffers were purchased from New England Biolabs, Frankfurt, Germany.
For detection of the neomycin resistance cassette 30 µg DNA was double-digested with SmaI/ApaI (50 units/µl). 0.4 µl 100 x BSA, 0.7 µl Spermidin and 0.3 µl RNase A was added and DNA was digested overnight at 25°C in a total volume of 40 µl. After 16 h of incubation additional 25 Units of each enzyme were added and further incubated. It was checked for complete digestion of the DNA on an agarose gel.

3.2.4.2. Electrophoresis and transfer

Digested genomic DNA was separated overnight at 25 V on a 0.7% agarose gel in 1x TAE (50 x TAE: dissolve 212 g (2 M) Tris-HCl in 500 ml H_2O, add 100 ml 0.5 M Na_2EDTA (pH 8.0) and 57.1 ml glacial acetic acid, ad 1000 ml) with Lamda-HindIII (Fermentas, St Leon-Rot, Germany) or Fermentas GeneRuler™ 1kb Plus DNA Ladder as a marker. The gels were then photographed on a UV transilluminator. For depurination the gel was shaken in 0.25 M HCl for 5-10 min, rinsed in tab water, denaturated in 0.5 M NaOH, 1.5M NaCl for 30 min, rinsed again in tab water and neutralised in 1.5 M NaCl, 1 M Tris-HCl pH 7.2 for 30 min. Capillary blot was performed as described (SAMBROOK *et al.* 1989) to transfer DNA onto Hybond-N^+ membranes (GE Healthcare, Freiburg, Germany). Blotting was performed overnight in 10x SSC (prepare from 20x SSC stock; 3 M NaCl, 300 mM sodium citrate; pH 7).

3.2.4.3. Probe preparation

A 498 bp probe against the neomycin resistance cassette was prepared by PCR with following primers:

Neo-fwd: 5´ - TGC TCG ACG TTG TCA CTG AAG C - 3´;

Neo-rev: 5´ - TAC CGT AAA GCA CGA GGA AGC G - 3´

and following PCR program:

95°C/5 min, 27 x (95°C/45 s, 55°C/45 s, 72°C/45 s), 72°C/5 min.

The PCR probe was purified by agarose gelelectrophoresis followed by gel-extraction using the NucleoSpin Extract II - kit (Machery-Nagel, Düren, Germany) according to the manufacturer´s instructions. Probe labeling was performed with Amersham Rediprime™ II DNA Labeling System (GE Healthcare, Freiburg, Germany) according to the manufacturer´s instructions. Briefly, 25 ng of template DNA in a volume of 45 µl TE was boiled at 95°C for 5 min and then placed on ice for 5 min. Afterwards the denatured template was transferred to the reaction tube, 5 µl [α-^{32}P] dCTP (3000 Ci/mmol, 50 µCi) (PerkinElmer, Rodgau, Germany) was added and mixed. The labeling reaction was carried out at 37°C for 10 min and then stopped by adding 5 µl EDTA solution provided by the supplier. The radioactive probe was purified using Illustra MicroSpin G-50 columns (GE Healthcare, Freiburg, Germany) according to the manufacturer´s instructions. Incorporation of the labeled nucleotide was checked with a scintillation counter.

3.2.4.4. Hybridisation

The membrane was put between hybridisation-mash, transferred to a hybridisation bottle und pre-hybridised with 30-40 ml pre-warmed hybridisation-buffer (hyb-Buffer) for 3-4 h at 65°C in a hybridisation-oven. To prepare 500 ml of hyb-buffer pre-warm separately 50 ml 50x Denhardt´s

solution (5 g Ficoll, 5 g Polyvinylpyrrolidine 5 g BSA, add 500 ml H_2O, filter, aliquot in 50 ml tubes and store at -20°C), 300 ml H_2O and 25 ml 10x SDS to 37°C. Add the Denhardt´s solution to the water, then add SDS and 125 ml 20x SSPE (175,3 g NaCl, 27,6 g NaH_2PO_4 x H_2O, 7,4 g Na_2EDTA add 800 ml H_2O, titrate to pH 7,4, ad 1000 ml, autoclave). After filtrating the solution, add 5 ml denatured ss-DNA (10 mg/ml), mix well, aliquot and store at -20°C. To prepare the hybridisation solution, the labeled probe was denatured by boiling for 5 min at 95°C. Then, ~1000000 cpm per 1 ml pre-warmed hyb-buffer was added (total volume for hybridisation: 5-10 ml), the prehybridisation buffer in the hybridisation bottles was exchanged by the hybridisation solution and incubated overnight at 65°C. The membranes were subjected to stringent washes with pre-heated (65°C) wash-buffers according to the following protocol: wash in 50 ml of 2x SSC/0.1% SDS for 30 min, then for 30 minutes in 50 ml of 0.2x SSC/0.1% SDS at 65°C. Afterwards it was checked with a hand radioactive counter whether radioactivity was below ~200 cpm, otherwise the membrane was put in 50 ml 0.1x SSC/0.1% SDS for another 30 min. For the detection of the signals membranes were rinsed with 2x SSC, sealed in plastic bags and exposed for 1-2 days to autoradiographic films (Kodak Biomax MS film, Sigma Aldrich, Munich, Germany) in Kodak cassettes with intensifying screens at -80°C.

3.2.5. Genotyping

Mice were routinely genotyped by following PCRs.

PCR 1:

Primer:	ASPA-fwd	5´- ATC TCA ATG TTA TTG TGT TAT ATT AGG -3´
	ASPA-rev	5´- GAT CTT TCT AAG GCT CCA CAA TGG -3´
PCR program:	95°C/3 min, 35 x (95°C/30 s, 60°C/30 s, 72°C/30 s), 72°C/5 min	

This PCR resulted in a 336 bp band for the wildtype allele and a 387 bp band for the synthetic allele.

Presence of the loxP site was detected by PCR 2 and yielded a 307 bp band.

PCR 2:

Primer	ASPA-fwd	5´-ATC TCA ATG TTA TTG TGT TAT ATT AGG-3´
	LoxRev	5´-TGA ACT GAT GGC GAG CTC AGA CC-3´
PCR program:	95°C/3 min, 35 x (95°C/30 s, 60°C/30 s, 72°C/30 s), 72°C/5 min	

3.2.6. RNA isolation and qRT-PCR

Animals were sacrificed by decapitation at P60, organs dissected quickly, and snap frozen. Brains were homogenised under liquid nitrogen using mortar and pestle. Total RNA was isolated using the Nucleo-Spin RNAII-Kit (Macherey-Nagel, Dueren, Germany). 450 ng of DNase-treated total RNA was reverse-transcribed using High Capacity cDNA Reverse Transcription Kit (Applied Biosystems, Carlsbad, CA). The cDNA equivalent to 22.5 ng RNA was amplified using commercial TaqMan assays (Applied Biosystems, Carlsbad, CA) for mouse aspartoacylase (aspa; Mm00480867_m1), glucoronidase beta (gusb; Mm00446953_m1) and folate hydrolase (folh1; Mm00489655_m1) with an ABI 7300 real time PCR cycler (Applied Biosystems, Carlsbad, CA). Quantitative realtime-PCR (qRT-PCR) reactions were performed in triplicates. Data analysis was done using a relative expression software tool (REST) using gusb as the reference gene (PFAFFL *et al.* 2002).

Relative abundances of *aspa* mRNA in different organs obtained from adult *aspa*$^{+/+}$ animals were determined by Dmitri Tkachev, Institute of Physiological Chemistry, University Medical Centre, Mainz, Germany.

3.2.7. Antibody generation

Expression of recombinant human aspartoacylase fused to a C-terminal 6x His tag using the bacterial expression vector pET-3a (New England Biolabs, Beverly, MA) was expressed in E. Coli (BL21) as described (KLUGMANN *et al.* 2003). After induction with IPTG (1 µM) for 4 h, bacteria were sonicated in a solubilisation buffer containing 20 mM Na-phosphate (pH 7.4), 0.5 M NaCl, 5 mM imidazole. Sonicated bacteria were pelleted, insoluble (pellet) and soluble (supernatant) fractions were separated by polyacrylamide gel electrophoresis (PAGE) and ASPA content was analysed by coomassie staining. Less than 5% of total ASPA protein was located in the supernatant. Recombinant soluble ASPA was purifed by affinity chromatography using Ni-charged agarose (Ni-NTA Agarose, Quiagen, Hilden, Germany). On the day of injection, purified ASPA (0.1 mg) was mixed with Freund's adjuvant and administered i.p. to a rabbit. Every two weeks the dose was repeated over a total of 12 weeks. Finally, the animal was sacrificed, blood collected and the serum isolated.

The anti-ASPA antibody was generted by Matthias Klugmann and Ruth Jelinek, Institute of Physiological Chemistry, University Medical Centre, Mainz, Germany.

3.2.8. Histology

3.2.8.1. Immunohistochemistry

For immunohistochemistry mice were deeply anesthetised with pentobarbital and trans-cardially perfused with phosphate bufferd saline (PBS) followed by phosphate buffered 4% paraformaldehyde (PFA). Brains were post-fixed in PFA overnight and cryoprotected in 30% sucrose/PBS for 2 days, then cut into 40 µm free-floating sections using a Microm HM-560 cryostat (Thermo Scientific, Waltham, MA) as described (KLUGMANN *et al.* 2005) and stored at 4°C in cryoprotection solution (25% glycerin, 25% ethylene glycol and 50% PBS) until use. After washing with PBS, permeabilisation with 0.2% TritonX-100 in PBS (PBS-Tx) and blocking in 4% normal goat serum (NGS) in PBS-Tx, sections were incubated overnight at 4°C with a combination of the following antibodies in 4% NGS in PBS-Tx: rabbit anti-aspa serum (1:1000); chicken anti-β-Galactosidase (1:500, abcam, Cambridge, UK); mouse anti-GFAP (1:1000, Sigma-Aldrich, Munich, Germany), respectively. For Iba-1 and β-Galactosidase detection, antigen retrieval was performed prior to permeabilisation by rinsing free floating sections two times in PBS followed by incubation in 10 mM sodium citrate buffer (pH 6.0) at 85°C for 30 min. Sections were allowed to cool down to room temperature in the same solution followed by permeabilisation with PBS-Tx, blocking for 30 min in PBS-Tx 1% BSA, and incubation with goat anti Iba-1 (1:500, Abcam, Cambridge, UK) in blocking solution overnight at 4°C. Sections were washed with PBS and incubated with appropriate Alexa-conjugated secondary antibodies (1:1000, Invitrogen, Carlsbad, CA) for 1-2 h at room temperature in 4% NGS in PBS-Tx, mounted on slides and coverslipped with Mowiol (Calbiochem, Darmstadt, Germany).

3.2.8.2. X-Gal staining

For LacZ immunohistochemistry, *aspa*$^{lacZ/+}$ animals were perfused in ice-cold 5% PFA, and tissues dissected and postfixed for 1 h followed by embedding in Kaiser's gelatine (Merck, Darmstadt, Germany). Vibratome sections (60 µm; Microm, HM650V; Thermo Scientific, Waltham, MA) were collected in PBS and incubated in X-gal solution (1.2 mg/ml X-gal, 5 mM potassium ferrocyanide and 2 mM $MgCl_2$ in PBS) for 4-12 h. After 3 washes in PBS sections were mounted and coverslipped in Mowiol.

X-Gal staining was performed by Dmitri Tkachev, Institute of Physiological Chemistry, University Medical Centre, Mainz, Germany.

3.2.8.3. Nissl staining

For Nissl staining, sections were mounted onto glass slides in PBS and air-dried, then stained for 10 s with toluidine blue (0.1% in dH_2O). Slides were washed two times with H_2O, destained for

15 s in 70% ethanol / 0.001% acetic acid, dehydrated in 100% ethanol and air-dried. After dipping in xylol, sections were mounted with Histokit (Carl Roth, Karlsruhe, Germany).

Immunostaining was visualised using a Leica DM IL LED inverted microscope (Leica Microsystems, Wetzlar, Germany) with the Leica application suite LAS EZ software and a Zeiss LSM 710 confocal microscope (Carl Zeiss MicroImaging, Jena, Germany) with Zeiss Zen software.

3.2.8.4. Teased sciatic nerve preparations

Teased sciatic nerve preparations were prepared as described (SHERMAN *et al.* 2001). Briefly, peripheral nerves were fixed by perfusion or immersion in 4% PFA in 0.1 M PBS, pH 7.4 for 30-60 min. After several washes with phosphate buffer, the epineurium was removed with fine forceps and the nerves were teased using acupuncture needles or fine forceps on TESPA-coated (2% TESPA (Sigma Aldrich, Munich, Germany) in acetone) SuperFrostPlus slides (Thermo Scientific, St. Leon-Rot, Germany) in a 50 µl drop containing PBS. Slides with nerve fibres were air dried and stored at -20°C until immunostaining. To coat slides with 3-Aminopropyl-trimethoxysilane (TESPA), slides were rinsed with dH_2O, washed with 95% ethanol for 2 min and dried at 100°C for 1 h. After cooling down to room temperature slides were coated with TESPA (2% TESPA in acetone) for 2 min. Slides were washed 3x for 40 s with acetone, 1x with dH_2O and dried overnight at 42°C.

For immunostaining, slides with teased fibres were encircled with a PAP-pen (Sigma Aldrich, Munich, Germany) to hold staining solutions. Immunostaining was carried out as described in the immunochemistry section, and rabbit anti-ASPA and rat anti-MBP (1:1000; Abcam, Cambridge, UK) were used as primary antibodies.

Teased sciatic nerves analysis was carried out by Philipp Röth, Institute of Physiological Chemistry, University Medical Centre, Mainz, Germany.

3.2.9. Electron microscopy

Animals were anesthetised with Avertin and transcardially perfused with warm HBSS followed by fixing solution (4% formaldehyde and 2.5% glutaraldehyde in phosphate buffer containing 0.5% NaCl as described (MOBIUS *et al.* 2010). The CNS was dissected and embedded in Epon (Serva) after postfixation with 2% OsO_4 (Science Services, Munich, Germany) and dehydration with ethanol and isopropanol and propylenoxid. Ultrathin sections were cut using an Ultracut S ultramicrotome (Leica, Austria), mounted on 100 mesh hexagonal copper EM grids (Plano, Germany) and poststained with 4% aqueous uranyl acetate (SPI-Supplies, USA) and lead citrate (REYNOLDS 1963). The sections were analysed in a LEO EM 912AB electron microscope (Zeiss, Jena, Germany), and pictures were taken with an on-axis 2048 x 2048 CCD camera (Proscan, Scheuring, Germany).

Electron microscopy was perfomed by Wiebke Möbius and Torben Ruhwedel at the Department of Neurogenetics, Max-Planck-Institute of Experimental Medicine, Göttingen, Germany.

3.2.10. Immunoblotting

Animals were sacrificed, organs dissected quickly and snap frozen. Brains were homogenised under liquid nitrogen using mortar and pestle. Aliquots were sonicated in tris buffered saline (TBS) containing protease inhibitors (cOmplete™ protease inhibitor cocktail tablets, Roche Applied Science, Mannheim, Germany) according to the manufacturer´s recommendation. Samples were centrifuged for 10 min at 13000 rcf and 4°C to remove cell debris. The supernatant was transferred to a new reaction tube and protein concentration was determined by the method of Bradford (BRADFORD 1976) using bovine serum albumin (NEB, Frankfurt, Germany) as standard. 20 µg of protein were mixed with 5x Laemmli reducing sample buffer (for 100 ml: 15.0 g SDS; 15.6 ml 2 M Tris-HCL pH 6.0; 57.5 g 87% glycerol; 16.6 ml β-mercaptoethanol, 0.4% (w/v) bromphenol blue), denatured for 5 min at 95°C and separated by SDS-PAGE. This was performed using a Bio-Rad electrophoresis system (Mini-PROTEAN 3) with Tris-glycin running-buffer (25 mM Tris-base, 190 mM glycine, 0.1 % SDS) according to manufacturer´s instruction manuals (Bio-Rad Laboratories GmbH, Munich, Germany). PageRuler™ Prestained Protein Ladder (Thermo Scientific, St. Leon-Rot, Germany) was used as a molecular weight marker. For Western blotting a tank transfer system (Mini Trans-Blot cell) was used according to the manufacturer´s instruction manuals (Bio-Rad Laboratories GmbH, Munich, Germany). The proteins were transferred in transfer buffer (25 mM Tris-base, 190 mM glycine, 20% ethanol (v/v)) onto nitrocellulose membranes (Protran, Whatman; GE Healthcare, Dassel, Germany). After blocking the membrane in blocking solution (TBS + 0.1% Tween20 (v/v) (TBST) + 5% non-fat dry milk (w/v)) for 1 h at room temperature under agitation to prevent non-specific background binding of the primary and/or secondary antibody, membranes were probed with the following antibodies with the dilutions made in blocking solution overnight at 4°C under agitation: rabbit anti-ASPA serum (1:1000), mouse anti-α-tubulin (1:400000, Sigma Aldrich, Munich, Germany), mouse anti-CNPase (1:1000, Abcam, Cambridge, UK), rat anti-MBP (1:1000; Abcam, Cambridge, UK), rat anti-PLP aa3 (1:1000, gift of J. Trotter). Antibodies were detected by the appropriate HRP-conjugated secondary antibodies (1:1000, Dianova, Hamburg, Germany) followed by ECL detection. For ECL detection of one membrane (~5x7cm) 1 ml of Solution A (200 ml 0.1 M Tris-HCL, pH 8.6; 50 mg Luminol; stored at 4°C) and 1 ml of Solution B (11 mg para-hydroxy coumaric acid in 10 ml DMSO) were mixed, 0.3 µl H_2O_2 was added, mixed and incubated for 2 min prior to detection on Amersham Hyperfilm™ ECL

films (GE Healthcare, Dassel, Germany). Data was analysed using the Image J software (U.S National Institute of Health, Bethesda, MA).

3.2.11. Behavioural testing

Differences in innate anxiety and general locomotor behaviour of male and female *aspa*$^{lacZ/lacZ}$ (males: n=8; females: n=7) and *aspa*$^{+/+}$ (males: n=8; females: n=6) mice were assessed in the open field test at P90. Animals were placed in the center of an arena (40x40x40 cm) under bright light conditions (100 lux) and monitored for 30 min. Total distance traveled and time spent in the center area and in the periphery was analysed using Smart software (Panlab, Madrid, Spain). Using the same cohorts of animals, motor learning was assessed using the rotarod test at P90. Mice were familiarised with the apparatus (Ugo Basile, Comerio, Italy) in 2 trials for 2 min at constant speed (4 rpm). In a series of 3 trials per animal, the time the mice remained on the accelerating roller (4-40 rpm in 4 min) was scored. Between trials the animals were allowed a 10 min period in their home cage. The individual performances were averaged over 2 days.

3.2.12. ^{1}H-MR spectroscopy

A male control mouse and an *aspa*$^{laZ/lacZ}$ mouse (4-month-old) were measured with ^{1}H-magnetic resonance spectroscopy on a 9.4T Bruker BioSpec scanner (Bruker, Rheinstetten, Germany) equipped with a cryogenic very low temperature, closed cycle cooled RF-coil. Mice were anesthetised by a gas mixture of O_2: 50% and air: 50% with ca. 1.8% isoflurane. Respiration rate was monitored throughout the experiment. Body temperature was maintained at 37°C by warm water circulation and verified by a rectal thermo sensor. For voxel positioning and high resolution images of the mouse brain were acquired with a T2-weighted RARE (rapid acquisition with relaxation enhancement) (TE = 11ms, TR = 2.5s, alpha = 20°, two averages; Resolution 66x66x500 um³). Spectra were acquired using a PRESS single voxel Sequence at an echo time of TE = 10 ms from a 12 µl (2x2x3 mm³) volume from the thalamic region, with a repetition time of TR = 4 s and 256 averages (NEX) resulting in a total acquisition time of 17 min per spectrum. Water suppression was done with the VAPOR (Variable pule powers and optimised relaxation delays) method interleaved with 6 outer-volume suppression slices. To ensure optimal B0 homogeneity 1st and 2nd order shimming was conducted with Fastmap over a volume of 5x5x5 mm³ prior each metabolite measurement resulting in a line width (fwhm) of the unsuppressed water signal of 12 Hz or better. An additional one shot

unsuppressed waterline (RF-off) was acquired for each voxel, which was used for eddy-current correction and water referencing. Quantification was done according with LCModel by fitting the *in vivo* spectra to phantom data of 16 metabolite solutions measured at the same scanner. Macromolecule contributions were fitted through simulated spectra at the relevant frequencies. Concentration values were referenced to an unsuppressed water signal acquired from the same voxel assuming a mean water-concentration of 46.1 M/l.

^{1}H MR spectroscopy was perfomed by Alexander Sartorius and Wolfgang Weber-Fahr at the Neuroimaging Department, Central Institute of Mental Health, Mannheim, Germany.

3.2.13. Statistics

All graphs and statistical analyses were done with GraphPad Prism 4 software (La Jolla, CA). Student's t-test was used for statistical analysis. Myelin protein levels were analysed with One-Way ANOVA followed by Bonferroni post-hoc test. Values are presented as the mean $\pm$ s.e.m and $p<0.05$ was considered as statistically significant. *$p<0.05$; **$p<0.01$, *** $p<0.001$.

3.3. Results

3.3.1. Disruption of *aspa* expression *aspa*^{lacZ} knockin mice

Based on a knockout-first strategy to produce a knockout at the RNA processing level (TESTA *et al.* 2004), targeting of the *aspa* locus in C57bl/6 ES cell was achieved by the European Mouse Mutagenesis Consortium (EUCOMM). A βgeo cassette (including the genes encoding β-galactosidase and neomycin) flanked by frt sites was inserted into intron 1 of the intact *aspa* gene. Additionally, exon 2 was flanked by loxP sites for optional conditional deletion of the targeted locus (Fig. 3.1). Two clones with homologous recombination events were injected into blastocysts (ASPA clone C09 and ASPA clone H09) and germ-line transmission was confirmed after appropriate matings. The C09-derived line was used for further experiments. Heterozygous *aspa*$^{lacZ/+}$ males and females were crossed to obtain *aspa*$^{+/+}$, *aspa*$^{lacZ/+}$ and *aspa*$^{lacZ/lacZ}$ littermates at the expected Mendelian ratios (24.9%, n=59; 51.9%, n=123; 23.2%, n=55) for the three genotypes.

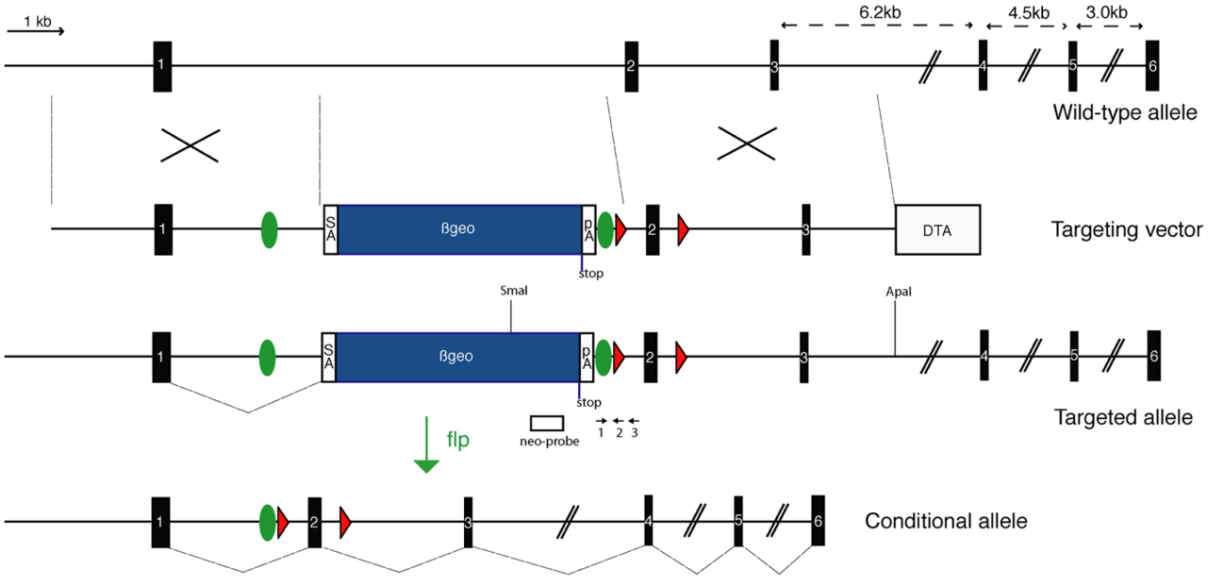

Figure 3.1: Generation of *aspa*^{lacZ} mice by homologous recombination.
Depicted is the genomic structure of the murine *aspa* locus, which spans 6 exons (black boxes). Homologous recombination of the targeting vector inserts the βgeo cassette (blue box), encoding β-Galactosidase (lacZ), into intron 1 of the intact *aspa* gene. This cassette is flanked by frt sites (green circles). Additional loxP sites flank exon 2 (red triangles). The vector includes a DTA cassette for negative selection. In the targeted allele, exon 1 is spliced to the splice acceptor site preceding βgeo, and transcription is terminated at the introduced pA site. The conditional *aspa*^{flox} allele is produced by breeding *aspa*^{lacZ} mutants to Flp-deleter mice (RODRIGUEZ *et al.* 2000) for recombination of the βgeo cassette *in vivo*. Note that frt and loxP sites are not drawn to scale. βgeo, β-galactosidase-neomycin-resistance cassette; SA, splice acceptor; pA, polyadenylation site, DTA, Diphteria toxin gene.

A single targeting event was confirmed by Southern blot analysis of genomic DNA obtained from liver of all three genotypes using a neomycin probe (Fig. 3.2 A). The modified *aspa* locus could also be identified by genotyping with producing amplicons of the expected sizes (Fig. 3.2 B). The βgeo cassette was flanked by an upstream 3' splice acceptor site and a downstream transcriptional termination sequence resulting in an exon1-βgeo fusion transcript. The corresponding fusion protein contains the N-terminal 77 amino acid residues of ASPA with no predicted enzymatic activity (BITTO *et al.* 2007). Because inactivation of the *aspa* gene was designed to attenuate transcription upstream of exon 2, d *aspa* mRNA levels in the brain of $aspa^{+/+}$, $aspa^{lacZ/+}$ and $aspa^{lacZ/lacZ}$ mice (n=3) were determined by quantitative real-time (qRT) PCR. Using a TaqMan probe binding to a downstream sequence, *aspa* mRNA levels were undetectable in $aspa^{lacZ/lacZ}$ mice. A 60.4 $\pm$ 4.3% (p=0.0001) reduction of mRNA expression was observed in $aspa^{lacZ/+}$ brains compared to controls (Fig. 3.2 C). To determine ASPA protein levels a rabbit anti-ASPA antibody was used in immunoblot analysis of whole brain homogenates of 2-month-old $aspa^{+/+}$, $aspa^{lacZ/+}$ and $aspa^{lacZ/lacZ}$ mice (n=3). In the presence of one functional allele in heterozygous $aspa^{lacZ/+}$ animals, ASPA was reduced to 74.5 $\pm$ 5.7% (p=0.048) of control levels and was completely abolished in homozygous $aspa^{lacZ/lacZ}$ mutants (Fig. 3.2 D, E). Analysis of β-Galactosidase levels showed the complementary profile with moderate levels in $aspa^{lacZ/+}$ mice and increased levels in $aspa^{lacZ/lacZ}$ mutants reflecting gene dosage effects (Fig. 3.2 D, E).

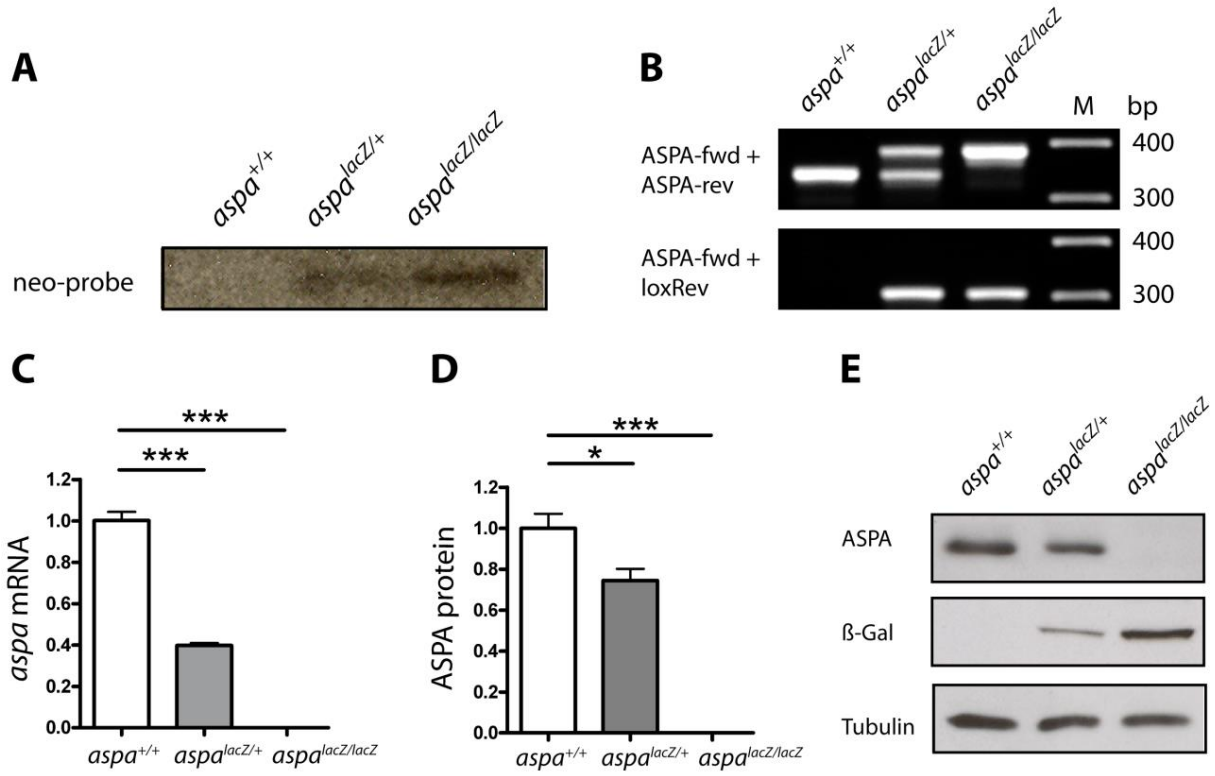

Figure 3.2: Molecular characterisation of *aspa*^{lacZ} mice.
(A) For Southern blot analysis genomic DNA was digested with SmaI/ApaI. The neo probe (white box in A) detected the expected 7.5 kb band in heterozygotes and homozygotes. **(B)** Genomic PCR of littermates with primers ASPA-fwd & ASPA-rev produces the expected amplicons in *aspa*$^{+/+}$ (336 bp), *aspa*$^{lacZ/+}$ (387 bp and 336 bp) and *aspa*$^{lacZ/lacZ}$ (387 bp) animals. The upstream loxP site was detected by PCR with primers ASPA-fwd & loxRev yielding a 307 bp band. **(C)** Q-RT-PCR using a TaqMan probe for quantification of *aspa* mRNA levels in brains of *aspa*$^{+/+}$, *aspa*$^{lacZ/+}$, and *aspa*$^{lacZ/lacZ}$ mice (n=3) confirms the attenuation of transcription downstream of exon 2 in the targeted allele. **(D)** Immunoblot detection of ASPA in whole brain lysates of a*spa*$^{+/+}$, *aspa*$^{lacZ/+}$ and *aspa*$^{lacZ/lacZ}$ mice (4-month-olds, n=3) revealed that in the presence of one functional allele in heterozygous *aspa*$^{lacZ/+}$ animals, ASPA was reduced to 74.5 ± 5.7% (p=0.048) of control levels and was completely abolished in homozygous *aspa*$^{lacZ/lacZ}$ mutants. Analysis of β-Galactosidase levels showed the complementary profile with moderate levels in *aspa*$^{lacZ/+}$ mice **(E)** Representative Western blot of the 37 kD ASPA protein was detected in *aspa*$^{+/+}$ and *aspa*$^{lacZ/+}$ mice but not in *aspa*$^{lacZ/lacZ}$ mutants. β-Galactosidase is expressed in *aspa*$^{lacZ/+}$ and *aspa*$^{lacZ/lacZ}$ brain but not controls. α-Tubulin was used as loading control.

Phenotypically, *aspa*$^{lacZ/lacZ}$ mutants were leaner (Fig. 3.3 A) and showed gait abnormalities starting before weaning. The body weight of *aspa*$^{lacZ/lacZ}$ mice was significantly decreased at P40 compared to controls for both sexes (*aspa*$^{+/+}$ 19.05 ± 0.83 g vs. *aspa*$^{lacZ/lacZ}$ 14.70 ± 0.67 g males, $p<0.001$; *aspa*$^{+/+}$ 16.84 ± 0.30 g vs. *aspa*$^{lacZ/lacZ}$ 13.93 ± 0.58 g females, $p<0.001$) (Fig. 3.3 B, C). Using Flp-deleter mice (DYMECKI 1996; RODRIGUEZ *et al.* 2000), the *aspa*$^{lacZ/lacZ}$ allele could be converted via excision of the βgeo cassette to the floxed *aspa*$^{f/f}$ allele (Fig. 3.1). The latter is phenotypically identical to the wildtype allele and will be instrumental for conditional deletion of the *aspa* gene via Cre-mediated recombination. However, the analysis of the conditional knockout animals was beyond the scope of this thesis.

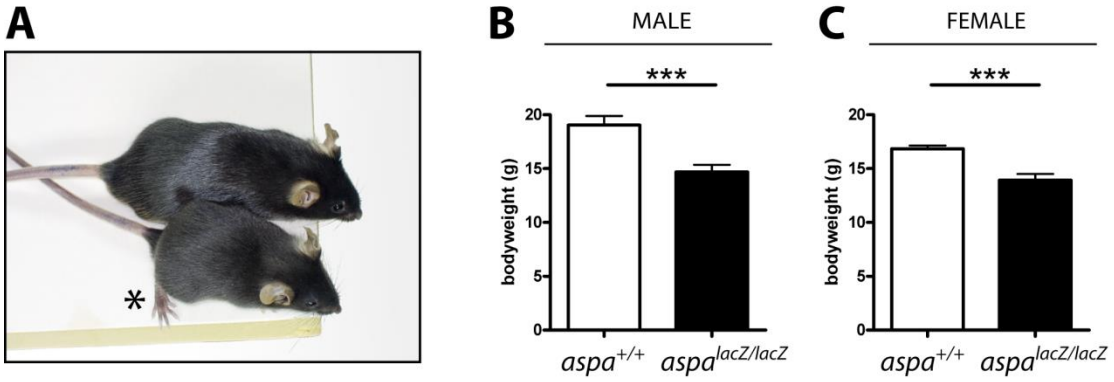

Figure 3.3: Assessment of the body weight of *aspa*^{lacZ} mice.
(A) Representative picture of a male *aspa*$^{lacZ/lacZ}$ mutant (asterisk) and an *aspa*$^{+/+}$ littermate at P70. **(B-C)** The body weight of male and female *aspa*$^{lacZ/lacZ}$ mice was determined at P40 and was significantly decreased compared to controls for both sexes (males: *aspa*$^{+/+}$ 19.05 ± 0.83 g vs. *aspa*$^{lacZ/lacZ}$ 14.70 ± 0.67 g, *p<0.001*; females: *aspa*$^{+/+}$ 16.84 ± 0.30 g vs. *aspa*$^{lacZ/lacZ}$ 13.93 ± 0.58 g, *p<0.001*).

3.3.2. ASPA expression domains

The genomic configuration of the modified locus was designed to recapitulate the activity of the *aspa* promoter and analysis of *aspa*$^{lacZ/+}$ heterozygots by X-Gal immunohistochemistry detected the presence of the soluble enzyme β-Galactosidase in central and peripheral tissues (Fig. 3.4 A-G). X-Gal was expressed by oligodendrocytes throughout the brain. Intense staining was observed in corpus callosum, but was also present in subcortical grey matter (Fig. 3.4 A). Fibre tracts in the thalamus showed strong X-Gal staining indicating the presence of β-Galactosidase in oligodendrocyte processes (Fig. 3.4 B). Brain stem and cerebellar white matter also displayed abundant X-Gal signals (Fig. 3.4 C). At higher magnification, X-gal signal was visualised in the soma and proximal processes of oligodendrocyte in the cerebellum (Fig. 3.4 D). Furthermore, activity of the *aspa* promoter in the peripheral organs was investigated by X-Gal staining. Highly abundant X-Gal staining was observed in small intestine and kidney (Fig. 3.4E, F) confirming previous reports on ASPA expression in these organs (HERSHFIELD *et al.* 2006; KLUGMANN and LEICHTLEIN 2006; SURENDRAN *et al.* 2006). X-Gal staining in the kidney was found in proximal tubules, but was absent from medulla and glomeruli. This expression pattern matches the distribution of ASPA immunoreactivity in this organ (HERSHFIELD *et al.* 2006). In addition, was observed X-Gal staining was observed in fibres of the sciatic nerve (Fig. 3.4 G). However, the histological approach did not resolve whether β-Galactosidase was localised to Schwann cells or the underlying axons.

To show that the newly generated anti-ASPA antibody specifically stains oligodendrocytes in the CNS, brain sections of homozygous Plp-dsRed-1 transgenic mice expressing the red fluorescent

protein (RFP) reporter under the control of the *plp-1* promoter (HIRRLINGER *et al.* 2005) were stained with the ASPA antibody. On the subcellular level, staining was detected in soma and proximal processes of oligodendrocytes (Fig. 3.4 H-J) confirming previous findings (KLUGMANN *et al.* 2003; MADHAVARAO *et al.* 2004). Double-immunostaining revealed that immunoreactivities of both β-galactosidase and ASPA exactly co-localised in the thalamus of a heterozygous $aspa^{lacZ/+}$ mouse further validating this reporter line as a genetic tool to monitor the activity of the *aspa* gene (Fig. 3.5).

To discern ASPA expression in the sciatic nerve, confocal analysis of ASPA immunoreactivity in teased nerve fibres of $aspa^{+/+}$ mice was performed (Fig. 3.4 K-M). ASPA was detected in protoplasmic domains of Schwann cells and segregated from the myelin marker MBP. These results show that this enzyme is present in myelinating glia of the central and peripheral nervous system. However, the histological approach precludes quantitative analyses. Therefore, qRT-PCR was conducted to determine the relative abundances of *aspa* mRNA in different organs obtained from adult $aspa^{+/+}$ animals. Expression levels in kidney, spinal cord, small intestine, and sciatic nerve were almost two-fold more than that in brain (Fig. 3.4 N). Since peripheral neurons were devoid of ASPA immunoreactivity (Fig. 3.4 K-M), the PCR data suggest that Schwann cells are the main source of *aspa* mRNA in the sciatic nerve. Moderate levels of expression were detected in muscle, testis and lung, and negligible in whole body preparation at embryonic day (E) E13.5 and E16.5.

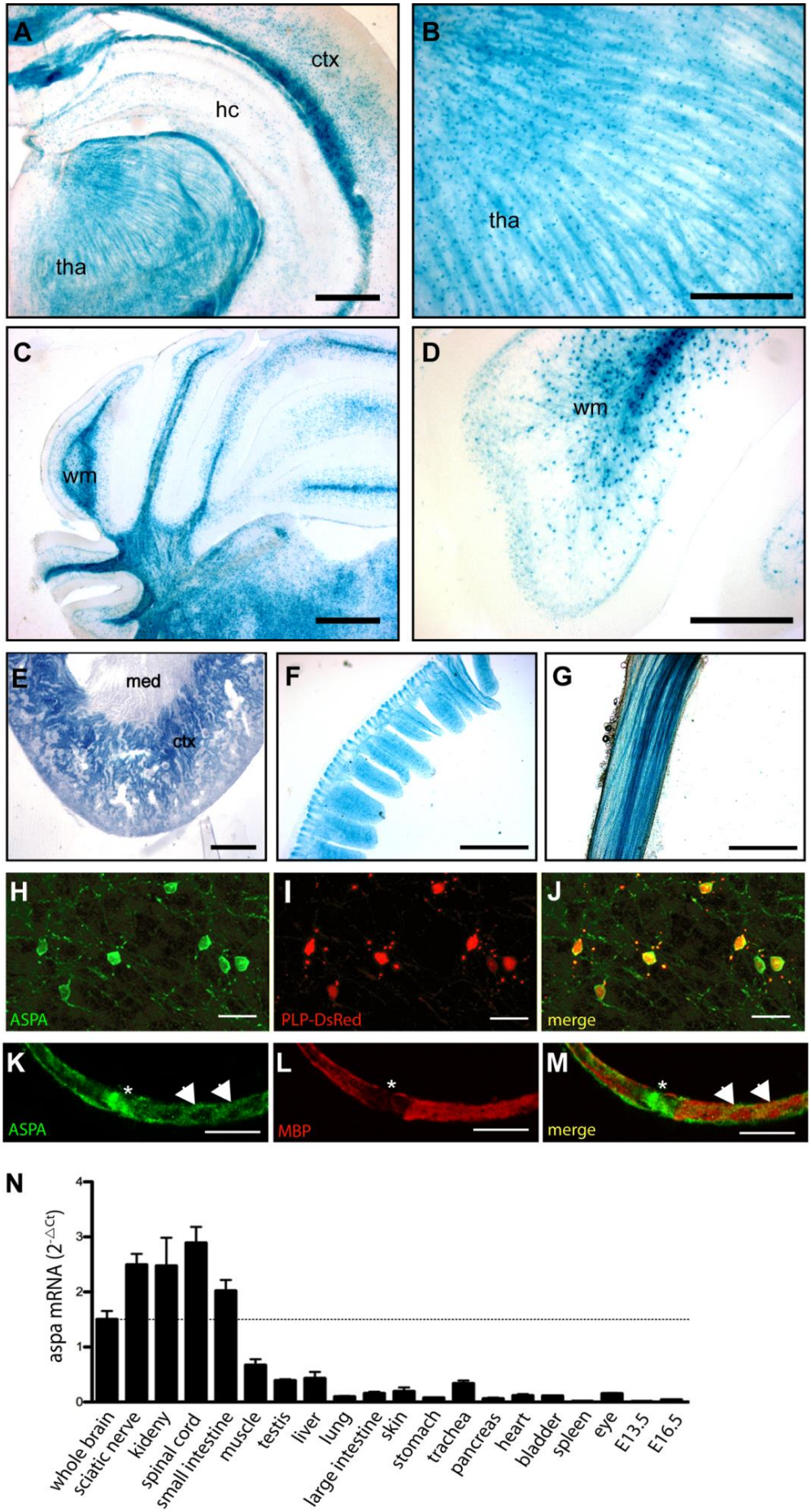
A
ctx
hc
tha
B
tha
C
wm
D
wm
E
med
ctx
F
G
H
ASPA
I
PLP-DsRed
J
merge
K
ASPA
L
MBP
M
merge
N
aspa mRNA (2-△Ct)
0
1
2
3
4
whole brain
sciatic nerve
kideny
spinal cord
small intestine
muscle
testis
liver
lung
large intestine
skin
stomach
trachea
pancreas
heart
bladder
spleen
eye
E13.5
E16.5

Figure 3.4: Analysis of *aspa* expression in CNS and periphery.
(A-D) Representative pictures of β-Galactosidase staining in adult *aspa*$^{lacZ/+}$ mouse tissues show activity of the *aspa* gene in oligodendrocytes of white and grey matter throughout the brain. Abundant staining was detected in white matter tracts in cerebellum and corpus callosum. While in the hippocampus and cortex X-Gal staining was found in oligodendrocyte cell bodies (**A**), lacZ-positive fibres were detected in the thalamus (**B**). In the cerebellum, proximal processes and somata of white matter oligodendrocytes were stained (**C, D**). **(E-G)** Outside the CNS, the cortex of the kidney (**E**), small intestine (**F**) and sciatic nerve fibres (**G**) show intense X-Gal staining. **(H-J)** Confocal detection of ASPA immunoreactivity (**H**) in cerebellar white matter of an adult Plp-dsRed-1 transgenic mouse expressing the red fluorescent reporter protein (**I**) in oligodendrocytes (HIRRLINGER *et al.* 2005). ASPA is expressed in somata and processes of oligodendrocytes. The pattern of ASPA-immunopositive cells matches the dsRed-expressing oligodendrocytes (**J**). **(K-M)** Confocal detection of ASPA immunoreactivity in cytosolic domains of wildtype Schwann cells. ASPA is enriched at the paranode (asterisk) and bands of Cajal (arrow heads) and segregates from MBP. **(N)** qRT-PCR analysis of *aspa* mRNA levels in different tissues of adult *aspa*$^{+/+}$ mice (n=6). hc, hippocampus; ctx, cortex; med, medulla; tha, thalamus; wm, white matter. Scale bars: 500 µm in A, C ,E; 200 µm in B, D; 400 µm in F, G; 20 µm in H-J; 10 µm in K-M.

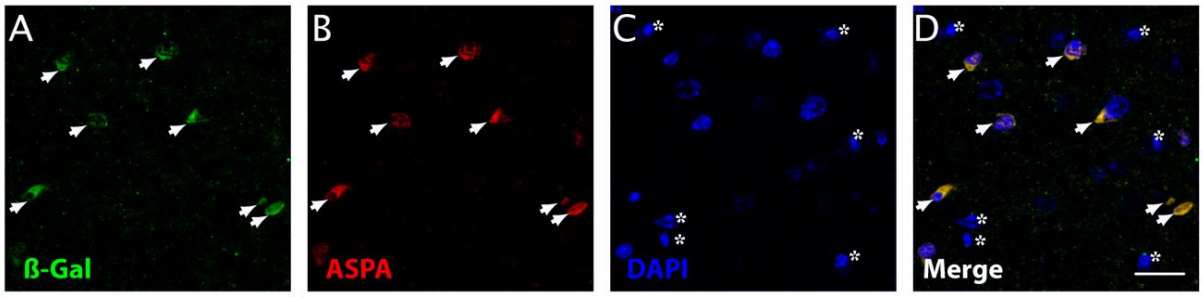

Figure 3.5: β-Galactosidase co-localises with ASPA.
Laser-confocal immunodetection of β-Galactosidase (**A**) and ASPA (**B**) in the thalamus of an *aspa*$^{lacZ/+}$ reporter mouse. **(C)** The nuclear DAPI staining shows all cells in the tissue. (**D**) The merged picture shows β-Galactosidase immunoreactivity in ASPA-positive oligodendrocytes (arrowheads) but not in other cells (asterisks). Scale bar: 20 µm.

3.3.3. Histological analysis of *aspa*$^{lacZ/lacZ}$ mutants

Histological analysis of Nissl-stained brain sections of *aspa*$^{lacZ/lacZ}$ mutants (4-month-old) revealed spongy degeneration throughout the CNS (Fig. 3.6). Vacuolisation was prominent in hippocampus, thalamus, brainstem, cerebellum, and spinal cord. In contrast, the white matter tracts of corpus callosum and optic nerve were remarkably intact (Fig. 3.7). In the hippocampus, vacuoles occurred specifically in the pyramidal cell layer while dentate granule cells were spared (Fig. 3.6 A, B). In contrast, the thalamus was uniformly affected (Fig. 3.6 C, D). Spongy degeneration was abundant in the dorsal region of the brain stem (Fig. 3.8 A, B, G, H).

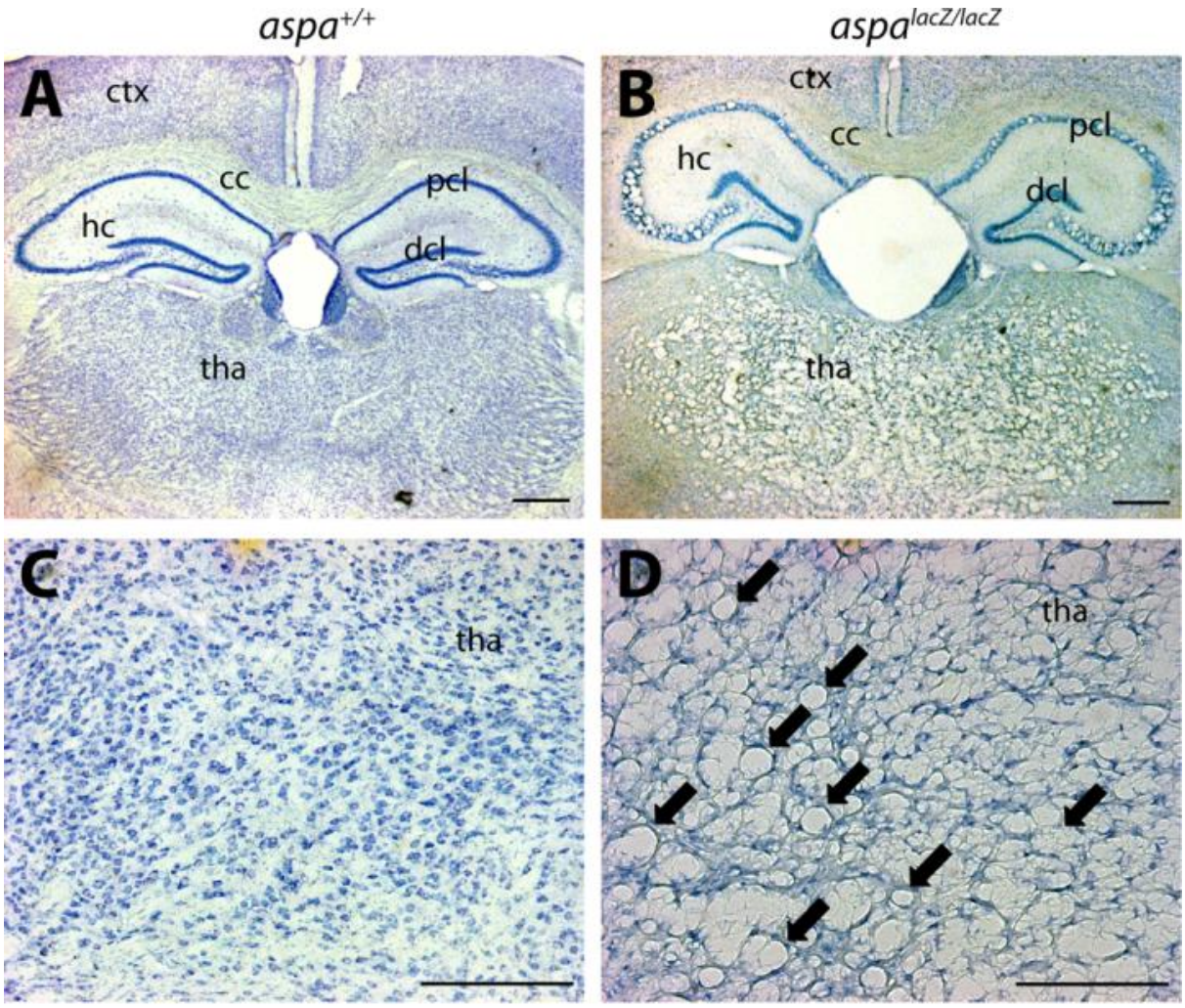

Figure 3.6: CNS vacuolisation in *aspa*$^{lacZ/lacZ}$ mutants.
Representative pictures of Nissl-stained brain sections of *aspa*$^{+/+}$ (**A,C**) and *aspa*$^{lacZ/lacZ}$ (**B,D**) mice (4-month-old). Vacuoles are abundant in forebrain grey matter of cortex and thalamus while the white matter of the corpus callosum is spared (**B**). In the hippocampus, the histopathology is exclusively seen in the pyramidal but not the dentate granule cell layer. Magnifications of thalamic areas show substantial spongy degeneration in the mutant (arrows in **D**) but not in the control (**C**). hc, hippocampus; cc, corpus callosum; ctx, cortex; dcl, granule cell layer; pcl, pyramidal cell layer; tha, thalamus. Scale bars: 400 µm (**A,B**), 200 µm (**C,D**).

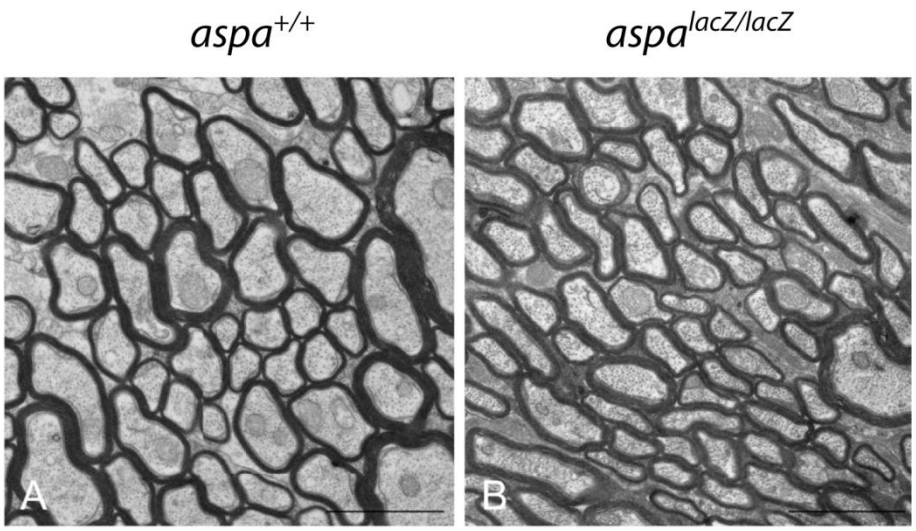

Figure 3.7: EM analysis of the optic nerve.
There are no obvious histological differences between the control (**A**) and mutant (**B**) optic nerve. Scale bar: 500 nm.

EM analysis revealed swollen and degenerated axons in the presence of normal myelin in the ventral aspect of the brain stem (Fig. 3.8 C, D). In the dorsal brain stem hypomyelination and axonal swellings were observed (Fig. 3.8 E, F). In the cerebellum, vacuolisation was detected in white matter, the granule cell layer and the Purkinje cell layer but not in the molecular layer (Fig 3.8 I, J, K, L). At the ultrastructural level, swollen Bergman glia showed accumulations of electron dense particles (Fig. 3.8 N, P). The nature of the latter could not be determined. Interestingly, the parallel fibres to Purkinje cell dendrite synapses appeared normal (Fig. 3.8 M, N).

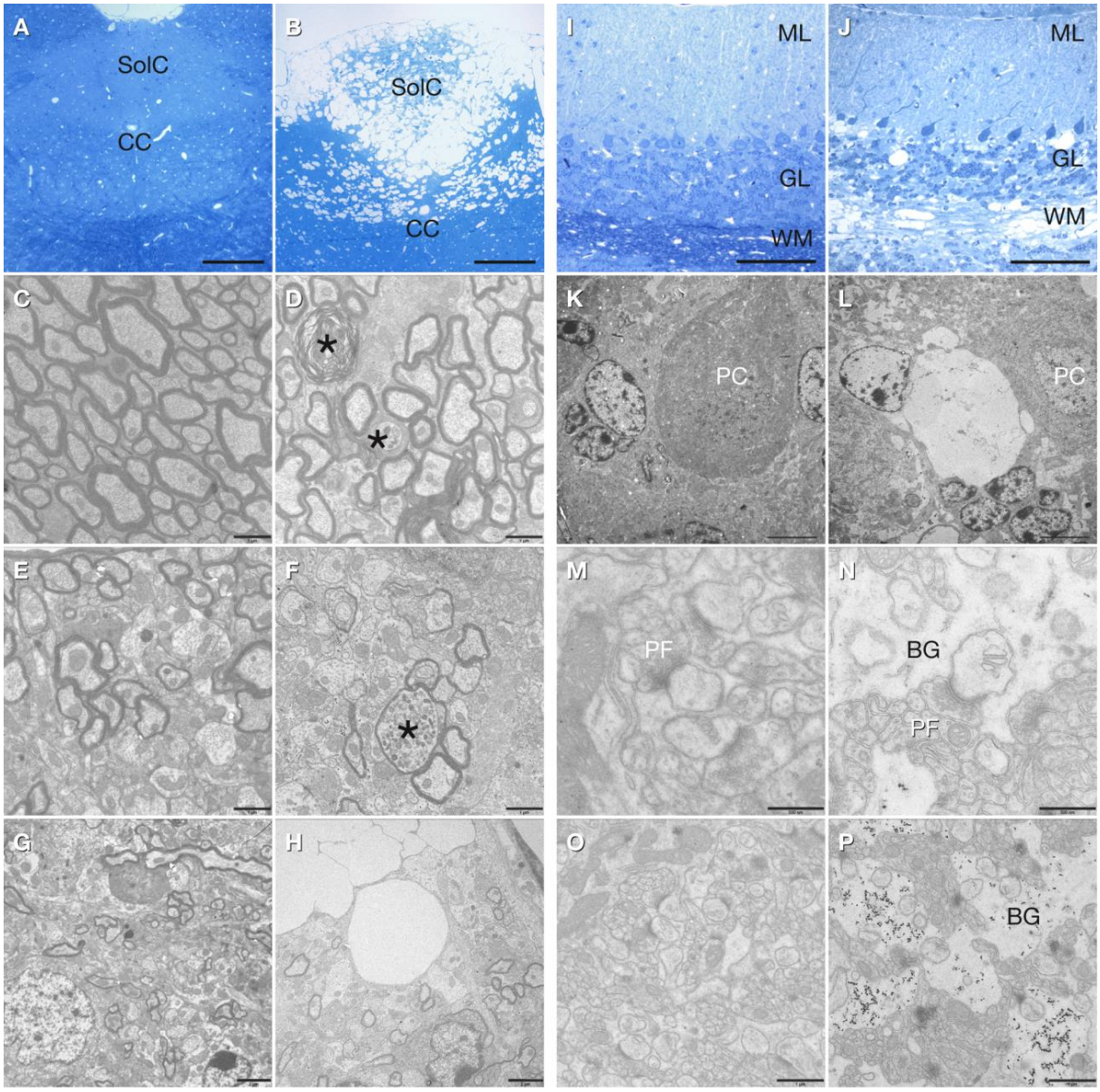

Figure 3.8: Histopathology of the brain stem and cerebellum in *aspa*$^{lacZ/lacZ}$ mice.
Caudal brain stem of controls (**A, C, E, G**) and *aspa*$^{lacZ/lacZ}$ mice (**B, D, F, H**): Vacuolisation is abundant in the dorsal region *aspa*$^{lacZ/lacZ}$ mice (solitary tract nu, commissural, SolC) as shown in semithin sections (**B**) and electron microscopy (**H**). In the pyramidal tract of mutant mice myelin appears normal, but axonal swellings and degeneration are present (**D**, asterisks). Axonal swellings as well as hypomyelination were found in the dorsal region with abundant vacuolisation (**F**, asterisk). Cerebellum of controls (**I, K, M, O**) and *aspa*$^{lacZ/lacZ}$ mice (**J, L, N, P**): In semithin sections of mutant cerebellum, vacuoles are detectable in the white matter (WM), granule cell layer (GL) and in the Purkinje cell layer (**J, L**). Parallel fibre to Purkinje cell dendrite synapses appear normal (**M, N**), but in *aspa*$^{lacZ/lacZ}$ mice the Bergman glia (BG) is swollen and shows accumulation of electron dense particles (**N, P**). BG, Bergman glia; CC, central canal; GL, granule cell layer; ML, molecular layer; PC, Purkinje cell; PF, parallel fibre; SolC, solitary tract nu, commissural; WM, white matter. Scale bars: 100 µm (**A, B, I, J**), 5 µm (**K, L**), 2 µm (**G, H**), 1 µm (**C, D, O, P**), 500 nm (**M, N**).

3.3.4. Regulation of myelin-associated proteins

Levels of myelin proteins were then investigated by immunoblot analysis of whole brain lysates of *aspa*$^{+/+}$, *aspa*$^{lacZ/+}$ and *aspa*$^{lacZ/lacZ}$ littermates (at 2 months of age; n=3 per group). In homozygous mutants, the major CNS myelin protein PLP and its smaller isoform, DM20, were reduced to 45.9 ± 1.4% (p=0.001) and 8.7 ± 2.7% (p=0.004), respectively (Fig. 3.9). The reason for the relatively stronger regulation of DM20 is unclear. The 21.5 kD and 18.5/17 kD MBP isoforms were reduced to 32.9 ± 0.9% (p<0.001) and 65.7 ± 3.8% (p=0.002), respectively. CNP was only moderately downregulated to 72.0 ± 4.8% (p=0.011). Heterozygous *aspa*$^{lacZ/+}$ mice did not differ from *aspa*$^{+/+}$ controls.

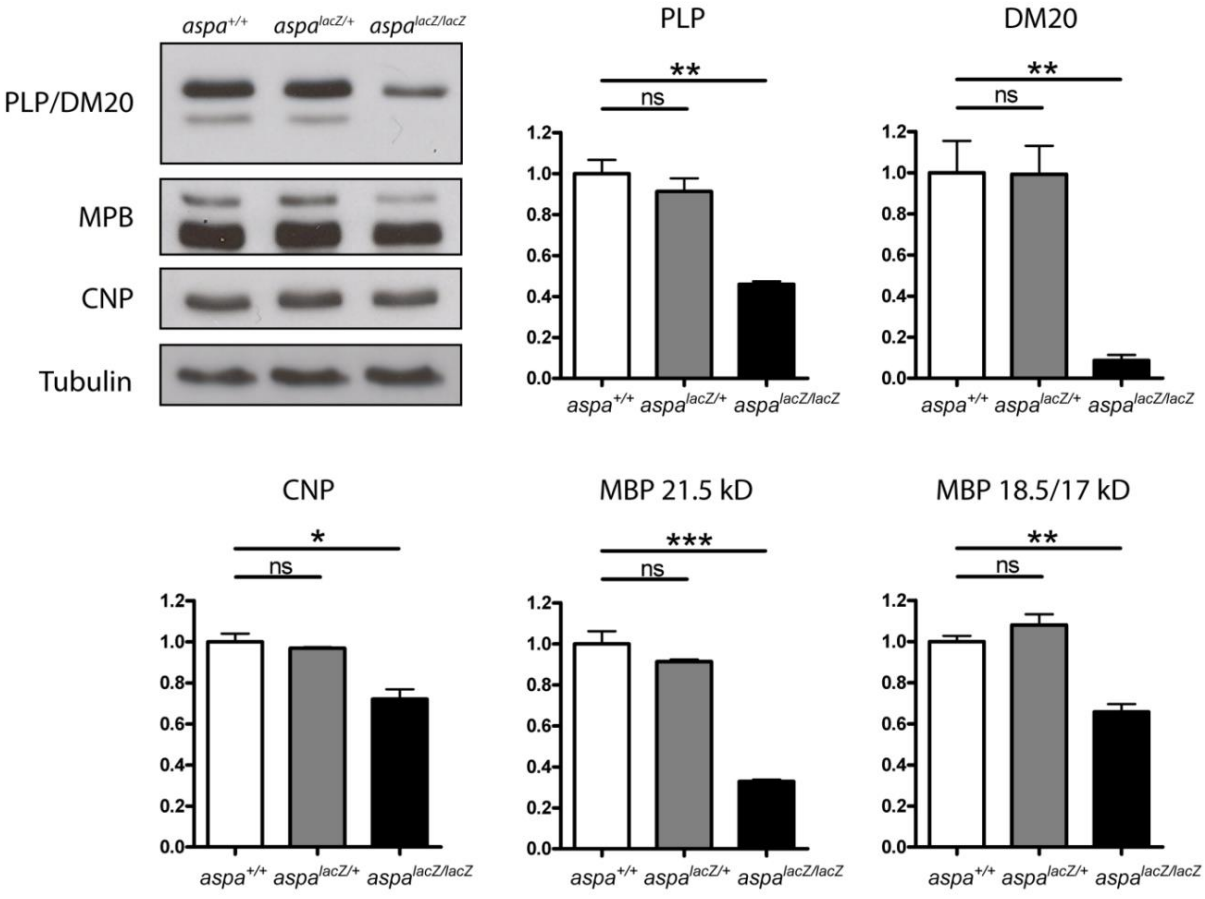

Figure 3.9: Myelin protein levels are reduced in *aspa*$^{lacZ/lacZ}$ mutants.
Western blot analysis of PLP, DM20, CNP and MBP levels in whole brain lysates of *aspa*$^{+/+}$, *aspa*$^{lacZ/+}$ and *aspa*$^{lacZ/lacZ}$ mice (P60, n=3). Quantification of immunoblots shows statistically significant decreases of all proteins tested in homozygous mutants while the presence of one functional aspa allele is sufficient to preserve protein quantities at control levels. Note: PLP, DM20, and the MBP 21.5 kD and MBP 18.5/17 kD isoforms were analysed separately.

3.3.5. Reactive gliosis in *aspa*$^{lacZ/lacZ}$ mutants

Increased numbers of astrocytes and microglia have been reported in CD (ADACHI *et al.* 1973). Therefore, immunohistochemical analyses was performed using brain sections of controls and mutants characterised by the presence (*aspa*$^{+/+}$) or absence (*aspa*$^{lacZ/lacZ}$) of ASPA immunoreactivity (Fig. 3.10). Microglia activation in the mutant thalamus was detected by Iba-1 immunohistochemistry (Fig. 3.10). Assessment of glial acidic fibrillary protein (GFAP) immunoreactivity revealed increased astrocyte numbers in the thalamus of *aspa*$^{lacZ/lacZ}$ mice.

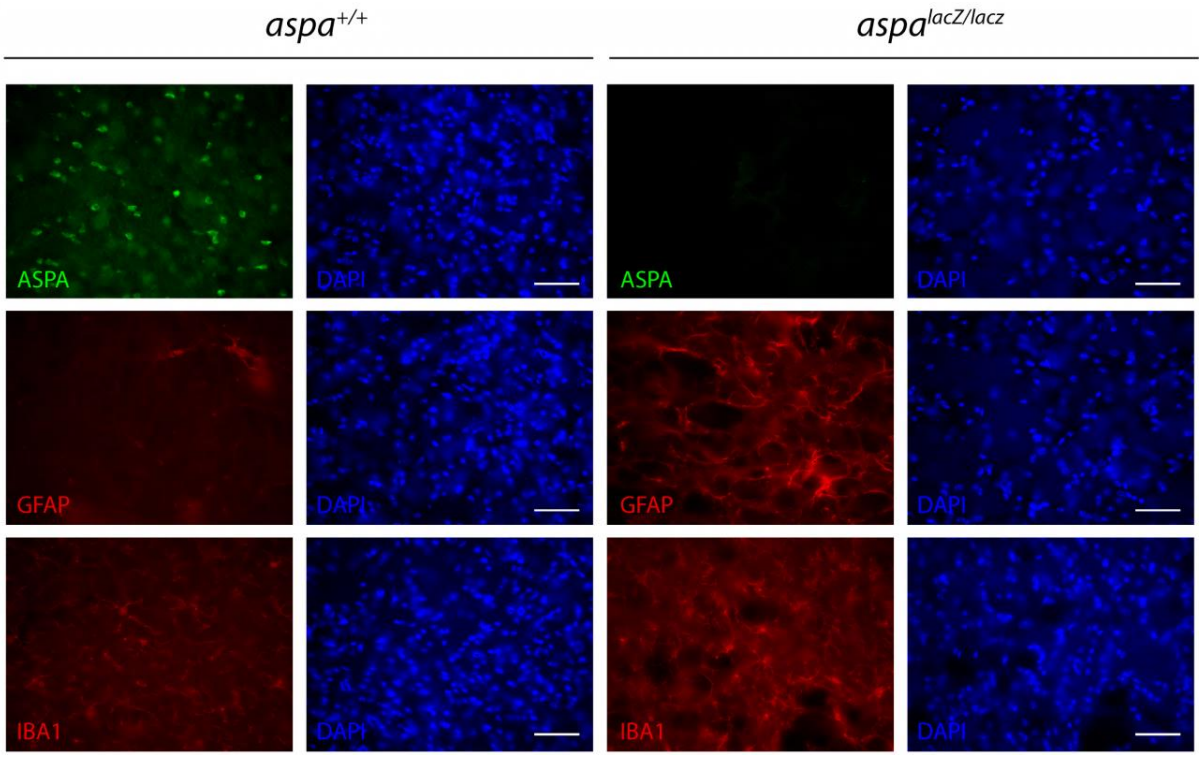

Figure 3.10: Reactive gliosis in *aspa*$^{lacZ/lacZ}$ mice.
Immunohistochemical staining in the thalamus of *aspa*$^{+/+}$ controls and *aspa*$^{lacZ/lacZ}$ mice showed substantially increased numbers of GFAP-positive astrocytes and Iba-1-positive microglia in the mutants (at 3 months of age). Note that ASPA immunoreactivity is present in the control but not in the mutant. Scale bars: 25 µm.

3.3.6. *In vivo* determination of brain metabolites in *aspa*$^{lacZ/lacZ}$ mice

The lack of ASPA leads to accumulation of its substrate NAA in brains of patients and CD models (KLUGMANN and LEICHTLEIN 2006; TRAKA *et al.* 2008). Ultrahigh field proton magnetic resonance spectroscopy (^{1}H-MRS) at 9.4T allows non-invasive quantification of metabolites, like NAA, glutamate, glutamine, GABA, taurine, and glucose in the living rodent brain (Fig. 3.11). It was focused

on the thalamus and prefrontal cortex because these regions showed high and low degree of vacuolisation, respectively. Analysis revealed substantially more of NAA (255.8%), myo-inositol (330.6%), taurine (204.4%) and glutamine (122.0%) in the *aspa*$^{lacZ/lacZ}$ thalamus compared to the control, while glutamate was reduced by 67% and GABA by 31.4% (Table 3.1). Due to limitations in resolution, the N-acetylaspartylglutamate (NAAG) peak could not be discerned from the NAA signal. While in the prefrontal cortex there was an increase in NAA (75.5%), myo-inositol (75.4%) and taurine (22.4%), these changes were not as prominent as in the thalamus. Of note, the reduction in GABA (26.4%) was similar to that seen in thalamus while creatine was virtually unchanged in both areas.

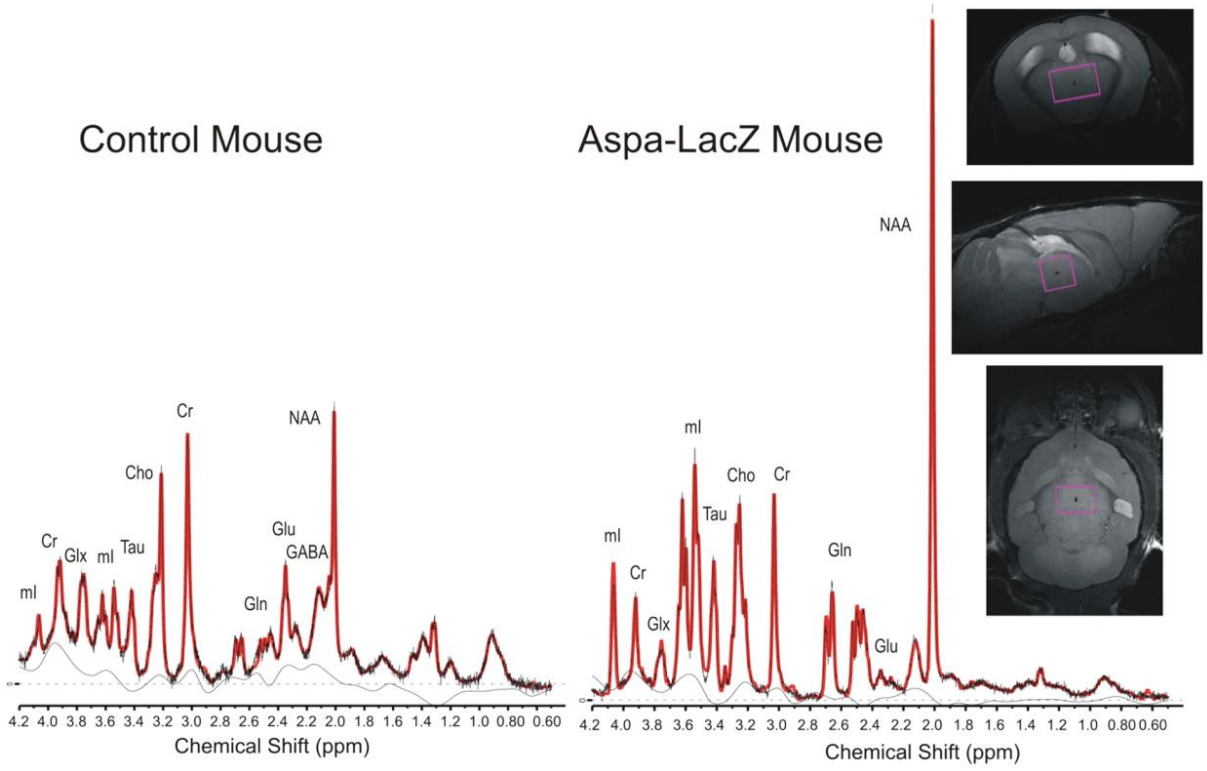

Figure 3.11: ^{1}H-MRS analysis.
Spectra were acquired from *aspa*$^{+/+}$ and *aspa*$^{lacZ/lacZ}$ littermates using a 2x2x3 mm³ single-voxel PRESS Sequence in the thalamus. Representative metabolites are marked in the spectra (Cr: Creatine and Phosphocreatine, NAA: NAA+NAAG, Cho: Phosphocholine and Glycerophosphorylcholine, Glu: Glutamate, Gln: Glutamine, mI: Myo-Inositol, Tau: Taurine, Glx: Glu+Gln). For metabolite concentrations see Table 3-1.

Table 3.1*: In vivo* metabolite concentrations determined by ^{1}H-MRS

	Thalamus			Prefrontal Cortex		
	Control mouse	Aspa-LacZ	Change	Control mouse	Aspa-LacZ	Change
	[mM/l] ± %SD	[mM/l] ± %SD	%	[mM/l] ± %SD	[mM/l] ± %SD	%
GABA	3.84 ± 4	2.63 ± 10	-31.4%	2.65 ± 7	1.95 ± 22	-26.4%
Glc	6.19 ± 6	4.63 ± 12	-25.2%	7.19 ± 5	N/A ± N/A	N/A
Tau	5.50 3	16.75 2	204.4%	11.53 2	14.1 ± 2 3	22.4%
Gln	3.65 ± 4	8.12 ± 3	122.2%	2.36 ± 6	2.38 ± 14	0.7%
Glu	9.28 ± 2	3.06 ± 9	-67.0%	11.21 ± 2	8.25 ± 5	-26.4%
mI	8.06 2	34.70 1	330.6%	6.59 3	11.5 ± 6 5	75.4%
Lac	5.08 ± 4	2.55 ± 12	-49.9%	3.90 ± 6	3.48 ± 16	-10.9%
Ch	2.58 ± 2	1.30 ± 4	-49.5%	2.35 ± 2	2.59 ± 5	10.4%
NAA	11.56 2	41.13 1	255.8%	11.21 2	19.6 ± 8 3	75.5%
Cr	9.66 ± 1	10.75 ± 2	11.4%	9.50 ± 2	9.50 ± 4	0.0%

Metabolite concentrations were measured over a 2x2x3 mm³ and 3x1.2x2.8 mm³ volume of interest in the thalamic region and the prefrontal cortex, respectively. The standard deviation of the metabolite concentrations (SD) corresponds to the Cramér-Rao lower bounds of the LCModel-fit and is given in %. SD-values below 20% are considered reliable. Error bars are derived through the fit-routine and indicate the quality of individual metabolite measurements. Cr: Creatine and Phosphocreatine, NAA: NAA+NAAG, Cho: Phosphocholine and Glycerophosphorylcholine, Glu: Glutamate, Gln: Glutamine, mI: Myo-Inositol, Tau: Taurine, Glc: Glucose.

Interstitial NAA levels can also increase via the hydrolysis of NAAG by the astrocyte-specific plasma membrane enzyme folh1/glutamate carboxypeptidase II (EC 3.4.17.21). Therefore, mRNA expression levels of this enzyme were determined. No changes were detectable in *aspa*$^{lacZ/+}$ animals (103.9 ± 6.9%; p=0.652) but a reduction of 48.1 ± 3.6% (p<0.0001) was found in *aspa*$^{lacZ/lacZ}$ mice (Fig. 3.12). This decrease was not due to a reduction in astrocyte numbers (Fig. 3.10) and might represent a cellular mechanism to prevent additional generation of NAA from NAAG in an environment of pathologically enriched NAA.

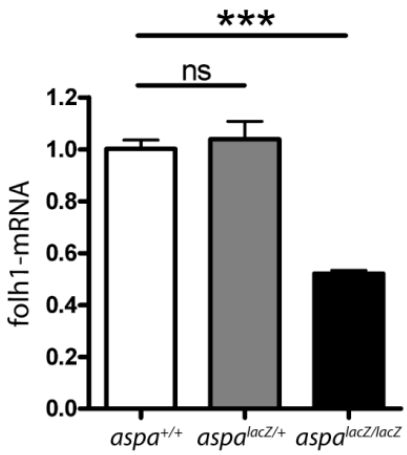

Figure 3.12: Downregulation of *folh1* expression in the absence of ASPA.
Q-PCR analysis for detection of folh1 in total RNA isolated from whole brains of *aspa*$^{+/+}$, *aspa*$^{lacZ/+}$ and *aspa*$^{lacZ/lacZ}$ littermates (P60, n=3) shows decreased *folh1* mRNA in homozygous mutants. *gusb* expression levels were used as a nominator.

3.3.7. Assessment of general locomotion and motor learning

CD is characterised by general muscle weakness and the failure to develop motor control. Male and female mutants, but not their respective littermate controls, displayed ataxia with splayed hind legs and a general lack of muscle tonus starting at the age of 3-4 weeks. These gait abnormalities progressed gradually to obvious deficits in motor co-ordination and weakness especially in the hind limbs. At the time of this thesis, the average life expectancy of *aspa*$^{lacZ/lacZ}$ was 14.9 $\pm$ 0.7 months (n=10) suggesting a reduced longevity. However, they showed progressive immobility and impaired motor function characterised by spasticity and jerky movements. In the beginning of the evaluation of general locomotion and motor learning aged-matched (P90) cohorts of mutant and wt mice were used that included pools of both sexes. However, inconsistent data was obtained. Therefore, male *aspa*$^{lacZ/lacZ}$ and *aspa*$^{+/+}$ littermates were analysed separately from the female cohorts. To quantify behavioural deficits in younger animals, motor coordination was assessed using the rotarod test. At P90, significant differences were observed between male and female cohorts (males: *aspa*$^{+/+}$ 203.3 $\pm$ 26.2 s vs. *aspa*$^{lacZ/lacZ}$ 100.2 $\pm$ 11.0 s; p=0.0012; two-tailed t-test; females: *aspa*$^{+/+}$ 210.5 $\pm$ 21.2 s vs. *aspa*$^{lacZ/lacZ}$ 120.9 $\pm$ 11.2 s; p=0.0046; two-tailed t-test) (Fig. 3.13 A).

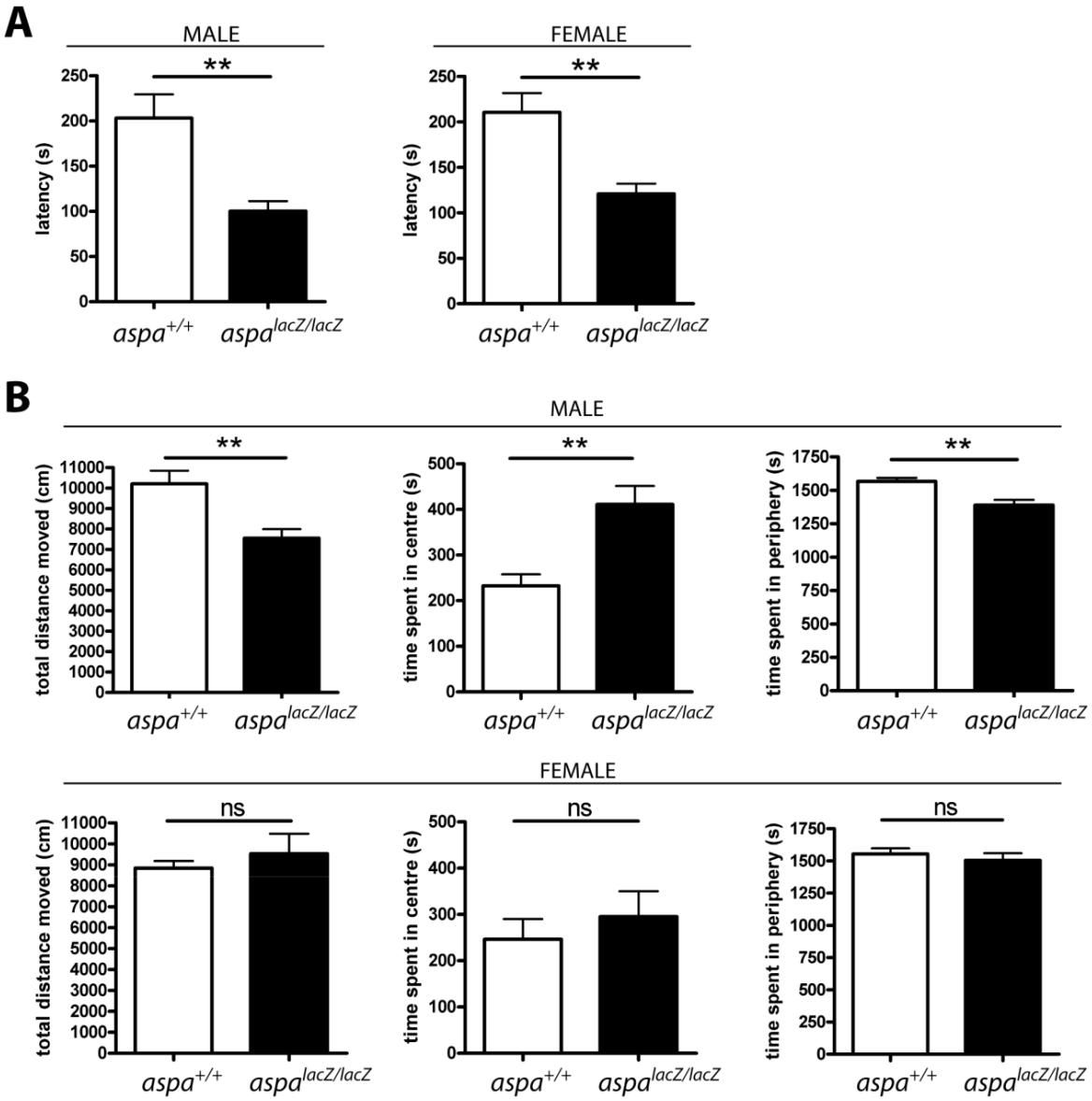

Figure 3.13: Special behavioural deficits in male but not female *aspa*$^{lacZ/lacZ}$ mutants.
(A) Analysis of motor coordination in the rotarod test shows impairment of both female and male *aspa*$^{lacZ/lacZ}$ mice compared to their *aspa*$^{+/+}$ controls at P90. **(B)** Spontaneous exploratory activity and aspects of anxiety-related behaviour of both sexes and genotypes were tested in an open field for 30 min (see Methods section). Male mutants (n=8) travelled less and spent more time in the centre than male controls (n=8). This behaviour is suggestive of impaired exploratory activity and anxiolysis. The behaviour of female mutants (n=6) did not differ from female controls (n=7).

Furthermore, the inherent locomotor and exploratory activity of both cohorts in was in an open-field test (Fig. 3.13B). Motor activity monitored by the total distance travelled over a 30 min period, was reduced in male (*aspa*$^{+/+}$ 10206 $\pm$ 642.1 s vs. *aspa*$^{lacZ/lacZ}$ 7547 $\pm$ 439.2 s; p=0.0042; two-tailed t-test) but not in female mutants compared to sex-matched controls (*aspa*$^{+/+}$ 8838 $\pm$ 340.9 s vs. *aspa*$^{lacZ/lacZ}$ 9527 $\pm$ 955.0 s; p=0.4849; two-tailed t-test). Male mutants spent more time in the centre

of the test arena than controls (*aspa*$^{+/+}$ 232.6 ± 25.3 s vs. *aspa*$^{lacZ/lacZ}$ 411.2 ± 40.1 s; p=0.0071; two-tailed t-test) and only slightly less time in the periphery (*aspa*$^{+/+}$ 1567 ± 25.3 s vs. *aspa*$^{lacZ/lacZ}$ 1389 ± 40.1 s; p=0.0021; two-tailed t-test), suggesting reduced anxiety-like behaviour. In contrast, there was no difference within the female cohort (Centre: *aspa*$^{+/+}$ 246.5 ± 44.0 s vs. *aspa*$^{lacZ/lacZ}$ 295.2 ± 55.2 s; p=0.4989; Periphery: *aspa*$^{+/+}$ 1554 ± 44.0 s vs. *aspa*$^{lacZ/lacZ}$ 1505 ± 55.2 s; p=0.4989; two-tailed t-test).

3.4. Discussion

3.4.1. *Aspa*$^{lacZ/lacZ}$ mice as a tool to study ASPA expression

The present study describes a novel ASPA-deficient mouse mutant obtained by a targeted insertion of the βgeo cassette in-frame with exon 1 of the *aspa* gene. The gene trap approach allowed to re-capitulate the activity of the endogenous *aspa* promoter by expression of the *lacZ* reporter in central and peripheral tissues. In fact, present data show that in the mouse, *aspa* mRNA quantities in kidney, small intestine and sciatic nerve were higher than in brain indicating a role for NAA deacetylation in normal peripheral tissues. The loss of ASPA in the periphery appears to be well-tolerated in humans because the pathology in CD is restricted to the CNS (MATALON *et al.* 1995). The failure to degrade NAA and/or other unknown substrates in ASPA expressing peripheral organs might have indirect toxic consequences for the CNS without inducing major histological abnormalities in the periphery. While a previous study employed *in situ* hybridisation and reported on the lack of *aspa* mRNA signals in sciatic nerve (KIRMANI *et al.* 2003), this study provides strong evidence for the presence of high levels of *aspa* mRNA in Schwann cells. NAA was reported in sciatic nerve and ASPA-dependent deacetylation might contribute to lipid synthesis during PNS myelination similar to the function of ASPA in oligodendrocytes (MADHAVARAO *et al.* 2005; ORY-LAVOLLEE *et al.* 1987). This raises the possibility that ASPA-deficiency might have detrimental effects for peripheral nerve integrity. However, *aspa*$^{lacZ/lacZ}$ sciatic nerve tissue showed no gross abnormalities confirming a report on the normal PNS of the spontaneous ASPA-null tremor rat (KONDO *et al.* 1991). Of the few reports on peripheral nerve tissue of CD patients, only one case showed axonopathy and demyelination, but no vacuolisation (SUZUKI 1968), suggesting that this unique peripheral lesion might represent a coincidence rather than a consequence of ASPA-deficiency. How can the remarkably abundant expression of ASPA in normal Schwann cells be reconciled with the unaffected integrity of ASPA-null

peripheral nerves? The physiology of peripheral nerve fibres differs from those in the CNS and Schwann cells might be more resistant to the effects of ASPA-deficiency (i.e. decreased pools of acetate, NAA toxicity) than oligodendrocytes. Alternatively, there might be subtle functional abnormalities in the ASPA-null PNS that are yet to be identified.

3.4.2. CD-like histopathology and metabolic imbalances in *aspa*$^{lacZ/lacZ}$ mutants

Ultrahigh field proton magnetic resonance spectroscopy revealed a substantial increase in levels of NAA but also taurine and myo-inositol in thalamus, and to a lesser extent in prefrontal cortex of *aspa*$^{lacZ/lacZ}$ mutants. Increased taurine in the *aspa*$^{lacZ/lacZ}$ brain may contribute to preservation of neuronal function via $GABA_A$-mediated hyperpolarisation of thalamic relay neurons (JIA *et al.* 2008). The profound increase in NAA in the CD brain is unique among neurological conditions and NAA-toxicity had been proposed as a reason for neuronal dysfunction (ASSADI *et al.* 2010; PEDERZOLLI *et al.* 2009). The efflux of NAA from neurons to the extracellular space is accompanied by a co-transport of water molecules, causing the interstitial pressure to rise (BASLOW 2002). Myo-inositol is a major osmolyte and serves as the precursor to phosphatidylinositol, a major membrane phospholipid. Extracellular tonicity induces the transport of myo-inositol from the outside to the inside of neurons and astrocytes (ULDRY *et al.* 2001). In the ASPA-deficient brain, the dramatic increase in astrocyte numbers and concomitant increase in interstitial pressure may lead to glial uptake of myo-inositol to prevent cytotoxic damage to hypertonic neurons. The contribution of myo-inositol to the metabolic pathology in CD patients might have been underestimated since studies using *in vivo* imaging of CD brains detected no or only a moderate increase in prefrontal cortex or cerebellar white matter, respectively (BLUML 1999; CAKMAKCI *et al.* 2010). These human data did not provide information on the thalamus. This results of this study show only a slight increase in prefrontal cortex myo-inositol. However, the changes in thalamus were severe, indicating that more dramatic metabolic changes might occur in the thalamus of the CD brain.

Although the NAAG signal was not determined, down-regulation of the NAAG-degrading enzyme folh1 in mutants indicates that levels of this metabolite may be increased. NAAG is neuroprotective in a number of neurological diseases by inhibiting the release of glutamate and GABA after activation of presynaptic mGluR3 (NEALE *et al.* 2005). In fact, both neurotransmitters were found to be decreased in the *aspa*$^{lacZ/lacZ}$ brain indicating that this neuroprotective mechanism might take place. ASPA is not expressed in astrocytes, yet this cell type appears to be particularly vulnerable for the osmotic downstream effects of accumulated NAA because astroglia are integral for the metabolism of NAAG, NAA and myo-inositol.

Swellings and vacuolisation appear within astrocytes before they become more prominent in the interstitium of CD patients (ADACHI *et al.* 1973). These abnormalities precede widespread neuronal damage and neurological deterioration suggesting that astroglia may buffer some of the excess metabolites to compensate extracellular tonicity, sustain axonal integrity and promote neuronal survival. Bergmann glia contained osmiophilic inclusions reminiscent of accumulations of glycogen granules. The identity of these electron-dense particles could not be determined and might represent advanced stages of intracellular digestion of phagocytosed material, or signs of direct damage to the Bergmann glia fibres.

Damaged CNS neurons have been reported in CD, the aspa^{Nur7} mutant, the tremor rat and the *aspa*^{lacZ} mouse (KAMOSHITA *et al.* 1967; KLUGMANN *et al.* 2005; TRAKA *et al.* 2008), suggesting that changes in axon integrity and metabolic status of the neuron contribute to the complex pathology. ASPA expression has been detected in wildtype neurons (MADHAVARAO *et al.* 2004) and one could speculate that ASPA-mediated degradation of NAA might become important in energetically challenged neurons (NAVE 2010). This concept is supported by reports on increased *aspa* gene activity in peripheral tissues in non-CNS diseases and is yet to be shown to occur in neurons (SURENDRAN *et al.* 2006; VAN DER HEUL-NIEUWENHUIJSEN *et al.* 2006). The distinct anatomical regions where spongy degeneration and hypomyelination occurred might be accounted for by the fact that different types of oligodendrocytes show regional variation in their connectivity to astrocytes via gap junctions, an important factor in regulating osmotic and metabolic homeostasis (ORTHMANN-MURPHY *et al.* 2008).

Congenital, infantile and juvenile forms of CD showing variable disease onset and severity have been suggested, with the moderate infantile category being the most frequent form by far (MATALON *et al.* 1995; TACKE *et al.* 2005). The pathology observed in *aspa*$^{lacZ/lacZ}$ mutants includes region specific spongy vacuolisation of the CNS, elevated NAA levels, demyelination, gliosis and impaired motor behaviour. As such, this mouse line is an accurate model of infantile CD. The *aspa*$^{lacZ/lacZ}$ line has been derived from C57BL/6J ES cells and shows a considerably milder phenotype compared to the previously described Aspa-ko mouse (MATALON *et al.* 2000). The latter line was obtained after the targeted deletion of the *aspa* gene in SV129 ES cells and shows motor seizures and premature death occurring as early as at 2 months of age. It is tempting to speculate that the genetic background can modify disease severity. Another major difference between the two lines is that the *aspa*^{lacZ} allele was targeted with a promoterless selection marker while in Aspa-ko mice the *neo* gene is driven by the strong *pgk* promoter that has been suggested to interfere with the activity of genes adjacent to *aspa* (OLSON *et al.* 1996; TRAKA *et al.* 2008). Consequently, the severe phenotype of the Aspa-ko mouse was suggested to be caused by multiple gene effects (TRAKA *et al.* 2008) that might

also account for subtle differences i.e. unchanged folh1 activity in Aspa-ko mice (SURENDRAN *et al.* 2004a) versus 50% *folh1* mRNA reduction in *aspa*$^{lacZ/lacZ}$ mice (this study). Interestingly, homozygous *aspa*^{Nur7} transgenic mice, carrying an *aspa* nonsense mutation identified in an ENU mutagenesis screen (TRAKA *et al.* 2008), show virtually the same mild neurological and histological abnormalities as the targeted *aspa*$^{lacZ/lacZ}$ line. Additional ENU-induced mutations in other genes of the *aspa*^{Nur7} mutant cannot be excluded, but both *aspa*^{lacZ} and *aspa*^{Nur7} mutants are on the C57BL/6J background eliminating genetic strain differences. In summary, the *aspa*^{lacZ} mouse is unique because the underlying genetic modification is restricted exclusively to the *aspa* gene, does not influence adjacent genes, and allows for screening of *aspa* gene activity.

3.4.3. Sexual dimorphism in behavioural outputs of *aspa*$^{lacZ/lacZ}$ mice

Behavioural phenotyping of *aspa*^{lacZ} mutants revealed sex-specific consequences of ASPA-deficiency. Rotarod performances were equally impaired in female and male mutants while different aspects of locomotor behaviour and inherent anxiety as monitored in the open field arena revealed sexual dimorphisms. There are no reports on gender-specific differences in behavioural test performance for the ASPA-ko or *aspa*^{Nur7} mouse lines. However, a recent study using the natural ASPA-null *tremor* rat (KITADA *et al.* 2000) showed that locomotor activity is less impaired in female *tremor* rats than males (ARUN *et al.* 2010). What mechanisms could account for these observations? Sexual dimorphism of oligodendrocytes in rodents and humans has been described and there is evidence for androgens to control oligodendrocyte differentiation and survival by signaling through their receptors expressed by oligodendroglia (reviewed in (CERGHET *et al.* 2009)). Therefore, the vulnerability of ASPA-deficient oligodenroglia may be different between female and male *aspa*$^{lacZ/lacZ}$ mutants and this could translate into differences at the behavioural level.

In summary, *aspa*$^{lacZ/lacZ}$ mice represent the accurate model of Canavan disease, and this line, as well as conditional *aspa*$^{f/f}$ mutants derived from this line, will be essential research tools to genetically dissect the mechanisms underlying CD and to design and test effective treatment strategies.

Chapter 4:

AAV-mediated transgene expression in oligodendrocytes

4. AAV-mediated transgene expression in oligodendrocytes

Recombinant adeno-associated viral (rAAV) vectors have become a versatile tool for gene transfer to the central nervous system because they are efficient, non-toxic and replication-deficient. Based on their inherent neurotropism, AAV-based gene delivery has entered the clinics for the treatment of neurodegenerative diseases. However, the lack of viral vectors with oligodendroglial tropism has precluded gene therapy for leukodystrophies, a group of hereditary disorders caused by oligodendrocyte dysfunction. This study aimed to determine whether the transduction profile of established AAV serotypes could be targeted towards oligodendrocytes via transcriptional tropism. To address the feasibility of that strategy, the tropism of AAV8, AAV1, and mosaic AAV1/2 vectors expressing the enhanced green fluorescent protein (EGFP) under the control of the myelin basic protein (MBP) promoter or the chicken β-actin (CBA) promoter was investigated. All vectors carrying the CBA promoter exclusively transduced neurons *in vitro* and *in vivo*. The MBP promoter was sufficient to restrict transgene expression to cultured oligodendrocytes for AAV1/2 and AAV8 while AAV1 showed some additional astroglial transduction. These results were confirmed after transfection of the unpackaged AAV constructs, suggesting that the CBA promoter is inactive in oligodendrocytes. AAV1/2-MBP-injection into the brain of adult mice resulted in robust, yet non-exclusive transduction of oligodendroglia *in vivo*, and these transduction characteristics were unaffected by the transgene and the purification method. The transduction specificity was further optimised by employing a novel conditional AAV expression system. These findings are going to be extended to the treatment of white matter diseases or whenever safe and efficient gene transfer to oligodendrocytes is required.

4.1. Introduction

Recombinant adeno-associated virus (rAAV) vectors are arguably the most popular vehicles for somatic gene transfer to the central nervous system (CNS) because they are inherently replication-deficient, non-pathogenic and readily infect post-mitotic cells (McCown 2005). AAV has become an attractive tool for both gene function studies and therapeutic approaches by genetic complementation or RNAi, because after transduction of post-mitotic cells, the recombinant vector genomes largely remain as episomal structures in the nucleus (McCarty *et al.* 2004) allowing for easy access by the cellular transcription machinery. This is the basis for long-term and robust expression of the transgene and avoids the problem of chromatin position effects observed for germ line transgenics.

It is widely accepted that the tropism of individual types of AAV vectors (serotypes) is determined by interactions between viral capsid proteins and specific cell surface receptors and co-receptors (BUNING *et al.* 2008). Virtually all AAV serotypes that were characterised in the context of CNS gene delivery transduce neurons with strong preference (CEARLEY and WOLFE 2006; KLEIN *et al.* 2008b; TAYMANS *et al.* 2007). The inherent neurotropism of AAV has been successfully employed for the treatment of neurodegenerative conditions in preclinical animal models and humans (FEIGIN *et al.* 2007; FRANICH *et al.* 2008; KAPLITT *et al.* 2007) but represents an obstacle for delivery of genes to oligodendroglia, the myelin forming cells in the CNS. Molecular abnormalities of oligodendrocytes (OLs) cause leukodystrophies, a group of hereditary disorders characterised by defects in the myelin sheath and the underlying axons. Therefore, somatic gene transfer to oligodendrocytes is essential for improvements in understanding of the pathophysiology of leukodystrophies, generation of animal models, and testing of genetic treatment strategies. Several approaches have been described to overcome the natural tropism (BUNING *et al.* 2008). Non-neuronal cellular promoters were employed to transduce the glial compartment after AAV-mediated delivery, yielding mixed results but generally suggesting the feasibility of this approach (CHEN *et al.* 1998; CHEN *et al.* 1999; LAWLOR *et al.* 2009; XU *et al.* 2001).

The aim of this study was to characterise the transcriptional tropism of AAV vectors expressing transgenes under the control of oligodendrocyte-specific or constitutive promoters. AAV2 vectors have been reported to be safe and efficient in clinical applications requiring focal transduction of neurons (KAPLITT *et al.* 2007; LEWITT *et al.* 2011). However, in this study AAV1/2 vectors were applied, which are mosaic virions that are AAV2-based, but show a superior transduction efficiency (RICHICHI *et al.* 2004). The proximal cis-acting fragment of the myelin-basic protein (MBP) gene was used to target transgene expression in oligodendrocytes.

This study shows that the MBP promoter conveys efficient and widespread transduction of oligodendrocytes *in vitro* and *in vivo*. These findings may help to pave the way for research directed at both the pathomechanisms and treatment of leukodystrophies.

4.2. Materials and Methods

4.2.1. Plasmid constructs

The enhanced green fluorescent protein (EGFP) cDNA was subcloned into a rAAV plasmid backbone under the control of the 1.1 kb CMV enhancer/chicken β-actin hybrid promoter (CBA) (FITZSIMONS *et al.* 2002) (Fig 4.1 A). The rAAV cassette contained the woodchuck hepatitis virus post-transcriptional regulatory element (WPRE) and the bovine growth hormone polyadenylation sequence (bGHpA) flanked by AAV2 inverted terminal repeats.

The 1.3 kb HindIII-fragment of the mouse MBP-promoter (IKENAKA *et al.* 1992), derived from plasmid MBP/IP250+ (TAMURA *et al.* 2001), was then cloned into the HindIII-site of pBluescriptKS and transferred using EcoRI (blunt) and Asp718 into the standard AAV cassette (Fig 4.1 B).

The EGFP cDNA was replaced by HA-tagged human aspa cDNA (KLUGMANN *et al.* 2005) for the assessment of the effects of the transgene on vector tropism (Fig 4.1 C, D).

A 340 bp transcriptional stop-cassette, designed to entail a herpes simplex virus thymidin kinase pA signal and a pA terminator from pGL3 (Promega, Madison, USA) flanked by loxP sites (GUGGENHUBER *et al.* 2010), was excised from pBlueScriptSK by EcoRV and HpaI, and was then cloned into the EcoRV-site downstream of the MBP promoter in pAAV-MBP-EGFP to obtain pAAV-MBP-Stop-EGFP (Fig 4.1 E).

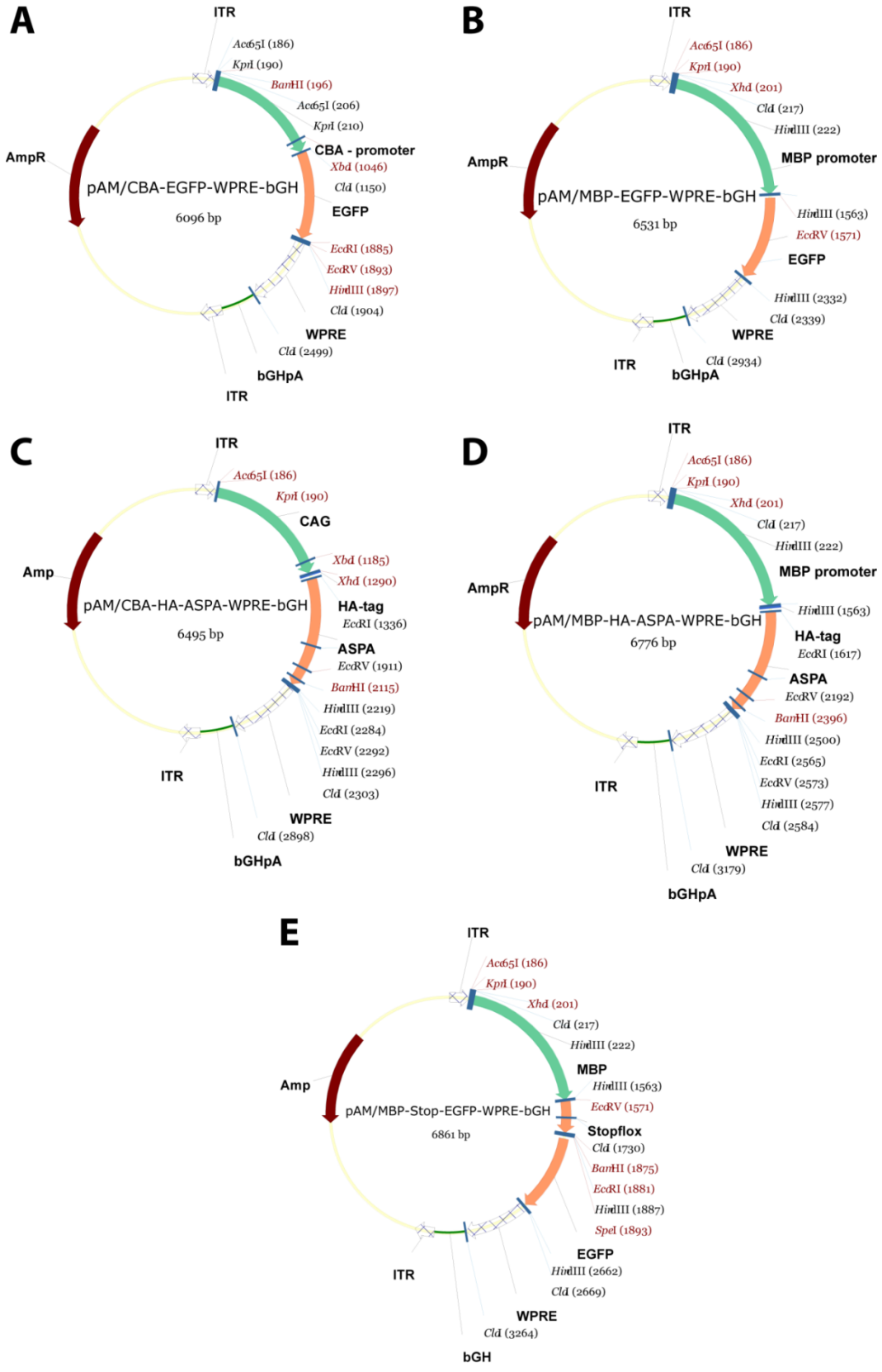

Figure 4.1: Schematic representation of the vectors used in the present study.
To generate plasmid pAM-MBP-EGFP-WPRE-bGH (**B**) the 1.1 kb CBA promoter from (**A**) was replaced by the 1.3 kb MBP promoter (IKENAKA and KAGAWA 1995). (**C, D**) The EGFP cDNA was replaced by HA-tagged human aspa cDNA (KLUGMANN *et al.* 2005) for the assessment of rAAV genome on vector tropism. (**E**) A transcriptional stop-cassette flanked by loxP sites was fused downstream to the MBP promoter to generate pAAV-MBP-Stop-EGFP-WPRE-bGH.

4.2.2. AAV vector production

4.2.2.1. HEK293 cell culture

Human Embryonic Kidney 293 (HEK293) cells were purchased from ATCC Manassas, USA. Tissue culture dishes were purchased from NUNC (Langenselbold, Germany)**.** Sterile plastic tubes (50 ml and 15 ml) were purchased from Greiner bio-one (Solingen, Germany). All cell culture reagents were purchased from LIFE Technologies GIBCO (Darmstadt, Germany), if not stated otherwise. Fetal calf serum (FCS) was purchased from PAA (Cölbe, Germany) and DMSO from Carl Roth (Karlsruhe, Germany). All solutions and media were sterile and pre-warmed before being added to the cells and cell culture was performed under a laminar flow hood.

One aliquot of HEK293 cells was thawed quickly in a 37°C water bath, transferred to a tube containing 10 ml HEK293 medium (HEK293 medium: Dulbecco´s Modified Eagles Medium (DMEM) supplemented with 10% FCS, 0.1 mM non-essential amino-acids (10 mM stock), 1 mM sodium pyruvate (100 mM stock), 100 U/ml penicillin and 100 U/ml streptomycin (10000 U/ml penicillin/streptomycin stock solution). Cells were centrifuged for 5 min at 800 rpm in a bench-top centrifuge, the cell pellet was then resuspended in 20 ml of HEK293 medium and plated onto 175 cm^2 cell culture flasks. Cells were grown in a humidified cell culture incubator (Hereaus, Germany) at 37°C with 5% CO_2. Medium was changed 12 h after plating.

To expand or subcultivate HEK293 cells, they were split twice a week. For splitting, medium was removed, the cells were washed twice with phosphate-buffered saline (PBS; 136 mM NaCl, 2.7 mM KCl, 10 mM Na_2HPO4, 1.8 mM KH_2PO4) and trypsinised with 6 ml of trypsin/EDTA for 2 min at 37°C. To stop the reaction, 9 ml HEK293 medium was added and the cells were centrifuged at 800 rpm for 5 min. Cells were resuspended in HEK293 medium and plated at a 1:7-1:8 ratio (manufacturer´s recommendation: 2 x 10^3 – 6 x 10^3 cells/cm^2).

4.2.2.2. Virus production

AAV vectors are produced in a helper-virus free manner as previously described (DURING *et al.* 2003; HAUCK *et al.* 2003). For the production of one heparin-purified AAV1/2 vector, two subconfluent 175 cm² cell-culture flasks were plated onto five 15 cm cell-culture dishes and for the production of other serotypes or viruses, to be purified by iodixanol-gradient ultracentrifugation, three 175 cm² flasks were plated onto ten 15 cm cell culture dishes on the day prior to transfection. On the day of transfection cell were ~70% confluent and the HEK293 medium was replaced 3 h before transfection by 25 ml pre-warmed transfection medium, which consist of Iscove´s Modified Dulbecco´s Medium (IMDM) supplemented with 5% foetal calf serum.

The transfection mixture for one AAV vector of the serotype 1/2 per 15 cm cell-culture dish was prepared by the following reagents added in the following order:

dH_2O	2.4 ml
2.5 M $CaCl_2$	330 µl
pFdelta6	25 µg
pNLrep (AAV2)	6 µg
pH21 (AAV1)	6.25 µg
rAAV plasmid	12.5 µg

For the production of AAV1, pRV-1 and pH21 are substituted for 12 µg pH21 and for the production of AAV8, 12 µg of the p5E18-VD2/8 plasmid was used. Adenoviral helper functions (E2A, E4 and VA) are provided by the plasmid pFdelta6 and E1 is encoded in the HEK293 genome.

The mixture was sterile filtered through a 0.2 µm syringe filter. While vortexing the mixture vigorously 13 ml 2 x HEBS buffer (50 mM HEPES, 280 mM NaCl, 1.5 mM Na_2HPO_4) was added, additional 15 s vortexed and left for 1 min 45 s to form a precipitate. Then, 5 ml of the solution was added dropwise to each culture dish. The dish was swirled gently to evenly distribute the reaction mixture. The medium was changed 16 h after transfection and replaced with fresh HEK293 medium.

4.2.2.3. Heparin column purification

The cells (5 dishes per virus) were harvested 60-65 h after transfection. Cells were washed with PBS, 25 ml of PBS was added to each dish, the cells were scraped off, equally distributed to three 50 ml tubes (containing ~1.65 dishes of cells) and centrifuged at 800 rpm for 10 min. Cell pellets were resuspended in 10 ml 150 mM NaCl, 50 mM Tris pH 8.0 per dish (makes ~16.5 ml per tube), pooled and redistributed to two tubes of 25 ml. Next, 1.25 ml of sodium deoxycholate (Sigma-Aldrich, Germany, CatNo: #D5670; 10 x stock solution) and 4.25 µl of benzonase endonuclease (Sigma-Aldrich, CatNo: #E1014) was added. The solution was incubated for 1 h at 37°C and cell debris was removed by centrifugation at 3000 rpm for 15 min at 4°C. The supernatant was transferred to a new tube, frozen at -20°C, thawed, centrifuged at 3000 rpm for 15 min at 4°C and the supernatant underwent a second round of freeze/thaw. AAV1/2 vectors can be purified by heparin affinity column chromatography. One 1 ml HiTrap Heparin column (Sigma-Aldrich, Germany, CatNo: #5-4836) was pre-equilibrated with 10 ml 150 mM NaCl, 20 mM Tris pH 8.0. The pump (Syringe pump PHD 2000 infusion; Harvard apparatus, Holliston, USA) was set at 25 cm diameter and 1 ml/min flow rate. The cell lysate (~50 ml) was loaded onto the column and afterwards the column was washed with 20 ml 100 mM NaCl, 20mM Tris pH 8.0. The next steps were performed by hand. First, the

column was washed once with 1 ml 200 mM NaCl, 20 mM Tris pH 8.0 and once with 1 ml 300 mM NaCl, 20 mM Tris pH 8.0. Afterwards, the virus was eluted with 1.5 ml 400 mM NaCl, 20 mM Tris pH 8.0 followed by 3 ml 450 mM NaCl, 20 mM Tris pH 8.0 and 1.5 ml 500 mM NaCl, 20 mM Tris pH 8.0. The 6 ml of virus solution were then concentrated using an Amicon Ultra-4 concentrator (MILLIPORE; Germany; CatNo: UFC810024). The virus solution was spun down to as small a volume as possible (~250 µl). The concentrator was then refilled twice with 3.5 ml of PBS and the solution was spun down again to ~250 µl. Both solutions were pooled, sterile filtered using a 13 mm 0.2 µm syringe filter, portioned in 20 µl aliquots and stored at -80°C. For quality control, 10 µl of the virus was analysed by SDS-PAGE followed by Coomassie-stain to visualise the viral proteins and verify purification.

4.2.2.4. Iodixanol-gradient ultracentrifugation

The cells (10 dishes per virus) were harvested 60-65 h after transfection. The cells were washed, collected in 25 ml PBS per dish and pelleted for 5 min at 800 rpm. The pellets were pooled and resuspended in a total of 10 ml (per dish) Tris/NaCl (50 mM/ 150 mM, pH 8.0). Next, sodium deoxycholate (Sigma-Aldrich St.Louis, MO, final concentration: 0.5%) and benzonase endonuclease (Sigma-Aldrich St.Louis, MO, final concentration: 50 U/ml) were added and the solution was incubated at 37°C for 30 min. After adding and dissolving of 584 mg NaCl (final concentration: 1 M) the solution was incubated for 30 min at 56°C. Afterwards, the cells were frozen at -20 °C and defrosted again. Precipitates were pelleted for 30 min followed by two additional freeze-thaw cycles. The supernatant (9 ml) was loaded on a discontinuous iodixanol (OptiPrep, Axis-Shield, City) gradient (3 ml of 54%, 3 ml of 40%, 3.5 ml of 25%, 6 ml of 15%) in tubes for a 60 Ti fixed-angle rotor (Beckman Coulter, Krefeld, Germany). The 40% phase was labelled with a pen on the outside of the tube. After centrifugation at 60.000 rpm for 1.5 h, the virus-containing 40% phase was retrieved, diluted with one volume of PBS containing 1 mM $MgCl_2$ and 2.5 mM KCl (PBS-MK) and concentrated 3x by refilling with PBS-MK using Amicon Ultra-4 concentrators (Millipore, Billerica, MA). When the volume was at 250 µl the virus solution was collected, the concentrator rinsed with an equal volume PBS-MK, solutions were pooled and sterile filtered.

4.2.2.5. Genomic titering of AAV

To extract the viral DNA, 2 µl of the virus solution was diluted in 10 µl 10 x ABI-buffer (500 mM KCL, 100 mM Tris pH 8.0, 50 mM $MgCl_2$) and 86 µl sterile H_2O. 1 µl DNase I (Roche, Basel, Switzerland) was added and the mixture was incubated for 30 min at 37°C to digest any non-viral DNA. After inactivation of DNase I at 70°C for 10 minutes, 1 µl of Proteinase K (10 µg/µl stock, Roche, Basel, Switzerland) was added to digest the capsid and set free the viral DNA. The mixture was

incubated for 1 h at 50°C followed by the inactivation of Proteinase K at 95°C for 20 min. The viral DNA was then stored at 4°C until real-time quantitative-PCR (qPCR).
A standard curve was prepared from a plasmid containing the WPRE element. Concentrations of 10^7, 10^6, 10^5 and 10^4 copies/µl were prepared. For qPCR, Power SYBR green (Applied Biosystems, Carlsbad, CA) was used.

One reaction contained:

H_20	3.4 µl
Power SYBR Green Master Mix	5.0 µl
Primer WPRE-fwd	0.3 µl
5´- GGC TGT TGG GCA CTG ACA AT -3´	
Primer WPRE-rev	0.3 µl
5´- CCG AAG GGA CGT AGC AGA AG -3´	
Template	1.0 µl
Final Volume	10.0 µl

The qPCR was performed in an ABI 7300 real-time PCR cycler (Applied Biosystems, Carlsbad, CA) with following PCR protocol: 40 cycles (95°C/30 s; 60°C/30 s ; 72°C/30 s).
The output data was analysed with ABI 7300 system software and Microsoft Excel and the genomic titre in copies/ml was calculated based on the standard curve.

4.2.3. Schwann cell culture

Sciatic nerves from postnatal day (P) P3 C57BL/6J mice were dissected, cleaned, and digested with 5 mg/ml of collagenase type 1 (Invitrogen, Darmstadt, Germany) at 37°C for 7 min, followed by 0.5% trypsin (Invitrogen) at 37°C for 5 min. Trypsin was neutralised by adding DMEM (Invitrogen) supplemented with 10% FCS, penicillin/streptomycin, and 20 U/ml of DNase I (Roche, Vienna, Austria). Trituration was done with a fire-polished Pasteur pipette and the cell suspension was centrifuged with 290 rcf for 5 min. The cell pellet was resuspended in DMEM / 10% FCS / PenStrep and plated at a density of about 1.2 x 10^5 cells/cm^2, onto glass cover slips coated with Poly-L-Lysine (PLL; Sigma, Vienna, Austria). The next day, the medium was changed to PNBM supplemented with NSF-1, L-glutamine and gentamicin/amphotericin-B (Lonza, Cologne, Germany) as well as 2 µM of cytosine arabinoside (Sigma, Vienna, Austria). AAV vectors (1 µl) were added as indicated. After six

days, cells were fixed with 4% PFA / 5% sucrose for 20 min and permeabilised with 0.1% Triton X-100 for 10 min. Schwann cells were stained with S100β antibody (Dako, Vienna, Austria; 1:1000) and transduced cells were detected by anti-GFP staining (Roche, Vienna, Austria; 1:1000).

Schwann cell experiments were performed by Rüdiger Schweigreiter at the Innsbruck Medical University, Biocenter, Division of Neurobiochemistry, Innsbruck, Austria.

4.2.4. Oligodendrocyte-enriched cultures

Primary cultures enriched in oligodendrocytes were prepared from embryonic day 14–16 mice as described (FELDMANN *et al.* 2009; TROTTER *et al.* 1989), with some minor modifications. Neural precursor cells growing on top of astrocyte monolayers were shaken off the astrocyte monolayers at day 13 after preparation (instead of day 15) and plated in modified Sato medium supplemented with B27, 1% horse serum, 10 ng/ml human recombinant platelet-derived growth factor (PDGF-AA), and 5 ng/ml basic fibroblast growth factor (bFGF) on Poly-L-Lysine coated coverslips (1 x 10^5 cells/11 mm coverslip). The cells were allowed to differentiate for 4 days *in vitro* before virus infection with 1 x 10^9 vg and then kept for additional 8 days. The resulting cultures were enriched in oligodendrocytes (60-70% of cells) but contained detectable numbers of astrocytes (20-30%) and also some neuronal cells (10-15%). Transfection of oligodendrocyte-enriched cultures was performed immediately after shake-off utilising AMAXA Biosystems technology according to the manufacturer's instructions (Amaxa®Nucleofector®Kit, Primary Neurons; program O-005). Transfected cells (4 x 10^6) were plated in a 6 cm dish containing PLL coated coverslips and analysed by immunofluorescence after 4 days in culture.

The preparation of oligodendrocyte-enriched cultures was done by technical staff of the Department of Molecular Cell Biology, Johannes Gutenberg University, Mainz. The transfection experiments were performed by Dominik Fröhlich, Department of Molecular Cell Biology, Johannes Gutenberg University, Mainz.

4.2.5. AAV vector administration

4.2.5.1. Vector infusion into adult mice

Adult male C57BL/6N or homozygous Plp-dsRed-1 transgenic mice expressing the red fluorescent reporter protein under the control of the plp promoter (HIRRLINGER *et al.* 2005) were anaesthetised (Fentanyl [0.005 mg/kg]/ Medetomidine (Domitor) [0.15 mg/kg]/ Midazolam

(Dormicum) [2.0 mg/kg] i. p.), and placed into a stereotaxic frame (Kopf instruments, Tujunga, CA). 1 µl of each AAV-EGFP serotype (adjusted at 5×10^{11} viral genomes (vg)/ml) was injected into the corpus callosum (+1.1 mm AP, ±1.3 mm ML, -2.3 mm DV from bregma), the striatum (+1.1 mm AP, ±1.7 mm ML, -3.5 mm DV from bregma) or the thalamus (-2.3 mm AP, ±1.5 mm ML, -3.5 mm DV from bregma) (PAXINOS and FRANKLIN 2001). Vector delivery was performed at a rate of 150 nl/min using a microprocessor controlled mini-pump (World Precision Instruments, Sarasota, FA, USA) with 34G bevelled needles (World Precision Instruments) and the needle was left in place for five minutes prior to slowly retracting the needle from the brain. Anaesthesia was antagonised using Narcanti (0.12 mg/kg)/ Antisedan (0.75 mg/kg)/ Anexate (0.2 mg/kg) i. p.

4.2.5.2. Vector infusion into neonatal mice

Neonatal mice underwent surgery as described (CETIN *et al.* 2006; PILPEL *et al.* 2009). Briefly, neonatal mice were cryo-anaesthetised by placing them in paper towels on crushed ice. They were then transferred into a custom-made Styrofoam-mold where the animal´s head was levelled horizontally and tightly fixed on both sides. The injections sites were marked on the animal´s head. A 34 G bevelled needle (World precision Instruments, Sarasota, FA, USA) was used for injection. 1 µl virus of either AAV1/2-MBP-EGFP or AAV1/2-CBA-EGFP (5×10^{11} viral genomes/ml) was injected at an injection rate of 150 nl/sec using a microprocessor controlled mini-pump equipped with a foot-switch (World precision Instruments) bilaterally into the striatum (+2.0 mm AP, ±1.5 mm ML, - 2.0 mm DV from lambda). After the injections the pups were warmed on a 37°C heating plate, rolled in used home cage embedding material and returned to their mother as a group to minimise rejection by the mother.

4.2.6. Immunocytochemistry and immunohistochemistry

Three weeks after vector infusion, when AAV1/2-mediated transgene protein expression has peaked to remain at stable levels (KLUGMANN *et al.* 2005), mice were deeply anesthetised with pentobarbital and transcardially perfused with PBS followed by phosphate buffered 4% paraformaldehyde (PFA). Brains were post-fixed in PFA overnight and cryoprotected in 30% sucrose/PBS for 2 days, then cut into 40 µm free-floating sections using a Microm HM-560 cryostat (Thermo Scientific, Waltham, MA), and stored at 4°C in cryoprotection solution (25% glycerin, 25% ethylene glycol and 50% PBS) until use. Oligodendrocyte-enriched cultures were fixed with 4% PFA for 5 min, washed with PBS, permeabilised with 0.2% TritonX-100 in PBS (PBS-Tx) for 5 min and blocked in 4% normal goat serum (NGS) in PBS-Tx for 15 min. The sections or cells were incubated overnight at 4°C with a combination of the following antibodies in 4% NGS in PBS-Tx: rabbit anti-aspa

serum (1:1000, (MERSMANN *et al.* 2011); mouse anti-HA (1:2000, Covance), mouse anti-GFAP (1:1000, Sigma-Aldrich, St. Louis, MO); mouse anti-NeuN (1:1000; Millipore, Billerica, MA); rabbit anti-EGFP serum (1:2000, made in-house); mouse anti-EGFP (1:2000, Roche, Basel, Switzerland) mouse anti-O4 (undiluted, a kind gift of J. Trotter), mouse anti-MOG (1:200, a kind gift of J. Trotter) and rabbit anti-CAII (1:250, a kind gift of S. Ghandour).

Sections/cells were washed with PBS and incubated with appropriate Alexa-conjugated secondary antibodies (1:1000, Invitrogen, Carlsbad, CA) for 1-2 h at room temperature in 4% NGS in PBS-Tx. After two washes in PBS-Tx, the cells/sections were counterstained with the nuclear chromophore 4´,6-Diamidino-2-phenylindole (DAPI; Hoechst, Germany; final concentration: 2 µg/ml), mounted on slides and coverslipped with Mowiol (Calbiochem, Darmstadt, Germany). Fluorescence was visualised using a Leica DMRA inverted microscope (Leica Microsystems, Wetzlar, Germany) or a Zeiss LSM 710 confocal microscope (Carl Zeiss MicroImaging, Jena, Germany).

4.2.7. Quantification of transduction efficiency

To quantify the cell types transduced by AAV1/2-MBP-EGFP, the vector was delivered stereotaxically into the striatum of 3-month-old homozygous Plp-dsRed-1 transgenic mice (n=3), expressing the RFP reporter under the control of the proteolipid protein (plp-1) promoter (HIRRLINGER *et al.* 2005). Brains were sectioned into 40 µm slices, stained for EGFP and for neuronal marker NeuN or GFAP as astroglial marker and every sixth slide was used to estimate the area of transduction. The area containing EGFP-positive cells was outlined and measured using ImageJ-software (NIH). CNP-Cre mice (LAPPE-SIEFKE *et al.* 2003) were used for the assessment of tropism of AAV1/2-MBP-Stop-EGFP and brains processed as described above. These sections were additionally stained for the oligodendrocyte marker ASPA.

4.2.8. Statistics

All graphs and statistical analyses were done with GraphPad Prism 4 software (La Jolla, CA). Student's t-test was used for statistical analysis. Values are presented as the mean ± s.e.m..

4.3. Results

4.3.1. Transduction of oligodendrocytes *in vitro*

The aim of this study was the identification of AAV vectors with oligodendroglial tropism. A total of four different AAV expression cassettes were packaged into AAV1, AAV1/2 and AAV8. The expression cassettes included the MBP promoter or the strong and ubiquitous CBA promoter to drive the expression of either HA-tagged human aspartoacylase (ASPA) or the cDNA encoding the EGFP reporter (Fig. 4.2).

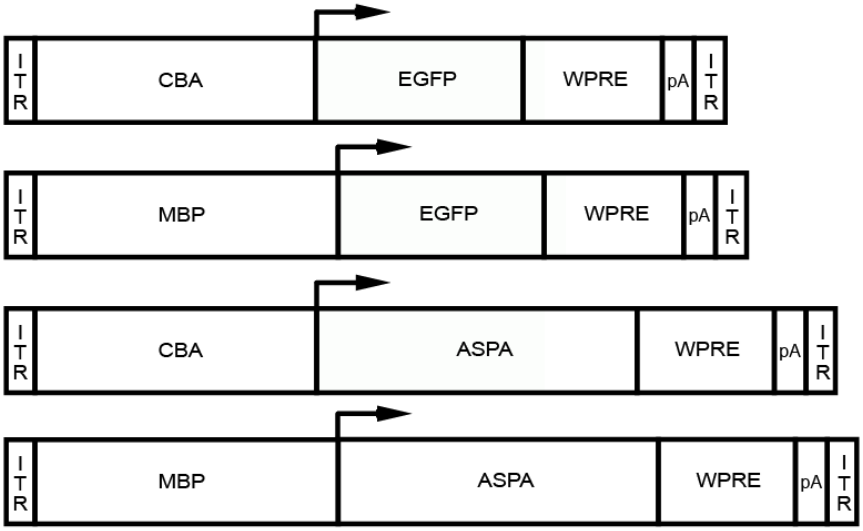

Figure 4.2: AAV expression cassettes.
The coding sequences of enhanced green fluorescent protein (EGFP) or the cytosolic enzyme aspartoacylase (ASPA) are under the control of the CMV enhancer/chicken ß-actin promoter (CBA) promoter or the myelin basic protein (MBP) promoter. Recombinant mRNAs expressed from these cassettes include the woodchuck hepatitis virus posttranscriptional regulatory element (WPRE) followed by the bovine polyadenylation signal (pA). The cassettes are flanked by AAV2 inverted terminal repeats (ITRs).

In order to identify a serotype/promoter combination with oligodendroglial tropism, vector stocks of six different EGFP-vectors were titer matched and added to the media of oligodendrocyte-enriched cultures (see Materials and Methods). Since these cultures contained all major neural cell types a potential non-oligodendroglial transgene expression could be monitored easily. At 4 days *in vitro*, these cultures were infected by 1 x 10^9 viral genomes (vg) and kept for additional 8 days in culture. Double immunofluorescent detection of the EGFP reporter and cell type specific markers (ASPA, MOG, O4 for oligodendrocytes; GFAP for astrocytes; NeuN for neurons) was performed to

assess the vector tropism *in vitro*. Figure 4.3 illustrates the result of a representative experiment including transduction of these primary cells following infection by the MBP/CBA-EGFP cassettes packaged into AAV1, AAV1/2, and AAV8. The AAV8 serotype was included in the study because it had previously been demonstrated to confer oligodendroglial transduction in rats *in vivo*. These results show that all vectors carrying the MBP promoter genomes transduced primary oligodendrocytes (Fig. 4.3 A-I), but not astrocytes (Fig. 4.3 J-L) or neurons (Fig. 4.3 M-O). While MBP genomes in AAV1/2 and AAV8 transduced all oligodendrocytes on a coverslip (100% transduction efficiency), AAV1-MBP virions only showed a 50% efficiency. Generally, the CBA promoter vectors spared oligodendrocytes (Fig. 4.3 A'-I'), but efficiently transduced astrocytes (Fig. 4.3 J'-L') and neurons (Fig. 4.3 M'-O').

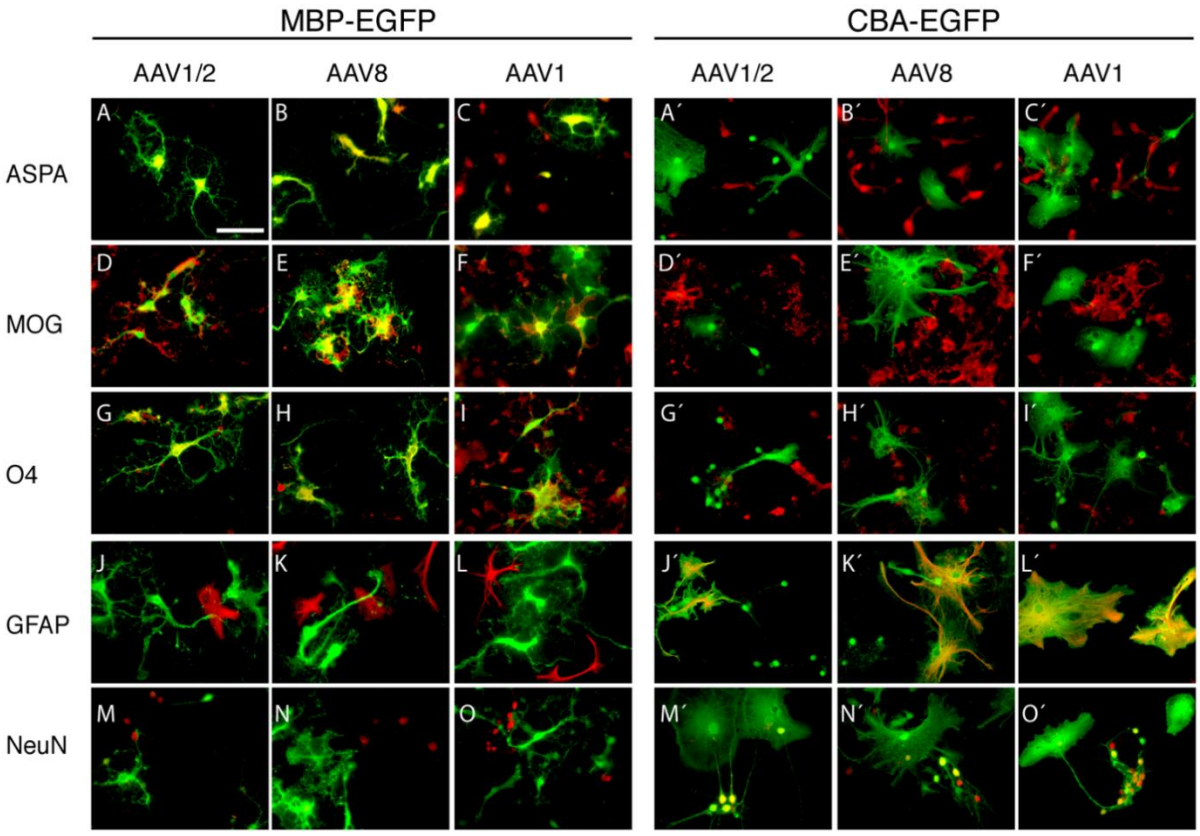

Figure 4.3: AAV-mediated transgene expression in oligodendrocytes *in vitro*.
Primary oligodendrocytes-enriched cultures were cultivated for four days before the administration of the indicated serotypes (1 x 10^9 vg) of AAV-MBP-EGFP (**A-O**) or AAV-CBA-EGFP (**A'-O'**) and further cultivated for additional eight days. Double-immunocytochemistry for EGFP (green) and cell type specific markers (oligodendrocytes: ASPA (**A-C**; **A´-C´**), MOG (**D-F**; **D´-F´**), O4 (**G-I**; **G´-I´**); astroglia: GFAP (**J-L**; **J´-L´**); neurons: NeuN (**M-O**; **M´-O´**); red) was performed to evaluate the vector tropism. Transduction of oligodendrocytes depends on the promoter but not on the serotype. Scale bar: 50 µm.

In summary, the MBP promoter appeared to confer oligodendrocyte-specific gene expression while the CBA promoter is inactive in oligodendrocytes. The primary virus entry depends on

interactions between the AAV capsid proteins and cell surface receptors followed by receptor-mediated endocytosis and it is widely accepted that this is the reason why different serotypes display cell type specific tropism. However, these data suggested that all serotypes tested generally infected neural cells and that cell type specific gene expression occurred at the transcriptional level. To exclude any potentially confounding effects of the viral capsid on the transduction profile, the naked AAV-plasmid DNA constructs (MBP-EGFP and CBA-EGFP) were delivered to the oligodendrocyte-enriched cultures and analysed by immunocytochemistry. Transfection of CBA-EGFP resulted in transgene expression in neurons (Fig. 4.4 A-D) but not in oligodendrocytes (Fig. 4.4 E-H). In contrast, MBP-driven GFP expression was restricted to oligodendrocytes (Fig. 4.4 I-L). These results indicate that gene expression in these primary cultures is promoter- but not serotype-dependent.

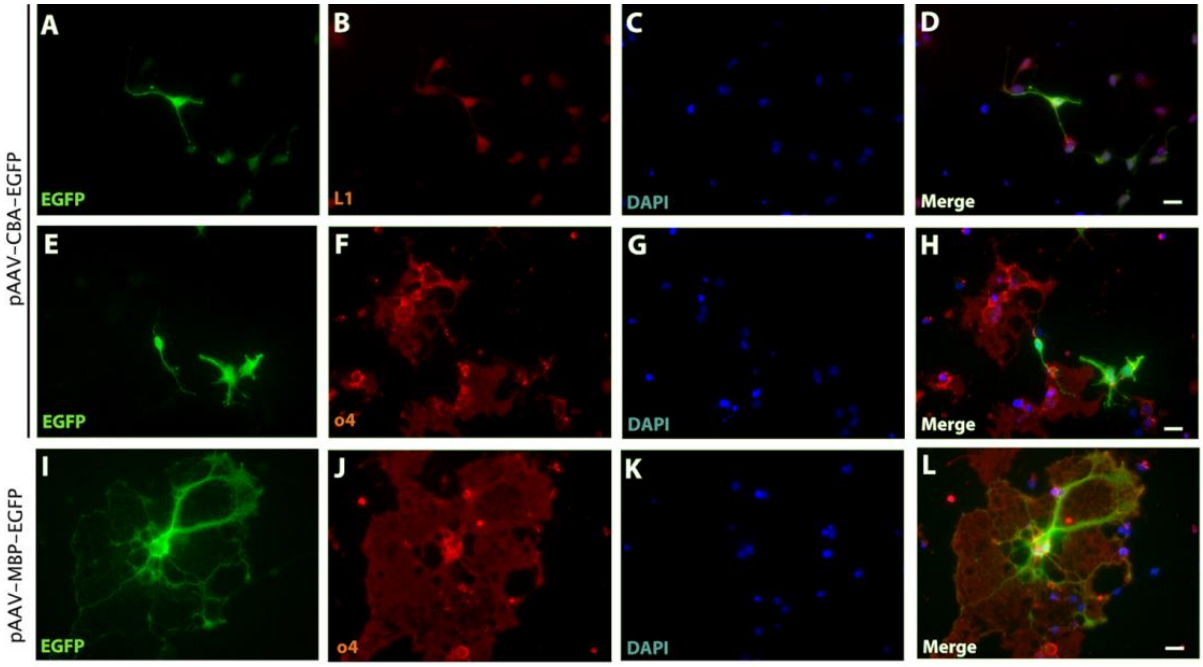

Figure 4.4: The CBA promoter is inactive in oligodendrocytes.
Representative pictures of primary oligodendrocyte-enriched cultures transfected with the AAV plasmids driving EGFP under the control of the CBA promoter (**A-H**) or the MBP promoter (**I-L**) followed by immunocytochemical detection of the reporter. **(A-D)** Expression of CBA-EGFP is restricted to L1-positive neurons. **(E-H)** CBA-EGFP immunoreactivity segregates from O4-postive oligodendrocytes. **(I-L)** MBP-EGFP is exclusively expressed in oligodendrocytes. Scale bars: 10 µm.

In order to address whether the transgene would interfere with the vector tropism, the EGFP cDNA was replaced with a DNA sequence encoding HA-tagged aspartoacylase (ASPA). This soluble enzyme is missing in Canavan disease (CD), a fatal white matter disease for which AAV-mediated *in vivo* gene therapy has been proposed (KLUGMANN and LEICHTLEIN 2006). The CBA-ASPA and MBP-ASPA cassettes (Fig. 4.2) were packaged into AAV1/2 and AAV8 and the tropism of these vectors was

determined in oligodendrocyte-enriched cultures by double-immunohistochemistry for the HA-tag (representing ectopic ASPA protein) and the oligodendrocyte marker carbonic anhydrase II (CAII) (SKOFF and GHANDOUR 1995). The CBA-ASPA vectors failed to transduce oligodendrocytes (Fig. 4.5 A, C), while the MBP-ASPA vectors efficiently transduced oligodendroglia, irrespective of the serotype (Fig. 4.5 B, D). In summary, the transgene does not change the tropism of the AAV vectors.

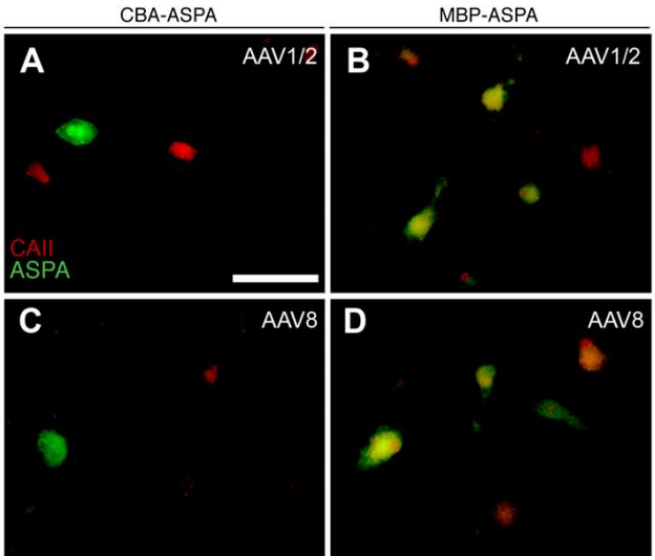

Figure 4.5: The type of transgene does not alter the tropism for oligodendrocytes *in vitro*.
Oligodendrocytes-enriched cultures were infected with AAV1/2 (**A, B**) or AAV8 vectors (**C, D**) containing the gene encoding HA-tagged ASPA under the control of either the CBA- or MBP-promoter as indicated. Transgenic ASPA (detected via the HA-tag; green) was detected in oligodendrocytes expressing the marker CAII (red) after infection with MBP vectors (**B, D**) but not with CBA vectors (**A, C**). Scale bar: 50 µm.

As the pathology of some leukodystrophies impedes both central and peripheral myelinating cells (BIFFI *et al.* 2011b), the capability of AAV1/2-MBP to transduce Schwann cells (SCs) was investigated. For this purpose, primary cultured SCs were infected with AAV1/2-CBA-EGFP and AAV1/2-MBP-EGFP and analysed by co-immunostaining for the reporter and the Schwann cell marker S100β. The transduction efficiencies for both vectors were generally poor and EGFP immunoreactivity in SCs was not detected (Fig. 4.6). While these results indicate that the vectors did not lead to transgene expression in SCs, it is not clear if this cell type is refractory to infection or if the promoters lack the required cis-elements to drive transgene expression in SCs.

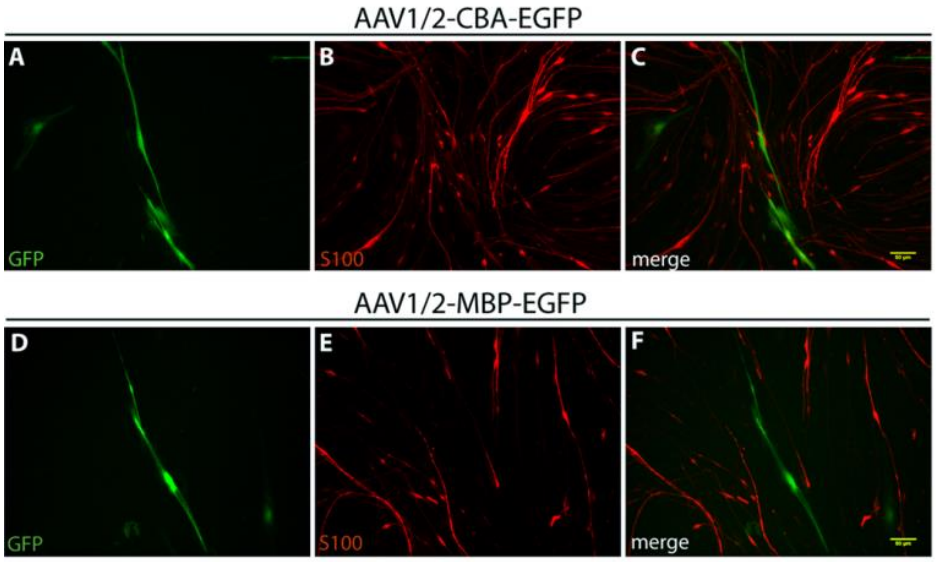

Figure 4.6: AAV-MBP does not transduce Schwann cells.
Primary Schwann cells were infected at the second day in culture with AAV1/2-CBA-EGFP (**A-C**) or AAV1/2-MBP-EGFP (**D-F**) vectors (1 µl of 7 x 10^{10} vg/ml), and analysed six days later for presence of EGFP immunoreactivity in S100β-positive Schwann cells. The merged pictures (**C, F**) do not show any EGFP immunoreactivity in SCs. A representative result of three independent experiments is shown. Scale bars: 50 µm.

4.3.2. Transduction of oligodendrocytes *in vivo*

To investigate the tropism *in vivo*, the 6 different vectors (AAV1/2, AAV8, AAV1 containing MBP/CBA-EGFP cassettes) were injected into the brain parenchyma of adult mice (n=3/vector). Vector delivery to the white matter tracts of the corpus callosum resulted in transduction of ASPA-positive oligodendrocytes for MBP cassettes in serotypes AAV1/2 and AAV1, but not for AAV8 (Fig. 4.7 A-C). The serotypes containing the CBA cassette did not show any GFP immunoreactivity in white matter oligodendrocytes but the vector spread caused GFP expression in neurons of the dorsal striatum (Fig. 4.7 D-F). Similarly, targeted intrastriatal vector delivery led to transgene expression in oligodendrocytes for AAV1/2-MBP, and AAV1-MBP, but not for AAV8-MBP (Fig. 4.7 G-I). The corresponding CBA-EGFP containing vectors showed an expression pattern complementary to the MBP vectors (Fig. 4.7 J-L). Although these results were not quantified, it seems that, at least in this study, AAV8 did not perform well regardless of the promoter used, whereas AAV1/2 and AAV1 appeared to show similar levels of efficacy *in vivo*. The superior oligodendroglial transduction rate of the mosaic serotype AAV1/2 over AAV1 *in vitro* (100% vs. 50%, see above) was the basis to select AAV1/2 for further experiments.

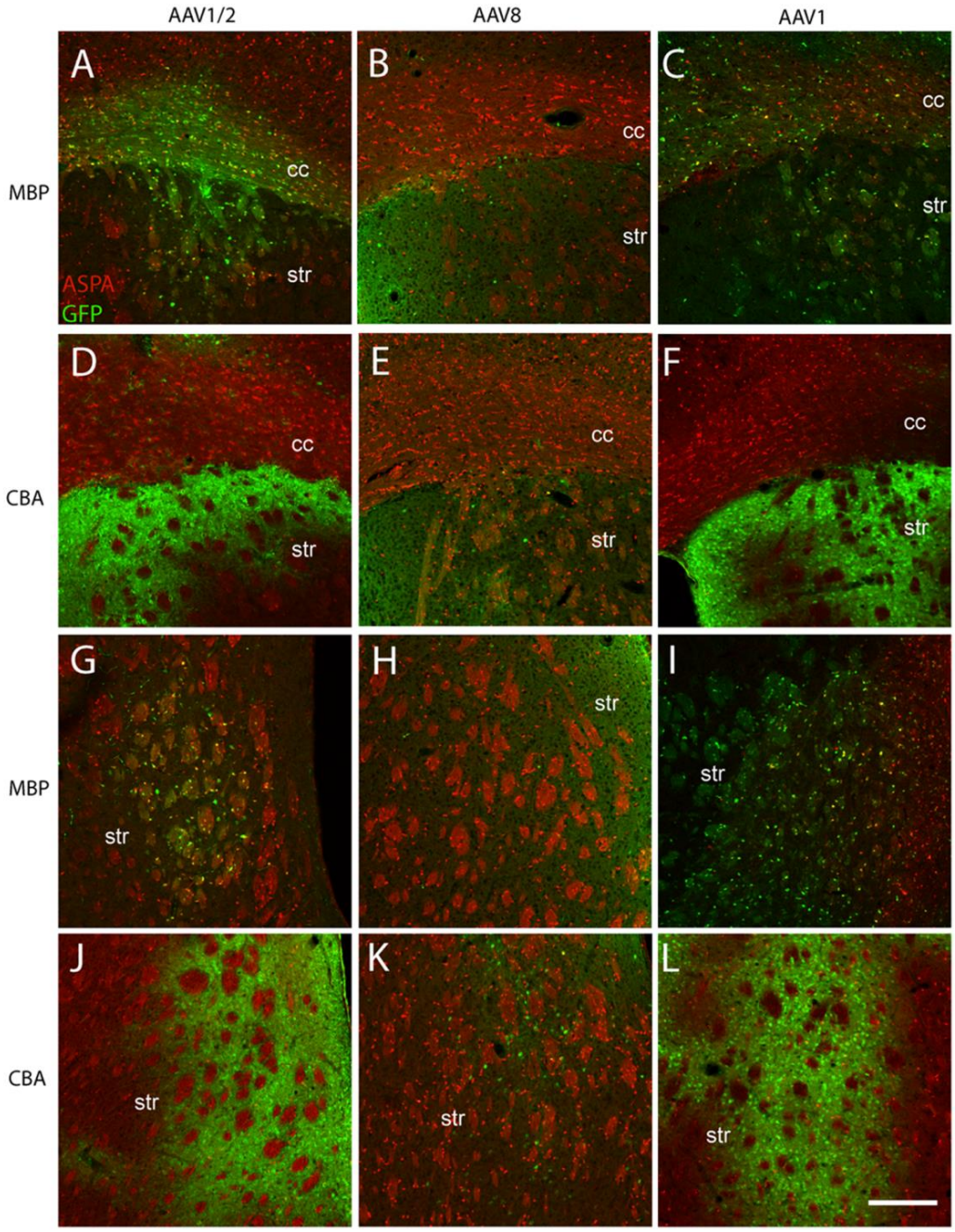

Figure 4.7: AAV-mediated transgene expression in oligodendrocytes *in vivo.*
Different AAV vectors (5 x 10^8 vg) were stereotaxically delivered to the corpus callosum (cc; **A-F**) or striatum (str; **G-L**) of adult mice followed by co-staining for EGFP (green) and the oligodendrocyte marker ASPA (red) three weeks later. AAV1/2 vectors transduced oligodendrocytes in the presence of the MBP promoter (**A, G**), and neurons when the CBA promoter was used (**D, J**). AAV8-mediated transduction resulted in neuronal transduction independent of the promoter (**B, E, H, K**). Tropism of AAV1 vectors (**C, F, I, L**) was similar to AAV1/2. Scale bar: 250 µm.

A detailed immunohistochemical analysis of the gen expression profile was performed by laser scanning confocal microscopy after delivery of AAV1/2-MBP-EGFP to the corpus callosum (Fig.

4.8 A-C), the striatum (Fig. 4.8 D-F) and the thalamus (Fig. 4.8 G-I) of adult mice. High levels of EGFP immunoreactivity were observed in all brain regions in cells expressing the oligodendrocyte marker ASPA (Fig. 4.8 A, D, G) or CAII (Fig. 4.8 J). In contrast, when injected into the thalamus, the control vector AAV1/2-CBA-EGFP showed the expected exclusive neuronal expression pattern (Fig. 4.8 J-K).

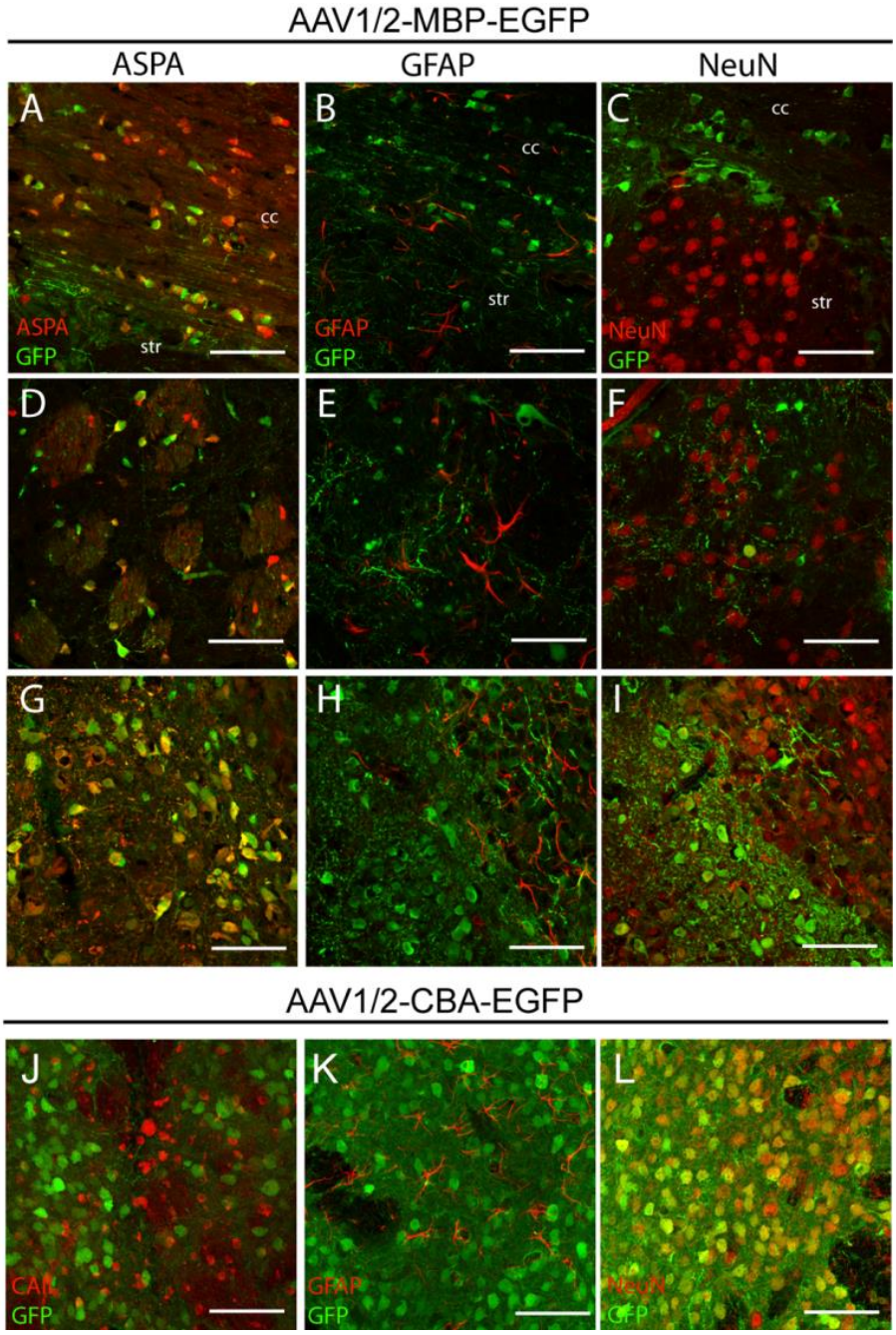

Figure 4.8: Histological analysis of cell types transduced by AAV1/2-MBP-EGFP.
Double immunostaining for EGFP (green) and cell type specific markers (red) for either oligodendrocytes (**A, D, G, J**), astroglia (**B, E, H, K**) or neurons (**C, F, I, L**) was performed three weeks after vector infusion into the corpus callosum (cc; **A-C**), striatum (str; **D-F**) or thalamus (**G-I**) of adult mice. Note that the MBP promoter drives robust transgene expression in oligodendrocytes while there is almost no EGFP immunoreactivity seen in astrocytes and neurons. **(J-L)** Representative results after AAV1/2-CBA-EGFP delivery to the thalamus show neuronal transgene expression. Scale bars: 50 µm.

It has been described that the purification method can alter vector tropism (KLEIN *et al.* 2008b). Therefore, the tropism of AAV1/2-MBP-EGFP vectors purified by either heparin affinity chromatography or discontinuous iodixanol density gradient ultracentrifugation was compared. Both vector preparations efficiently transduced oligodendrocytes *in vitro* (Fig. 4.9 A, B) and *in vivo* after delivery into the striatum (Fig. 4.9 C, D) or subcortical white matter (Fig. 4.9 E, F). These findings suggest that both purification methods can be used interchangeably without affecting the oligodendroglial tropism.

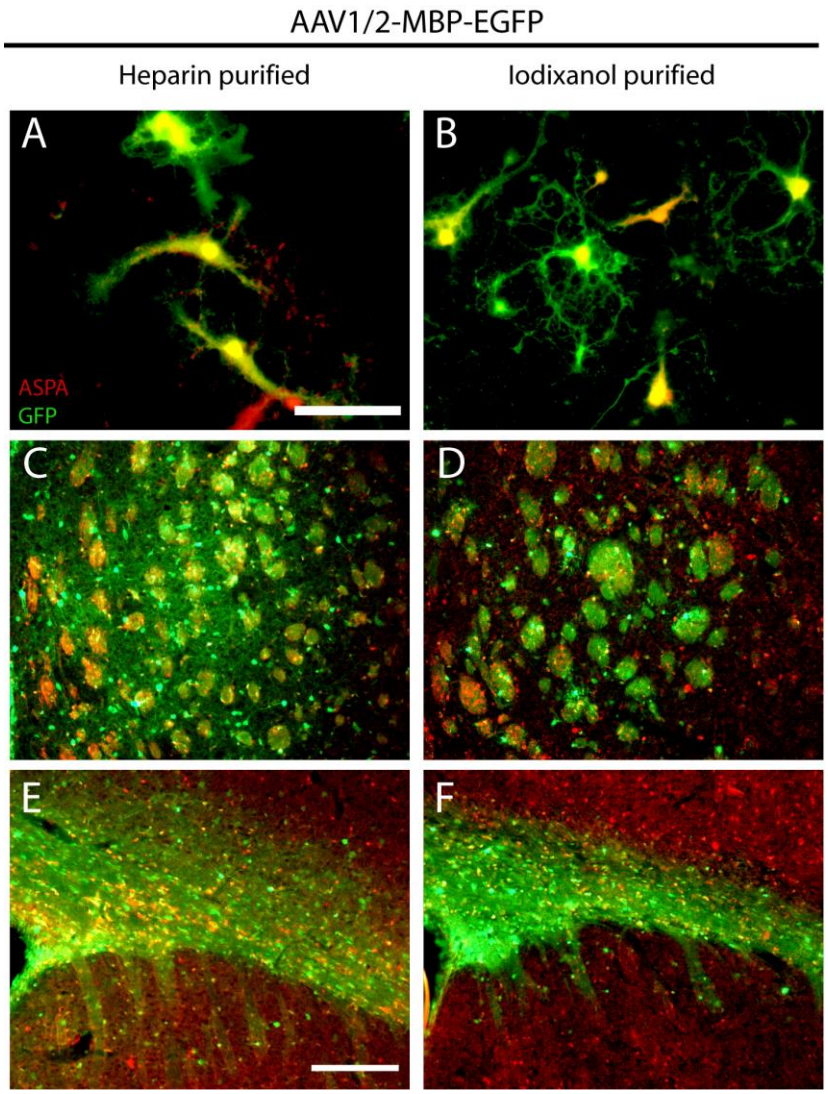

Figure 4.9: The type of purification does not alter the tropism for oligodendrocytes *in vitro* and *in vivo*.
AAV1/2-MBP-EGFP purified by heparin affinity chromatography (**A, C, E**) or iodixanol gradient centrifugation (**B, D, F**) used to infect cultured primary oligodendrocytes (A, B) or stereotaxically delivered to 3-month-old mice (**C-F**). Transduction of oligodendrocytes was determined by double-immunohistochemistry for ASPA (red) and GFP (green). Scale bars: 50 µm in A, B; 250 µm in C-F.

Since many leukodystrophies manifest in early childhood, it is likely that the success of gene replacement strategies depends on the timing of intervention. Hence, AAV1/2-MBP-EGFP and AAV1/2-CBA-EGFP were injected into neonatal mice to test for the capability of these vectors to transduce oligodendrocytes or oligodendrocyte progenitors cells (OPCs) of neonatal mice (Fig. 4.10). The infusion of MBP vectors resulted in the oligodendroglial transgene expression, yet with a poor efficiency. In contrast, transgene expression was detected in neuronal cell bodies and the neuropil when CBA vectors were used, which is consistent with previous studies (PILPEL *et al.* 2009).

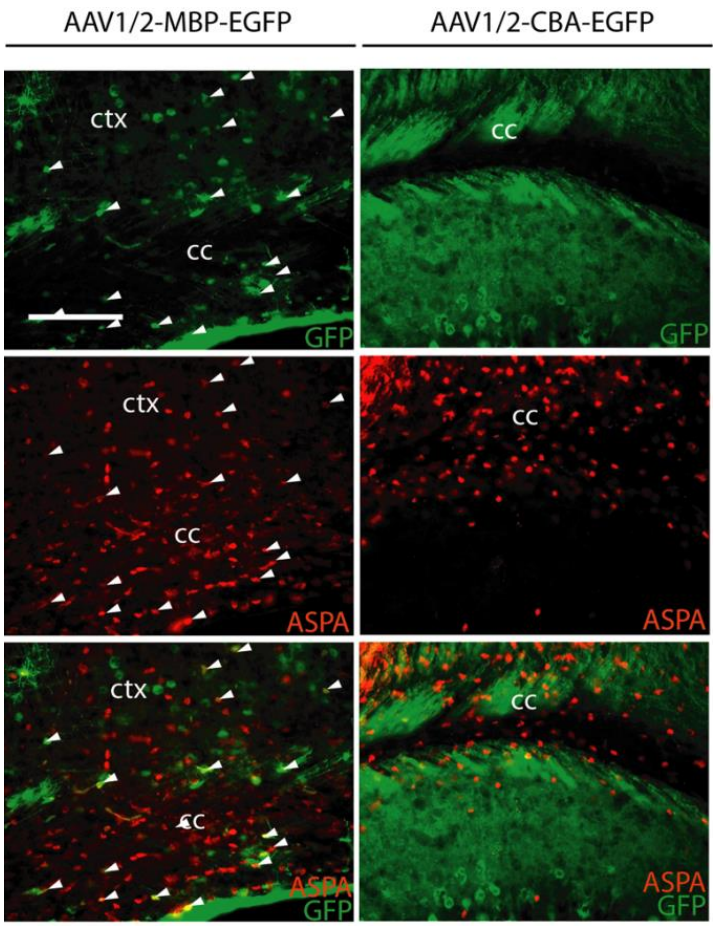

Figure 4.10: Limited transduction of oligodendroglia after neonatal vector administration.
Neonatal mice were injected with AAV1/2-MBP-EGFP or AAV1/2-CBA-EGFP and brains subjected to immunohistochemical analysis after 3 weeks. AAV1/2-MBP-EGFP transduced ASPA-positive oligodendrocytes (red) indicated by arrowheads. In contrast, GFP immunoreactivity is detected in the neuronal cell bodies and neuropil in AAV1/2-CBA-EGFP treated animals. cc, corpus callosum; ctx, neocortex. Scale bar: 100 µm.

A prerequisite for the successful treatment of leukodystrophies is the aibility of the therapeutic vector to spread throughout the CNS. To address this, the rostrocaudal extent of AAV1/2-MBP-mediated transgene expression was determined after unilateral intrastriatal vector delivery of 1 µl (5×10^8 vg) into adult mice. This resulted in EGFP expression between +0.8 mm and -2.2 mm anterior and posterior to the injection site (Fig. 4.11).

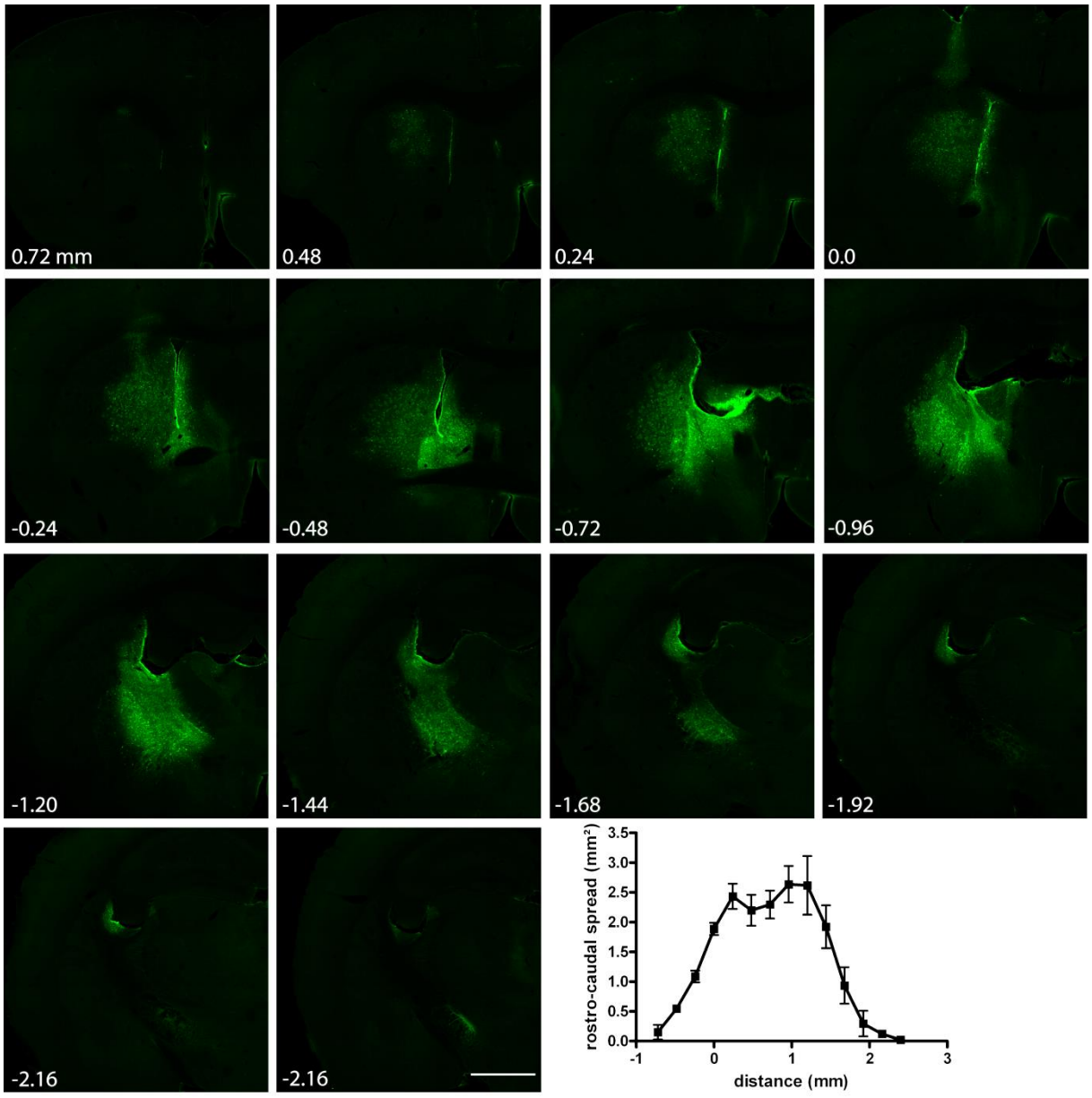

Figure 4.11: Vector spread after AAV1/2-MBP-EGFP delivery to the CNS.
The vector (5×10^8 vg in 1 µl) was delivered unilaterally to the striatum of 3-month-old mice (n=3). Three weeks later brains were processed into 40 µm sections, immunostained for EGFP (green) and every 6th section was used to determine the infected area using ImageJ software. The numbers indicate the distance from the injection site (= 0 mm). Scale bar: 1 mm.

The ratios of transduced cell types were quantified after AAV1/2-MBP-EGFP injection in the striatum of PLP-dsRed transgenic mice expressing the fluorescent reporter ds-Red under the promoter of the proteolipid protein (*plp-1*) gene. It was shown previously that expression of ds-Red reliably occurs in oligodendrocytes (HIRRLINGER *et al.* 2005). Therefore, this mouse line was utilised in order to reduce potentially confounding influences of immunostainings. The relative numbers of all transduced (EGFP-positive) cells were 78.2 ± 4.4% oligodendrocytes and 21.6 ± 3.3% neurons (Fig. 4.12; $p<0.0001$, two-tailed t-test). Transduction of astrocytes was negligible at 0.23 ± 0.23%.

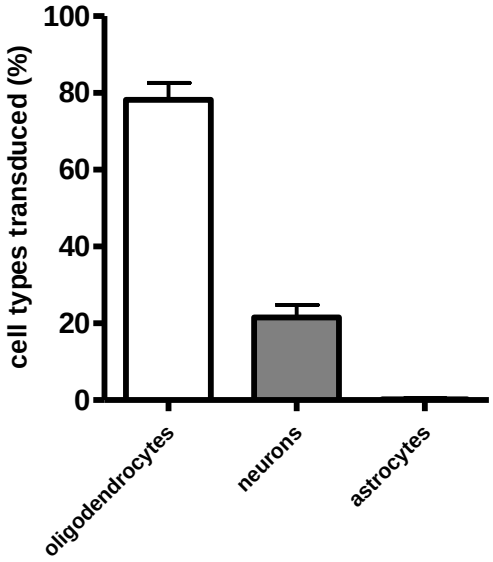

Figure 4.12: Tropism of AAV1/2-MBP-EGFP in the mouse brain.
AAV1/2-MBP-EGFP was injected in the striatum of transgenic mice expressing the fluorescent reporter dsRed in oligodendrocytes. Three weeks later, the relative numbers of transduced cell types were determined by EGFP co-labelling with dsRed (oligodendrocytes), NeuN (neurons) and GFAP (astrocytes). The relative numbers of all transduced (EGFP-positive) cells were 78.2 ± 4.4% oligodendrocytes, 21.6 ± 3.3% neurons and 0.23 ± 0.23% astrocytes.

4.3.3. Combining the AAV platform with the Cre/loxP technique

Although the residual ectopic activity of the MBP promoter in neurons can be tolerated in gene therapy applications for leukodystrophies, it may be undesirable for specific gene function studies in oligodendrocytes. In order to restrict transgene expression to oligodendrocytes expressing Cre-recombinase, an AAV-expression cassette was designed containing a transcriptional stop-cassette flanked by loxP sites preceding the transgene (Fig. 4.13). An AAV1/2-MBP-stop-EGFP vector was generated and used for infection of primary oligodendrocytes-enriched cultures obtained from wildtype pups or from transgenics expressing Cre-recombinase under the control of the

oligodendrocyte 2´, 3´-cyclic nucleotide 3´-phosphodiesterase (CNP) promoter (CNP-Cre mice) (LAPPE-SIEFKE *et al.* 2003). As expected, no EGFP expression was detected in the absence of Cre-recombinase (Fig. 4.13 A-D). In contrast, Cre-dependent recombination occurred specifically in CNP-Cre oligodendrocytes (Fig. 4.13 E-H). Similarly, no EGFP-expression was detected after AAV1/2-MBP-stop-EGFP delivery to the CNS of adult wildtype mice (Fig. 4.13 I), while EGFP expression occurred in the brain of CNP-Cre animals (Fig. 4.13 J). Quantification of the transduction efficacy *in vivo* showed that of all transduced (EGFP-positive) cells, 92.2 ± 5.3% were ASPA-positive oligodendrocytes and 7.8 ± 0.7% were NeuN-positive neurons (Fig. 4.13 K; $p<0.0001$, two-tailed t-test). Transgene expression in astrocytes was not observed. This translates into a 63.9% reduction of neuronal expression compared with the non-conditional AAV-system (Fig. 4.12). These results suggest that the AAV platform can be successfully combined with conditional expression systems when restricted transduction of oligodendrocytes is required.

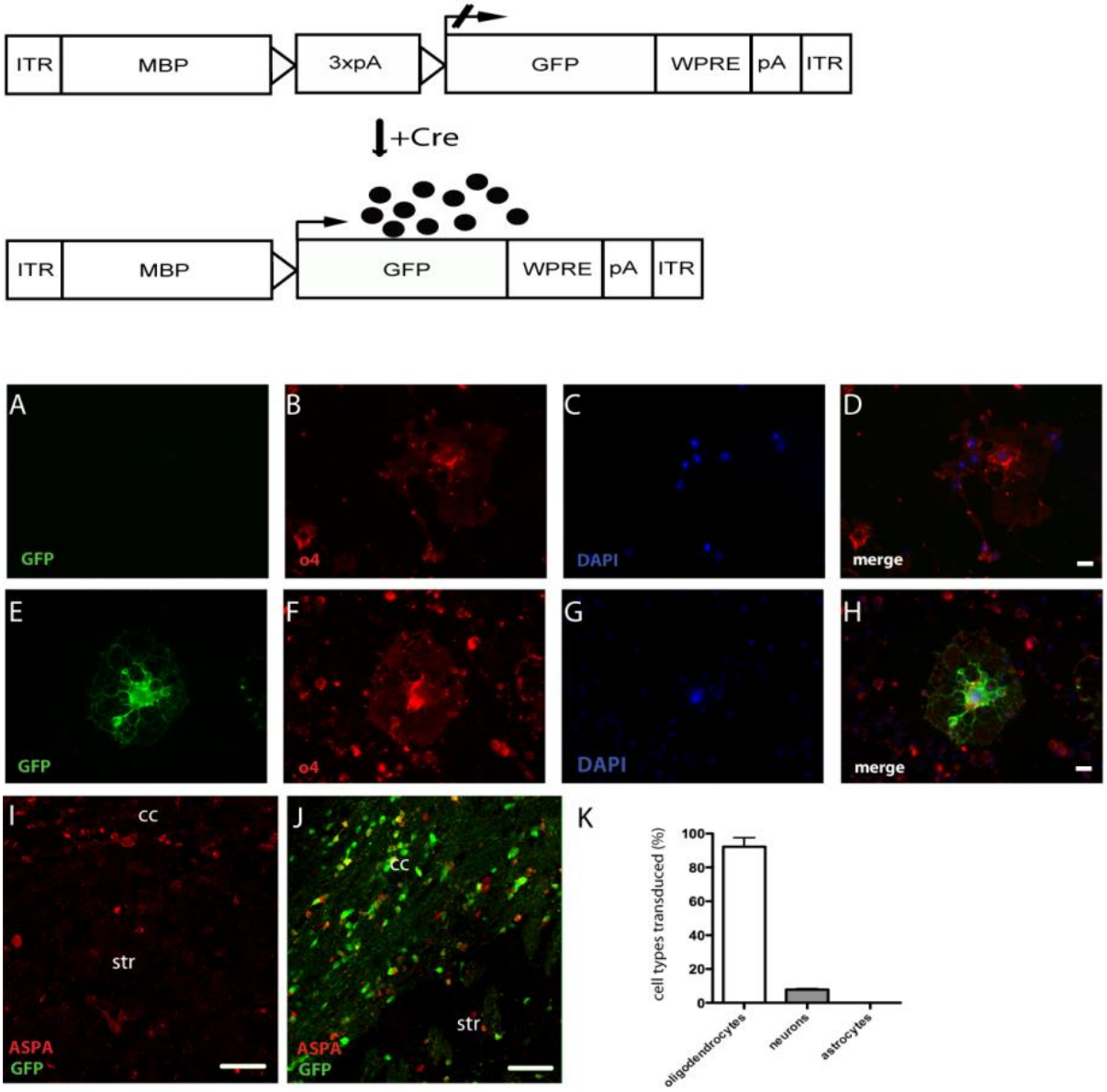

Figure 4.13: AAV-mediated conditional overexpression in oligodendrocytes.

Top, Silencing of transgene expression by a transcriptional termination cassette (stop-cassette) containing three polyadenylation sites (3xpA) flanked by loxP sites (triangles). Cre-recombinase-mediated excision of the stop cassette leads to transcription of the transgene. AAV1/2-MBP-stop-EGFP was used to infect primary oligodendrocytes generated from C57BL/6 mice (**A-D**) and from transgenic mice (**E-H**) expressing Cre under the control of the CNP promoter. **(I)** Direct delivery of AAV1/2-MBP-stop-EGFP to the corpus callosum (cc) and striatum (str) of wildtype mice did not result in transduction. Oligodendrocytes were identified by the marker ASPA (red). **(J)** Cre-dependent recombination of the AAV genome leads to oligodendroglial gene expression in CNP-Cre mice. **(K)** Quantification of relative numbers of cells transduced after delivery of AAV1/2-MBP-stop-EGFP to CNP-Cre mice. The relative numbers of all transduced (EGFP-positive) cells were 92.2 ± 5.3% ASPA-positive oligodendrocytes and 7.8 ± 0.7% NeuN-positive neurons. Gene expression in astrocytes was not observed. Scale bars: 10 µm in D, H; 50 µm in I, J.

4.4. Discussion

Current gene therapy strategies for the treatment of selected leukodystrophies include an *ex vivo* approach where hematopoietic stem cells are transduced by lentivirus (LV) to target microglial precursors, and an *in vivo* approach based on intracerebral injection of neurotropic AAV or LV. Both strategies are efficient largely because the transduced microglia and neurons secrete the therapeutic gene products that can lead to cross-correction of non-transduced oligodendrocytes (BIFFI *et al.* 2011b; LATTANZI *et al.* 2010). Other leukodystrophies, such as CD, are caused by the deficiency in a non-secreted enzyme normally expressed in oligodendrocytes. The widespread AAV-mediated neuronal gene delivery has not been successful in conferring functional recovery in CD animal models, suggesting that direct genetic correction of the affected oligodendrocytes is required for clinical efficiacy. (KLUGMANN and LEICHTLEIN 2006; KLUGMANN *et al.* 2005). However, AAV vectors that inherently target oligodendrocytes are lacking.

It is widely accepted that vector tropism depends on the surface of the capsid since it is involved in cell binding, internalisation and intracellular trafficking (VAN VLIET *et al.* 2008). Hence, the characterisation of novel natural serotypes or high-throughput random diversification and selection has yielded AAV vectors that showed transduction of astroglia (FOUST *et al.* 2009; KOERBER *et al.* 2009; LAWLOR *et al.* 2009). While these approaches did not identify vectors with robust tropism in oligodendroglia, AAV8 had been shown to target oligodendrocytes in the rat brain when the transgene was controlled by the MBP promoter, and some intrinsic preference for oligodendrocytes has been reported for AAV1 after delivery to the mouse brain (LAWLOR *et al.* 2009; WANG *et al.* 2003). In the light of the potential to use AAV vectors in clinical applications, this study focused on the well-characterised serotypes AAV1, AAV8, and AAV1/2 that have shown to be efficient in the brains of rodents and monkeys (KLEIN *et al.* 2008a; MARKAKIS *et al.* 2010; MASAMIZU *et al.* 2010; REIMSNIDER *et al.* 2007; TAYMANS *et al.* 2007). The hypothesis was that the utilisation of the MBP promoter would lead to the expression of transgenes in oligodendrocytes.

After adding the AAV vectors to oligodendrocyte-enriched cultures, all MBP-promoter vectors specifically drove transgene expression in oligodendrocytes, while the CBA-promoter vectors spared oligodendrocytes but led to expression in neurons and astroglia. These findings were confirmed for AAV1/2 and AAV1 after vector delivery to the brain.

It is difficult to reconcile these results with the dogma that tropism is determined by the capsid structure, since the uptake of fluorescently labelled rAAV capsid after delivery to the rodent brain has been reported to be restricted to neurons (BARTLETT *et al.* 1998). One possible explanation may be a scenario where the natural AAV capsid tropism leads to primary infection of neurons,

followed by the transfer of virions or AAV genomes to oligodendrocytes where transgene expression specifically occurs under the control of the MBP promoter. This transfer could be mediated by exosomes or microvesicles released into the extracellular medium by a range of cell types including neurons, since they provide means for intercellular distribution of proteins and nucleic acids (LACHENAL *et al.* 2011). Another explanation could be that all serotypes delivered the rAAV genome to all cell types alike, but cell type-specific transgene expression occurred in a promoter-dependent fashion. Both possibilities are hypotetical at this stage but regardless of the actual mechanism, it appears that transcriptional tropism can be targeted by the use of cell type specific promoters. This notion was supported when primary oligodendrocyte-enriched cultures were transfected with the AAV plasmids. In this experiment, the MBP promoter- but not the CBA promoter-construct was active in oligodendrocytes. Although the cells were not tested for the presence of vector genomes after gene delivery, these results suggest that the CBA promoter lacks activity in oligodendrocytes and that binding and internalisation of putative neurotropic vectors might occur in non-neuronal cells where transgene expression is then ultimately controlled by transcriptional regulation. This is surprising given that the CBA promoter, consisting of cis-elements of the chicken beta-actin gene and the CMV immediate early enhancers, is considered to be ubiquitous.

AAV8 vector delivery to the mouse brain resulted in a lower transduction efficiency compared to AAV1 and AAV1/2 vectors regardless of the promoter used (Fig. 4.7). Various efficacies have been reported for AAV8-mediated transduction, but differences in promoter-usage, purification-method, targeted brain region, species and injection parameters are confounding factors for direct comparisons between studies (DE BACKER *et al.* 2010; KLEIN *et al.* 2002; LAWLOR *et al.* 2009). Based on the initial comparison of the performance of the serotypes expressing the MBP constructs *in vivo*, this study focused on the detailed characterisation of mosaic AAV1/2 vectors, because they combine the benefits of both parental serotypes (superior transduction efficiency of AAV1 over AAV2, and optional affinity purification utilising the known AAV2 receptor heparan sulfate proteoglycans [HSPG]). While these vector preparations consist of virions with heterogeneous capsid composition, the majority is likely to carry equal ratios of AAV1 and AAV2 capsid proteins, because of the use of equimolar quantities of helper plasmids for vector packaging. In fact, in the course of this work, inter-batch variability with respect to tropism was not observed. This even applied when vector preparations obtained by different purification protocols were compared (Fig. 4.9). Moreover, the transduction profiles of mosaic AAV1/2 appear to closely resemble those described for AAV1 vectors (HAUCK *et al.* 2003). The same appears to be true for AAV1/2-MBP preparations since these results suggest that AAV1/2-MBP and AAV1-MBP vectors display comparable efficiency *in vitro* and *in vivo*.

A strong preference of AAV1/2-MBP to target oligodendrocytes over neurons *in vivo* (78% vs. 22%) was observed. The non-exclusive oligodendroglial activity can most likely be attributed to the limited size of the MBP promoter (compromising transcriptional specificity). Some transcriptional activity in neurons might even be desired for the treatment of CD since the missing enzyme ASPA is probably also expressed in some neuronal nuclei (MOFFETT *et al.* 2011). Moreover, in the case of metachromatic leukodystrophy (MLD), transduction of neurons resulted in cross-correction of oligodendrocytes (SEVIN *et al.* 2006) so the neuronal activity of MBP promoter would still be beneficial for clinical application.

While robust oligodendrocyte transduction was observed after vector delivery to the adult brain, AAV-MBP-mediated gene transfer into the neonatal CNS did not efficiently target oligodendrocytes. It is tempting to speculate that most of the oligodendrocytes and oligodendrocyte progenitors*in vivo* do not get infected at this stage of maturation probably because they do not yet express specific receptors, which are a prerequisite for the initial interaction between the virus and the cell and the subsequent internalisation process. This hypothesis is supported by the findings that for AAV2, HSPGs are known to be the primary receptors and HSPG synthesis on oligodendrocytes is upregulated by adhesion-induced regeneration and/or differentiation (Szuchet et al. 2000).

Schwann cells (SCs), the myelinating cells of the peripheral nervous system, are also affected in MLD. While MBP is endogenously expressed in the periphery, AAV1/2-MBP did not lead to transgene expression in primary SCs. Two possibilities can account for this result. SCs could be refractory to infection by AAV1/2 (serotype-dependent). Alternatively, infection might occur but transgene expression is precluded because the MBP-promoter is inactive in SCs. Although this study did not distinguish these two scenarios, the latter one appears likely given that the short MBP promoter fragment used in this study does not contain the SC enhancer elements known to be critical for transcriptional activity in this cell type (FARHADI *et al.* 2003).

The present findings indicate that there is a need for a range of recombinant promoters that are active in myelinating glia and can be used to drive AAV-mediated transgene expression. To our knowledge, the MBP promoter is the only one that is small enough (AAV has a packaging limit of ca. 5 kb) and yet specific. The 1.3 kb upstream sequence of the MBP transcriptional start was employed in this study, the 1.9 kb version might help to restrict the transcriptional tropism to oligodendrocytes (CHEN *et al.* 1999). While a single injection of 1 µl of AAV1/2-MBP yielded a vector spread over 3 mm in the mouse brain, the transgene expression was not oligodendrocytes exclusive. If this AAV platform is used for basic research, a more restricted gen expression profile might be required. To address this, an AAV-MBP expression cassette that required Cre-dependent recombination of a stop-cassette located upstream of the EGFP cDNA was generated. After delivery of the corresponding

AAV1/2 vector to the brain of CNP-Cre mice, transgene expression was detected almost exclusively in oligodendroglia. Although CNP is a widely used marker protein of oligodendrocytes, transgene expression was also observed in a few neurons, an observation that could be explained by the transfer of Cre-activity from oligodendrocytes to neurons (e.g. via exosomes), by low-level activity of the CNP promoter in neurons, or by 'leakiness' of the stop cassette. Numerous studies have confirmed the specificity of the CNP-Cre line in the context of oligodendrocyte-specific deletion of genomic loci (KASSMANN *et al.* 2007; SAHER *et al.* 2005) and the conditional AAV system appears to be tight at least in neurons (GUGGENHUBER *et al.* 2010). However, rAAV genomes are maintained as episomal structures in the nucleus, providing supraphysiological access for DNA-modifying enzymes (including Cre-recombinase). Therefore, the recombination in neurons revealed by the highly sensitive AAV system might virtually be considered a 'false' positive when compared with results obtained by conventional germ line transgenics.

The highly efficient AAV-mediated gene transfer to oligodendrocytes will be useful for gene function studies, the generation of animal models of abnormal myelination, and for gene therapy strategies for leukodystrophies e.g. Canavan disease (see Chapter 5).

Chapter 5:

Successful gene therapy for a mouse model of Canavan disease

5. Successful gene therapy for a mouse model of Canavan disease

Canavan disease (CD) is a rare leukodystrophy, caused by mutations in the gene encoding aspartoacylase (ASPA), an oligodendrocyte enriched enzyme. It is characterised by the accumulation of its substrate N-acetylaspartate (NAA) in the brain, leading to a spongiform vacuolisation, severe motoric and cognitive impairment and premature death. To date, no therapy is available due to the lack of gene transfer systems restoring ASPA in oligodendrocytes. However, the monogenetic nature of CD in combination with the pathology restricted to the CNS allows the development of gene transfer strategies to target the causative pathological mechanism of this disease. To achieve oligodendroglial transgene expression an adeno-associated virus (AAV)-based gene transfer system was established with the *aspa* gene driven by the oligodendrocyte-specific myelin basic protein (MBP) promoter. Using a multi-site injection strategy this vector was delivered directly to the brain of juvenile ASPA-deficient mice and the effects on clinical signs were monitored up to six months. *Aspa* gene transfer resulted in transduction of oligodendrocytes in grey and white matter throughout the brain. Histological abnormalities were ameliorated and NAA levels reduced. AAV-aspa treatment resulted in normalisation of body weight and motor function. Furthermore, species-typical nest-building behaviour was restored. These data provide a proof-of-concept for a successful genetic treatment of CD and might pave the way towards translation into clinical application.

5.1. Introduction

Canavan disease (CD) is an autosomal recessive neurogenetic disorder caused by mutations in the gene encoding aspartoacylase (ASPA; EC 3.5.1.15)) resulting in a loss of ASPA function and the progressive accumulation of its substrate N-acetyl-aspartate (NAA) in brain, blood and urine (CANAVAN 1931; KAUL *et al.* 1993; MATALON *et al.* 1988). Histopathological findings in CD patients as well as in animal models comprise spongiform vacuolisation of the brain, dysmyelination and gliosis, leading to developmental delay, mental retardation, macrocephaly, hypotonia and later spasticity, seizures and premature death (MATALON and MICHALS-MATALON 2000; SURENDRAN *et al.* 2003b).

The etiology and progression of CD is thought to be related to the accumulation of NAA. Although many facts of NAA biochemistry still remain elusive, several functions in the brain have been proposed. This includes the maintenance of the osmotic-hydrostatic pressure (BASLOW 2003), the usage as an acetate source for myelin lipids (CHAKRABORTY *et al.* 2001; MADHAVARAO *et al.* 2005). Furthermore, excess NAA can promote oxidative stress (PEDERZOLLI *et al.* 2010a; PEDERZOLLI *et al.*

2007; SURENDRAN 2010) and may contribute to the induction of seizures (AKIMITSU *et al.* 2000; YAN *et al.* 2003). Thus, increased NAA levels might contribute to the deleterious effects in CD patients.

Pharmacological interventions aim at neutralising NAA toxicity and included lowering the NAA levels with lithium salts (ASSADI *et al.* 2010; BASLOW *et al.* 2002; JANSON *et al.* 2005) and the administration of antioxidants (PEDERZOLLI *et al.* 2010b). Furthermore, attempts were made to supplement acetate by the administration of glyceryltriacetate (ARUN *et al.* 2010; SEGEL *et al.* 2011). Moreover, enzyme replacement strategies as well as the transplantation of neural progenitor cells to compensate for oligodendrocyte loss have been proposed for CD therapy (SURENDRAN *et al.* 2004c; ZANO *et al.* 2011), but none of these strategies did result in an effective treatment. However, the monogenetic nature of CD in combination with the pathology restricted to the CNS allows the development of gene transfer strategies to target the causative pathological mechanism of this disease. Indeed, the pioneering study involving a liposome-based *aspa* gene delivery to CD patients was the first gene therapy attempt for a non-malignant CNS disease (LEONE *et al.* 2000). Virus-mediated gene transfer is a versatile tool for the genetic engineering of somatic cells (JANSON and DURING 2001). Hence, further studies included *aspa* gene transfer using recombinant adenoviruses and recombinant adeno-associated viruses serotype 2 (rAAV2) or chimeric rAAV1/2 into the brains of CD patients or CD animal models (KITADA *et al.* 2000; MATALON *et al.* 2000) . The rationale for the usage of neurotropic vectors in these studies to deliver ASPA into neurons is based on the hypothesis that excess NAA is the toxic agent causing CD pathology and that the degradation of NAA at the origin of its synthesis can subsequently ameliorate CD symptoms (JANSON *et al.* 2002b; KLUGMANN *et al.* 2005; MATALON *et al.* 2003; MCPHEE *et al.* 2005b; SEKI *et al.* 2002; SEKI *et al.* 2004). The result of these studies was a general lack of neurological efficacy due to inadequacies of the timing of treatment and insufficiencies of the vector system delivering *aspa* to neurons instead of oligodendrocytes. Hence, ectopic neuronal overexpression does not compensate for the lack of ASPA in oligodendrocytes and the restoration of ASPA at its physiological site should be the aim to ultimately correct CD pathophysiology.

This study evaluates the therapeutic efficacy of *aspa* gene transfer to oligodendrocytes in young *aspa*$^{-/-}$ mice. This approach is based on the use of an AAV-vector system with oligodendroglial tropism (see Chapter 4) for the treatment of an mouse model of CD (see Chapter 3).

5.2. Material & Methods

5.2.1. AAV construct

All enzymes for cloning were purchased from New England Biolabs (NEB, Frankfurt, Germany) and used according the manufacturer´s instructions. Agarose gel electrophoresis was carried out using electrophoresis equipment purchased from Biometra and visualised with the UVsolo TS imaging system (Biometra, Göttingen, Germany). DNA fragments were separated using 1xTBE (0.09 M Tris base, 0.09 M boric acid, 2 mM EDTA (pH 8.0)) as running buffer and extracted from the gel using Nucleospin II plasmid extraction kit (Macherey-Nagel, Düren, Germany) according to the manufacturer's instructions. The production of chemocompetent *E.coli* DH5α cells as well as the transformation of these cells was carried out using standard molecular biology techniques (SAMBROOK *et al.* 1989). Mini- and Maxipreparations of plasmid DNA were performed with PureLink™ Quick Plasmid Miniprep Kit and PureLink™ HiPure Plasmid Maxiprep Kit (Invitrogen, Carlsbad, CA) according to the manufacturer's instructions.

For the generation of pAAV-MBP-HA-ASPA (pAM-MBP-HA-ASPA-WPRE-bGH; pAAV-aspa) the 1.1 kb CMV enhancer/chicken β-actin (CBA) promoter was excised with Acc65I and XhoI from the plasmid used in a previous study (KLUGMANN *et al.* 2005). Sticky ends of the vector backbone carrying the HA-tagged ASPA were filled in and dephosphorylated with calf intestine phosphatase (CIP). The 1.3 kb MBP-promoter (IKENAKA and KAGAWA 1995) (a kind gift of Prof. Ikenaka) was excised from a pBluescript KS vector with Acc65I and EcoRV, the ends were filled in and ligated to the vector backbone. In addition, a pAAV backbone without cDNA (pAM-CBA-pL-WPRE-bGHpA; pAAV-empty) from our lab was used as a vector control. Both plasmids carry a woodchuck hepatitis virus posttranscriptional regulatory element (WPRE), the bovine growth hormone poly(A) (bGH) and an ampicillin-resistance cassette. A schematic representation of the vectors is depicted in Fig. 5.1.

The production of pseudotyped mosaic AAV1/2 vectors in HEK cells and determination of genomic titers using the ABI 7300 real time PCR cycler (Applied Biosystems, Carlsbad, CA) were performed as described (DURING *et al.* 2003) and explained in Chapter 4. The vectors used in this study were purified via iodixanol-gradient ultracentrifugation.

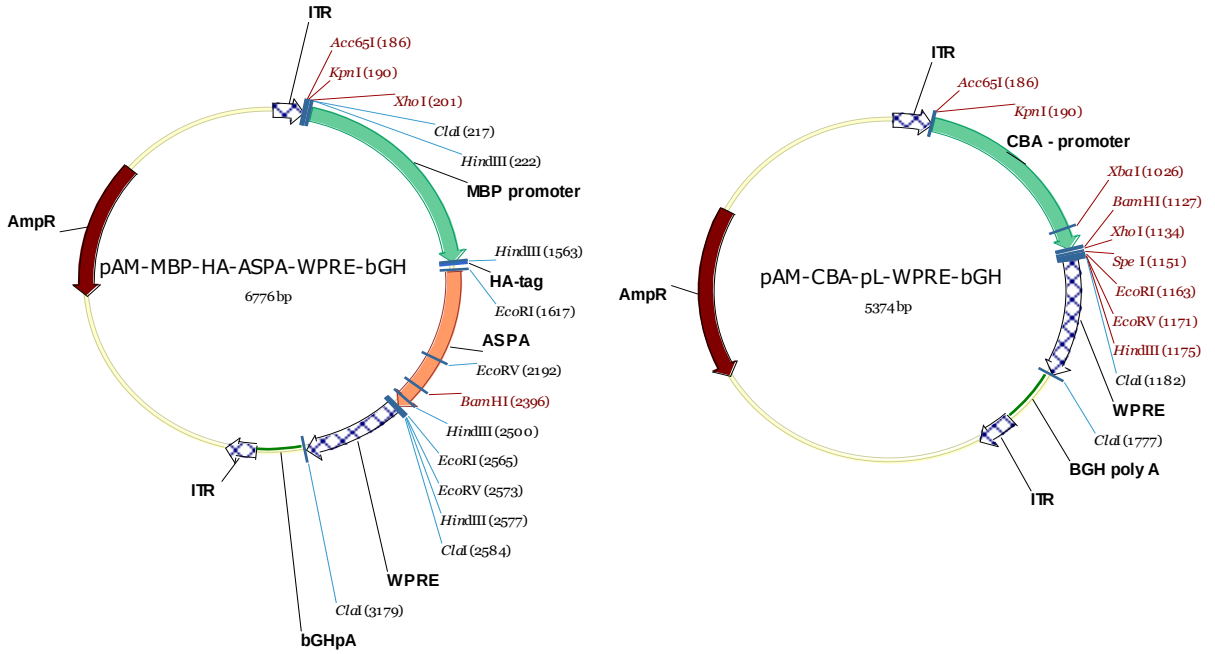

Figure 5.1: Schematic representation of the vectors used for the gene-therapy study.
To generate plasmid pAM-MBP-HA-ASPA-WPRE-bGH (pAAV-aspa) the 1.1 kb CBA promoter used in a previous study (KLUGMANN *et al.* 2005) was replaced by the 1.3 kb MBP promoter (IKENAKA and KAGAWA 1995). A pAAV backbone without cDNA (pAM-CBA-pL-WPRE-bGH; pAAV-empty) was used as a vector control.

5.2.2. Vector administration

Biopsies were taken from the tail of all mice at postnatal day (P) P1 or P2 and the mice were marked with a foot tattoo using the Aramis Animal Microtattoo System (Ketchum Manufacturing Inc., Brockville, ON, Canada) equipped with a 30 G needle. After genotyping, male mice underwent surgery at P9-P10 as described (CETIN *et al.* 2006; PILPEL *et al.* 2009). For anesthesia mice were pre-medicated with 0.02 mg/kg atropine injected subcutaneously into the scuff at the back of their necks to reduce bronchial secretion and improve breathing. 10 min after injection of atropine a mixture of 40 mg/kg ketamine and 5 mg/kg xylazine was injected i.p.. Mice were transferred to a custom-made Styrofoam-mold were the animal´s head was leveled horizontally and tightly fixed on both sides. A midline incision was made with small surgical scissors, small hooks were used to keep the area open and the skull was gently cleaned. A 34G beveled needle (World precision Instruments, Sarasota, FA, USA) was used for injection as it can easily penetrate the scull of P9-P10 mice without using a drill. 1 µl virus of either AAV-aspa (3.5 x 10^{12} vg/ml) or AAV-empty (3.4 x 10^{12} vg/ml) was injected at an injection rate of 150 nl/sec using a microprocessor controlled mini-pump equipped with a foot-switch (World precision Instruments) bilaterally into each of the following brain regions: striatum

(+4.0 mm AP, ± 1.8 mm ML, - 2.3 mm DV from lambda), thalamus (+2.0 mm AP, ± 1.7 mm ML, - 2.5 mm DV from lambda) and cerebellum (-2.3 mm AP, ± 2.0 mm ML, - 2.8 mm DV from lambda). The skin was sutured, the animal was kept warm until full recovery from anesthesia and then placed back into its home cage.

5.2.3. Immunoblotting

Animals were sacrificed by decapitation, organs dissected quickly and snap frozen in liquid nitrogen. Brains were homogenised under liquid nitrogen using mortar and pestle. Aliquots were sonicated in tris-buffered saline (TBS) containing protease inhibitors (cOmplete™ protease inhibitor cocktail tablets, Roche Applied Science, Mannheim, Germany) according to the manufacturer´s recommendation. Samples were centrifuged for 10 min at 13000 rpm and 4°C to remove cell debris. The supernatant was transferred to a new reaction tube and protein concentration was determined by the method of Bradford (BRADFORD 1976) using bovine serum albumin (NEB, Frankfurt, Germany) as standard. 20 µg of protein were mixed with 5x Laemmli reducing sample buffer (for 100 ml: 15.0 g SDS; 15.6 ml 2 M Tris-HCL pH 6.0; 57.5 g 87% glycerol; 16.6 ml β-mercaptoethanol, 0.4% (w/v) bromphenol blue), denatured for 5 min at 95°C and separated by SDS-PAGE. This was performed using a Bio-Rad electrophoresis system (Mini-PROTEAN 3) with Tris-glycin running-buffer (25 mM Tris-base, 190 mM glycine, 0.1% SDS) according to manufacturer´s instruction manuals (Bio-Rad Laboratories GmbH, Munich, Germany). PageRuler™ Prestained Protein Ladder (Thermo Scientific, St. Leon-Rot, Germany) was used as a molecular weight marker. For Western blotting a tank transfer system (Mini Trans-Blot cell) was used according to the manufacturer´s instruction manuals (Bio-Rad Laboratories GmbH, Munich, Germany). The proteins were transferred in transfer buffer (25 mM Tris-base, 190 mM glycine, 20% ethanol (v/v)) onto nitrocellulose membranes (Protran, Whatman; GE Healthcare, Dassel, Germany). After blocking the membrane in blocking solution (TBS + 0.1% Tween20 (v/v) (TBST) + 5% non-fat dry milk (w/v)) for 1 h at room temperature under agitation to prevent non-specific background binding of the primary and/or secondary antibody, membranes were probed with the following antibodies with the dilutions made in blocking solution overnight at 4°C under agitation: rabbit anti-aspa serum (1:1000) and mouse anti-α-tubulin (1:400.000, Sigma-Aldrich, St. Luis, MO). Antibodies were detected by the appropriate HRP-conjugated secondary antibodies (1:1000, Dianova, Hamburg, Germany) followed by ECL-detection. For ECL detection of one membrane (~5x7 cm) 1 ml of solution A (200 ml 0.1 M Tris-HCL, pH8.6; 50 mg Luminol; stored at 4°C) and 1 ml of solution B (11 mg para-hydroxy coumaric acid in 10 ml DMSO) were mixed, 0.3 µl H_2O_2 was added, mixed and incubated for 2 min prior to

detection with the FusionSL™ chemiluminescence detection system equipped with the Fusion detection software (Peqlab, Erlangen, Germany). Data was analysed using the bio-ID quantification software (Peqlab, Erlangen, Germany).

5.2.4. ^{1}H nuclear magnetic resonance (^{1}H-NMR)

5.2.4.1. Extraction of mouse brain using $CHCl_3$/MeOH/Water

Extractions were made according to standard protocols (BECKONERT *et al.* 2007). Briefly, homogenised mouse brain tissue was weighed and placed on ice. 4 ml/g of tissue of ice-cold methanol (HPLC grade) and 0.85 ml/g of H_2O (HPLC grade) were added to the tubes and vortexed. 4 ml/g of tissue of ice-cold chloroform (HPLC grade) and 2 ml/g of H_2O (HPLC grade) were added to the samples and vortexed again. Samples were allowed to rest on ice for 15 min before centrifugating at 18000 rcf and 4°C for 15 minutes. The upper aqueous phase and the lower organic phase were carefully transferred into separate glass vials. The remaining protein pellet was re-extracted as above and combined with the earlier fractions. The organic phase was allowed to dry in the fume cupboard overnight before being reconstituted in 600 µl deuterated chloroform, transferred into 5 mm NMR tubes and stored at -40°C. The aqueous phase was deep frozen in liquid nitrogen for 10 minutes and then lyophilised. Aqueous brain extracts were reconstituted in 600 µl of 100 mM phosphate buffer containing 20% D_2O and 100 µM TSP. Samples were mixed by vortexing and 550 µl each were transferred into 5 mm NMR tubes.

5.2.4.2. Pulse parameters, spectral processing and structural assignment

NMR spectra were acquired on a Bruker DRX600 spectrometer operating at 600.13 MHz ^{1}H-NMR frequency and 298 K. Gradient shimming was used immediately prior to spectral acquisition. ^{1}H-NMR spectra of the samples were acquired using 1D excitation sculpting pulse sequence. For all spectra 128 free induction decays (FIDs) were collected into 32K complex data points, using a spectral width of 12,019 Hz (20 ppm), with a 5 s relaxation delay between pulses. Data were zero-filled by a factor of 2 and the FIDs were multiplied by an exponential weighting function equivalent to a line broadening of 1 Hz prior to Fourier transformation (FT) using XWINNMR software. The acquired NMR spectra were corrected for phase and baseline distortions, referenced internally to TSP δ0.0 and normalised to creatine. ^{1}H-NMR assignments were made based on previous knowledge of metabolite spectra found in NMR database libraries (BMRB, www.brmb.wisc.edu; The Human Metabolome Project, www.metabolomics.ca) and by comparison of the chemical shifts with published values of known compounds at the same pH (FAN *et al.* 1986; NICHOLSON *et al.* 1995).

NMR spectroscopy was performed by Orla Teahan, Translational Neuroscience Facility, Department of Physiology, School of Medical Science, UNSW, Sydney, Australia.

5.2.5. Histology

For immunohistochemistry mice were deeply anesthetised with pentobarbital and trans-cardially perfused with phosphate bufferd saline (PBS) followed by phosphate buffered 4% paraformaldehyde (PFA). Brains were post-fixed in PFA overnight. The right hemisphere of the cerebellum and brainstem was then cut and kept in 1% PFA for EM analysis. The remaining part of the brain was cryoprotected in 30% sucrose/PBS for 2 days, then cut into 40 µm free-floating sections using a Microm HM-560 cryostat (Thermo Scientific, Waltham, MA) and stored at 4 °C in cryoprotection solution (25% glycerin, 25% ethylene glycol and 50% PBS) until use.

For ASPA and NeuN co-detection, antigen retrieval was performed prior to permeabilisation by rinsing free floating sections twice in PBS followed by incubation in 10 mM sodium citrate buffer (pH 6.0) at 85°C for 30 min. Sections were allowed to cool down to room temperature in the same solution followed by permeabilisation with 0.2% TritonX-100 in PBS (PBS-Tx) for 10 min and blocking for 30 min in PBS-Tx 4% normal goat serum (NGS). Sections were incubated overnight at 4°C with a combination of the following antibodies in blocking solution: rabbit anti-aspa serum (1:1000 (MERSMANN *et al.* 2011)); mouse anti-NeuN (1:1000, Millipore, Schwalbach, Germany) and mouse anti-GFAP (1:1000, Sigma-Aldrich, St. Louis, MO). Sections were washed with PBS and incubated with appropriate Alexa-conjugated secondary antibodies (1:1000, Invitrogen, Carlsbad, CA) for 1-2 h at room temperature in the dark in 4% NGS in PBS-Tx. After counterstaining the cell nuclei with a mixture of DRAQ5 (1:1000) and DAPI (1:10000) for 15 minutes, sections were mounted on slides and coverslipped with Mowiol (Calbiochem, Darmstadt, Germany).

For Nissl staining, sections were mounted onto glass slides in PBS and air-dried, then stained for 10 s with toluidine blue (0.1% in H_2O). Slides were washed twice with H_2O, destained for 15 s in 70% ethanol / 0.001% acetic acid, dehydrated in 100% ethanol and air-dried. After dipping in xylol, sections were mounted with Histokit (Carl Roth, Karlsruhe, Germany).

Immunostaining was visualised using a Leica DM IL LED inverted microscope (Leica Microsystems, Wetzlar, Germany) with the Leica application suite LAS EZ software and a Zeiss LSM 710 confocal microscope (Carl Zeiss MicroImaging, Jena, Germany) with Zeiss Zen software. The overview on ASPA expression (Fig. 5-4) was done in the '*tile scan mode*' composing 5x5 tiles using a 10x objective.

5.2.6. Behavioural Testing

Behavioural testing was performed at 4 months of age. Two groups of male *aspa*$^{-/-}$ mice, either injected with AAV-aspa (n=6) or with AAV-empty (n=6) were tested and compared to uninjected male wildtype littermates (*aspa*$^{+/+}$, n=10) as a control group unless stated otherwise.

5.2.6.1. Rotarod test

Motor coordination and balance were tested in an accelerating rotarod paradigm. Mice were first familiarised with the apparatus (Ugo Basile, Comerio, Italy) in two trials for 2 min at constant speed (4 rpm). For testing, the mice were placed onto the accelerating rod (4-40 rpm in 4 min) and the latency to fall from the rod was determined. Individual performance was averaged over 6 trials (three trials on two consecutive days with a 10 min resting period in their home cages between the trials). If the mouse held on to the rod without active movement, the time of the second rotation was reported as the time of falling off the rod. Nine *aspa*$^{+/+}$ mice were used as a control group.

5.2.6.2. Wire suspension test

This test was performed as previously described (PAYLOR *et al.* 1998; SHAHBAZIAN *et al.* 2002). Mice were suspended from a 2 mm wire placed 30 cm above the ground padded with soft embedding material, and the latency to fall was determined. Cut-off time was 60 s. One test-trial was performed to habituate the mice to the apparatus and after a 5 min resting period in their home cage the test was performed.

5.2.6.3. Dowel Test

This test was performed as previously described (SHAHBAZIAN *et al.* 2002). Mice were placed onto the middle of a wooden dowel (1 cm diameter), which was placed horizontally about 30 cm above the ground padded with soft embedding material. The latency to fall off the dowel was recorded. The performance was averaged over a series of 3 trials (cut-off time: 2 min) per animal with a 5 min resting period in the home cage between the trials. If mice walked across and off the dowel, they were placed back onto the middle of the dowel.

5.2.7. Statistics

All graphs and statistical analyses were done with GraphPad Prism 4 software (La Jolla, CA). Behavioural tests were analysed with One-Way ANOVA followed by Bonferroni *post-hoc* test. The body weight was analysed using a repeated measures Two-Way (group x time) ANOVA for months 2, 3 and 4. Data from month 6 were analysed with One-Way ANOVA followed by Bonferroni *post-hoc*

test, due to the smaller cohort of animals (2, 3, 4 months: *aspa*$^{-/-}$ AAV-aspa: n=6; *aspa*$^{-/-}$ AAV-empty: n=6; *aspa*$^{+/+}$: n=10; 6 months: *aspa*$^{-/-}$ AAV-aspa: n=3; *aspa*$^{-/-}$ AAV-empty: n=3; *aspa*$^{+/+}$: n=3). The data are expressed as mean ± s.e.m. and $p<0.05$ was considered as statistically significant. *$p<0.05$; **$p<0.01$, *** $p<0.001$.

5.3. Results

5.3.1. Study design and viral gene delivery into the brain of young *aspa*$^{-/-}$ mice

Based on earlier findings (Chapter 4) the use of the MBP-promoter is sufficient to drive transgene expression in oligodendrocytes *in vivo*. Moreover, the mosaic AAV1/2 serotype was identified to be the most efficient vector for gene transfer to oligodendrocytes (OLs). Consequently, AAV1/2-MBP-Aspa was selected as the vector of choice for the gene therapy approach.

Timing of intervention is a crucial element in CD therapy. Ideally, the treatment should start before the onset of potentially irreversible brain damage. Based on the findings from Chapter 3, revealing that CD pathology already becomes apparent before weaning in *aspa*$^{-/-}$ animals (≙ *aspa*$^{lacZ/lacZ}$ from Chapter 3*)* and AAV-mediated transgene expression takes several weeks to reach maximum levels, gene transfer should take place as early as possible (KLUGMANN *et al.* 2005). However, results of this thesis (Chapter 4) point out that AAV-MBP mediated gene transfer to neonatal mice resulted in a poor transduction efficiency. Based on the spatio-temporal expression profile of ASPA (KIRMANI *et al.* 2003; KLUGMANN *et al.* 2003), vector infusion was performed at postnatal day (P) 9 or 10. In order to define the injection sites the lambda demarcation was used as a basis and the coordinates were determined according to previous studies in young mice (PAXINOS *et al.* 2006; PILPEL *et al.* 2009). To achieve a widespread viral transduction, the vectors were injected bilateral into the striatum, the thalamus and the cerebellum (Fig. 5.2 C-E), which are severely affected brain regions in CD patients and CD animal models (see Chapter 3).

Aspa$^{-/-}$ mice were injected in a freehand injection procedure, due to the lack of equipment for stereotaxic guidance in juvenile mice, with AAV-MBP-aspa (*aspa*$^{-/-}$ AAV-aspa; n=6; a total of 2.1 x 10^{10} viral genomes per mouse) or with AAV-empty as a vector control (*aspa*$^{-/-}$ AAV-empty; n=6; a total of 2.0 x 10^{10} viral genomes per mouse). The body weight and motor functions were assessed as depicted in the experimental outline (Fig. 5.2 A). Furthermore, cohorts of AAV-aspa and AAV-empty infused *aspa*$^{-/-}$ animals and *aspa*$^{+/+}$ controls (n=3 for each group) were sacrificed to perform histological and biochemical analysis.

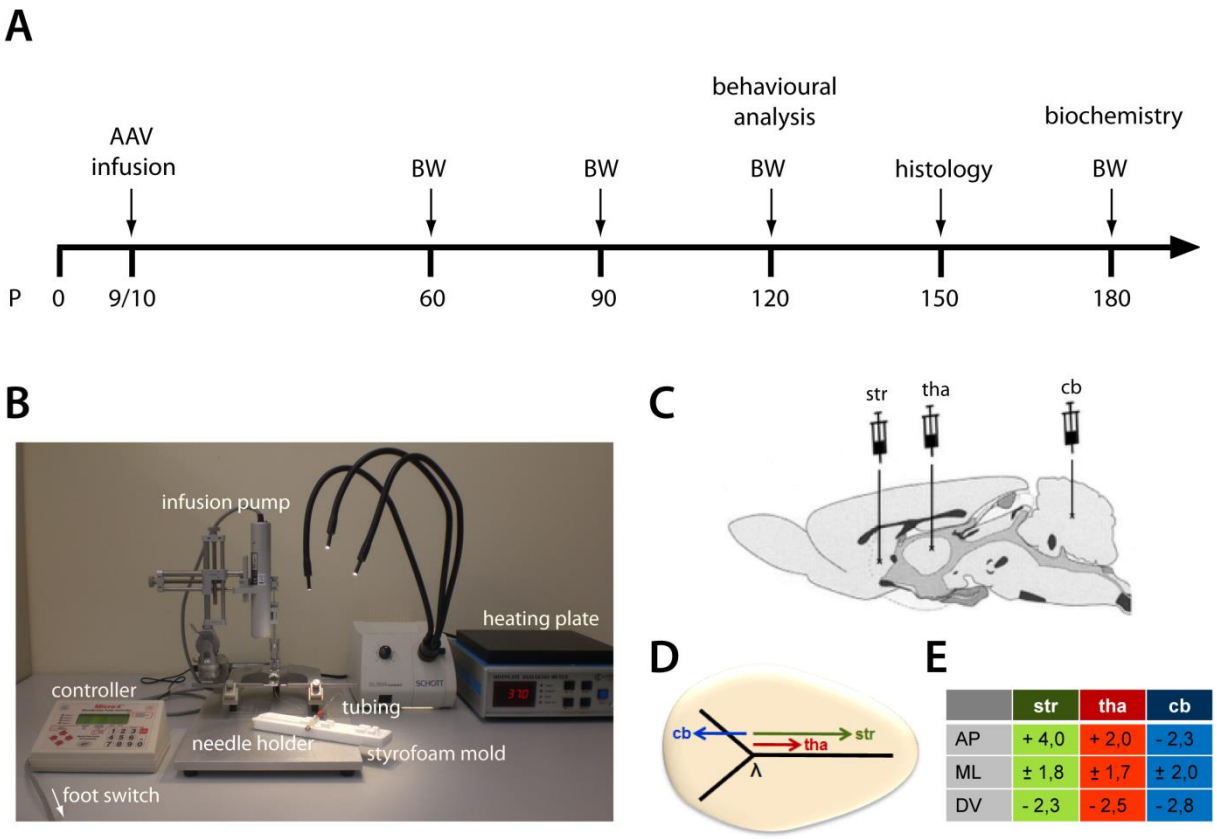

Figure 5.2: Study design and experimental setup.
(A) Experimental time line. AAV injections were carried out P9 or P10. The body weight (BW) was measured on a regular basis, behavioural analysis was performed after 4 months, followed by histological and biochemical analysis. **(B)** Injection setup. The infusion pump was equipped with a 100 µl syringe and connected to a 34G bevelled needle via plastic tubing and a needle holder. The injection was controlled by a microprocessor connected to a foot switch. During the surgery the mouse was placed in a Styrofoam mold to fixate the head and body and afterwards put on a heating plate until recovery. (**C, D**) Scheme of a rodent brain with the injection sites on a sagittal section (**C**) (modified from (KLUGMANN *et al.* 2005)) and on top view (**D**). **(E)** Table of the injection coordinates.

5.3.2. Effects on ASPA expression and NAA levels

ASPA protein levels were assessed by Western Blot analysis of whole brain lysates 6 months after viral gene delivery (n=3 for each group). Previous studies using a vector with a hemagglutinin tag (HA-tag, YPYDVPDYA) fused to the N-terminus of recombinant ASPA revealed no adverse effects of the HA-tag in ASPA gene transfer to neurons, but benefited from highly sensitive HA-immunoreactivity (KLUGMANN *et al.* 2005). Therefore, HA-tagged ASPA was used for the gene therapy of *aspa*$^{-/-}$ mice. However, in a previous study Klugmann and co-workers have shown, that the HA-tagged ASPA construct resulted in two bands in Western-Blot analysis: One band at 38 kDa representing fusion-protein and a possible 37 kDa band corresponding to the expected ASPA size, indicating that the HA-tag may be cleaved off through a form of posttranscriptional processing in a

subpopulation of cells (KLUGMANN *et al.* 2005). In the present study, only one single band at 37 kDa was detectable, indicating quantitative removal of the HA-tag.

This band was detected in *aspa*$^{+/+}$ as well as in *aspa*$^{-/-}$ AAV-aspa injected animals but not in the in *aspa*$^{-/-}$ AAV-empty injected mice (Fig. 5.3.A). One of the AAV-aspa injected knockouts (8th lane) showed only poor ASPA expression, leading to the strong variation of expression levels in Fig. 5.3.B. (ASPA protein: *aspa*$^{+/+}$: 1.00 ± 0.10 %; *aspa*$^{-/-}$ AAV-empty: 0.00 ± 0.00 %; *aspa*$^{-/-}$ AAV-aspa 0.59 ± 0.31 %; $F_{2,8}$= 7.24; p<0.0251).

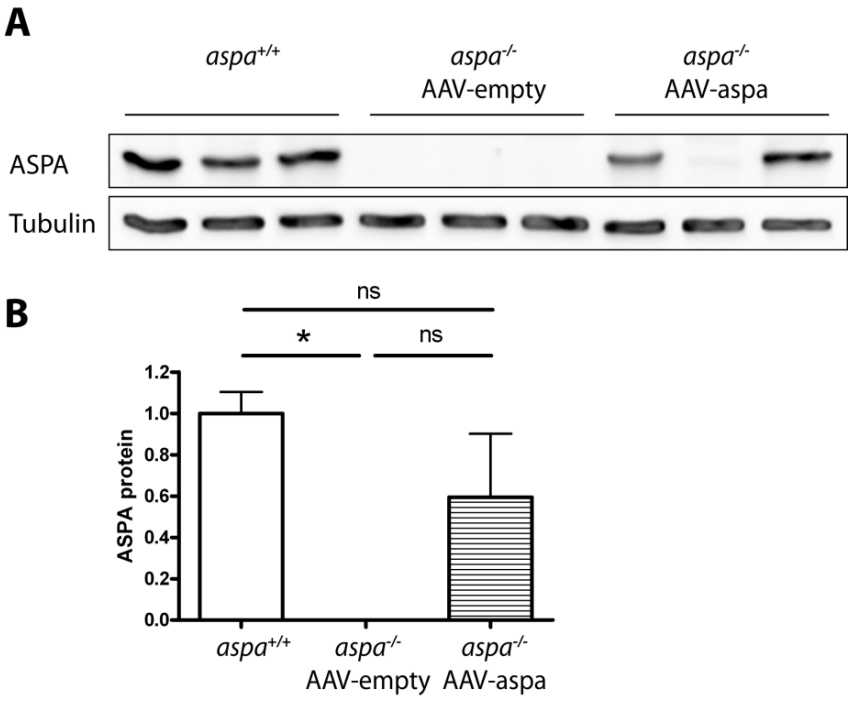

Figure 5.3: Western blot analysis of ASPA protein levels.
(A) Western blot analysis of whole brain lysates 6 months after virus injection (n=3 for each group). The 37 kD ASPA protein was detected in *aspa*$^{+/+}$ and *aspa*$^{-/-}$ AAV-aspa injected mice but not in *aspa*$^{-/-}$ AAV-empty treated animals. α-Tubulin was used as loading control. **(B)** Quantification of ASPA protein levels: *aspa*$^{+/+}$: 1.00 ± 0.10 %; *aspa*$^{-/-}$ AAV-empty: 0.00 ± 0.00 %; *aspa*$^{-/-}$ AAV-aspa 0.59 ± 0.31 %; $F_{2,8}$= 7.24; p<0.0251.

Next, the biological functionality of the restored ASPA protein was assessed by determination of NAA levels in brain homogenates using ^{1}H-NMR spectroscopy 6 months after treatment. NAA concentrations were decreased in all mice treated with AAV-aspa and in two two-thirds of the AAV-aspa treated animals a reduction to wildtype levels was achieved, demonstrating the functionality of ASPA protein (Fig. 5.4). As whole brain lysates were used for this experiment, these results strongly suggests the restoration of ASPA throughout the brain. However, due to the freehand injection procedure, variances in the reduction of NAA levels were expected. Indeed, the animal displaying the lowest ASPA expression in the Western blot analysis also contained the highest amount of NAA.

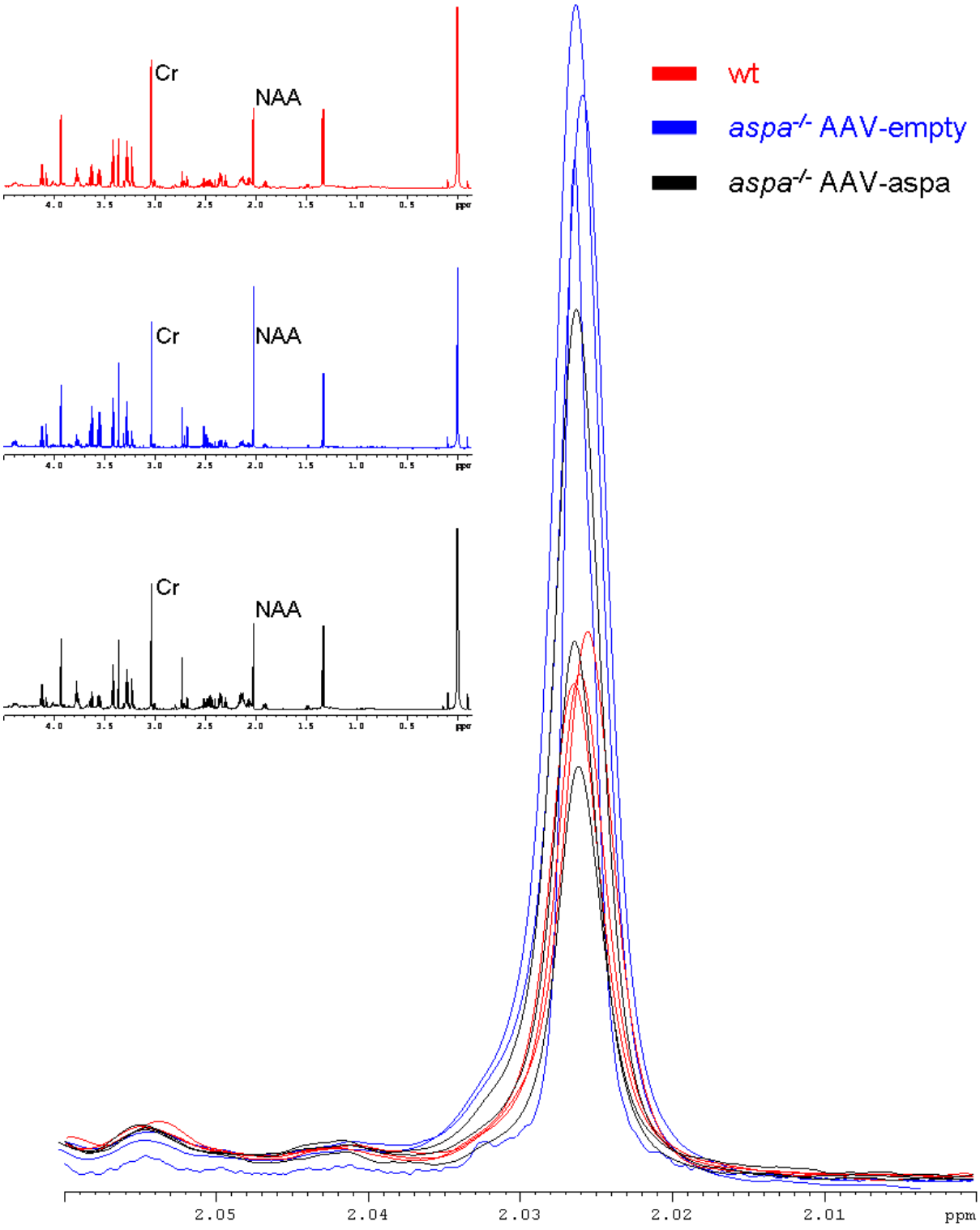

Figure 5.4: ^{1}H-NMR analysis of NAA levels.
Left: Representative ^{1}H-NMR spectra of whole brain lysates from *aspa*$^{+/+}$ (red), *aspa*$^{-/-}$ AAV-empty injected animals (blue) and *aspa*$^{-/-}$ AAV-aspa injected mice (black) 6 months after virus infusion. Right: Overlay of the NAA peak of all animals investigated (n=3 per group). NAA levels were lowered in all AAV-aspa treated mice including a reduction to normal levels in 2 out of 3 animals, confirming the functionality of the restored enzyme. NAA levels are presented as a ratio with Creatine (Cr).

5.3.3. Histological findings

Vector spread

Brain sections of 5-month-old mice were stained with an anti-ASPA antibody to evaluate viral transduction efficiency. Immunohistochemical analysis of representative brain sections from *aspa*$^{+/+}$ mice revealed robust ASPA expression throughout the brain with highest expression levels in subcortical and cerebellar white matter tracts (Fig. 5.5 A-C). AAV-empty injected *aspa*$^{-/-}$ mice did not exhibit any ASPA immunoreactivity (Fig. 5.5 G-I). However, ASPA expression was restored in *aspa*$^{-/-}$ via AAV-mediated gene transfer (Fig. 5.5 M-O). In *aspa*$^{-/-}$ AAV-aspa injected mice the transgene was robustly expressed throughout the brain with highest expression levels in the targeted regions striatum, thalamus and cerebellum. Moreover, ASPA-positive cell bodies were present in regions distal to the injection sites such as the corpus callosum, hippocampus, neocortex and brain stem comparable to the expression pattern of the endogenous protein in *aspa*$^{+/+}$ mice.

Tropism

Furthermore, the brain sections were used to examine the cell types transduced by the vectors. To verify the non-neuronal gene delivery, double-immunostaining for the transgene and the neuronal marker NeuN was performed. The transduction pattern was analysed by confocal microscopy and Figure 5.6 shows ASPA expression in the thalamus as a representative example for one of the target regions. In naïve *aspa*$^{+/+}$ mice endogenous ASPA expression clearly segregated from neurons. No ASPA protein was detectable in *aspa*$^{-/-}$ AAV-empty injected mice. However, AAV-aspa injected *aspa*$^{-/-}$ animals displayed strong ASPA expression, which is excluded from neurons. Hence, neuronal *aspa* gene delivery could be excluded. Furthermore, ASPA immunoreactivity was not found in astrocytes (Fig 5.7).

The co-labeling of ASPA with an oligodendrocyte marker was prevented up to now, because there was no antibody available staining oligodendroglial somata in a double-immunostaining with the anti-ASPA antibody. In addition, the co-labeling with an antibody against the HA-tag was not successful (data not shown), probably because the HA-tag was cleaved off (see 5.3.2). Hence, for the present study oligodendroglial gene transfer had to be determined based on morphological criteria such as small cell bodies and high density of both the cytoplasm and the nucleus (BAUMANN and PHAM-DINH 2001). In the brains of naïve as well as *aspa*$^{-/-}$ AAV-aspa animals ASPA immunoreactivity was present in small cell bodies (Fig. 5.6 A, G and Fig. 5.7 A, G), which is distinctive for oligodendrocyte-specific protein expression in the cytoplasm of these cells and indicating oligodendroglial gene transfer.

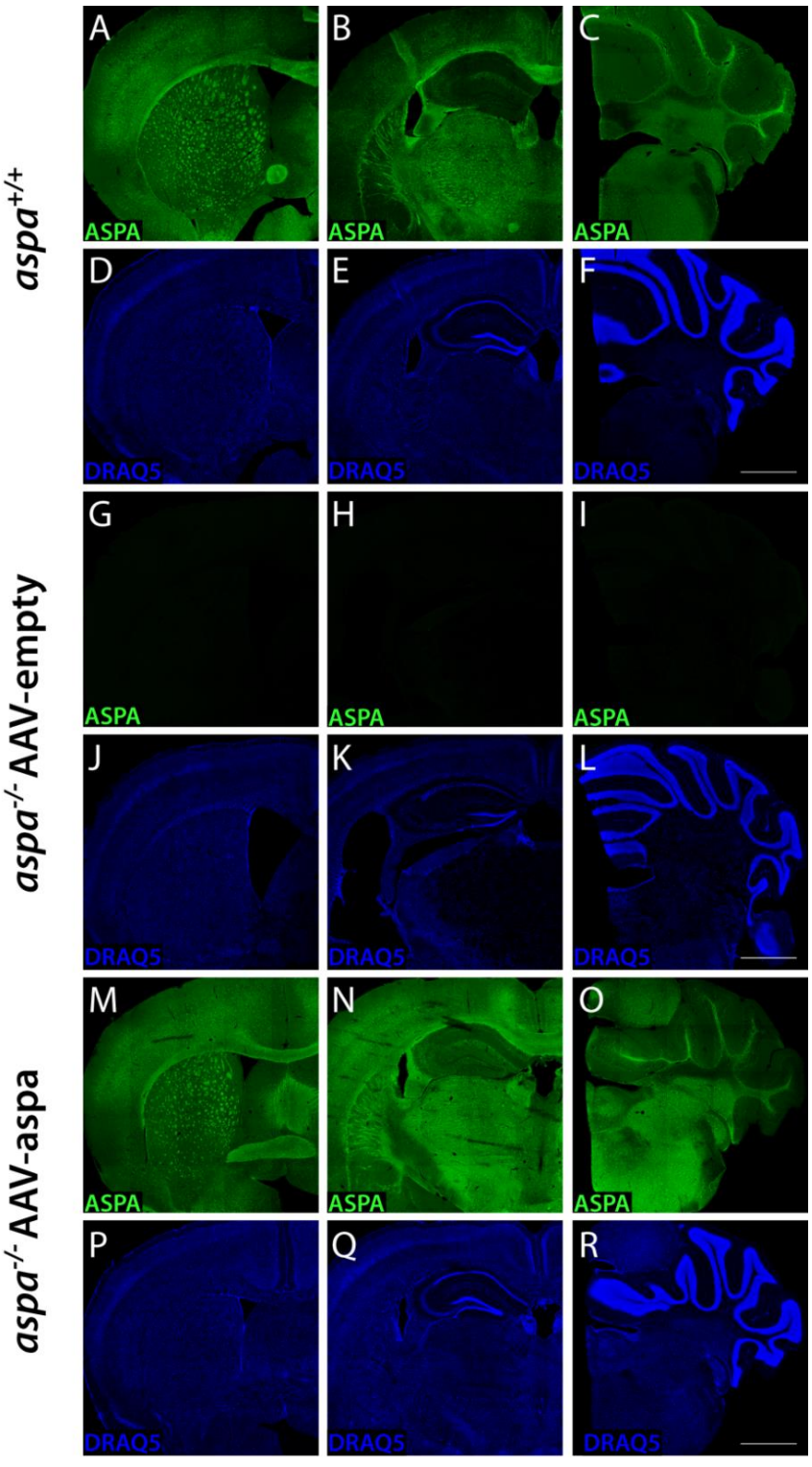

Figure 5.5: Overview on the ASPA expression.

Immunohistochemical analysis of one hemisphere showing the striatum, corpus callosum and cortex (**A, D, G, J, M, P**), the thalamus, hippocampus, corpus callosum and cortex (**B, E, H, K, N, Q**) and the cerebellum and brainstem (**C, F, I, L, O, R**). Panels (**A-C**), (**G-I**) and (**M-O**) show ASPA immunoreactivity, while panels (**D-F**), (**J-L**) and (**P-R**) show the corresponding staining of the cell nuclei with DRAQ5. (**A-F**) Highest ASPA-expression in naïve *aspa*$^{+/+}$ controls was observed in white matter tracts such as the corpus callosum and the white matter tracts of the cerebellum, but also striatum, thalamus and brainstem displayed strong ASPA expression. (**G-L**) *aspa*$^{-/-}$ AAV-empty injected mice do not show any ASPA immunoreactivity. (**M-R**) In contrast, AAV-aspa injected *aspa*$^{-/-}$ animals display strong ASPA expression throughout the brain and especially in white matter tracts. Scale bars: 1 mm.

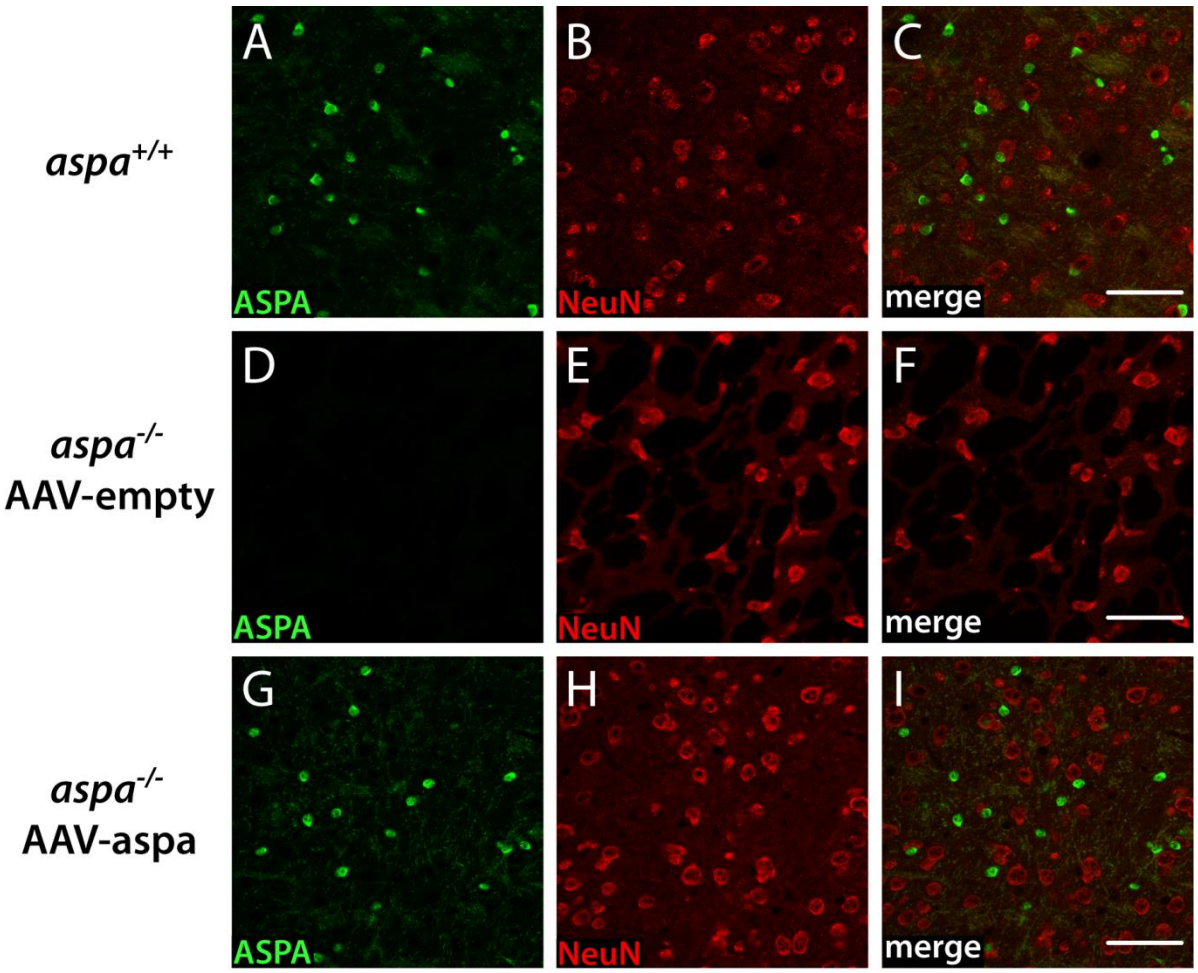

Figure 5.6: Non-neuronal ASPA expression.

The panels show the in-depth histological analysis of ASPA expression via confocal microscopy (**A, D, G**) and the co-labeling with the neuronal marker NeuN (**B, E, H**) in the thalamus. **(A-C)** In naïve *aspa*$^{+/+}$ mice ASPA is not expressed in neurons. **(D-F)** *aspa*$^{-/-}$ AAV-empty injected mice do not show any ASPA immunoreactivity. **(G-I)** However, AAV-aspa injected *aspa*$^{-/-}$ animals display strong ASPA expression, which segregates from neurons. The immunostaining exhibited by small cell bodies is distinctive for oligodendrocyte-specific cytoplasmatic protein expression. Scale bars: 50 µm.

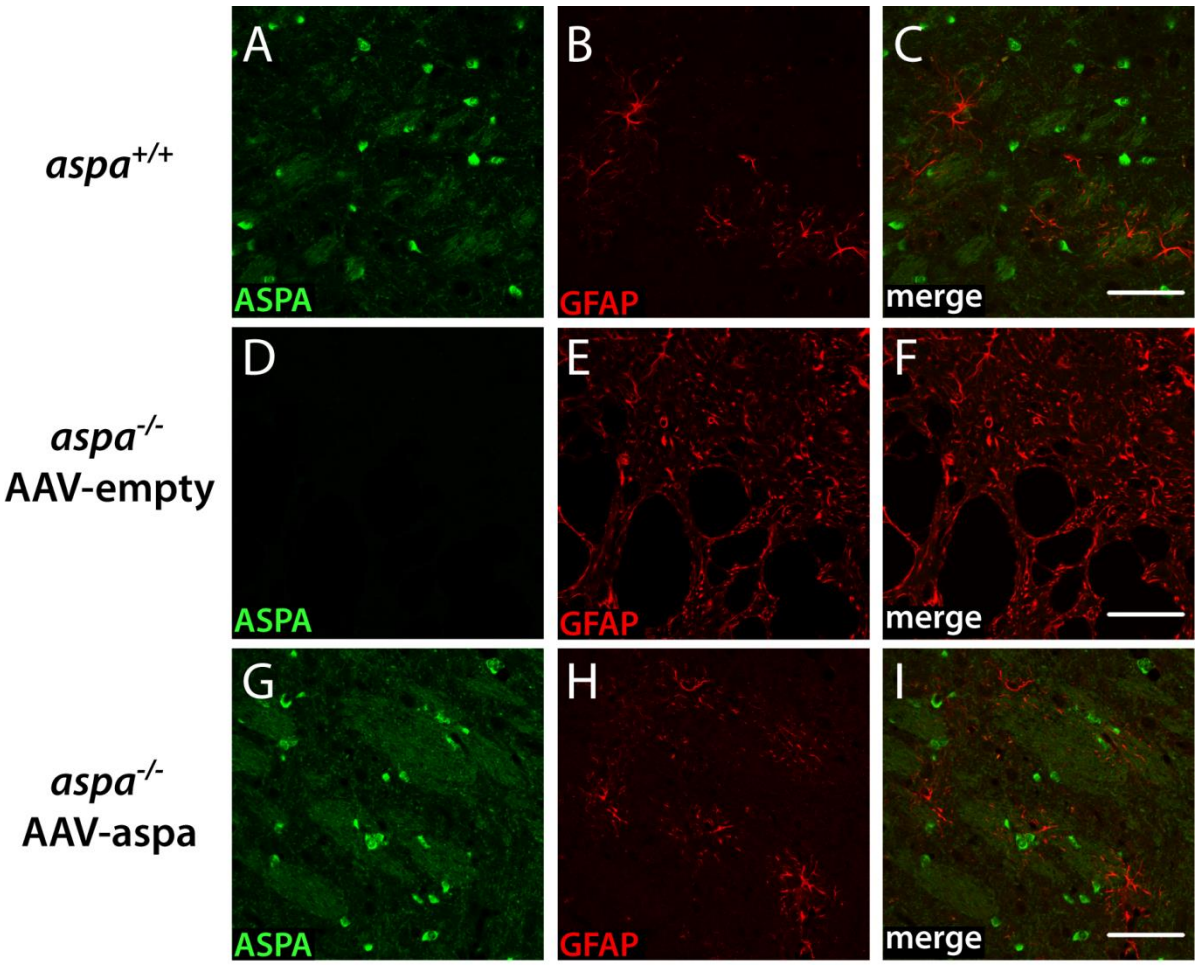

Figure 5.7: Non-astroglial ASPA expression.
The panels show the in-depth histological analysis of ASPA expression via confocal microscopy (**A, D, G**) and the co-labeling with the astroglial marker GFAP (**B, E, H**) in the thalamus. **(A-C)** In naïve *aspa*$^{+/+}$ mice ASPA is not expressed in astrocytes. **(D-F)** *aspa*$^{-/-}$ AAV-empty injected mice do not show any ASPA immunoreactivity. **(G-I)** However, AAV-aspa injected *aspa*$^{-/-}$ animals display strong ASPA expression, which segregates from astrocytes. The immunostaining exhibited by small cell bodies is distinctive for oligodendrocyte-specific cytoplasmatic protein expression. Scale bars: 50 µm.

A hallmark of CD is the massive and progressive vacuolisation accompanied by the enlargement of the ventricles (KITADA *et al.* 2000; SURENDRAN *et al.* 2005a; TRAKA *et al.* 2008). To investigate this, histological analysis was performed by Nissl staining of brain sections 5 months after AAV-aspa or AAV-empty infusion (Fig 5.8).

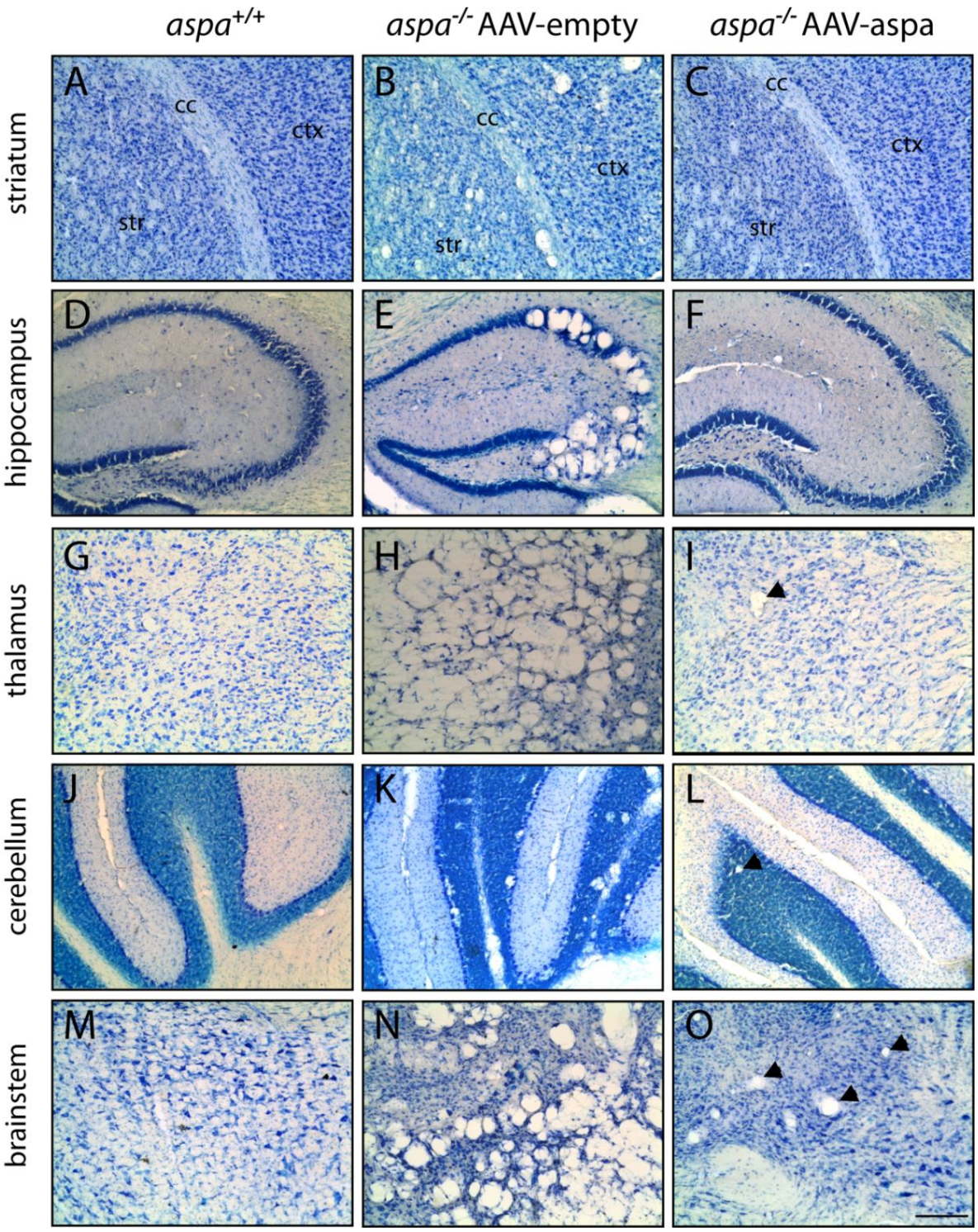

Figure 5.8: Amelioration of the vacuolisation in different brain regions.
Representative Nissl stained sections of wildtype mice (**A, D, G, J, M**), AAV-empty injected *aspa*$^{-/-}$ mice (**B, E, H, K, N**) and AAV-aspa injected *aspa*$^{-/-}$ mice (**C, F, I, L, O**) at 5 months of age. Vacuolisation was present in the striatum (str), cerebral cortex (ctx) and corpus callosum (cc) of *aspa*$^{-/-}$ AAV-empty injected, but not in corresponding wildtype and AAV-aspa injected mice (**A, B, C**). Vacuolisation in the CA1-CA3 region of the hippocampus (**D, E, F**) was reduced and so was the substantial spongy degeneration of the thalamus (**G, H, I**). In the cerebellum (**J, K, L**) vacuoles were present in the purkinje cell layer, granular cell layer and the white matter in control vector group, whereas the molecular layer appeared normal. In all affected layers a reduction of the vacuolisation was achieved by the injection of AAV-aspa. The extensive vacuolisation of the dorsal brainstem was diminished (**M, N, O**). Remaining vacuols are indicated by arrowheads. Scale bar: 200 µm.

Vacuolisation in *aspa*$^{-/-}$ AAV-empty injected mice was prominent in the hippocampus, thalamus, cerebellum and the dorsal brain stem. The thalamus and the dorsal brain stem were uniformly affected (Fig. 5.8 H, N). In contrast, in the hippocampus vacuoles specifically occurred in in the CA1-CA3 region, whereas the dentate gyrus granule cells were spared (Fig. 5.8 E). In the cerebellum vacuoles were present in the white matter tracts, the purkinje cell layer and the granular cell layer, while the molecular layer appeared normal (Fig. 5.8 K).

Furthermore, vacuoles were observed in the cerebral cortex and the corpus callosum in aged mutants (Fig. 5.8 B), but not before 5 months (see Chapter 3), indicating the progressive nature of the vacuolisation. By infusion of AAV-aspa into the striatum, thalamus and cerebellum of *aspa*$^{-/-}$ mice the spongiform vacuolisation was significantly reduced in all regions analysed (Fig. 5.8 C, F, I, L, O) but most effectively in the thalamus. It is noteworthy that spongy degeneration of regions distal from the injection sites such as hippocampus and corpus callosum was also diminished. Table 5.1 gives an overview on the extent of vacuolisation after AAV-mediated *aspa* gene transfer.

Table 5.1: Reduction of the spongiform vacuolisation in different brain regions.

	aspa$^{-/-}$ AAV-empty	*aspa*$^{-/-}$ AAV-aspa
Striatum	++	+
Corpus callosum	+	-
Cerebral cortex	+	-
Hippocampus		
CA1-CA3	+++	-/+
Dentate gyrus	-	-
Thalamus	++++	+
Cerebellum		
Granule cell layer	+	-/+
Purkinje cell layer	+	-
White matter	++	+
Brainstem	+++	+/++
Ventricle size	massively enlarged	enlarged/normal

The extent of vacuolisation was examined in Nissl-stained sections at 5 months of age. The presence of vacuoles was characterised according to (TRAKA *et al.* 2008) as: -: absent, +: low, ++: moderate, +++: severe.

5.3.4. Evaluation of body weight and motor functions

The body weight of *aspa*$^{-/-}$ mice is significantly reduced compared to *aspa*$^{+/+}$ mice throughout the whole lifespan (see Chapter 3) and was therefore evaluated after *aspa* gene transfer (Fig.5.9). Repeated-measures Two-Way ANOVA analysis for months 2, 3 and 4, respectively, revealed no significant interaction effect ($F_{4,38}$=1.13; p=0.3554), but a significant effect on time ($F_{2,38}$=227.90; p<0.0001), on the group ($F_{2,38}$=25.01; p<0.0001) and on the subject ($F_{19,38}$=5.839; p<0.0001). Thus, the subjects of all groups gained weight during the study, but only the body weight of AAV-aspa treated *aspa*$^{-/-}$ mice was restored to *aspa*$^{+/+}$ mice levels. The body weight at month 6 was evaluated separately by One-Way ANOVA followed by Bonferroni *post-hoc* test due to a smaller group size ($F_{2,6}$=17.42; p=0.0032). Although *aspa*$^{-/-}$ AAV-aspa mice gained less weight than *aspa*$^{+/+}$ controls, there was no significant difference between these groups (p>0.05) and the body weight of *aspa*$^{-/-}$ AAV-empty mice was reduced until the end of the study with a trend towards a decrease of body weight during disease progression.

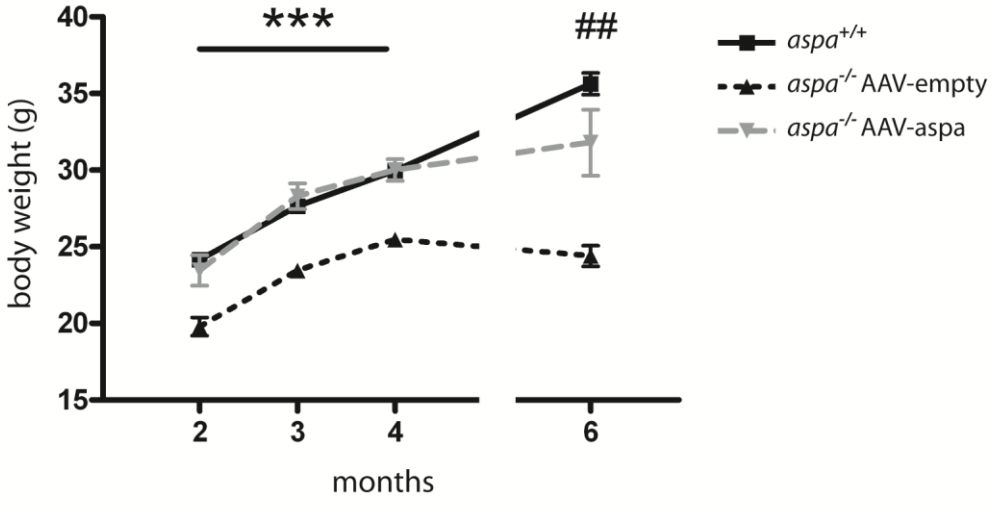

Figure 5.9: Time curve of the body weight of *aspa*$^{+/+}$, *aspa*$^{-/-}$ AAV-empty and *aspa*$^{-/-}$ AAV-aspa mice.
The body weight of *aspa*$^{-/-}$ mice is significantly reduced compared to *aspa*$^{+/+}$ mice throughout the whole lifespan. The body weight was analysed using repeated measures Two-Way ANOVA analysis for months 2, 3 and 4. There was no significant interaction effect ($F_{4,38}$=1.13; p=0.3554), but a significant effect on time ($F_{2,38}$=227.90; p<0.0001), on the group ($F_{2,38}$=25.01; p<0.0001) and on the subject ($F_{19,38}$=5.839; p<0.0001). The body weight at month 6 was evaluated separately by a One-Way ANOVA followed by Bonferroni *post-hoc* test due to the smaller group size ($F_{2,6}$=17.42; p=0.0032).

CD patients as well as CD animal models suffer from motor impairments such as ataxia and spasticity. Hence, the central aim of CD therapy is to restore motor functions. To address the

therapeutic benefits on neurological function all groups of animals were subjected to a battery of behavioural tests.

Motor learning was assessed in an accelerating rotarod paradigm at 4 months of age. A significant decrease in the time spent on the rotarod in *aspa*$^{-/-}$ AAV-empty injected mice was observed compared to wildtype animals. The latency for *aspa*$^{-/-}$ AAV-aspa mice was increased and comparable to *aspa*$^{+/+}$ levels (Fig. 5.10 A) (*aspa*$^{+/+}$: 180.9 ± 17.3 s; *aspa*$^{-/-}$ AAV-empty: 77.2 ± 22.9 s; *aspa*$^{-/-}$ AAV-aspa 167.6 ± 21.9 s; $F_{2,18}$=7.46; p=0.044). To further evaluate motor functions, a wire suspension test was performed (Fig. 5.9 B) forcing the mice to suspend themselves from a thin metal wire. Whereas *aspa*$^{+/+}$ mice were able to hold onto the wire, AAV-empty injected *aspa*$^{-/-}$ mice showed a significant decrease in suspension time. In contrast to the AAV-empty injected *aspa*$^{-/-}$ mice, the AAV-aspa treated *aspa*$^{-/-}$ mice showed a significantly improved performance in this test (*aspa*$^{+/+}$: 49.0 ± 5.7 s; *aspa*$^{-/-}$ AAV-empty: 3.8 ± 1.0 s; *aspa*$^{-/-}$ AAV-aspa 49.9 ± 7.1 s; $F_{2,19}$=19.38; p<0.0001). In addition, the ability to balance on a thin wooden dowel was restored in AAV-aspa injected *aspa*$^{-/-}$ mice (Fig. 5.10 C) (*aspa*$^{+/+}$: 117.1 ± 2.0 s; *aspa*$^{-/-}$ AAV-empty: 15.89 ± 4.9 s; *aspa*$^{-/-}$ AAV-aspa 100.3 ± 16.4 s; $F_{2,19}$=42.03; p<0.0001).

Interestingly, AAV-aspa injected *aspa*$^{-/-}$ mice exhibited normal nest-building behaviour including rumpling and shredding of the supplied nest-building material in contrast to the AAV-empty injected *aspa*$^{-/-}$ controls (Fig. 5.10 D-F). Depicted are representative photos 3 days after the change of the home cage of single-housed mice indicating the restoration of complex behaviour in *aspa*$^{-/-}$ mice after AAV-mediated *aspa* gene transfer.

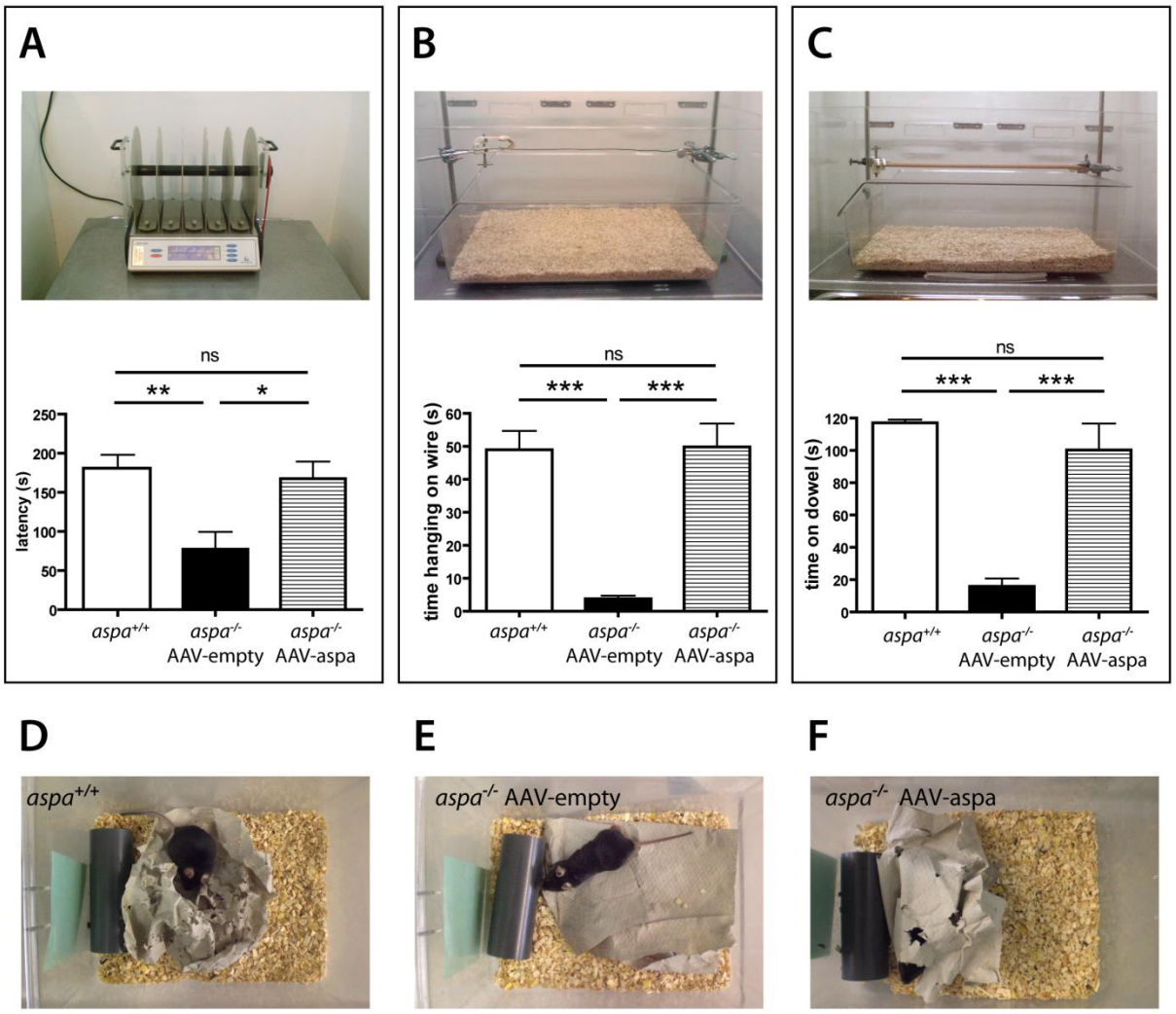

Figure 5.10: Amelioration of behavioral deficits after AAV-aspa injection.

(**A**) The analysis of motor functions in an accelerating rotarod paradigm revealed a significant improvement of performance after AAV-aspa treatment. (**B**) AAV-empty injected *aspa*$^{-/-}$ mice were not able to hang onto a thin metal wire in the wire suspension test compared to their wildtype littermates and the AAV-aspa treated knockouts. (**C**) In the dowel test paradigm wildtype mice remained on the wooden dowel for the maximum time of 2 min whereas AAV-empty injected, but not AAV-aspa injected mice tend to fall down. *$p < 0.05$; **$p < 0.01$, *** $p < 0.001$ in the Bonferroni *post-hoc* test for *aspa*$^{-/-}$ AAV-aspa vs. *aspa*$^{-/-}$ AAV-empty and *aspa*$^{+/+}$. (**D, E, F**) Nest building behavior was restored in AAV-aspa injected mice. Depicted are representative photos three days after the change of the home cage of single-housed mice.

5.4. Discussion

5.4.1. The study design

Canavan disease is an autosomal recessive leukodystrophy caused by loss-of-function mutations in the *aspa* gene. This leads to a loss of ASPA function and subsequently to the progressive accumulation of its substrate N-acetylaspartate (NAA), which is cleaved by ASPA under physiological conditions into aspartate and acetate. With its monogenetic nature and the pathology confined to the CNS, CD provides a strong rationale for a gene transfer approach to target the causative pathological mechanism of this disease. Due to the lack of a gene-transfer system, which is able to transduce oligodendrocytes, previous studies used neurotropic vectors to degrade NAA at the origin of its synthesis (KLUGMANN *et al.* 2005; MATALON *et al.* 2003; MCPHEE *et al.* 2005b; SEKI *et al.* 2002; SEKI *et al.* 2004). However, these attempts resulted in hardly any improvements of clinical parameters, suggesting that neuronal ASPA expression cannot compensate for oligodendrocyte dysfunction. Hence, the inadequacies of the vector system hampered a better outcome and provide the rationale for the restoration of ASPA at its physiological site to ultimately correct CD pathophysiology.

Since CD is a disorder manifesting in early childhood, it is likely that the success of a replacement strategy depends on the timing of intervention. It has been shown previously that mRNA levels are detectable beyond postnatal day 11 in the mouse brain (KIRMANI *et al.* 2003) and ASPA enzyme reaches significant levels at day 12 in the postnatal rat brain (KLUGMANN *et al.* 2003). Thus, gene therapy should take place as early as possible, suggesting *in utero* gene transfer (KLUGMANN *et al.* 2005). Nevertheless, previous studies have used adult CD animal models for viral-mediated *aspa*-transfer and could hardly improve CD pathophysiology, demonstrating the ill-conceived timing of these studies (MATALON *et al.* 2003; MCPHEE *et al.* 2005b; SEKI *et al.* 2002; SEKI *et al.* 2004). However, results from Chapter 4 revealed that AAV mediated gene transfer into neonatal mice with the transgene driven by the MBP-promoter resulted in a very low transduction rate, precluding efficient gene transfer with the MBP-HA-ASPA AAV1/2 virus at this time point. It is tempting to speculate that oligodendrocyte progenitors (OPCs) do not get infected at this stage of maturation, probably because they do not yet express specific receptors, which are the prerequisite for an initial interaction between the virus and the cell and the subsequent internalisation process. This hypothesis is supported by the findings that synthesis of the primary AAV2 receptors, heparan sulfate proteoglycans (HSPG), on oligodendrocytes is upregulated by adhesion-induced regeneration and/or differentiation (SZUCHET *et al.* 2000). Therefore, a time point later in development (P9/P10) was selected.

For the present study, a genetically engineered CD mouse model was used displaying all signs of CD pathology such as the spongiform vacuolisation, moderate neurological impairments, metabolic changes and behavioural deficits (see Chapter 3). In line with previous preclinical and clinical studies (JANSON *et al.* 2002a; KLUGMANN *et al.* 2005) a multi-site injection strategy was chosen to ensure most widespread transduction efficiency and the efficacy of this treatment was assessed.

5.4.2. AAV mediated *aspa* gene transfer restores ASPA expression and lowers NAA levels

The expression of ASPA protein in AAV-aspa injected *aspa*$^{-/-}$ mice was confirmed via Western blot analyses of whole brain lysates 6 months after virus infusion. ASPA protein was detectable in *aspa*$^{+/+}$ and in *aspa*$^{-/-}$ AAV-aspa injected animals, but not in the in *aspa*$^{-/-}$ AAV-empty injected mice, demonstrating the successful restoration of this enzyme. However, ASPA levels were not significantly increased compared to *aspa*$^{-/-}$ AAV-empty injected mice. This might be a cause of the broad variance in expression levels, which is a consequence of variances of the injection parameters due to the freehand injection procedure. However, this does not necessarily hamper clinical application, as a variation in the injection coordinates can be prevented by stereotaxically guided intraparenchymal injections, which were not available for intervention in P9/P10 mice.

To validate the functionality of the enzyme the levels of ASPA substrate were assessed by measuring NAA levels *ex vivo* in whole brain lysates 6 months after virus infusion. ^{1}H-NMR spectroscopy revealed an increase of NAA levels in ASPA-deficient mice confirming the MRI data (see Chapter 3). The decrease of the NAA signal after AAV-aspa treatment confirms the functionality of the restored ASPA enzyme and correlates with the ASPA expression levels. This is indicated by the finding, that the *aspa*$^{-/-}$ AAV-aspa injected animal, displaying the lowest ASPA expression in the Western blot analysis, also contained the highest amount of NAA. In fact, NAA levels were normalised in two out of three of the animals, demonstrating the positive effects of AAV-aspa treatment. However, the variations in NAA reduction can again be explained by the freehand-injection procedure.

5.4.3. *aspa* gene transfer to OLs ameliorates CD histopathology

In CD the whole brain is affected, most strikingly visible by the extent of spongiform vacuolisation. Hence, an ideal therapy should aim at a widespread transduction of OLs. For that

reason, a multi-site injection strategy was pursued, targeting the striatum, thalamus and cerebellum of P9/P10 mice. *Aspa* gene transfer resulted in a robust and widespread rostro-caudal and medio-lateral extent of transduction 5 months after virus infusion. Whereas AAV-empty injected *aspa*$^{-/-}$ mice did not exhibit any ASPA immunoreactivity, ASPA expression was restored in *aspa*$^{-/-}$ AAV-aspa injected animals. When compared to *aspa*$^{+/+}$ mice, the cohort of *aspa*$^{-/-}$ mice infused with the therapeutic vector exhibited almost the same transduction pattern peaking in white matter tracts, striatum and thalamus. Furthermore, the restored ASPA expression pattern was remarkably overlapping with the expression pattern in wildtype animals as shown in X-Gal stainings depicted in Chapter 3. In addition to the expression at the injection sites, ASPA-positive cell bodies were present in regions distal to the injection sites such as the corpus callosum, hippocampus, neocortex and brain stem, thus demonstrating the efficiency of the vector used. The extent of transduction may also be influenced synergistically by the choice of the time-point of intervention. Gliogenesis peaks within the first few postnatal weeks and OPCs emigrate from the subventricular zone into the striatum and white matter as well as into the medial, dorsal, and lateral regions of the cerebral cortex, where they develop into mature oligodendrocytes (LEVISON *et al.* 1993; LEVISON and GOLDMAN 1993; MARSHALL *et al.* 2003). Therefore, postnatal days 9 and 10 were chosen to profit from still migrating OPCs already expressing the cell surface receptors needed for viral entry, thus enhancing the extent of transduction.

In-depth histological analysis of the thalamus revealed the non-neuronal expression of ASPA after AAV-mediated gene transfer as colocalisation between the neural marker NeuN and ASPA did not occur. Based on morphological criteria the ASPA-positive cells were identified to be oligodendrocytes. Furthermore, the immunoreactivity exhibited by small cell bodies is distinctive for oligodendrocyte-specific cytoplasmatic protein expression (KLUGMANN *et al.* 2003) and demonstrates the correct intracellular protein localisation.

This study revealed an age-dependent progressive vacuolisation in the corpus callosum, which has not been reported in other CD models so far (TRAKA *et al.* 2008). The formation of vacuoles is not fully understood. However, swellings and vacuolisation appear within astrocytes before they become more prominent in the interstitium of CD patients (ADACHI *et al.* 1973). In addition, ectopic ASPA expression in neurons with concurrent decrease of NAA does not lead to an improvement of brain morphology (KLUGMANN *et al.* 2005), suggesting that oligodendrocyte as well as astrocyte impairment causes the spongiform degeneration. The results of this study indicate that the restoration of ASPA in oligodendrocytes is sufficient to prevent vacuole formation. Vacuolisation was reduced throughout the brain, but most effectively in the vector infused regions suggesting that the extent of vacuolisation correlates with the restored ASPA expression levels. Furthermore, the

massively enlarged ventricles in *aspa*$^{-/-}$ mice were reduced to slightly enlarged to normal dimensions in AAV-aspa treated *aspa*$^{-/-}$ mice, implying the amelioration of all histopathological signs after AAV-aspa treatment.

5.4.4. Amelioration of motor deficits and the reduced body weight

The regulation of the body weight is closely linked with the regulation of energy balance involving complex CNS circuits. Signals from the gastrointestinal systems like cholecystokinin enter the solitary tract nucleus (STN) located in the caudal brain stem via the vagus nerve to evoke satiation, but intact reciprocal neuronal connections between the STN and parabrachial nucleus (PBN) and the hypothalamus are a prerequisite for the control of eating (BLEVINS and BASKIN 2010). As it was shown in Chapter 3 the STN was severely vacuolated, hypomyelinated and showed signs of axonal swellings in *aspa*$^{-/-}$ mice. This, together with the loss of neuronal integrity in the hypothalamus, may cause the lower body weight of *aspa*$^{-/-}$ mice. However, by *aspa* gene transfer histopathological alteration and neuronal integrity in the thalamus as well as in the brain stem were ameliorated and resulted in an increase of body weight comparable to *aspa*$^{+/+}$mice levels in AAV-aspa infused *aspa*$^{-/-}$ animals lasting over the whole study period.

None of the studies restoring ASPA in neurons have shown comprehensive results regarding the amelioration of motor deficits (KLUGMANN and LEICHTLEIN 2006). Hence, the present study is the first reporting the successful restoration of motor functions in *aspa*$^{-/-}$ mice. In all paradigms tested comprising rotarod-testing, the dowel test and the wire suspension test, AAV-aspa treated *aspa*$^{-/-}$ animals performed significantly better than AAV-empty infused *aspa*$^{-/-}$ mice and equal to *aspa*$^{+/+}$ controls.

Moreover, AAV-aspa treated *aspa*$^{-/-}$ mice show a general normalisation of species-typical behaviour. This includes the increase of alertness and climbing on the cage lid as well as the lack of hypotonia and the splayed legs. Additionally, even complex behaviour such as nest-building requiring step-by-step planning and organisation was restored after AAV-aspa infusion. It is known that cytotoxic lesions in the hippocampus, prefrontal cortex, preoptic area and septum can impair nesting behaviour in rodents (DEACON *et al.* 2002; KOLB 1984; LIN *et al.* 2007; NUMAN 1974; SLOTNICK and NIGROSH 1975). In addition, nest-building in female rodents is influenced by hormone and reproductive status. In contrast to *aspa*$^{+/+}$ and AAV-aspa injected *aspa*$^{-/-}$ mice AAV-empty infused *aspa*$^{-/-}$ animals do not build nests, but only hole up under the paper sheets. This behavior is probably caused by lesions in the above-mentioned regions and further potentiated by the motor deficits of

these mice. Taken together, AAV mediated *aspa* delivery to OLs restores motor function as well as species-typical behaviour in *aspa*$^{-/-}$ mice.

5.4.5. Conclusions and outlook

The present study demonstrates the safety and therapeutic efficacy of AAV-aspa gene delivery in correcting the CD phenotype with no evidence of adverse events. It was shown that the restoration of ASPA in oligodendrocytes and the subsequent rescue of oligodendroglial biochemistry leads to an improvement of motor as well as complex functions and the amelioration of histological aberrations in *aspa*$^{-/-}$ mice, which cannot be achieved by neuronal ASPA expression. Hence, this study helps understanding CD pathophysiology and is an important step towards human CD therapy. The key for success was the appropriate vector system in combination with the right timing of intervention. Although this is a proof-of-concept for the genetic treatment of CD, possible implications reach far beyond CD. This vector system can be applied whenever gene transfer to oligodendrocytes is required, ranging from leukodystrophies originating from loss-of-function mutations to leukodystrophies, which are caused by gain-of-function mutations as RNAi methods can be applied. Moreover, AAVs are widely used in clinical settings making it likely to translate these preclinical findings into the clinic.

References

References

ADACHI, M., L. SCHNECK, J. CARA and B. W. VOLK, 1973 Spongy degeneration of the central nervous system (van Bogaert and Bertrand type; Canavan's disease). A review. Hum Pathol **4:** 331-347.

ADACHI, M., J. TORII, L. SCHNECK and B. W. VOLK, 1972 Electron microscopic and enzyme histochemical studies of the cerebellum in spongy degeneration (van Bogaert and Bertrans type). Acta Neuropathol **20:** 22-31.

AKACHE, B., D. GRIMM, K. PANDEY, S. R. YANT, H. XU *et al.*, 2006 The 37/67-kilodalton laminin receptor is a receptor for adeno-associated virus serotypes 8, 2, 3, and 9. J Virol **80:** 9831-9836.

AKIMITSU, T., K. KURISU, R. HANAYA, K. IIDA, Y. KIURA *et al.*, 2000 Epileptic seizures induced by N-acetyl-L-aspartate in rats: in vivo and in vitro studies. Brain Res **861:** 143-150.

ALLEN, N. J., and B. A. BARRES, 2009 Neuroscience: Glia - more than just brain glue. Nature **457:** 675-677.

ANDREW, R. D., M. W. LABRON, S. E. BOEHNKE, L. CARNDUFF and S. A. KIROV, 2007 Physiological evidence that pyramidal neurons lack functional water channels. Cereb Cortex **17:** 787-802.

ARIYANNUR, P. S., J. R. MOFFETT, P. MANICKAM, N. PATTABIRAMAN, P. ARUN *et al.*, 2010 Methamphetamine-induced neuronal protein NAT8L is the NAA biosynthetic enzyme: implications for specialized acetyl coenzyme A metabolism in the CNS. Brain Res **1335:** 1-13.

ARUN, P., C. N. MADHAVARAO, J. R. MOFFETT, K. HAMILTON, N. E. GRUNBERG *et al.*, 2010 Metabolic acetate therapy improves phenotype in the tremor rat model of Canavan disease. J Inherit Metab Dis **33:** 195-210.

ASSADI, M., C. JANSON, D. J. WANG, O. GOLDFARB, N. SURI *et al.*, 2010 Lithium citrate reduces excessive intra-cerebral N-acetyl aspartate in Canavan disease. Eur J Paediatr Neurol **14:** 354-359.

ATCHISON, R. W., B. C. CASTO and W. M. HAMMON, 1965 Adenovirus-associated defective virus particles. Science **149:** 754-756.

BALLARD, F. J., 1972 Supply and utilization of acetate in mammals. Am J Clin Nutr **25:** 773-779.

BARRES, B. A., and M. C. RAFF, 1994 Control of oligodendrocyte number in the developing rat optic nerve. Neuron **12:** 935-942.

BARTLETT, J. S., R. J. SAMULSKI and T. J. MCCOWN, 1998 Selective and rapid uptake of adeno-associated virus type 2 in brain. Hum Gene Ther **9:** 1181-1186.

BARTLETT, J. S., R. WILCHER and R. J. SAMULSKI, 2000 Infectious entry pathway of adeno-associated virus and adeno-associated virus vectors. J Virol **74:** 2777-2785.

BASLOW, M. H., 1999a The existence of molecular water pumps in the nervous system: a review of the evidence. Neurochem Int **34:** 77-90.

BASLOW, M. H., 1999b Molecular water pumps and the aetiology of Canavan disease: a case of the sorcerer's apprentice. J Inherit Metab Dis **22:** 99-101.

BASLOW, M. H., 2002 Evidence supporting a role for N-acetyl-L-aspartate as a molecular water pump in myelinated neurons in the central nervous system. An analytical review. Neurochem Int **40:** 295-300.

BASLOW, M. H., 2003 N-acetylaspartate in the vertebrate brain: metabolism and function. Neurochem Res **28:** 941-953.

BASLOW, M. H., 2010 Evidence that the tri-cellular metabolism of N-acetylaspartate functions as the brain's "operating system": how NAA metabolism supports meaningful intercellular frequency-encoded communications. Amino Acids **39:** 1139-1145.

BASLOW, M. H., and D. N. GUILFOYLE, 2009 Are astrocytes the missing link between lack of brain aspartoacylase activity and the spongiform leukodystrophy in Canavan disease? Neurochem Res **34:** 1523-1534.

BASLOW, M. H., K. KITADA, R. F. SUCKOW, B. L. HUNGUND and T. SERIKAWA, 2002 The effects of lithium chloride and other substances on levels of brain N-acetyl-L-aspartic acid in Canavan disease-like rats. Neurochem Res **27:** 403-406.

BASLOW, M. H., and S. YAMADA, 1997 Identification of N-acetylaspartate in the lens of the vertebrate eye: a new model for the investigation of the function of N-acetylated amino acids in vertebrates. Exp Eye Res **64:** 283-286.

BAUMANN, N., and D. PHAM-DINH, 2001 Biology of oligodendrocyte and myelin in the mammalian central nervous system. Physiol Rev **81:** 871-927.

BECKER, I., J. LODDER, V. GIESELMANN and M. ECKHARDT, 2010 Molecular characterization of N-acetylaspartylglutamate synthetase. J Biol Chem **285:** 29156-29164.

BECKONERT, O., H. C. KEUN, T. M. EBBELS, J. BUNDY, E. HOLMES *et al.*, 2007 Metabolic profiling, metabolomic and metabonomic procedures for NMR spectroscopy of urine, plasma, serum and tissue extracts. Nat Protoc **2:** 2692-2703.

BHAKOO, K. K., T. J. CRAIG and P. STYLES, 2001 Developmental and regional distribution of aspartoacylase in rat brain tissue. J Neurochem **79:** 211-220.

BHAKOO, K. K., and D. PEARCE, 2000 In vitro expression of N-acetyl aspartate by oligodendrocytes: implications for proton magnetic resonance spectroscopy signal in vivo. J Neurochem **74:** 254-262.

BIFFI, A., P. AUBOURG and N. CARTIER, 2011a Gene therapy for leukodystrophies. Hum Mol Genet.

BIFFI, A., P. AUBOURG and N. CARTIER, 2011b Gene therapy for leukodystrophies. Hum Mol Genet **20:** R42-53.

BITTO, E., C. A. BINGMAN, G. E. WESENBERG, J. G. MCCOY and G. N. PHILLIPS, JR., 2007 Structure of aspartoacylase, the brain enzyme impaired in Canavan disease. Proc Natl Acad Sci U S A **104:** 456-461.

BLACKBURN, S. D., R. A. STEADMAN and F. B. JOHNSON, 2006 Attachment of adeno-associated virus type 3H to fibroblast growth factor receptor 1. Arch Virol **151:** 617-623.

BLEVINS, J. E., and D. G. BASKIN, 2010 Hypothalamic-brainstem circuits controlling eating. Forum Nutr **63:** 133-140.

BLUML, S., 1999 In vivo quantitation of cerebral metabolite concentrations using natural abundance 13C MRS at 1.5 T. J Magn Reson **136:** 219-225.

BOWLES, D. E., J. E. RABINOWITZ and R. J. SAMULSKI, 2003 Marker rescue of adeno-associated virus (AAV) capsid mutants: a novel approach for chimeric AAV production. J Virol **77:** 423-432.

BRADFORD, M. M., 1976 A rapid and sensitive method for the quantitation of microgram quantities of protein utilizing the principle of protein-dye binding. Anal Biochem **72:** 248-254.

BRADLEY, A., M. EVANS, M. H. KAUFMAN and E. ROBERTSON, 1984 Formation of germ-line chimaeras from embryo-derived teratocarcinoma cell lines. Nature **309:** 255-256.

BRISMAR, J., G. BRISMAR, G. GASCON and P. OZAND, 1990 Canavan disease: CT and MR imaging of the brain. AJNR Am J Neuroradiol **11:** 805-810.

BROEKMAN, M. L., R. C. BAEK, L. A. COMER, J. L. FERNANDEZ, T. N. SEYFRIED *et al.*, 2007 Complete correction of enzymatic deficiency and neurochemistry in the GM1-gangliosidosis mouse brain by neonatal adeno-associated virus-mediated gene delivery. Mol Ther **15:** 30-37.

BUFFOLI, 2010 Aquaporin biology and nervous system. Curr Neuropharmacol **8:** 97-104.

BUNING, H., L. PERABO, O. COUTELLE, S. QUADT-HUMME and M. HALLEK, 2008 Recent developments in adeno-associated virus vector technology. J Gene Med **10:** 717-733.

BURGER, C., K. NASH and R. J. MANDEL, 2005 Recombinant adeno-associated viral vectors in the nervous system. Hum Gene Ther **16:** 781-791.

BURRI, R., C. STEFFEN and N. HERSCHKOWITZ, 1991 N-acetyl-L-aspartate is a major source of acetyl groups for lipid synthesis during rat brain development. Dev Neurosci **13:** 403-411.

CAKMAKCI, H., Y. PEKCEVIK, U. YIS, A. UNALP and S. KURUL, 2010 Diagnostic value of proton MR spectroscopy and diffusion-weighted MR imaging in childhood inherited neurometabolic brain diseases and review of the literature. Eur J Radiol **74:** e161-171.

CANAVAN, M. M., 1931 Schilder's Encephalitis Periaxialis Diffusa. Arch Neurol Psychiatr **25:** 299-308.

CEARLEY, C. N., L. H. VANDENBERGHE, M. K. PARENTE, E. R. CARNISH, J. M. WILSON *et al.*, 2008 Expanded repertoire of AAV vector serotypes mediate unique patterns of transduction in mouse brain. Mol Ther **16:** 1710-1718.

CEARLEY, C. N., and J. H. WOLFE, 2006 Transduction characteristics of adeno-associated virus vectors expressing cap serotypes 7, 8, 9, and Rh10 in the mouse brain. Mol Ther **13:** 528-537.

CECCHINI, S., T. VIRAG and R. M. KOTIN, 2011 Reproducible high yields of recombinant adeno-associated virus produced using invertebrate cells in 0.02 to 200 liter cultures. Hum Gene Ther.

CERGHET, M., R. P. SKOFF, M. SWAMYDAS and D. BESSERT, 2009 Sexual dimorphism in the white matter of rodents. Journal of the Neurological Sciences **286:** 76-80.

CETIN, A., S. KOMAI, M. ELIAVA, P. H. SEEBURG and P. OSTEN, 2006 Stereotaxic gene delivery in the rodent brain. Nat Protoc **1:** 3166-3173.

CHAKRABORTY, G., P. MEKALA, D. YAHYA, G. WU and R. W. LEDEEN, 2001 Intraneuronal N-acetylaspartate supplies acetyl groups for myelin lipid synthesis: evidence for myelin-associated aspartoacylase. J Neurochem **78:** 736-745.

CHEN, H., D. M. MCCARTY, A. T. BRUCE and K. SUZUKI, 1998 Gene transfer and expression in oligodendrocytes under the control of myelin basic protein transcriptional control region mediated by adeno-associated virus. Gene Ther **5:** 50-58.

CHEN, H., D. M. MCCARTY, A. T. BRUCE and K. SUZUKI, 1999 Oligodendrocyte-specific gene expression in mouse brain: use of a myelin-forming cell type-specific promoter in an adeno-associated virus. J Neurosci Res **55:** 504-513.

CHRISTINE, C. W., P. A. STARR, P. S. LARSON, J. L. EBERLING, W. J. JAGUST *et al.*, 2009 Safety and tolerability of putaminal AADC gene therapy for Parkinson disease. Neurology **73:** 1662-1669.

D'ADAMO, A. F., JR., L. I. GIDEZ and F. M. YATSU, 1968 Acetyl transport mechanisms. Involvement of N-acetyl aspartic acid in de novo fatty acid biosynthesis in the developing rat brain. Exp Brain Res **5:** 267-273.

D'ADAMO, A. F., JR., and F. M. YATSU, 1966 Acetate metabolism in the nervous system. N-acetyl-L-aspartic acid and the biosynthesis of brain lipids. J Neurochem **13:** 961-965.

DAADI, M. M., P. PIVIROTTO, J. BRINGAS, J. CUNNINGHAM, J. FORSAYETH *et al.*, 2006 Distribution of AAV2-hAADC-transduced cells after 3 years in Parkinsonian monkeys. Neuroreport **17:** 201-204.

DAVIDSON, B. L., and X. O. BREAKEFIELD, 2003 Viral vectors for gene delivery to the nervous system. Nat Rev Neurosci **4:** 353-364.

DAVIS, K. L., and V. HAROUTUNIAN, 2003 Global expression-profiling studies and oligodendrocyte dysfunction in schizophrenia and bipolar disorder. Lancet **362:** 758.

DE BACKER, M. W., M. A. BRANS, M. C. LUIJENDIJK, K. M. GARNER and R. A. ADAN, 2010 Optimization of adeno-associated viral vector-mediated gene delivery to the hypothalamus. Hum Gene Ther **21:** 673-682.

DEACON, R. M., A. CROUCHER and J. N. RAWLINS, 2002 Hippocampal cytotoxic lesion effects on species-typical behaviours in mice. Behav Brain Res **132:** 203-213.

DEELCHAND, D. K., A. A. SHESTOV, D. M. KOSKI, K. UGURBIL and P. G. HENRY, 2009 Acetate transport and utilization in the rat brain. J Neurochem **109 Suppl 1:** 46-54.

DOETSCH, F., J. M. GARCIA-VERDUGO and A. ALVAREZ-BUYLLA, 1997 Cellular composition and three-dimensional organization of the subventricular germinal zone in the adult mammalian brain. J Neurosci **17:** 5046-5061.

DUAN, D., P. SHARMA, J. YANG, Y. YUE, L. DUDUS *et al.*, 1998 Circular intermediates of recombinant adeno-associated virus have defined structural characteristics responsible for long-term episomal persistence in muscle tissue. J Virol **72:** 8568-8577.

DUAN, D., Y. YUE and J. F. ENGELHARDT, 2001 Expanding AAV packaging capacity with trans-splicing or overlapping vectors: a quantitative comparison. Mol Ther **4:** 383-391.

DUAN, D., Y. YUE, Z. YAN and J. F. ENGELHARDT, 2000 A new dual-vector approach to enhance recombinant adeno-associated virus-mediated gene expression through intermolecular cis activation. Nat Med **6:** 595-598.

DUGAS, J. C., Y. C. TAI, T. P. SPEED, J. NGAI and B. A. BARRES, 2006 Functional genomic analysis of oligodendrocyte differentiation. J Neurosci **26:** 10967-10983.

DURING, M., 1996 Gene therapy in New Zealand. Science **272:** 467.

DURING, M. J., D. YOUNG, K. BAER, P. LAWLOR and M. KLUGMANN, 2003 Development and optimization of adeno-associated virus vector transfer into the central nervous system. Methods Mol Med **76:** 221-236.

DYMECKI, S. M., 1996 Flp recombinase promotes site-specific DNA recombination in embryonic stem cells and transgenic mice. Proc Natl Acad Sci U S A **93:** 6191-6196.

EDDLESTON, M., and L. MUCKE, 1993 Molecular profile of reactive astrocytes--implications for their role in neurologic disease. Neuroscience **54:** 15-36.

ENG, L. F., and R. S. GHIRNIKAR, 1994 GFAP and astrogliosis. Brain Pathol **4:** 229-237.

FAN, T. W., R. M. HIGASHI, A. N. LANE and O. JARDETZKY, 1986 Combined use of 1H-NMR and GC-MS for metabolite monitoring and in vivo 1H-NMR assignments. Biochim Biophys Acta **882:** 154-167.

FARHADI, H. F., P. LEPAGE, R. FORGHANI, H. C. FRIEDMAN, W. ORFALI *et al.*, 2003 A combinatorial network of evolutionarily conserved myelin basic protein regulatory sequences confers distinct glial-specific phenotypes. J Neurosci **23:** 10214-10223.

FEIGIN, A., M. G. KAPLITT, C. TANG, T. LIN, P. MATTIS *et al.*, 2007 Modulation of metabolic brain networks after subthalamic gene therapy for Parkinson's disease. Proc Natl Acad Sci U S A **104:** 19559-19564.

FELDMANN, A., C. WINTERSTEIN, R. WHITE, J. TROTTER and E. M. KRAMER-ALBERS, 2009 Comprehensive analysis of expression, subcellular localization, and cognate pairing of SNARE proteins in oligodendrocytes. J Neurosci Res **87:** 1760-1772.

FITZSIMONS, H. L., R. J. BLAND and M. J. DURING, 2002 Promoters and regulatory elements that improve adeno-associated virus transgene expression in the brain. Methods **28:** 227-236.

FOUST, K. D., E. NURRE, C. L. MONTGOMERY, A. HERNANDEZ, C. M. CHAN *et al.*, 2009 Intravascular AAV9 preferentially targets neonatal neurons and adult astrocytes. Nat Biotechnol **27:** 59-65.

FRANICH, N. R., H. L. FITZSIMONS, D. M. FONG, M. KLUGMANN, M. J. DURING *et al.*, 2008 AAV vector-mediated RNAi of mutant huntingtin expression is neuroprotective in a novel genetic rat model of Huntington's disease. Mol Ther **16:** 947-956.

FRIEDMANN, T., and R. ROBLIN, 1972 Gene therapy for human genetic disease? Science **175:** 949-955.

GAO, G., L. H. VANDENBERGHE, M. R. ALVIRA, Y. LU, R. CALCEDO *et al.*, 2004 Clades of Adeno-associated viruses are widely disseminated in human tissues. J Virol **78:** 6381-6388.

GAO, G. P., M. R. ALVIRA, L. WANG, R. CALCEDO, J. JOHNSTON *et al.*, 2002 Novel adeno-associated viruses from rhesus monkeys as vectors for human gene therapy. Proc Natl Acad Sci U S A **99:** 11854-11859.

GOW, A., V. L. FRIEDRICH, JR. and R. A. LAZZARINI, 1992 Myelin basic protein gene contains separate enhancers for oligodendrocyte and Schwann cell expression. J Cell Biol **119:** 605-616.

GUGGENHUBER, S., K. MONORY, B. LUTZ and M. KLUGMANN, 2010 AAV vector-mediated overexpression of CB1 cannabinoid receptor in pyramidal neurons of the hippocampus protects against seizure-induced excitoxicity. PLoS One **5:** e15707.

HAGENFELDT, L., I. BOLLGREN and N. VENIZELOS, 1987 N-acetylaspartic aciduria due to aspartoacylase deficiency--a new aetiology of childhood leukodystrophy. J Inherit Metab Dis **10:** 135-141.

HALBERT, C. L., E. A. RUTLEDGE, J. M. ALLEN, D. W. RUSSELL and A. D. MILLER, 2000 Repeat transduction in the mouse lung by using adeno-associated virus vectors with different serotypes. J Virol **74:** 1524-1532.

HARTLINE, D. K., and D. R. COLMAN, 2007 Rapid conduction and the evolution of giant axons and myelinated fibers. Curr Biol **17:** R29-35.

HAUCK, B., L. CHEN and W. XIAO, 2003 Generation and characterization of chimeric recombinant AAV vectors. Mol Ther **7:** 419-425.

HERGA, S., J. G. BERRIN, J. PERRIER, A. PUIGSERVER and T. GIARDINA, 2006 Identification of the zinc binding ligands and the catalytic residue in human aspartoacylase, an enzyme involved in Canavan disease. FEBS Lett **580:** 5899-5904.

HERSHFIELD, J. R., C. N. MADHAVARAO, J. R. MOFFETT, J. A. BENJAMINS, J. Y. GARBERN *et al.*, 2006 Aspartoacylase is a regulated nuclear-cytoplasmic enzyme. Faseb J **20:** 2139-2141.

HIGASHIGUCHI, T., T. SERIKAWA, T. YAMADA, K. KOGISHI, A. KONDO *et al.*, 1991 Semidominant expression of absence-like seizure in tremor rats. Behav Genet **21:** 537-545.

HIRRLINGER, P. G., A. SCHELLER, C. BRAUN, M. QUINTELA-SCHNEIDER, B. FUSS *et al.*, 2005 Expression of reef coral fluorescent proteins in the central nervous system of transgenic mice. Mol Cell Neurosci **30:** 291-303.

IKENAKA, K., and T. KAGAWA, 1995 Transgenic systems in studying myelin gene expression. Dev Neurosci **17:** 127-136.

IKENAKA, K., K. NAKAHIRA, K. NAKAJIMA, I. FUJIMOTO, T. KAGAWA *et al.*, 1992 Detection of brain-specific gene expression in brain cells in primary culture: a novel promoter assay based on the use of a retrovirus vector. New Biol **4:** 53-60.

ISHIBASHI, T., K. A. DAKIN, B. STEVENS, P. R. LEE, S. V. KOZLOV *et al.*, 2006 Astrocytes promote myelination in response to electrical impulses. Neuron **49:** 823-832.

JANG, J. H., J. T. KOERBER, J. S. KIM, P. ASURI, T. VAZIN *et al.*, 2011 An Evolved Adeno-associated Viral Variant Enhances Gene Delivery and Gene Targeting in Neural Stem Cells. Mol Ther **19:** 667-675.

JANSON, C., S. MCPHEE, L. BILANIUK, J. HASELGROVE, M. TESTAIUTI *et al.*, 2002a Clinical protocol. Gene therapy of Canavan disease: AAV-2 vector for neurosurgical delivery of aspartoacylase gene (ASPA) to the human brain. Hum Gene Ther **13:** 1391-1412.

JANSON, C., S. MCPHEE, L. BILANIUK, J. HASELGROVE, M. TESTAIUTI *et al.*, 2002b Gene Therapy of Canavan Disease: AAV-2 Vector for Neurosurgical Delivery of Aspartoacylase Gene (ASPA) to the Human Brain. Hum Gene Ther **13:** 1391-1412.

JANSON, C. G., M. ASSADI, J. FRANCIS, L. BILANIUK, D. SHERA *et al.*, 2005 Lithium citrate for Canavan disease. Pediatr Neurol **33:** 235-243.

JANSON, C. G., and M. J. DURING, 2001 Viral vectors as part of an integrated functional genomics program. Genomics **78:** 3-6.

JIA, F., M. YUE, D. CHANDRA, A. KERAMIDAS, P. A. GOLDSTEIN *et al.*, 2008 Taurine is a potent activator of extrasynaptic GABA(A) receptors in the thalamus. J Neurosci **28:** 106-115.

KALUDOV, N., K. E. BROWN, R. W. WALTERS, J. ZABNER and J. A. CHIORINI, 2001 Adeno-associated virus serotype 4 (AAV4) and AAV5 both require sialic acid binding for hemagglutination and efficient transduction but differ in sialic acid linkage specificity. J Virol **75:** 6884-6893.

KAMOSHITA, S., G. B. REED, JR. and M. J. AGUILAR, 1967 Axonal dystrophy in a case of Canavan's spongy degeneration. Neurology **17:** 895-898.

KAPLITT, M. G., A. FEIGIN, C. TANG, H. L. FITZSIMONS, P. MATTIS *et al.*, 2007 Safety and tolerability of gene therapy with an adeno-associated virus (AAV) borne GAD gene for Parkinson's disease: an open label, phase I trial. Lancet **369:** 2097-2105.

KAPLITT, M. G., P. LEONE, R. J. SAMULSKI, X. XIAO, D. W. PFAFF *et al.*, 1994 Long-term gene expression and phenotypic correction using adeno-associated virus vectors in the mammalian brain. Nat Genet **8:** 148-154.

KASHIWAKURA, Y., K. TAMAYOSE, K. IWABUCHI, Y. HIRAI, T. SHIMADA *et al.*, 2005 Hepatocyte growth factor receptor is a coreceptor for adeno-associated virus type 2 infection. J Virol **79:** 609-614.

KASSMANN, C. M., C. LAPPE-SIEFKE, M. BAES, B. BRUGGER, A. MILDNER *et al.*, 2007 Axonal loss and neuroinflammation caused by peroxisome-deficient oligodendrocytes. Nat Genet **39:** 969-976.

KAUL, R., K. BALAMURUGAN, G. P. GAO and R. MATALON, 1994 Canavan disease: genomic organization and localization of human ASPA to 17p13-ter and conservation of the ASPA gene during evolution. Genomics **21:** 364-370.

KAUL, R., J. CASANOVA, A. B. JOHNSON, P. TANG and R. MATALON, 1991 Purification, characterization, and localization of aspartoacylase from bovine brain. J Neurochem **56:** 129-135.

KAUL, R., G. P. GAO, K. BALAMURUGAN and R. MATALON, 1993 Cloning of the human aspartoacylase cDNA and a common missense mutation in Canavan disease. Nat Genet **5:** 118-123.

KAY, M. A., 2011 State-of-the-art gene-based therapies: the road ahead. Nat Rev Genet.

KIRMANI, B. F., D. M. JACOBOWITZ and M. A. NAMBOODIRI, 2003 Developmental increase of aspartoacylase in oligodendrocytes parallels CNS myelination. Brain Res Dev Brain Res **140:** 105-115.

KITADA, K., T. AKIMITSU, Y. SHIGEMATSU, A. KONDO, T. MAIHARA *et al.*, 2000 Accumulation of N-acetyl-L-aspartate in the brain of the tremor rat, a mutant exhibiting absence-like seizure and spongiform degeneration in the central nervous system. J Neurochem **74:** 2512-2519.

KLEIN, R. L., R. D. DAYTON, N. J. LEIDENHEIMER, K. JANSEN, T. E. GOLDE *et al.*, 2006 Efficient neuronal gene transfer with AAV8 leads to neurotoxic levels of tau or green fluorescent proteins. Mol Ther **13:** 517-527.

KLEIN, R. L., R. D. DAYTON, J. B. TATOM, C. G. DIACZYNSKY and M. F. SALVATORE, 2008a Tau expression levels from various adeno-associated virus vector serotypes produce graded neurodegenerative disease states. Eur J Neurosci **27:** 1615-1625.

KLEIN, R. L., R. D. DAYTON, J. B. TATOM, K. M. HENDERSON and P. P. HENNING, 2008b AAV8, 9, Rh10, Rh43 vector gene transfer in the rat brain: effects of serotype, promoter and purification method. Mol Ther **16:** 89-96.

KLEIN, R. L., M. E. HAMBY, Y. GONG, A. C. HIRKO, S. WANG *et al.*, 2002 Dose and promoter effects of adeno-associated viral vector for green fluorescent protein expression in the rat brain. Exp Neurol **176:** 66-74.

KLUGMANN, M., 2007 Adeno-assoiated virus for gene delivery to the central nervous system: Novel strategies in functional genomics and the treatment of neurologic disorders, pp. in *Habilitationsschrift zur Erlangung der venia legendi für das Fach Zellbiologie der Fakultät für Biowissenschaften der Ruprecht-Karls-Universität Heidelberg*.

KLUGMANN, M., and C. B. LEICHTLEIN, 2006 Clinical trials of gene therapy for Canavan Disease, pp. 303-316. in *Gene therapy in the central nervous system*, edited by M. G. KAPLITT and M. J. DURING. Elsevier, San Diego.

KLUGMANN, M., C. B. LEICHTLEIN, C. W. SYMES, T. SERIKAWA, D. YOUNG *et al.*, 2005 Restoration of aspartoacylase activity in CNS neurons does not ameliorate motor deficits and demyelination in a model of Canavan disease. Mol Ther **11:** 745-753.

KLUGMANN, M., C. W. SYMES, B. K. KLAUSSNER, C. B. LEICHTLEIN, T. SERIKAWA *et al.*, 2003 Identification and distribution of aspartoacylase in the postnatal rat brain. Neuroreport **14:** 1837-1840.

KOERBER, J. T., R. KLIMCZAK, J. H. JANG, D. DALKARA, J. G. FLANNERY *et al.*, 2009 Molecular evolution of adeno-associated virus for enhanced glial gene delivery. Mol Ther **17:** 2088-2095.

KOLB, B., 1984 Functions of the frontal cortex of the rat: a comparative review. Brain Res **320:** 65-98.

KONDO, A., H. NAGARA, K. AKAZAWA, J. TATEISHI, T. SERIKAWA *et al.*, 1991 CNS pathology in the neurological mutant rats zitter, tremor and zitter-tremor double mutant (spontaneously epileptic rat, SER). Exaggeration of clinical and neuropathological phenotypes in SER. Brain **114:** 979-999.

KOTIN, R. M., R. M. LINDEN and K. I. BERNS, 1992 Characterization of a preferred site on human chromosome 19q for integration of adeno-associated virus DNA by non-homologous recombination. EMBO J **11:** 5071-5078.

KRAWCZYK, H., and W. GRADOWSKA, 2003 Characterisation of the 1H and 13C NMR spectra of N-acetylaspartylglutamate and its detection in urine from patients with Canavan disease. J Pharm Biomed Anal **31:** 455-463.

KRONN, D., C. ODDOUX, J. PHILLIPS and H. OSTRER, 1995 Prevalence of Canavan disease heterozygotes in the New York metropolitan Ashkenazi Jewish population. Am J Hum Genet **57:** 1250-1252.

KUMAR, S., J. C. BIANCOTTI, R. MATALON and J. DE VELLIS, 2009 Lack of aspartoacylase activity disrupts survival and differentiation of neural progenitors and oligodendrocytes in a mouse model of Canavan disease. J Neurosci Res **87:** 3415-3427.

KUMAR, S., N. S. MATTAN and J. DE VELLIS, 2006 Canavan disease: a white matter disorder. Ment Retard Dev Disabil Res Rev **12:** 157-165.

LACHENAL, G., K. PERNET-GALLAY, M. CHIVET, F. J. HEMMING, A. BELLY *et al.*, 2011 Release of exosomes from differentiated neurons and its regulation by synaptic glutamatergic activity. Mol Cell Neurosci **46:** 409-418.

LAPPE-SIEFKE, C., S. GOEBBELS, M. GRAVEL, E. NICKSCH, J. LEE *et al.*, 2003 Disruption of Cnp1 uncouples oligodendroglial functions in axonal support and myelination. Nat Genet **33:** 366-374.

LATTANZI, A., M. NERI, C. MADERNA, I. DI GIROLAMO, S. MARTINO *et al.*, 2010 Widespread enzymatic correction of CNS tissues by a single intracerebral injection of therapeutic lentiviral vector in leukodystrophy mouse models. Hum Mol Genet **19:** 2208-2227.

LAWLOR, P. A., R. J. BLAND, A. MOURAVLEV, D. YOUNG and M. J. DURING, 2009 Efficient gene delivery and selective transduction of glial cells in the mammalian brain by AAV serotypes isolated from nonhuman primates. Mol Ther **17:** 1692-1702.

LE COQ, J., H. J. AN, C. LEBRILLA and R. E. VIOLA, 2006 Characterization of human aspartoacylase: the brain enzyme responsible for canavan disease. Biochemistry **45:** 5878-5884.

LEONE, P., C. G. JANSON, L. BILANIUK, Z. WANG, F. SORGI *et al.*, 2000 Aspartoacylase gene transfer to the mammalian central nervous system with therapeutic implications for Canavan disease. Ann Neurol **48:** 27-38.

LEONE, P., C. G. JANSON, S. J. MCPHEE and M. J. DURING, 1999 Global CNS gene transfer for a childhood neurogenetic enzyme deficiency: Canavan disease. Curr Opin Mol Ther **1:** 487-492.

LEVISON, S. W., C. CHUANG, B. J. ABRAMSON and J. E. GOLDMAN, 1993 The migrational patterns and developmental fates of glial precursors in the rat subventricular zone are temporally regulated. Development **119:** 611-622.

LEVISON, S. W., and J. E. GOLDMAN, 1993 Both oligodendrocytes and astrocytes develop from progenitors in the subventricular zone of postnatal rat forebrain. Neuron **10:** 201-212.

LEWITT, P. A., A. R. REZAI, M. A. LEEHEY, S. G. OJEMANN, A. W. FLAHERTY *et al.*, 2011 AAV2-GAD gene therapy for advanced Parkinson's disease: a double-blind, sham-surgery controlled, randomised trial. Lancet Neurol **10:** 309-319.

LIN, L., G. CHEN, H. KUANG, D. WANG and J. Z. TSIEN, 2007 Neural encoding of the concept of nest in the mouse brain. Proc Natl Acad Sci U S A **104:** 6066-6071.

LU, Z. H., G. CHAKRABORTY, R. W. LEDEEN, D. YAHYA and G. WU, 2004 N-Acetylaspartate synthase is bimodally expressed in microsomes and mitochondria of brain. Brain Res Mol Brain Res **122:** 71-78.

LUX, K., N. GOERLITZ, S. SCHLEMMINGER, L. PERABO, D. GOLDNAU *et al.*, 2005 Green fluorescent protein-tagged adeno-associated virus particles allow the study of cytosolic and nuclear trafficking. J Virol **79:** 11776-11787.

MADHAVARAO, C. N., P. ARUN, Y. ANIKSTER, S. R. MOG, O. STARETZ-CHACHAM *et al.*, 2009 Glyceryl triacetate for Canavan disease: a low-dose trial in infants and evaluation of a higher dose for toxicity in the tremor rat model. J Inherit Metab Dis **32:** 640-650.

MADHAVARAO, C. N., P. ARUN, J. R. MOFFETT, S. SZUCS, S. SURENDRAN *et al.*, 2005 Defective N-acetylaspartate catabolism reduces brain acetate levels and myelin lipid synthesis in Canavan's disease. Proc Natl Acad Sci U S A **102:** 5221-5226.

MADHAVARAO, C. N., J. R. MOFFETT, R. A. MOORE, R. E. VIOLA, M. A. NAMBOODIRI *et al.*, 2004 Immunohistochemical localization of aspartoacylase in the rat central nervous system. J Comp Neurol **472:** 318-329.

MAKAROVA, K. S., and N. V. GRISHIN, 1999 The Zn-peptidase superfamily: functional convergence after evolutionary divergence. J Mol Biol **292:** 11-17.

MANDEL, R. J., F. P. MANFREDSSON, K. D. FOUST, A. RISING, S. REIMSNIDER *et al.*, 2006 Recombinant adeno-associated viral vectors as therapeutic agents to treat neurological disorders. Mol Ther **13:** 463-483.

MARKAKIS, E. A., K. P. VIVES, J. BOBER, S. LEICHTLE, C. LERANTH *et al.*, 2010 Comparative transduction efficiency of AAV vector serotypes 1-6 in the substantia nigra and striatum of the primate brain. Mol Ther **18:** 588-593.

MARSHALL, C. A., S. O. SUZUKI and J. E. GOLDMAN, 2003 Gliogenic and neurogenic progenitors of the subventricular zone: who are they, where did they come from, and where are they going? Glia **43:** 52-61.

MASAMIZU, Y., T. OKADA, H. ISHIBASHI, S. TAKEDA, S. YUASA *et al.*, 2010 Efficient gene transfer into neurons in monkey brain by adeno-associated virus 8. Neuroreport **21:** 447-451.

MASTAKOV, M. Y., K. BAER, C. W. SYMES, C. B. LEICHTLEIN, R. M. KOTIN *et al.*, 2002 Immunological aspects of recombinant adeno-associated virus delivery to the Mammalian brain. J Virol **76:** 8446-8454.

MATALON, R., and K. MICHALS-MATALON, 1999 Biochemistry and molecular biology of Canavan disease. Neurochem Res **24:** 507-513.

MATALON, R., K. MICHALS and R. KAUL, 1995 Canavan disease: from spongy degeneration to molecular analysis. J Pediatr **127:** 511-517.

MATALON, R., K. MICHALS, D. SEBESTA, M. DEANCHING, P. GASHKOFF *et al.*, 1988 Aspartoacylase deficiency and N-acetylaspartic aciduria in patients with Canavan disease. Am J Med Genet **29:** 463-471.

MATALON, R., P. L. RADY, K. A. PLATT, H. B. SKINNER, M. J. QUAST *et al.*, 2000 Knock-out mouse for Canavan disease: a model for gene transfer to the central nervous system. J Gene Med **2:** 165-175.

MATALON, R., S. SURENDRAN, P. L. RADY, M. J. QUAST, G. A. CAMPBELL *et al.*, 2003 Adeno-associated virus-mediated aspartoacylase gene transfer to the brain of knockout mouse for canavan disease. Mol Ther **7:** 580-587.

MATALON, R. M., and K. MICHALS-MATALON, 2000 Spongy degeneration of the brain, Canavan disease: biochemical and molecular findings. Front Biosci **1:** D307-311.

MATHEW, R., P. ARUN, C. N. MADHAVARAO, J. R. MOFFETT and M. A. NAMBOODIRI, 2005 Progress toward acetate supplementation therapy for Canavan disease: glyceryl triacetate administration increases acetate, but not N-acetylaspartate, levels in brain. J Pharmacol Exp Ther **315:** 297-303.

MATTAN, N. S., C. A. GHIANI, M. LLOYD, R. MATALON, D. BOK *et al.*, 2010 Aspartoacylase deficiency affects early postnatal development of oligodendrocytes and myelination. Neurobiol Dis **40:** 432-443.

MCCARTY, D. M., S. M. YOUNG, JR. and R. J. SAMULSKI, 2004 Integration of adeno-associated virus (AAV) and recombinant AAV vectors. Annu Rev Genet **38:** 819-845.

MCCOWN, T. J., 2005 Adeno-associated virus (AAV) vectors in the CNS. Curr Gene Ther **5:** 333-338.

MCPHEE, S., J. S. FRANCIS, C. G. JANSON, T. SERIKAWA, K. HYLAND *et al.*, 2005a Effects of AAV-2-mediated aspartoacylase gene transfer in the tremor rat model of Canavan disease. Molecular Brain Research **in press**.

MCPHEE, S. W., J. FRANCIS, C. G. JANSON, T. SERIKAWA, K. HYLAND *et al.*, 2005b Effects of AAV-2-mediated aspartoacylase gene transfer in the tremor rat model of Canavan disease. Brain Res Mol Brain Res **135:** 112-121.

MCPHEE, S. W., C. G. JANSON, C. LI, R. J. SAMULSKI, A. S. CAMP *et al.*, 2006 Immune responses to AAV in a phase I study for Canavan disease. J Gene Med **8:** 577-588.

MERSMANN, N., D. TKACHEV, R. JELINEK, P. T. ROTH, W. MOBIUS *et al.*, 2011 Aspartoacylase-LacZ Knockin Mice: An Engineered Model of Canavan Disease. PLoS One **6:** e20336.

MICHAELIS, T., K. D. MERBOLDT, H. BRUHN, W. HANICKE and J. FRAHM, 1993 Absolute concentrations of metabolites in the adult human brain in vivo: quantification of localized proton MR spectra. Radiology **187:** 219-227.

MIYAKE, M., Y. KAKIMOTO and M. SORIMACHI, 1981 A gas chromatographic method for the determination of N-acetyl-L-aspartic acid, N-acetyl-alpha-aspartylglutamic acid and beta-citryl-L-glutamic acid and their distributions in the brain and other organs of various species of animals. J Neurochem **36:** 804-810.

MOBIUS, W., B. COOPER, W. A. KAUFMANN, C. IMIG, T. RUHWEDEL *et al.*, 2010 Electron microscopy of the mouse central nervous system. Methods Cell Biol **96:** 475-512.

MOFFETT, J. R., P. ARUN, P. S. ARIYANNUR, J. Y. GARBERN, D. M. JACOBOWITZ *et al.*, 2011 Extensive aspartoacylase expression in the rat central nervous system. Glia.

MOFFETT, J. R., and M. A. NAMBOODIRI, 1995 Differential distribution of N-acetylaspartylglutamate and N-acetylaspartate immunoreactivities in rat forebrain. J Neurocytol **24:** 409-433.

MOFFETT, J. R., M. A. NAMBOODIRI, C. B. CANGRO and J. H. NEALE, 1991 Immunohistochemical localization of N-acetylaspartate in rat brain. Neuroreport **2:** 131-134.

MORI, S., L. WANG, T. TAKEUCHI and T. KANDA, 2004 Two novel adeno-associated viruses from cynomolgus monkey: pseudotyping characterization of capsid protein. Virology **330:** 375-383.

NADLER, J. V., and J. R. COOPER, 1972 N-acetyl-L-aspartic acid content of human neural tumours and bovine peripheral nervous tissues. J Neurochem **19:** 313-319.

NAMBOODIRI, A. M., A. PEETHAMBARAN, R. MATHEW, P. A. SAMBHU, J. HERSHFIELD *et al.*, 2006 Canavan disease and the role of N-acetylaspartate in myelin synthesis. Mol Cell Endocrinol **26:** 26.

NAVE, K. A., 2010 Myelination and the trophic support of long axons. Nat Rev Neurosci **11:** 275-283.

NEALE, J. H., T. BZDEGA and B. WROBLEWSKA, 2000 N-Acetylaspartylglutamate: the most abundant peptide neurotransmitter in the mammalian central nervous system. J Neurochem **75:** 443-452.

NEALE, J. H., R. T. OLSZEWSKI, L. M. GEHL, B. WROBLEWSKA and T. BZDEGA, 2005 The neurotransmitter N-acetylaspartylglutamate in models of pain, ALS, diabetic neuropathy, CNS injury and schizophrenia. Trends Pharmacol Sci **26:** 477-484.

NICHOLSON, J. K., P. J. FOXALL, M. SPRAUL, R. D. FARRANT and J. C. LINDON, 1995 750 MHz 1H and 1H-13C NMR spectroscopy of human blood plasma. Anal Chem **67:** 793-811.

NIWA, M., A. NITTA, H. MIZOGUCHI, Y. ITO, Y. NODA *et al.*, 2007 A novel molecule "shati" is involved in methamphetamine-induced hyperlocomotion, sensitization, and conditioned place preference. J Neurosci **27:** 7604-7615.

NOCTOR, S. C., A. C. FLINT, T. A. WEISSMAN, R. S. DAMMERMAN and A. R. KRIEGSTEIN, 2001 Neurons derived from radial glial cells establish radial units in neocortex. Nature **409:** 714-720.

NUMAN, M., 1974 Medial preoptic area and maternal behavior in the female rat. J Comp Physiol Psychol **87:** 746-759.

OLSON, E. N., H. H. ARNOLD, P. W. RIGBY and B. J. WOLD, 1996 Know your neighbors: three phenotypes in null mutants of the myogenic bHLH gene MRF4. Cell **85:** 1-4.

OLSON, J. K., A. M. GIRVIN and S. D. MILLER, 2001 Direct activation of innate and antigen-presenting functions of microglia following infection with Theiler's virus. J Virol **75:** 9780-9789.

ORTHMANN-MURPHY, J. L., C. K. ABRAMS and S. S. SCHERER, 2008 Gap junctions couple astrocytes and oligodendrocytes. J Mol Neurosci **35:** 101-116.

ORY-LAVOLLEE, L., R. D. BLAKELY and J. T. COYLE, 1987 Neurochemical and immunocytochemical studies on the distribution of N-acetyl-aspartylglutamate and N-acetyl-aspartate in rat spinal cord and some peripheral nervous tissues. J Neurochem **48:** 895-899.

PATEL, T. B., and J. B. CLARK, 1979 Synthesis of N-acetyl-L-aspartate by rat brain mitochondria and its involvement in mitochondrial/cytosolic carbon transport. Biochem J **184:** 539-546.

PAXINOS, G., and K. J. B. FRANKLIN, 2001 *The Mouse Brain in Stereotaxic Coordinates*.

PAXINOS, G., G. HALLIDAY, C. WATSON, Y. KOUTCHEROV and H. WANG, 2006 Atlas of the Developing Mouse Brain at E17.5, P0 and P6. Academic Press.

PAYLOR, R., M. NGUYEN, J. N. CRAWLEY, J. PATRICK, A. BEAUDET *et al.*, 1998 Alpha7 nicotinic receptor subunits are not necessary for hippocampal-dependent learning or sensorimotor gating: a behavioral characterization of Acra7-deficient mice. Learn Mem **5:** 302-316.

PEDERZOLLI, C. D., C. P. MESCKA, A. S. MAGNUSSON, K. B. DECKMANN, E. DE SOUZA STRECK *et al.*, 2010a N-acetylaspartic acid impairs enzymatic antioxidant defenses and enhances hydrogen peroxide concentration in rat brain. Metab Brain Dis **25:** 251-259.

PEDERZOLLI, C. D., C. P. MESCKA, F. SCAPIN, F. J. ROCKENBACH, A. M. SGARAVATTI *et al.*, 2007 N-acetylaspartic acid promotes oxidative stress in cerebral cortex of rats. Int J Dev Neurosci **25:** 317-324.

PEDERZOLLI, C. D., F. J. ROCKENBACH, F. R. ZANIN, N. T. HENN, E. C. ROMAGNA *et al.*, 2009 Intracerebroventricular administration of N-acetylaspartic acid impairs antioxidant defenses and promotes protein oxidation in cerebral cortex of rats. Metab Brain Dis **24:** 283-298.

PEDERZOLLI, C. D., A. P. ROSA, A. S. DE OLIVEIRA, J. G. COELHO, L. BECKER DDA *et al.*, 2010b Neuroprotective role of lipoic acid against acute toxicity of N-acetylaspartic acid. Mol Cell Biochem **344:** 231-239.

PEEL, A. L., and R. L. KLEIN, 2000 Adeno-associated virus vectors: activity and applications in the CNS. J Neurosci Methods **98:** 95-104.

PEKNY, M., and M. NILSSON, 2005 Astrocyte activation and reactive gliosis. Glia **50:** 427-434.

PFAFFL, M. W., G. W. HORGAN and L. DEMPFLE, 2002 Relative expression software tool (REST) for group-wise comparison and statistical analysis of relative expression results in real-time PCR. Nucleic Acids Res **30:** e36.

PILPEL, N., N. LANDECK, M. KLUGMANN, P. H. SEEBURG and M. K. SCHWARZ, 2009 Rapid, reproducible transduction of select forebrain regions by targeted recombinant virus injection into the neonatal mouse brain. J Neurosci Methods **182:** 55-63.

QING, K., C. MAH, J. HANSEN, S. ZHOU, V. DWARKI *et al.*, 1999 Human fibroblast growth factor receptor 1 is a co-receptor for infection by adeno-associated virus 2. Nat Med **5:** 71-77.

RABINOWITZ, J. E., D. E. BOWLES, S. M. FAUST, J. G. LEDFORD, S. E. CUNNINGHAM *et al.*, 2004 Cross-dressing the virion: the transcapsidation of adeno-associated virus serotypes functionally defines subgroups. J Virol **78:** 4421-4432.

RABINOWITZ, J. E., F. ROLLING, C. LI, H. CONRATH, W. XIAO *et al.*, 2002 Cross-packaging of a single adeno-associated virus (AAV) type 2 vector genome into multiple AAV serotypes enables transduction with broad specificity. J Virol **76:** 791-801.

REIMSNIDER, S., F. P. MANFREDSSON, N. MUZYCZKA and R. J. MANDEL, 2007 Time course of transgene expression after intrastriatal pseudotyped rAAV2/1, rAAV2/2, rAAV2/5, and rAAV2/8 transduction in the rat. Mol Ther **15:** 1504-1511.

REYNOLDS, E. S., 1963 The use of lead citrate at high pH as an electron-opaque stain in electron microscopy. J Cell Biol **17:** 208-212.

RICHICHI, C., E. J. LIN, D. STEFANIN, D. COLELLA, T. RAVIZZA *et al.*, 2004 Anticonvulsant and antiepileptogenic effects mediated by adeno-associated virus vector neuropeptide y expression in the rat hippocampus. J Neurosci **24:** 3051-3059.

RODRIGUEZ, C. I., F. BUCHHOLZ, J. GALLOWAY, R. SEQUERRA, J. KASPER *et al.*, 2000 High-efficiency deleter mice show that FLPe is an alternative to Cre-loxP. Nat Genet **25:** 139-140.

SAHER, G., B. BRUGGER, C. LAPPE-SIEFKE, W. MOBIUS, R. TOZAWA *et al.*, 2005 High cholesterol level is essential for myelin membrane growth. Nat Neurosci **8:** 468-475.

SAMBROOK, S., E. F. FRITSCH and T. MANIATIS, 1989 Molecular Cloning: A Laboratory Manual. Cold Spring Harbor Laboratory Press; 2nd edition.

SAMULSKI, R. J., K. I. BERNS, M. TAN and N. MUZYCZKA, 1982 Cloning of adeno-associated virus into pBR322: rescue of intact virus from the recombinant plasmid in human cells. Proc Natl Acad Sci U S A **79:** 2077-2081.

SANTELLO, M., and A. VOLTERRA, 2009 Synaptic modulation by astrocytes via Ca2+-dependent glutamate release. Neuroscience **158:** 253-259.

SCHMIDT, M., E. GROT, P. CERVENKA, S. WAINER, C. BUCK *et al.*, 2006 Identification and characterization of novel adeno-associated virus isolates in ATCC virus stocks. J Virol **80:** 5082-5085.

SEGEL, R., Y. ANIKSTER, S. ZEVIN, A. STEINBERG, W. A. GAHL *et al.*, 2011 A safety trial of high dose glyceryl triacetate for Canavan disease. Mol Genet Metab.

SEKI, T., H. MATSUBAYASHI, T. AMANO, K. KITADA, T. SERIKAWA *et al.*, 2002 Adenoviral gene transfer of aspartoacylase into the tremor rat, a genetic model of epilepsy, as a trial of gene therapy for inherited epileptic disorder. Neurosci Lett **328:** 249-252.

SEKI, T., H. MATSUBAYASHI, T. AMANO, K. KITADA, T. SERIKAWA *et al.*, 2004 Adenoviral gene transfer of aspartoacylase ameliorates tonic convulsions of spontaneously epileptic rats. Neurochem Int **45:** 171-178.

SERIKAWA, T., and J. YAMADA, 1986 Epileptic seizures in rats homozygous for two mutations, zitter and tremor. J Hered **77:** 441-444.

SEVIN, C., A. BENRAISS, D. VAN DAM, D. BONNIN, G. NAGELS *et al.*, 2006 Intracerebral adeno-associated virus-mediated gene transfer in rapidly progressive forms of metachromatic leukodystrophy. Hum Mol Genet **15:** 53-64.

SHAHBAZIAN, M., J. YOUNG, L. YUVA-PAYLOR, C. SPENCER, B. ANTALFFY *et al.*, 2002 Mice with truncated MeCP2 recapitulate many Rett syndrome features and display hyperacetylation of histone H3. Neuron **35:** 243-254.

SHERMAN, D. L., C. FABRIZI, C. S. GILLESPIE and P. J. BROPHY, 2001 Specific disruption of a schwann cell dystrophin-related protein complex in a demyelinating neuropathy. Neuron **30:** 677-687.

SHERWOOD, C. C., C. D. STIMPSON, M. A. RAGHANTI, D. E. WILDMAN, M. UDDIN *et al.*, 2006 Evolution of increased glia-neuron ratios in the human frontal cortex. Proc Natl Acad Sci U S A **103:** 13606-13611.

SHIELDS, D. C., K. E. SCHAECHER, T. C. SAIDO and N. L. BANIK, 1999 A putative mechanism of demyelination in multiple sclerosis by a proteolytic enzyme, calpain. Proc Natl Acad Sci U S A **96:** 11486-11491.

SIMMONS, M. L., C. G. FRONDOZA and J. T. COYLE, 1991 Immunocytochemical localization of N-acetyl-aspartate with monoclonal antibodies. Neuroscience **45:** 37-45.

SKOFF, R. P., and M. S. GHANDOUR, 1995 Oligodendrocytes in female carriers of the jimpy gene make more myelin than normal oligodendrocytes. J Comp Neurol **355:** 124-133.

SLOTNICK, B. M., and B. J. NIGROSH, 1975 Maternal behavior of mice with cingulate cortical, amygdala, or septal lesions. J Comp Physiol Psychol **88:** 118-127.

SMALL, R. K., P. RIDDLE and M. NOBLE, 1987 Evidence for migration of oligodendrocyte--type-2 astrocyte progenitor cells into the developing rat optic nerve. Nature **328:** 155-157.

SOMIA, N., and I. M. VERMA, 2000 Gene therapy: trials and tribulations. Nat Rev Genet **1:** 91-99.

SONNTAG, F., S. BLEKER, B. LEUCHS, R. FISCHER and J. A. KLEINSCHMIDT, 2006 Adeno-associated virus type 2 capsids with externalized VP1/VP2 trafficking domains are generated prior to passage through the cytoplasm and are maintained until uncoating occurs in the nucleus. J Virol **80:** 11040-11054.

SUMMERFORD, C., J. S. BARTLETT and R. J. SAMULSKI, 1999 AlphaVbeta5 integrin: a co-receptor for adeno-associated virus type 2 infection. Nat Med **5:** 78-82.

SUMMERFORD, C., and R. J. SAMULSKI, 1998 Membrane-associated heparan sulfate proteoglycan is a receptor for adeno-associated virus type 2 virions. J Virol **72:** 1438-1445.

SURENDRAN, S., 2010 Upregulation of N-acetylaspartic acid resulting nitric oxide toxicity induces aspartoacylase mutations and protein interaction to cause pathophysiology seen in Canavan disease. Med Hypotheses **75:** 533-534.

SURENDRAN, S., G. A. CAMPBELL, S. K. TYRING and R. MATALON, 2005a Aspartoacylase gene knockout results in severe vacuolation in the white matter and gray matter of the spinal cord in the mouse. Neurobiol Dis **18:** 385-389.

SURENDRAN, S., E. L. EZELL, M. J. QUAST, J. WEI, S. K. TYRING *et al.*, 2004a Aspartoacylase deficiency does not affect N-acetylaspartylglutamate level or glutamate carboxypeptidase II activity in the knockout mouse brain. Brain Res **6:** 268-271.

SURENDRAN, S., E. L. EZELL, M. J. QUAST, J. WEI, S. K. TYRING *et al.*, 2004b Mental retardation and hypotonia seen in the knock out mouse for Canavan disease is not due to succinate semialdehyde dehydrogenase deficiency. Neurosci Lett **358:** 29-32.

SURENDRAN, S., K. M. MATALON, S. SZUCS, S. K. TYRING and R. MATALON, 2003a Metabolic changes in the knockout mouse for Canavan's disease: implications for patients with Canavan's disease. J Child Neurol **18:** 611-615.

SURENDRAN, S., R. MATALON and S. K. TYRING, 2006 Upregulation of aspartoacylase activity in the duodenum of obesity induced diabetes mouse: Implications on diabetic neuropathy. Biochem Biophys Res Commun **11:** 11.

SURENDRAN, S., K. MICHALS-MATALON, M. J. QUAST, S. K. TYRING, J. WEI *et al.*, 2003b Canavan disease: a monogenic trait with complex genomic interaction. Mol Genet Metab **80:** 74-80.

SURENDRAN, S., L. S. SHIHABUDDIN, J. CLARKE, T. V. TAKSIR, G. R. STEWART *et al.*, 2004c Mouse neural progenitor cells differentiate into oligodendrocytes in the brain of a knockout mouse model of Canavan disease. Brain Res Dev Brain Res **153:** 19-27.

SURENDRAN, S., S. SZUCS, S. K. TYRING and R. MATALON, 2005b Aspartoacylase gene knockout in the mouse: impact on reproduction. Reprod Toxicol **20:** 281-283.

SUZUKI, K., 1968 Peripheral nerve lesion in spongy degeneration of the central nervous system. Acta Neuropathol **10:** 95-98.

SZUCHET, S., K. WATANABE and Y. YAMAGUCHI, 2000 Differentiation/regeneration of oligodendrocytes entails the assembly of a cell-associated matrix. Int J Dev Neurosci **18:** 705-720.

TACKE, U., H. OLBRICH, J. O. SASS, A. FEKETE, J. HORVATH *et al.*, 2005 Possible genotype-phenotype correlations in children with mild clinical course of Canavan disease. Neuropediatrics **36:** 252-255.

TALLAN, H. H., 1957 Studies on the distribution of N-acetyl-L-aspartic acid in brain. J Biol Chem **224:** 41-45.

TALLAN, H. H., S. MOORE and W. H. STEIN, 1956 N-Acetyl-L-aspartic acid in brain. J Biol Chem **219:** 257-264.

TAMURA, K., M. TAMURA, K. IKENAKA, T. YOSHIMATSU, Y. MIYAO *et al.*, 2001 Eradication of murine brain tumors by direct inoculation of concentrated high titer-recombinant retrovirus harboring the herpes simplex virus thymidine kinase gene. Gene Ther **8:** 215-222.

TAYMANS, J. M., L. H. VANDENBERGHE, C. V. HAUTE, I. THIRY, C. M. DEROOSE *et al.*, 2007 Comparative analysis of adeno-associated viral vector serotypes 1, 2, 5, 7, and 8 in mouse brain. Hum Gene Ther **18:** 195-206.

TESTA, G., J. SCHAFT, F. VAN DER HOEVEN, S. GLASER, K. ANASTASSIADIS *et al.*, 2004 A reliable lacZ expression reporter cassette for multipurpose, knockout-first alleles. Genesis **38:** 151-158.

THOMAS, D. L., L. WANG, J. NIAMKE, J. LIU, W. KANG *et al.*, 2009 Scalable recombinant adeno-associated virus production using recombinant herpes simplex virus type 1 coinfection of suspension-adapted mammalian cells. Hum Gene Ther **20:** 861-870.

TKACHEV, D., M. L. MIMMACK, M. M. RYAN, M. WAYLAND, T. FREEMAN *et al.*, 2003 Oligodendrocyte dysfunction in schizophrenia and bipolar disorder. Lancet **362:** 798-805.

TRAKA, M., R. L. WOLLMANN, S. R. CERDA, J. DUGAS, B. A. BARRES *et al.*, 2008 Nur7 is a nonsense mutation in the mouse aspartoacylase gene that causes spongy degeneration of the CNS. J Neurosci **28:** 11537-11549.

TROTTER, J., D. BITTER-SUERMANN and M. SCHACHNER, 1989 Differentiation-regulated loss of the polysialylated embryonic form and expression of the different polypeptides of the neural cell adhesion molecule by cultured oligodendrocytes and myelin. J Neurosci Res **22:** 369-383.

TUSZYNSKI, M. H., 2007 Nerve growth factor gene therapy in Alzheimer disease. Alzheimer Dis Assoc Disord **21:** 179-189.

ULDRY, M., M. IBBERSON, J. D. HORISBERGER, J. Y. CHATTON, B. M. RIEDERER *et al.*, 2001 Identification of a mammalian H(+)-myo-inositol symporter expressed predominantly in the brain. EMBO J **20:** 4467-4477.

URENJAK, J., S. R. WILLIAMS, D. G. GADIAN and M. NOBLE, 1992 Specific expression of N-acetylaspartate in neurons, oligodendrocyte-type-2 astrocyte progenitors, and immature oligodendrocytes in vitro. J Neurochem **59:** 55-61.

VAN BOGAERT, L., and I. BERTRAND, 1949 Sur une idiotie familiale avec degeresce sponglieuse de neuraxe (note preliminaire). Acta Neurol Belg **49:** 572-587.

VAN DER HEUL-NIEUWENHUIJSEN, L., P. J. HENDRIKSEN, T. H. VAN DER KWAST and G. JENSTER, 2006 Gene expression profiling of the human prostate zones. BJU Int **98:** 886-897.

VAN VLIET, K. M., V. BLOUIN, N. BRUMENT, M. AGBANDJE-MCKENNA and R. O. SNYDER, 2008 The role of the adeno-associated virus capsid in gene transfer. Methods Mol Biol **437:** 51-91.

VIRCHOW, R., 1846 Über das granulirte Aussehen der Wandungen der Gehirnventrikel. Allg Z Psychat **3:** 242-250.

WANG, C., C. M. WANG, K. R. CLARK and T. J. SFERRA, 2003 Recombinant AAV serotype 1 transduction efficiency and tropism in the murine brain. Gene Ther **10:** 1528-1534.

WANG, J., P. LEONE, G. WU, J. S. FRANCIS, H. LI *et al.*, 2009 Myelin lipid abnormalities in the aspartoacylase-deficient tremor rat. Neurochem Res **34:** 138-148.

WANG, J., R. MATALON, G. BHATIA, G. WU, H. LI *et al.*, 2007 Bimodal occurrence of aspartoacylase in myelin and cytosol of brain. J Neurochem **101:** 448-457.

WARRINGTON, K. H., JR., and R. W. HERZOG, 2006 Treatment of human disease by adeno-associated viral gene transfer. Hum Genet **119:** 571-603.

WIAME, E., D. TYTECA, N. PIERROT, F. COLLARD, M. AMYERE *et al.*, 2010 Molecular identification of aspartate N-acetyltransferase and its mutation in hypoacetylaspartia. Biochem J **425:** 127-136.

WITTSACK, H. J., H. KUGEL, B. ROTH and W. HEINDEL, 1996 Quantitative measurements with localized 1H MR spectroscopy in children with Canavan's disease. J Magn Reson Imaging **6:** 889-893.

WU, Z., A. ASOKAN and R. J. SAMULSKI, 2006 Adeno-associated virus serotypes: vector toolkit for human gene therapy. Mol Ther **14:** 316-327.

WU, Z., H. YANG and P. COLOSI, 2010 Effect of genome size on AAV vector packaging. Mol Ther **18:** 80-86.

WYSS-CORAY, T., J. D. LOIKE, T. C. BRIONNE, E. LU, R. ANANKOV *et al.*, 2003 Adult mouse astrocytes degrade amyloid-beta in vitro and in situ. Nat Med **9:** 453-457.

XU, R., C. G. JANSON, M. MASTAKOV, P. LAWLOR, D. YOUNG *et al.*, 2001 Quantitative comparison of expression with adeno-associated virus (AAV-2) brain-specific gene cassettes. Gene Ther **8:** 1323-1332.

YAN, H. D., K. ISHIHARA, T. SERIKAWA and M. SASA, 2003 Activation by N-acetyl-L-aspartate of acutely dissociated hippocampal neurons in rats via metabotropic glutamate receptors. Epilepsia **44:** 1153-1159.

YANG, J., W. ZHOU, Y. ZHANG, T. ZIDON, T. RITCHIE *et al.*, 1999 Concatamerization of adeno-associated virus circular genomes occurs through intermolecular recombination. J Virol **73:** 9468-9477.

ZANO, S., R. MALIK, S. SZUCS, R. MATALON and R. E. VIOLA, 2011 Modification of aspartoacylase for potential use in enzyme replacement therapy for the treatment of Canavan disease. Mol Genet Metab **102:** 176-180.

ZOLOTUKHIN, S., M. POTTER, I. ZOLOTUKHIN, Y. SAKAI, S. LOILER *et al.*, 2002 Production and purification of serotype 1, 2, and 5 recombinant adeno-associated viral vectors. Methods **28:** 158-167.

Appendix

Abbreviations

°C	degree Celsius
A	Adenosine
a/p	anterior/posterior
AAV	Adeno-associated virus
ad	adjust
ANAT	acetyl CoA/aspartate N-acetyltransferase
ASPA	Aspartoacylase
bFGF	basic fibroblast growh factor
BG	Bergman glia
bGH(pA)	Bovine growth hormone (polyadenylation signal)
Bp	base pairs
C	Cytidine
CAII	Carbonic anhydrase II
CAM	Cell adhesion molecule
CBA	CMV enhancer/chicken β-actin (promoter)
cc	Corpus callosum or Central canal
CD	Canavan Disease
CMV	Cytomegalovirus
CNP(ase)	2', 3'-cyclic nucleotide 3'-phosphodiesterase
CNS	Central nervous system
cpm	counts per minute
Cr	Creatinine
Cre	Causes recombination; Cre recombinase from bacteriophage P1
ctx	Cortex
d/v	dorso/ventral
DAPI	4´,6-Diamidino-2-phenylindole
dcl	Dentate gyrus granular cell layer
DMEM	Dulbecco´s modified Eagle´s medium
DMSO	Dimethylsulfoxid
DNA	Deoxyribonucleic acid
DNase	Deoxyribonuclease
DTA	Diphteria toxin
E	Embryonic day
EDTA	Ethylenediaminetetraacetic acid
EGFP	Enhanced green fluorescent protein
ENU	*N*-ethyl-*N*-nitrosourea
ESC	Embryonic stem cell
EUCOMM	European Mouse Mutagenesis Program
FCS	Foetal calf serum
Fig.	Figure
Flp	Flippase
Folh1	folate hydrolase 1; glutamate carboxypeptidase II; NAAG peptidase
Frt	Flp recombination target
g	gravitational force
G	Guanosine

GCP-II	Glutamate carboxypeptidase II; Folh1
GFAP	Glial fibrillary acidic protein
GFP	Green fluorescent protein
GL	Granular cell layer
Glc	Glucose
GM	Grey matter
GPRC	G-protein coupeled receptor
hc	Hippocampus
HEK	Human embryonic kidney cell
HEPES	4-(2-Hydroxyethyl)piperazine-1-ethanesulfonic acid
HSPG	heparan sulfate proteoglycan
i.c.v	intracerebroventricular
i.p.	intraparenchymal
IMDM	Iscove´s modified Dulbecco´s medium
ITR	Inverted terminal repeats
kb	kilo base
kDa	kilo Dalton
ko	knock out
lacZ	gene encoding β-galactosidase
LIF	Leukemia inhibitory factor
loxP	Locus of X-ing over P1
m/l	medio/lateral
MBP	Myelin basic protein
MEF	Mouse embryonic fibroblast
mI	Myo-Inositol
MLD	Metachromatic Leukodystrophy
MMC	Mitomycin C
MOG	Myelin oligodendrocyte glycoprotein
MRI	Magnetic resonance imaging
NAA	N-acetyl-L-aspartate
NAAG	N-acetyl-L-aspartate
NAAGS	N-acetyl-aspartylglutamate synthase
NeuN	neuronal nuclei
NSCs	Neural stem cells
nu	Nucleus
O4	Oligodendrocyte-antigen 4
OL	Oligodendrocyte
OPC	Oligodendrocyte precursor cell
ORF	Open-reading frame
P	Postnatal day
pA	Polyadenylation signal
PAGE	Polyacrylamide gel electrophoresis
PBS	Phosphate-buffered saline
PC	Purkinje cell
pcl	Pyramidal cell layer
PCR	Polymerase chain reaction
PDGF	Platelet-derived growth factor
PF	Parallel fibre
PFA	Paraformaldehyde
PLP	Proteolipidprotein
PNS	Peripheral nervous system

rcf	relative centrifugal force
RFP	Red fluorescent protein
RNA	Ribonucleic acid
RNase	Ribonuclease
rpm	Revolutions per minute
SA	Splice acceptor
SC	Schwann cell
SDS	Sodium dodecyl sulfate
SEM	Standard error of mean
SolC	Solitary tract nucleus
str	Striatum
T	Tesla
T	Thymidine
Tau	Taurin
TBS	Tris-buffered saline
TESPA	3-Aminopropyl-trimethoxysilane
tha	Thalamus
Tris	Tris(hydroxymethyl)aminomethane
v/v	Volume per volume
vg	viral genomes
w/v	Weight per volume
WM	White matter
WPRE	Woodchuck hepatitis virus posttranscriptional regulatory element
wt	wild type
X-Gal	5-bromo-4-chloro-3-indolyl-beta-D-galactopyranoside
βgeo	β-galacosidase-neomycin-resistance cassette

Further abbeviations were used according the international system of units (SI). The one letter code of amino acids was used for proteins.

List of figures

List of tables

Danksagung

Curriculum Vitae – Nadine Mersmann